



**Pharmacological  
exposure optimisation  
of anticancer agents  
during clinical development**

*Lisa Tamara van der Heijden*



**Pharmacological  
exposure optimisation  
of anticancer agents  
during clinical development**

*Lisa Tamara van der Heijden*

The research described in this thesis was performed at the Department of Pharmacy & Pharmacology, the Netherlands Cancer Institute – Antoni van Leeuwenhoek Hospital, Amsterdam, The Netherlands, in collaboration with other institutes.

Printing of this thesis was financially supported by the Oncology Graduate School Amsterdam.

ISBN: 978-94-6483-329-4

**Cover design and layout**

© evelienjagtman.com

**Print**

Ridderprint

© Lisa T. van der Heijden, 2023

# **Pharmacological exposure optimisation of anticancer agents during clinical development**

**Optimaliseren van de farmacologische blootstelling van oncologische  
geneesmiddelen tijdens klinische ontwikkeling**

(met een samenvatting in het Nederlands)

**Proefschrift**

ter verkrijging van de graad van doctor aan de Universiteit Utrecht  
op gezag van rector magnificus, prof. dr. H.R.B.M. Krummeling  
ingevolge het besluit van het college voor promoties  
in het openbaar te verdedigen op

dinsdag 12 december 2023 des middags te 2.15 uur

door

**Lisa Tamara van der Heijden**

Geboren op 12 juli 1994  
te Capelle aan den IJssel

**Promotoren:**

Prof. dr. A.D.R. Huitema

Prof. dr. J.H. Beijnen

**Copromotoren:**

Dr. T.P.C. Dorlo

Dr. H. Rosing

**Beoordelingscommissie**

Prof. dr. N.P. van Erp

Prof. dr. M. van den Heuvel-Eibrink

Prof. dr. O.W. Kranenburg

dr. M.M. Malingré

Prof. dr. R.M. Schiffelers

*Not all those who wander are lost*

J.R.R. Tolkien



**Chapter 1** A naïve pooled data approach for extrapolation of Phase 0 microdose trials to therapeutic dosing regimens  
*Clinical Translational Science*. 2023;16(2):258-268 21

**Chapter 2** An ultra-sensitive liquid chromatography tandem mass spectrometry method for the simultaneous quantification of  $^3\text{H}_6$ -alelectinib and alelectinib in human plasma for the support of a microtracer food-effect trial  
*Manuscript in preparation* 51

**Chapter 3** The use of microtracers in food-effect trials: An alternative study design for toxic drugs with long half-lives exemplified by the case for alelectinib  
*Accepted in Clinical Translational Science* 75

**Chapter 4** The use of microdosing for *in vivo* phenotyping of Cytochrome P450: Where do we stand?  
*Submitted* 101

**Chapter 5** Safety of the triple combination lapatinib, binimetinib, and vinorelbine for RAS mutated metastatic colorectal cancer patients: A preliminary analysis of the first dose levels from the RASTRIC Phase I/II clinical trial  
*Interim analysis* 159

**Chapter 6** Quantification of the exposure-toxicity relationship of combined MEK and pan-HER inhibitors in patients with KRAS mutated tumours  
*Interim analysis* 187

## PART 1

Novel applications  
of microdoses and  
microtracers

## PART 2

Dose finding of  
targeted agents in  
combination therapy



**Chapter 7** Dose optimization of oral docetaxel in combination with ritonavir for patients with metastatic castration resistant prostate cancer  
*Manuscript in preparation* 217

**Chapter 8** Is higher docetaxel clearance in prostate cancer patients explained by higher CYP3A: An *in vivo* phenotyping study with midazolam  
*Accepted in Journal of Clinical Pharmacology* 247

## PART 3

Dose finding of oral docetaxel for patients with metastatic castration resistant prostate cancer

**Chapter 9** A highly sensitive bioanalytical method for the quantification of vinblastine, vincristine, vinorelbine and 4-O-deacetylvinorelbine in human plasma using LC-MS/MS  
*Journal of Pharmaceutical and Biomedical Analysis*. 2022;215:114772 273

**Chapter 10** A sensitive liquid chromatographic-mass spectrometry method for the quantification of vincristine in whole blood collected with volumetric absorptive microsampling  
*Journal of Pharmaceutical and Biomedical Analysis*. 2023;225:115232 291

**Chapter 11** Age-dependent vincristine binding to  $\beta$ -tubulin explains non-linear pharmacokinetics of vincristine: a physiologically based pharmacokinetic approach  
*Manuscript in preparation* 317

**Chapter 12** Development of a Therapeutic Drug Monitoring strategy for the optimization of vincristine treatment in paediatric oncology populations in Africa  
*Therapeutic Drug Monitoring*. 2023;45(3):354–363 339

## Appendices

Summary	383
Nederlandse samenvatting	389
Author affiliations	397
Author contribution	403
List of Publications	407
Dankwoord	411
Curriculum vitae	417

Optimisation of vincristine exposure in paediatric populations

## PART 4



**Chapter 13** Conclusions and Perspectives 367



# Preface



## PREFACE

Over the past decades, the pharmacological treatment of cancer has switched focus. The increasing knowledge of cancer biology enabled the development of novel anticancer agents targeting specific molecular pathways responsible for tumour growth (often referred to as targeted therapies). As a result, the focus of drug development changed from conventional cytotoxic chemotherapeutics to targeted therapies. Despite this switch in therapy, the design of dose finding clinical trials to select the dose for further clinical development of a drug has not changed. The most frequently used design for Phase I trials still consists of dose-escalating cohorts, which are designed to find the maximum tolerated dose (MTD) [1]. This so-called MTD paradigm, is based on several assumptions. The first assumption is that the drug has an exposure–efficacy relationship that parallels exposure–toxicity relationship (Figure 1A) [1–4]. In other words, a higher dose will result in more effect of the drug but will also result in more toxicity. Secondly, the drug has a small range of exposure where the drug is effective but not toxic (narrow therapeutic window). Thirdly, dose limiting toxicity occurs early during treatment and is dose related. Lastly, overdosing and the associated toxicity is considered more acceptable than underdosing due to the rapidly progression of chemo-sensitive disease [1,3].

While the above-described assumptions hold up for conventional chemotherapy [1–4], they are not necessarily appropriate for targeted therapies. Due to their more specific mechanism of action, the exposure–efficacy relationship might be different than their exposure–toxicity relationship, resulting in an optimal dose, defined as the dose with an optimal balance between efficacy and toxicity, which is potentially lower than the MTD (Figure 1B) [2,5]. Therefore, patients may be exposed to doses higher than necessary for efficacy and consequently more at risk for toxicity than needed. Furthermore, toxicities from targeted therapies can be either acute, chronic, or cumulative in nature [2,6]. Toxicities which occur later in the treatment period or after end of therapy are poorly characterized in clinical trials, and not considered in dose recommendations [7–10]. Approximately 50% of (severe) toxicities of targeted therapies occur after the end of the period in which dose limiting toxicities are considered [7–9]. Thus, the current dose finding framework might not be suitable for new, more targeted, anticancer agents.

Poorly optimised doses can have negative consequences for patients, including frequent dose reductions, impaired therapy adherence, and premature discontinuation and therefore missed opportunity of drug benefit, or limitations to subsequent therapy due to persistent or irreversible toxicities [3,6]. In worst-case

scenarios, toxicities could be associated with a reduced overall survival or removal of a drug from the market [11]. Lastly, poor dose optimisation might contribute to unsuccessful development programs for promising drug candidates [12].

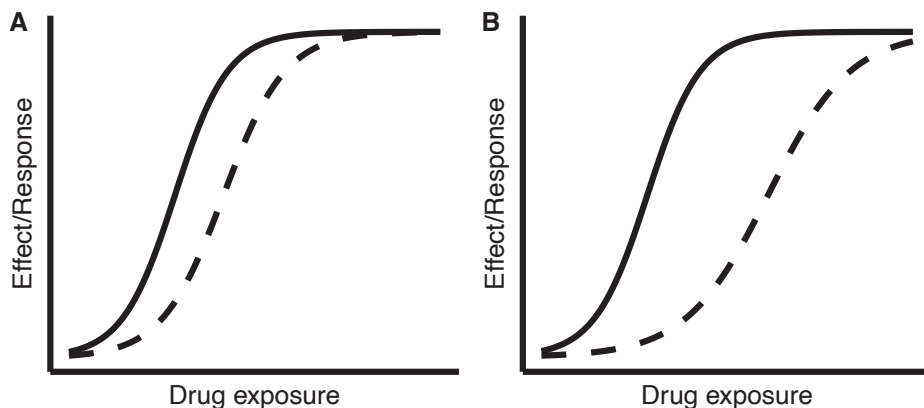


**Figure 1.** Exposure-efficacy and exposure-toxicity relationship for a drug. For scenario A, the maximum tolerated dose (MTD) is appropriate for dose selection, while for scenario B, the MTD is less appropriate for dose selection. The solid line represents efficacy and the dashed line represent toxicity.

Taken all this in consideration, there is a need to improve dose selection in early development of targeted anticancer agents. Characterisation of exposure-efficacy and exposure-toxicity relationships is essential for this aim [13]. Moreover, validated pharmacodynamic biomarkers to link exposure-response relationships to clinical outcomes (e.g., overall survival) are desired [2,14]. Despite the recommendations of harmonized guidelines, most oncology Phase I trials conducted in 2022 still aimed to define a recommended Phase 2 dose based on toxicity [1]. Moreover, in the period 2019 to 2021, approximately 1/3<sup>rd</sup> of the small molecules and antibody-drug conjugates registered by the US Food and Drug Administration (FDA) for oncology, the selected dose was the MTD or the maximum administered dose if the MTD was not reached [6].

To help the field to reform the paradigm for dose optimisation and dose selection in oncology drug development, the FDA's Oncology Center for Excellence launched an initiative called Project OPTIMUS. The goal of Project OPTIMUS is to change the dose finding and dose optimisation paradigm in oncology to emphasize the selection of a dose or doses that optimise drug exposure based on efficacy, safety, and tolerability [2,15]. To enable the paradigm shift, novel study designs

and strategies are needed to obtain the essential data on exposure-response relationships earlier in drug development. Two factors are essential to obtain this data. The first is the conduct of more informative dose finding trials, including novel trial designs. The second factor is the use of powerful data analysis tools, such as models to describe exposure-response relationships (pharmacometrics) to fully characterise exposure-response relationships and finding doses with an optimal efficacy-toxicity balance. Moreover, optimal doses might not be similar across different patient populations (e.g., adults vs paediatric patients or across different tumour types). Therefore, methods for extrapolation of exposure-response relationships across populations need to be investigated.

## THESIS OUTLINE

This thesis aims to contribute to the shift in dose-finding paradigm within oncology by investigating novel methods for dose optimisation and dose extrapolation. Separate objectives of this thesis are: 1) development and validation of bioanalytical methods for the quantification of drug concentrations necessary for an improved understanding of drug exposure (pharmacokinetics), 2) demonstration of the feasibility of using microdosing and microtracers for exposure characterisation in early drug development, and 3) application of pharmacometrics methods for the characterisation of exposure-response relationships and the extrapolation to different patient populations.

In **Part 1** the application of microdoses and microtracers to improve understanding of *in vivo* pharmacokinetics is described. **Chapter 1** describes a novel strategy to extrapolate microdose pharmacokinetics to therapeutic pharmacokinetics to inform dose selection for Phase I clinical trials. **Chapters 2** and **3** describes the use of microtracers to determine the food-effect on the pharmacokinetics toxic drugs with long half-lives exemplified by the tyrosine kinase inhibitor alectinib. **Chapter 4** gives an overview of the application of microdoses to *in vivo* phenotyping. Recommendations for microdose phenotyping tests are provided based on the literature.

**Part 2** demonstrates the challenging dose optimisation of the combination of human epidermal growth factor receptor (pan-HER) inhibitors and mitogen-activated protein kinase kinase (MEK) inhibitors for the treatment of RAS mutated solid tumours. **Chapter 5** describes the interim analysis of a Phase I study of patients with colorectal carcinoma who are treated with triple therapy of lapatinib (pan-HER inhibitor), binimetinib (MEK inhibitor), and vinorelbine (microtubule targeting agent). **Chapter 6** aims to quantify the exposure-toxicity relationship of the combination therapy of MEK and pan-HER inhibitors. Recommendations for rational dosing strategies are provided based on a pharmacokinetic-pharmacodynamic model.

In **Part 3** dose optimisation for oral docetaxel in combination with the oral booster ritonavir for patients with metastatic castration resistant prostate cancer (mCRPC) is described. **Chapter 7** focusses on the quantification of the difference in pharmacokinetics of oral docetaxel between mCRPC patients and patients with other solid tumours. Recommendations for a Phase 2 dose are provided based on dose simulations using a population pharmacokinetic model. **Chapter 8** compares



the *in vivo* CYP3A activity of patients with prostate cancer and male patients with other solid tumours. In this *in vivo* phenotyping study midazolam clearance is compared between the two patient groups to test the hypothesis if CYP3A contributes to the observed differences in pharmacokinetics of oral docetaxel.

In **Part 4** the pharmacokinetics is described of an old cytotoxic drug, vincristine, of which no dose optimisation has been performed and despite its long use in clinical practice many factors regarding the variability in pharmacokinetics is unknown. **Chapter 9** and **10** focuses on the quantification of vincristine and two other vinca-alkaloids and a metabolite in human plasma and vincristine in whole blood collected with volumetric absorptive microsampling (VAMS), respectively. **Chapter 11** explores the role of  $\beta$ -tubulin in tissues and blood cells in the complex pharmacokinetics of vincristine in adult and paediatric patients. The physiologically-based pharmacokinetic (PBPK) model forms the basis for further optimisation of paediatric dosing guidelines of vincristine. **Chapter 12** provides a pharmacometric nomogram for the classification of vincristine exposure in African paediatric patients into low and adequate exposure groups. This pharmacometric nomogram could help optimise vincristine dosing in this special population.

Finally, the general conclusion of the work included in this thesis as well as future perspectives are discussed in **Chapter 13**, followed by a summary of all individual chapters.

## REFERENCES

1. Araujo D, Greystoke A, Bates S, Bayle A, Calvo E, Castelo-Branco L, de Bono J, Drilon A, Garralda E, Ivy P, Kholmanskikh O, Melero I, Pentheroudakis G, Petrie J, Plummer R, Ponce S, Postel-Vinay S, Siu L, Spreafico A, Stathis A, Steeghs N, Yap C, Yap TA, Ratain M, Seymour L (2023) Oncology phase I trial design and conduct: time for a change - MDICT Guidelines 2022. *Ann Oncol* 34 (1):48-60. doi:10.1016/j.annonc.2022.09.158
2. Murphy R, Halford S, Symeonides SN (2023) Project Optimus, an FDA initiative: Considerations for cancer drug development internationally, from an academic perspective. *Front Oncol* 13:1144056. doi:10.3389/fonc.2023.1144056
3. Shah M, Rahman A, Theoret MR, Pazdur R (2021) The Drug-Dosing Conundrum in Oncology - When Less Is More. *N Engl J Med* 385 (16):1445-1447. doi:10.1056/NEJMp2109826
4. Takimoto CH (2009) Maximum tolerated dose: clinical endpoint for a bygone era? *Target Oncol* 4 (2):143-147. doi:10.1007/s11523-009-0108-y
5. Postel-Vinay S, Arkenau HT, Olmos D, Ang J, Barriuso J, Ashley S, Banerji U, De-Bono J, Judson I, Kaye S (2009) Clinical benefit in Phase-I trials of novel molecularly targeted agents: does dose matter? *Br J Cancer* 100 (9):1373-1378. doi:10.1038/sj.bjc.6605030
6. Fourie Zirkelbach J, Shah M, Vallejo J, Cheng J, Ayyoub A, Liu J, Hudson R, Sridhara R, Ison G, Amiri-Kordestani L, Tang S, Gwise T, Rahman A, Pazdur R, Theoret MR (2022) Improving Dose-Optimization Processes Used in Oncology Drug Development to Minimize Toxicity and Maximize Benefit to Patients. *J Clin Oncol* 40 (30):3489-3500. doi:10.1200/jco.22.00371
7. Postel-Vinay S, Gomez-Roca C, Molife LR, Anghan B, Levy A, Judson I, De Bono J, Soria JC, Kaye S, Paoletti X (2011) Phase I trials of molecularly targeted agents: should we pay more attention to late toxicities? *J Clin Oncol* 29 (13):1728-1735. doi:10.1200/jco.2010.31.9236
8. Postel-Vinay S, Collette L, Paoletti X, Rizzo E, Massard C, Olmos D, Fowst C, Levy B, Mancini P, Lacombe D, Ivy P, Seymour L, Le Tourneau C, Siu LL, Kaye SB, Verweij J, Soria JC (2014) Towards new methods for the determination of dose limiting toxicities and the assessment of the recommended dose for further studies of molecularly targeted agents--dose-Limiting Toxicity and Toxicity Assessment Recommendation Group for Early Trials of Targeted therapies, an European Organisation for Research and Treatment of Cancer-led study. *Eur J Cancer* 50 (12):2040-2049. doi:10.1016/j.ejca.2014.04.031
9. Edgerly M, Fojo T (2008) Is there room for improvement in adverse event reporting in the era of targeted therapies? *J Natl Cancer Inst* 100 (4):240-242. doi:10.1093/jnci/djm324
10. Altzerinakou MA, Collette L, Paoletti X (2019) Cumulative Toxicity in Targeted Therapies: What to Expect at the Recommended Phase II Dose. *J Natl Cancer Inst* 111 (11):1179-1185. doi:10.1093/jnci/djz024
11. Norsworthy KJ, Ko CW, Lee JE, Liu J, John CS, Przepiorcka D, Farrell AT, Pazdur R (2018) FDA Approval Summary: Mylotarg for Treatment of Patients with Relapsed or Refractory CD33-Positive Acute Myeloid Leukemia. *Oncologist* 23 (9):1103-1108. doi:10.1634/theoncologist.2017-0604

12. Sacks LV, Shamsuddin HH, Yasinskaya YI, Bouri K, Lanthier ML, Sherman RE (2014) Scientific and regulatory reasons for delay and denial of FDA approval of initial applications for new drugs, 2000-2012. *Jama* 311 (4):378-384. doi:10.1001/jama.2013.282542
13. Kawakatsu S, Bruno R, Kågedal M, Li C, Girish S, Joshi A, Wu B (2021) Confounding factors in exposure-response analyses and mitigation strategies for monoclonal antibodies in oncology. *Br J Clin Pharmacol* 87 (6):2493-2501. doi:10.1111/bcp.14662
14. Bottino DC, Patel M, Kadakia E, Zhou J, Patel C, Neuwirth R, Iartchouk N, Brake R, Venkatakrishnan K, Chakravarty A (2019) Dose Optimization for Anticancer Drug Combinations: Maximizing Therapeutic Index via Clinical Exposure-Toxicity/Preclinical Exposure-Efficacy Modeling. *Clin Cancer Res* 25 (22):6633-6643. doi:10.1158/1078-0432.Ccr-18-3882
15. US Food and Drug Administration (FDA) (2023) Project Optimus: Reforming the dose optimization and dose selection paradigm in oncology. <https://www.fda.gov/about-fda/oncology-center-excellence/project-optimus> Accessed 31 May 2023





# Part 1

**Novel applications of  
microdoses and microtracers**



# Chapter 1

## **A naïve pooled data approach for extrapolation of Phase 0 microdose trials to therapeutic dosing regimens**

*Clinical Translational Science. 2023;16(2):258-268*

Lisa T. van der Heijden  
Merel van Nuland  
Jos H. Beijnen  
Alwin D.R. Huitema  
Thomas P.C. Dorlo

## ABSTRACT

Microdosing is a strategy to obtain knowledge of human pharmacokinetics prior to Phase I clinical trials. The most frequently used method to extrapolate microdose ( $\leq 100 \mu\text{g}$ ) pharmacokinetics to therapeutic doses is based on linear extrapolation from a non-compartmental analysis (NCA) with a two-fold acceptance criterion between pharmacokinetic metrics of the extrapolated microdose and the therapeutic dose. The major disadvantage of NCA is the assumption of linear extrapolation of NCA metrics. In this study, we used a naïve pooled data (NPD) modelling approach to extrapolate microdose pharmacokinetics to therapeutic pharmacokinetics. Gemcitabine and anastrozole were used as examples of intravenous and oral drugs, respectively. Data from microdose studies were used to build a parent-metabolite model for gemcitabine and its metabolite 2',2'-difluorodeoxyuridine (dFdU) and a model for anastrozole. The pharmacokinetic microdose models were extrapolated to therapeutic doses. Extrapolation of the microdose showed differences in pharmacokinetic shape for gemcitabine and dFdU between the simulated and observed therapeutic concentrations, whereas the observed therapeutic concentrations for anastrozole were captured by the extrapolation. This study demonstrated the possible use and feasibility of an NPD modelling approach for the evaluation and application of microdose studies in early drug development. Lastly, physiologically-based pharmacokinetic modelling might be an alternative for microdose extrapolation of drugs with complex pharmacokinetics such as gemcitabine.



# 1 INTRODUCTION

The concept of microdosing was introduced in the 1990s as a method to obtain early *in vivo* human pharmacokinetic data [1]. The first study using microdosing was published in 2003 [1]. Subsequently, the European Medicines Agency (EMA) and the US Food and Drug Administration (FDA) first addressed microdosing trials in 2004 and 2006, respectively [2,3]. This resulted in the current International Conference on Harmonization (ICH) M3[R2] guideline on experimental investigational new drug studies by the EMA [4]. During this period, a microdose was defined as 1/100<sup>th</sup> of the anticipated therapeutic dose with a maximum of 100 µg [3].

The original idea of microdosing was assessment of the pharmacokinetics of a new drug in an early phase prior to Phase I clinical studies [5]. Because microdosing trials precede Phase I clinical trials, they are often referred to as Phase 0 studies. In these Phase 0 studies, a small population of healthy volunteers (and sometimes patients [6]) is administered a microdose of the drug candidate. The aim of these studies is to quickly establish whether a novel drug has an appropriate pharmacokinetic profile in the human body without therapeutic or diagnostic purpose [6]. Consequently, Phase 0 microdose studies enhance early selection of promising drug candidates and help in selecting the starting dose, thereby reducing costs and time, and improving efficiency of drug development [7].

The concept of microdosing is based on the assumption that pharmacokinetics of a microdose can be extrapolated to therapeutic doses. The most frequently used method to evaluate the pharmacokinetic extrapolation of microdose to therapeutic dose is by performing a non-compartmental analysis (NCA) and determine the fold-difference in dose-normalised pharmacokinetic metrics between the microdose and therapeutic dose [8,9]. The acceptance criterion is typically a two-fold difference, which is commonly used in allometry [8,9]. Based on this criterion, the predictability of microdose to therapeutic pharmacokinetics has been summarized previously, where the predictability of orally administered drugs was 62% (n=25) [10] and 68% (n=41) [11], while the predictability of intravenously (IV) administered drugs was 100% (n=12) [10] and 94% (n=16) [11]. Phase 0 microdose studies appear to be more successful in predicting therapeutic human pharmacokinetics compared to the traditionally used techniques for *in vitro* to *in vivo* extrapolation (IVIVE) such as allometry or physiologically based pharmacokinetics (PBPK). A predictability of 51-79% for IVIVE is reported in literature for both oral and IV administered drugs and with a two-fold error [12-15].

Assessing microdose predictability using NCA with a two-fold criterion, however, has several disadvantages. Drugs with pharmacokinetic metrics just outside the two-fold criterion are classified as not predictive. However, it is debatable whether drugs with metrics just outside this interval are relevantly different from drugs with metrics just inside the interval. Additionally, the two-fold criterion is difficult to interpret for pharmacokinetic parameters or metrics that have boundaries. For example, bioavailability, cannot be larger than 100% and organ clearance is bound by blood flow. Furthermore, the current evaluation method ignores the overall shape of the pharmacokinetic curve when only summary measures for exposure are used for evaluation (e.g., a similar area-under-the-concentration-time-curve [AUC] value could represent two different pharmacokinetic curves).

An alternative approach to assess microdose predictability is a naïve pooled data (NPD) modelling approach. In this approach, a population pharmacokinetic model is developed by fitting the combined data of all individuals while ignoring individual differences. The aim of the current study was to demonstrate the feasibility of an NPD modelling approach for extrapolation of a microdose to therapeutic dosing. The NPD approach will be demonstrated with data from two microdose studies [16-18] using gemcitabine, and its metabolite 2',2'-difluorodeoxyuridine (dFdU) as example of an IV administered drug and anastrozole as an example for an oral administered drug. Pharmacokinetic models were developed using the microdose data and used for the extrapolation to therapeutic dosing. The observed therapeutic data were used to evaluate the predictive value of microdose-based extrapolations.

## 2 METHODS

### 2.1 Study design, subjects and data

Data were used from three studies: a gemcitabine Phase 0 microdose study<sup>16</sup>, an anastrozole microdose study [17] and an anastrozole clinical dose finding study [18]. Demographic characteristics of the subjects included in the studies are depicted in Table S1.

#### 2.1.1 Gemcitabine study

The gemcitabine Phase 0 microdose study was a prospective, sequential, open-label, single arm microdose study performed at the Antoni van Leeuwenhoek Hospital, the Netherlands. In this study patients received gemcitabine as a microdose and as a therapeutic dose. The trial received institutional ethical approval, was conducted in accordance with the principles of the Declaration of Helsinki and was registered in the Netherlands Trial Register (NTR6183). The study design and results of the NCA have been described in detail previously [16].

Ten patients (>18 years old) with solid tumours and an indication for treatment with gemcitabine according to standard of care were included in the study. Patient characteristics are described in Table S1. Patients received 100 µg gemcitabine and 1250 mg/m<sup>2</sup> gemcitabine within a 24-hour interval [16]. Both the microdose and therapeutic dose were administered as a 30-minute IV infusion. Blood samples were taken 0, 0.25, 0.5, 0.75, 1, 1.25, 1.5, 1.75, 2, 4, and 8 hours after the start of the infusion. Plasma concentrations of gemcitabine and dFdU after administration of the microdose were quantified using a validated liquid-chromatography-tandem mass spectrometry (LC-MS/MS) method with a lower limit of quantification (LLOQ) of 5 pg/mL and 500 pg/mL, respectively [19]. Furthermore, gemcitabine and dFdU concentrations after administration of the therapeutic dose were quantified using a validated LC-MS/MS method with a LLOQ of 0.5 ng/mL and 50 ng/mL, respectively<sup>20</sup>. The accuracy and precision of both assays were within 15% [19,20].

#### 2.1.2 Anastrozole studies

Anastrozole data was derived from two studies [17,18] using Plot Digitizer (<https://sourceforge.net/projects/plotdigitizer/>, version 2.6.8). The microdose study included six healthy Japanese men (Table S1). Anastrozole was dosed orally at 1.98 µg simultaneously with cetrozole and TDM-322 [17]. Blood samples were taken predose and over a 72-hour period after dosing. Anastrozole plasma concentrations were quantified using a validated LC-MS/MS method with a LLOQ of 0.2 pg/mL [17]. The accuracy and precision of this assay were not reported.

In the clinical dose finding study six postmenopausal women with advanced breast cancer were included in the study (Table S1) [18]. Patients received a single oral dose of 1 mg anastrozole. Blood samples were taken predose and over a 100-hour period after dosing. Anastrozole plasma concentration were quantified with gas chromatography [18]. The performance of the bioanalytical method was not reported. The study designs and results have been described in detail elsewhere [17,18].

## 2.2 Software

Plasma concentrations of gemcitabine, dFdU and anastrozole were analysed using non-linear mixed-effects modelling software NONMEM (version 7.3, ICON Development Solutions, Ellicott City MD). Pirana (version 2.9.2), R (version 3.4.3) and Perl-speaks-NONMEM (PsN, version 5.22.4) were used for the numerical and visual evaluation of the model output.

## 2.3 Model development

### 2.3.1 Gemcitabine and 2',2'-difluorodeoxyuridine model (dFdU)

For the structural model, 1 and 2 compartment models with linear elimination were tested for gemcitabine and dFdU based on previously published models with therapeutic dose data [21-23]. Model development of gemcitabine and dFdU was performed sequentially. The Laplacian estimation method and subroutine ADVAN13 (with TOL equals 9) were used. Full conversion of gemcitabine to dFdU was assumed and described with a first-order conversion rate constant. This assumption was made to account for the missing plasma concentrations of other metabolites so the renal clearance of gemcitabine would be reliably estimated. Residual errors were described by a proportional error model for gemcitabine observations above LLOQ (Equation 1), a combined error model for gemcitabine observations lower than LLOQ but above the limit of detection (LOD) (Equation 2) and a combined error model for dFdU observations (Equation 2).

$$C_{obs,ij} = C_{pred,ij} * (1 + \varepsilon_{prop,ij}) \quad (\text{Equation 1})$$

$$C_{obs,ij} = C_{pred,ij} * (1 + \varepsilon_{prop,ij}) + \varepsilon_{add,ij} \quad (\text{Equation 2})$$

where  $C_{obs,ij}$  is the  $j$ th observed concentration of the  $i$ th subject,  $C_{pred,ij}$  the predicted concentration for the  $j$ th observed concentration of the  $i$ th subject, and  $\varepsilon_{prop,ij}$  the proportional residual error and  $\varepsilon_{add,ij}$  the additive error both assumed to be distributed following  $N(0, \sigma^2)$ .

The additive errors for gemcitabine and dFdU were fixed to half of their respective LLOQ to reduce overparameterisation of the model. Beal's M3 method was used to handle observations below the limit of detection (<LOD) [24]. Bayesian estimation was used to obtain Conditional Weighted Residuals (CWRES).

### 2.3.2 Anastrozole model

For the structural model of anastrozole, 1 and 2 compartment models with linear elimination were evaluated. First order absorption and zero order absorption were tested to describe anastrozole absorption. Residual errors were described by a proportional error model (Equation 1). The first-order conditional estimation method with the interaction option and subroutine ADVAN4 TRANS4 were used.

## 2.4 Model selection and evaluation

Model evaluation was performed throughout model building by consideration of the physiological and scientific plausibility, general Goodness-of-Fit (GOF), individual fit, precision of parameter estimates and change in objective function value (OFV). A decrease in OFV  $\geq 7.879$  ( $P < 0.005$  based on  $\chi^2$  distribution with one degree of freedom) was considered statistically significant for hierarchical models. Sampling Importance Resampling (SIR) was performed on the final models to obtain 95% confidence intervals (CI) of the parameter estimates. Furthermore, the predictability of the model was evaluated with Visual Predictive Checks.

## 2.5 Extrapolation to therapeutic dosing

The final models were used for extrapolation to therapeutic pharmacokinetics with the therapeutic dosing regimens of gemcitabine (1250 mg/m<sup>2</sup>)<sup>and</sup> anastrozole (1 mg) [17]. Plasma concentrations after therapeutic dosing were simulated 1000 times using the final microdose model. The geometric mean was calculated from these simulated concentrations at each time point. The geometric mean concentrations over time were plotted using a two-fold error margin around the geometric mean. A two-fold error was deemed acceptable due to its frequent use in allometry [8,9], and its use in the NCA evaluation of microdose studies. This two-fold error margin represented the acceptable discrepancy between the extrapolated therapeutic pharmacokinetics from a microdose and the expected therapeutic pharmacokinetics. The width of the error margin can be adjusted according to the expected or desired therapeutic window of a new drug entity. Since in this study, therapeutic pharmacokinetics were known, the observed therapeutic plasma concentrations were visually compared to the simulated therapeutic plasma concentrations. The fraction of observed therapeutic plasma concentrations within the two-fold error margin were calculated. Since

extrapolation rather than accurate prediction is the aim of microdose Phase 0 studies, extrapolation to therapeutic dosing was considered adequate if 70% of the observed therapeutic plasma concentrations fell within the two-fold error margin. For anastrozole, the mean plasma concentrations were compared instead of the geometric means since the original publication only reported mean plasma concentrations.

## 3 RESULTS

### 3.1 Gemcitabine and 2,'2-difluorodeoxyuridine (dFdU) model

A total of 99 gemcitabine plasma concentrations from 9 patients and 88 dFdU plasma concentrations from 8 patients were included in the data analysis, of which 7 (7.1%) were less than the LOD. Two patients were excluded from the original dataset. One patient was excluded due to dosing errors, receiving 1 mg instead of 100 µg. Another patient was excluded from the dFdU analysis due to exhibiting highly different dFdU pharmacokinetics. This individual caused CWRES to fall outside the  $\pm 4$  range.

The data were best described by a 2-compartment model for gemcitabine and a 1-compartment model for dFdU with a first-order conversion rate constant from gemcitabine into dFdU and a first order elimination for dFdU. The final model estimates are depicted in Table 1 and GOF plots are depicted in Figure 1 and 2. Overall, the model adequately described the data. CWRES versus time and versus observations are depicted in Figures 1b and 1c for gemcitabine and Figures 2b and 2c for dFdU respectively. CWRES showed a bias towards high concentrations which could not be improved with further model development. The final model adequately predicted the gemcitabine and dFdU concentrations over time (see Supplemental Figure S1 and S2).

### 3.2 Anastrozole model

A total of 66 anastrozole plasma concentrations from 6 patients were included in the data analysis. A 2-compartment model with linear elimination best described the data. The absorption phase could not be captured by first order absorption. Therefore, zero order absorption was modelled as zero order absorption with a duration of 1 hour. Estimation of the duration of the zero-order absorption resulted in instability of the model. The additive error was omitted because it was estimated to be close to zero.

The final model estimates are depicted in Table 2. The GOF plots are depicted in Figure 3. Predictions versus observations were evenly distributed around the line of unity (Figure 3a). CWRES distribution demonstrated a small bias at low and higher concentrations which could not be improved with further model development. However, the final model predicted the data well (Figure S3).

**Table 1.** Final model parameter estimates for the gemcitabine-dFdU population pharmacokinetics model and naïve pooled data approach.

Parameter	Final model estimate	
	NPD	95% CI (SIR)
<b>Fixed effects</b>		
$V_{c,dFdC}$ (L)	32.4	26.3-39.5
$V_{p,dFdC}$ (L)	128	67.7-218
$Q_{dFdC}$ (L/min)	0.294	0.202-0.422
$Cl_{trans}$ (L/min)	2.87	2.42-3.38
$V_{c,dFdU}$ (L)	38.1	33.7-43.3
$Cl_{dFdU}$ (L/min)	0.0307	0.0113-0.0499
<b>Residual variability (<math>\sigma^2</math>)</b>		
$\sigma^2$ proportional <sub>dFdC</sub>	0.569	0.481-0.715
$\sigma^2$ additive <sub>dFdC</sub>	0.00125*	-
$\sigma^2$ proportional <sub>dFdU</sub>	0.461	0.394-0.573
$\sigma^2$ additive <sub>dFdU</sub>	0.25*	-

Abbreviations: 95% CI, 95% confidence interval; BSV, between subject variability;  $Cl_{trans}$ , conversion clearance from gemcitabine to 2',2'-difluorodeoxyuridine; dFdC, gemcitabine; dFdU, 2',2' difluorodeoxyuridine; NPD, Naïve pooled data; SIR, Sampling Importance Resampling; Q, intercompartmental clearance;  $V_c$ , Volume of distribution of the central compartment;  $V_p$ , Volume of distribution of the peripheral compartment.

\*Fixed parameter

**Table 2.** Final model parameter estimates for the anastrozole population pharmacokinetics model and naïve pooled data approach.

Parameter	Final model estimate (RSE%)	
	NPD	95% CI SIR
<b>Fixed effects</b>		
$V_c$ (L)	4.52	0.43-9.62
$V_p$ (L)	79.5	71.6-87.1
Cl (L/h)	1.57	1.44-1.72
Q (L/h)	139	109-177
F	1*	-
D2	1*	-
<b>Residual variability (<math>\sigma^2</math>)</b>		
$\sigma^2$ proportional	0.0428	0.0309-0.0633
$\sigma^2$ additive	0*	-

Abbreviations: 95% CI, 95% confidence interval; BSV, between subject variability; Cl, clearance; D2, duration of dosing in the dosing compartment (= compartment 2); F, bioavailability; NPD, naïve pooled data; SIR, Sampling Importance Resampling; Q, intercompartmental clearance;  $V_c$ , central volume of distribution;  $V_p$ ; peripheral volume of distribution.

\*Fixed parameter.



### 3.3 Extrapolation to therapeutic dosing.

Therapeutic plasma concentrations of gemcitabine, dFdU, and anastrozole were extrapolated with the models described above. The geometric mean of the extrapolated therapeutic plasma concentrations is depicted with the observed therapeutic plasma concentrations in Figure 4.

Therapeutic pharmacokinetics of gemcitabine are depicted in Figure 4a. Visual comparison indicated that the extrapolated therapeutic pharmacokinetics from a microdose underestimated the initial distribution phase and largely overestimated the terminal elimination phase. This is confirmed by the numerical comparison: the fractions of the therapeutic observations within the two-fold error margin of the geometric mean were 75-100% between 9.39 and 50.5 minutes after infusion and 0-50% between 50.5 minutes and 10 h after infusion (see Table S2).

The simulated therapeutic pharmacokinetics of gemcitabine would possibly underestimate a recommended dose for Phase I studies due to overestimation of the terminal elimination phase. However, the range of concentrations were similar between extrapolated and observed pharmacokinetics.

The simulated and observed therapeutic pharmacokinetics of dFdU are depicted in Figure 4b. Comparing the extrapolated concentrations and the observed concentrations visually revealed a major difference in pharmacokinetic profile. Therefore, a microdose of gemcitabine is not predictable of therapeutic dFdU pharmacokinetics and would potentially result in misguided dose recommendations for phase I studies. However, the numerical comparison indicated good predictability with 70-100% of the observed concentrations within two-fold of the geometric mean between 9.39 minutes and 3 hours after infusions (see Table S2). This discrepancy between visual and numerical comparison demonstrates the importance of visual comparison.

The therapeutic data of anastrozole is depicted as a mean with a standard deviation (Figure 4c). Extrapolated therapeutic pharmacokinetics showed a similar pharmacokinetic profile compared to observed therapeutic pharmacokinetics indicating good predictability. This was supported with numerical comparison: All mean observed concentrations were within two-fold of the extrapolated mean concentration. Continuing, the standard deviations of ten out of eleven concentration-time points also fell within two-fold of the extrapolated mean concentration. While the last observation ( $C_{last}$ ) differentiated most from the extrapolated mean concentration, the numerical differences were relatively small

between the extrapolated and observed therapeutic plasma concentrations for  $C_{\text{last}}$  (2.0 vs. 4.1  $\mu\text{g/L}$ , respectively). From Figure 4c it was concluded that extrapolated therapeutic anastrozole concentrations based on microdose pharmacokinetic model would be informative for dose recommendations for phase I clinical trials.

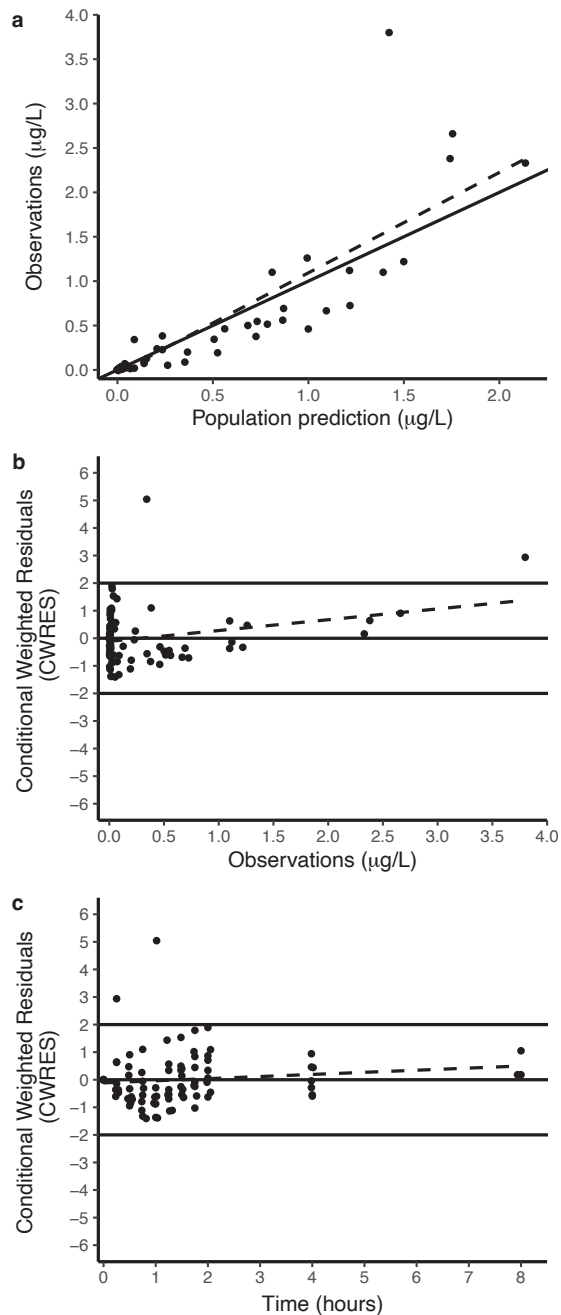


**Figure 1.** Diagnostic plots for the final naïve pooled data modeling approach of gemcitabine. **a**, Observations vs populations predictions. **b,c** Conditional Weighted Residuals (CWRES) vs observations and time after dose, respectively. The black dashed line depicts the trend in the data.

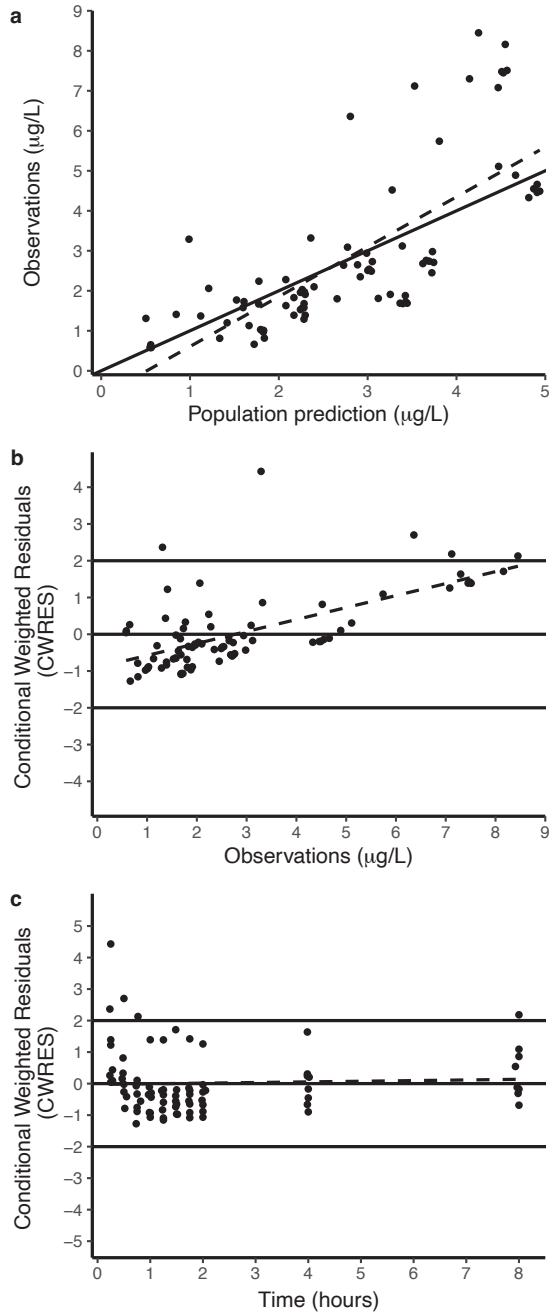


**Figure 2.** Diagnostic plots for the final naïve pooled data modeling approach of 2',2'-difluorodeoxyuridine. **a**, Observations vs populations predictions. **b,c** Conditional Weighted Residuals (CWRES) vs observations and time after dose, respectively. The black dashed line depicts the trend in the data.

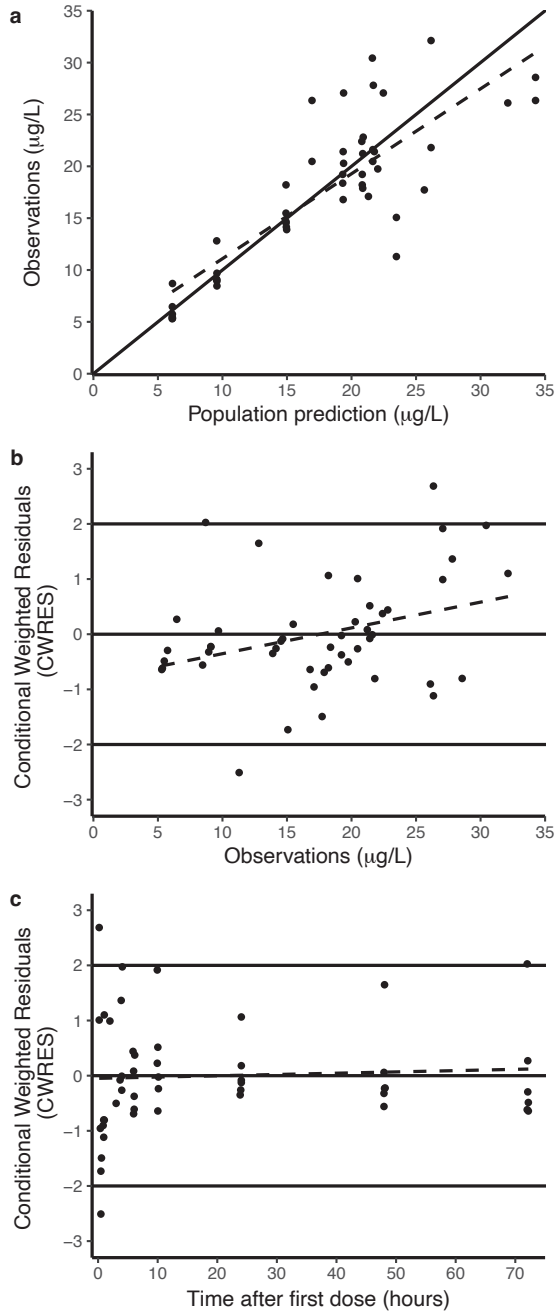


**Figure 3.** Diagnostic plots for the final naïve pooled data modeling approach of anastrozole. a, Observations vs populations predictions. b,c Conditional Weighted Residuals (CWRES) vs observations and time after first dose, respectively. The black dashed line depicts the trend in the data.

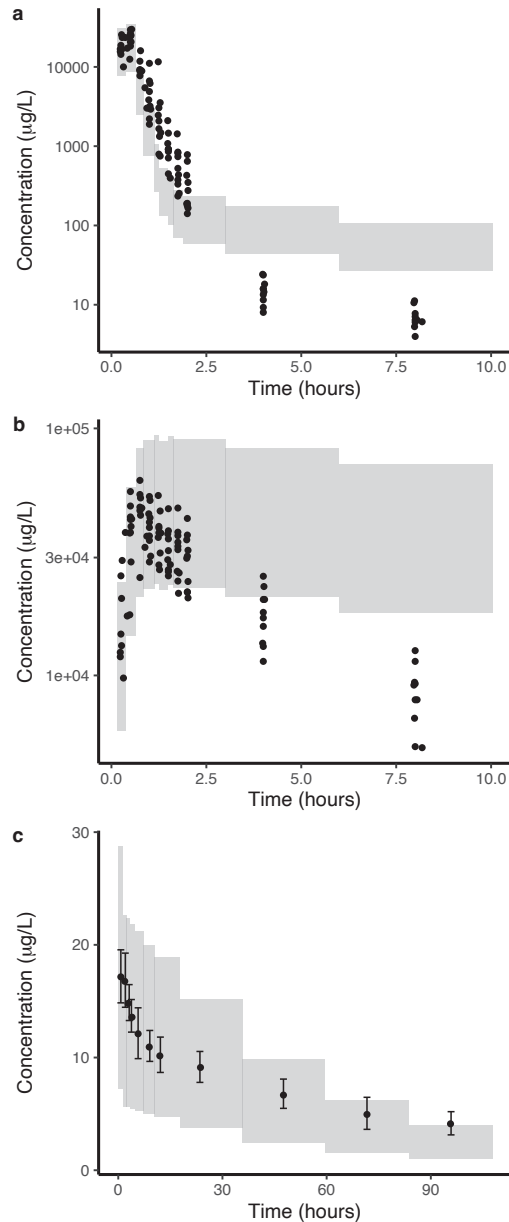


**Figure 4.** The Visual Predictive Checks of the microdose models: a, gemcitabine. b, 2',2'-difluorodeoxyuridine. c, anastrozole. The Visual Predictive Checks were achieved by simulating ( $n = 1000$ ) the therapeutic doses  $1,250 \text{ mg/m}^2$  (IV) for gemcitabine and  $1 \text{ mg}$  for anastrozole (oral), using the final NPD pharmacokinetic models. The gray area is the two-fold range around the geometric mean for gemcitabine and 2',2'-difluorodeoxyuridine and the mean for anastrozole of the extrapolated concentrations. The dots represent the observed therapeutic concentrations.

## 4 DISCUSSION

This study demonstrated the feasibility of using an NPD modelling approach for extrapolation of a microdose to therapeutic dosing. Pharmacokinetic models using the NPD approach were developed for gemcitabine, dFdU and anastrozole based on microdose data. These microdose pharmacokinetic models were used to extrapolate plasma concentrations over time after administration of the therapeutic dose currently used in the clinic. Because therapeutic plasma concentrations were available, the observed therapeutic plasma concentrations were visually compared to the extrapolated therapeutic plasma concentrations. Extrapolation of the microdose models to therapeutic doses demonstrated that the simulated therapeutic plasma concentrations fell within similar ranges to the observed therapeutic plasma concentrations. Although the predictive performance of microdose pharmacokinetics might not be perfect, the similar range of predicted plasma concentrations and observed plasma concentrations demonstrated the suitability of microdose studies to acquire early knowledge about *in vivo* exposure. However, possible discrepancies between the predicted therapeutic pharmacokinetics and the observed therapeutic pharmacokinetics should be taken into account when microdose studies are used to inform therapeutic doses for Phase I clinical trials. Figure 4 depicts differences in the shape of the pharmacokinetic curve for gemcitabine and dFdU between the extrapolated concentrations and observed concentrations. These discrepancies could misinform therapeutic dose recommendations. The possible discrepancies could be taken into account by the error margin, visualising a predefined acceptable error between the extrapolated therapeutic pharmacokinetics and observed therapeutic pharmacokinetics. Based on the extrapolated therapeutic pharmacokinetics and the predefined error margin, therapeutic dose recommendations for Phase I clinical studies can be defined.

The results from the NPD modelling approach were not fully in accordance with the previously published evaluation of gemcitabine, dFdU and anastrozole microdose predictability based on NCA (see Table 3) [11,16]. The gemcitabine Phase 0 microdose reported predictability for the gemcitabine pharmacokinetic metrics  $AUC_{0-8}$ ,  $AUC_{inf}$ , maximum concentration ( $C_{max}$ ) and Cl, whereas elimination rate constant, terminal half-life ( $t_{1/2}$ ) and volume of distribution fell outside the two-fold. In addition, the NPD modelling approach demonstrated a difference in shape of the pharmacokinetics profile between the microdose and therapeutic dose despite having similar AUC-values. This non-linearity has been attributed to the saturation of the nucleoside uptake transporter (hENT1), cytidine

deaminase (CDA) and deoxycytidine kinase (dCK) [16]. CDA is responsible for the rapid and extensive metabolism of gemcitabine to dFdU in plasma, liver, kidneys and other tissues [25] whereas dCK is the rate-limiting enzyme for the phosphorylation of gemcitabine to its nucleotide analogs (see Figure S4) [26]. Saturation of hENT1 is supported by intracellular data [16]. Saturation of cellular uptake and intracellular phosphorylation of gemcitabine might be an explanation of the difference seen in dFdU elimination between microdose and therapeutic dose (Figure 4b). At therapeutic doses, saturation would result in increased availability of gemcitabine for metabolism to dFdU by CDA in the liver and other tissues, whereas at microdose level the in part reversible phosphorylation could result a balance between gemcitabine phosphorylation and dFdU formation [26,27]. For anastrozole, extrapolation of microdose pharmacokinetics described the therapeutic pharmacokinetics well [11]. The dose-normalised AUC of the microdose and therapeutic dose (16.8 and 10.4 ng\*h/mL, respectively) met the two-fold criterion [17,18]. This study showed in addition that the shape of the anastrozole pharmacokinetic curve as well as the individual concentration-time points were adequately predicted by the NPD modelling approach.

The aim of microdose Phase 0 studies is to obtain knowledge of *in vivo* human pharmacokinetics prior to Phase I clinical trials. Information obtained from these microdose Phase 0 studies could be used for decision making during further drug development. The NPD modelling approach presented here has several advantages compared to NCA. First, the NPD modelling approach allows the possibility to apply and to evaluate more complex and physiologically relevant models (e.g., multiple compartment models) and thereby improving the extrapolation to therapeutic pharmacokinetics compared to NCA. Secondly, the visual evaluation allows the simultaneous assessment of the extrapolation of individual concentration-time points and the shape of the pharmacokinetic curve (comparison between (geometric) mean of the therapeutic concentrations and the extrapolated therapeutic concentrations). Visual comparison is important since two different pharmacokinetic profiles can lead to an equivalent AUC but nevertheless result in differences in target attainment. Furthermore, a numerical comparison can be made by calculating the fraction of therapeutic observations within the prior determined error margin (e.g., two-fold error margin) which can be dependent on the therapeutic window of the drug. Additionally, numerical evaluation of the NPD modelling approach is also possible by performing a numerical predictive check. Lastly, NCA assumes mono-exponential linear elimination for the extrapolation of the AUC to infinity and subsequent calculation of clearance [16]. This assumption holds for drugs with biphasic elimination



(such as gemcitabine or anastrozole) when there are enough observations in the terminal elimination phase. However, it might be a limitation during early drug development when *in vivo* human pharmacokinetics is unknown, and the terminal elimination phase has not been captured. A direct comparison of the NCA-method and the NPD modelling approach is shown in Table 3.

**Table 3.** Direct comparison between the non-compartmental analysis method and the naïve pooled data modelling approach.

	Method		
	NCA	NPD	
Criterion	PK metrics ± two-fold <sup>#</sup>	≥70% of observations within two-fold error margin <sup>§</sup>	Similar trend in PK
<b>Compound</b>			
Gemcitabine	Yes <sup>16,‡</sup>	No	No
dFdU	Yes <sup>16</sup>	Yes	No
Anastrozole	Yes <sup>11</sup>	Yes	Yes
<b>Characteristics</b>			
Simplicity	Good	Moderate	
Evaluation of physiologically relevant models	Not possible	Possible	
Visual evaluation	Possible	Possible	
Numerical comparison	Not possible	Possible	
Assumes mono-exponential linear elimination	Yes	No	
Application for clinical trial simulation	Not possible	Possible	

Abbreviations: dFdU, 2',2'-difluorodeoxyuridine; NCA, Non-compartmental analysis; NPD, Naïve Pooled Data; PK, pharmacokinetics.

<sup>#</sup> The extrapolation of the microdose to therapeutic pharmacokinetics was considered good when the dose-normalised pharmacokinetic metrics of the microdose and therapeutic dose fell within two-fold of each other.

<sup>§</sup> The extrapolation to the microdose to therapeutic dosing was considered adequate if 70% of the observed therapeutic plasma concentrations fell within the two-fold error margin.

<sup>‡</sup> Area-Under-the-Concentration-Time Curve (AUC) from zero to 8 hours, AUC extrapolated to infinity, maximum concentration, and clearance met the two-fold criterion while elimination rate constant, half-life, and volume of distribution did not [16]

The major advantage of the NPD modelling approach compared to NCA is its ability to extrapolate different therapeutic doses. The different therapeutic doses could be compared in their exposure but also in attainment of a desired target (e.g., time above or below a desired threshold concentration). Visualisations of

the extrapolated pharmacokinetics of different therapeutic doses with a relevant error margin (e.g., a two-fold error margin as used here) could be used in decision making to define the start dose of a future Phase I clinical trial. Furthermore, Figure 4 depicts a similar range between the extrapolated concentrations and the observed concentrations. While the exact pharmacokinetic profile is not always captured by the extrapolation, the extrapolations based on microdose pharmacokinetics were indicative for the anticipated range of exposure. Therefore, microdose Phase 0 trials have the potential to reduce the number of dose levels in Phase I clinical trials.

In addition to the here presented NPD modelling approach, a full population pharmacokinetic model could also be used to evaluate microdose predictability. An NPD modelling approach might be more appropriate for microdose studies for two reasons. First, the aim of Phase 0 microdose studies is a quick assessment of the human pharmacokinetics of a new drug entity [5]. Estimation of between subject variability and/or explanation of variability in pharmacokinetics might be more relevant in later stages of drug development, when larger and more heterogeneous populations are being exposed to the drug. Second, microdose Phase 0 studies typically consist of a very small study population (mostly <10 subjects) [28]. Due to the small sample size, the final datasets of these microdose Phase 0 studies are modest in size increasing the risk of overparameterization. Furthermore, estimated between-subject variability in these studies might not be an accurate representation of true between-subject variability in a larger patient population. Therefore, it could result in unreliable extrapolation towards therapeutic dosing. A possible next step could be the combination of PBPK modelling and microdosing [28]. Preclinical data (e.g., *in vitro* enzyme/transporter kinetics studies) could be used to develop a PBPK model for the new drug entity, while *in vivo* human pharmacokinetic data from a microdose study could be used to optimise the model. This method could potentially improve the microdose predictability for drugs with complex pharmacokinetics like gemcitabine and metabolites. However, drugs with pharmacokinetic behaviour less dependent on complex enzyme or transporters systems (e.g., anastrozole) may be well extrapolated with the NPD modelling approach.

## 5 CONCLUSION

This study demonstrated the use and feasibility of an NPD modelling approach for the evaluation and application of microdose studies in early drug development. The method was shown to adequately describe microdose pharmacokinetics and the extrapolation to therapeutic dosing was informative for the therapeutic exposure. Furthermore, the method allows visual comparison between extrapolated microdose pharmacokinetics and therapeutic pharmacokinetics. This method can further be adjusted to the specific characteristics and requirements of a new drug entity.

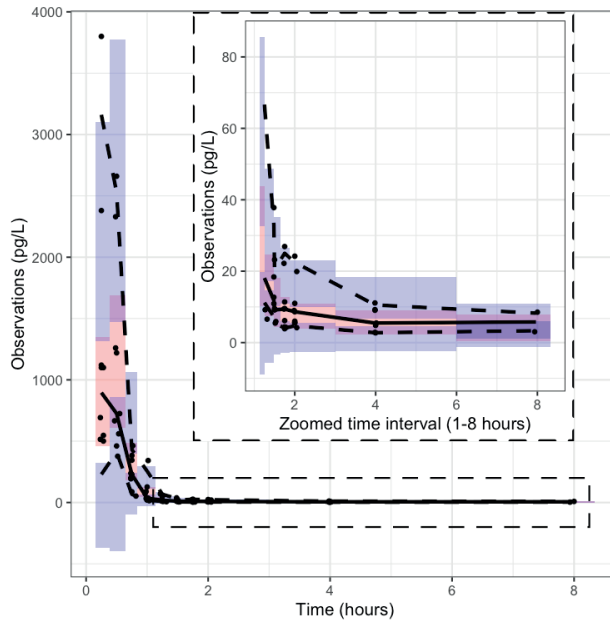
## REFERENCES

1. Lappin G, Garner RC (2003) Big physics, small doses: the use of AMS and PET in human microdosing of development drugs. *Nat Rev Drug Discov* 2 (3):233-240. doi:10.1038/nrd1037
2. European Medicines Agency (EMA) (2004) Position paper on non-clinical safety studies to support clinical trials with a single microdose. <https://iaa-ams.co.jp/wp-content/uploads/2020/10/MD1.pdf> Accessed April 2020
3. US Food and Drug Administration (FDA) (2006) Guidance for the industry, investigators and reviewers: exploratory IND studies. *Biotechnol Law Rep* 25:167-174
4. European Medicines Agency (EMA) (2009) ICH M3 (R2): Note for guidance on non-clinical safety studies for the conduct of human clinical trials and marketing authorization for pharmaceuticals. <https://www.ema.europa.eu/en/ich-m3-r2-non-clinical-safety-studies-conduct-human-clinical-trials-pharmaceuticals-scientific> Accessed April 2020
5. Garner RC, Lappin G (2006) The phase 0 microdosing concept. *Br J Clin Pharmacol* 61 (4):367-370. doi:10.1111/j.1365-2125.2006.02575.x
6. Heuveling DA, de Bree R, Vugts DJ, Huisman MC, Giovannoni L, Hoekstra OS, Leemans CR, Neri D, van Dongen GA (2013) Phase 0 microdosing PET study using the human mini antibody F16SIP in head and neck cancer patients. *J Nucl Med* 54 (3):397-401. doi:10.2967/jnumed.112.111310
7. Marchetti S, Schellens JH (2007) The impact of FDA and EMEA guidelines on drug development in relation to Phase 0 trials. *Br J Cancer* 97 (5):577-581. doi:10.1038/sj.bjc.6603925
8. Lappin G, Garner RC (2008) The utility of microdosing over the past 5 years. *Expert Opin Drug Metab Toxicol* 4 (12):1499-1506. doi:10.1517/17425250802531767
9. Rowland M (2007) Commentary on ACCP position statement on the use of microdosing in the drug development process. *J Clin Pharmacol* 47 (12):1595-1596; author reply 1597-1598. doi:10.1177/0091270007310548
10. Lappin G, Noveck R, Burt T (2013) Microdosing and drug development: past, present and future. *Expert Opin Drug Metab Toxicol* 9 (7):817-834. doi:10.1517/17425255.2013.786042
11. van Nuland M, Rosing H, Huitema ADR, Beijnen JH (2019) Predictive Value of Microdose Pharmacokinetics. *Clin Pharmacokinet* 58 (10):1221-1236. doi:10.1007/s40262-019-00769-x
12. Nair A, Morsy MA, Jacob S (2018) Dose translation between laboratory animals and human in preclinical and clinical phases of drug development. *Drug Dev Res*. doi:10.1002/ddr.21461
13. Jones RD, Jones HM, Rowland M, Gibson CR, Yates JW, Chien JY, Ring BJ, Adkison KK, Ku MS, He H, Vuppugalla R, Marathe P, Fischer V, Dutta S, Sinha VK, Bjornsson T, Lave T, Poulin P (2011) PhRMA CPCDC initiative on predictive models of human pharmacokinetics, part 2: comparative assessment of prediction methods of human volume of distribution. *J Pharm Sci* 100 (10):4074-4089. doi:10.1002/jps.22553

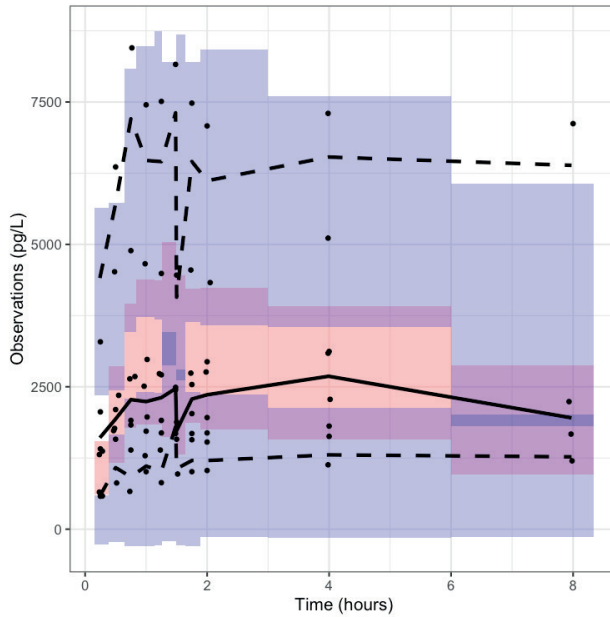
14. Ring BJ, Chien JY, Adkison KK, Jones HM, Rowland M, Jones RD, Yates JW, Ku MS, Gibson CR, He H, Vuppugalla R, Marathe P, Fischer V, Dutta S, Sinha VK, Bjornsson T, Lave T, Poulin P (2011) PhRMA CPCDC initiative on predictive models of human pharmacokinetics, part 3: comparative assessment of prediction methods of human clearance. *J Pharm Sci* 100 (10):4090-4110. doi:10.1002/jps.22552
15. Vuppugalla R, Marathe P, He H, Jones RD, Yates JW, Jones HM, Gibson CR, Chien JY, Ring BJ, Adkison KK, Ku MS, Fischer V, Dutta S, Sinha VK, Bjornsson T, Lave T, Poulin P (2011) PhRMA CPCDC initiative on predictive models of human pharmacokinetics, part 4: prediction of plasma concentration-time profiles in human from in vivo preclinical data by using the Wajima approach. *J Pharm Sci* 100 (10):4111-4126. doi:10.1002/jps.22551
16. Van Nuland M, Rosing H, Thijssen B, Burgers JA, Huitema ADR, Marchetti S, Schellens JHM, Beijnen JH (2020) Pilot Study to Predict Pharmacokinetics of a Therapeutic Gemcitabine Dose From a Microdose. *Clin Pharmacol Drug Dev*. doi:10.1002/cpdd.774
17. Kusuhara H, Takashima T, Fujii H, Takashima T, Tanaka M, Ishii A, Tazawa S, Takahashi K, Takahashi K, Tokai H, Yano T, Kataoka M, Inano A, Yoshida S, Hosoya T, Sugiyama Y, Yamashita S, Hojo T, Watanabe Y (2017) Comparison of pharmacokinetics of newly discovered aromatase inhibitors by a cassette microdosing approach in healthy Japanese subjects. *Drug Metab Pharmacokinet* 32 (6):293-300. doi:10.1016/j.dmpk.2017.09.003
18. Nomura Y, Koyama H, Ohashi Y, Watanabe H (2000) Clinical Dosage Determination of a New Aromatase Inhibitor, Anastrozole, in Postmenopausal Japanese Women with Advanced Breast Cancer. *Clinical Drug Investigation* 20 (5):357-369. doi:10.2165/00044011-200020050-00007
19. van Nuland M, Hillebrand MJX, Rosing H, Burgers JA, Schellens JHM, Beijnen JH (2018) Ultra-sensitive LC-MS/MS method for the quantification of gemcitabine and its metabolite 2',2'-difluorodeoxyuridine in human plasma for a microdose clinical trial. *J Pharm Biomed Anal* 151:25-31. doi:10.1016/j.jpba.2017.12.048
20. Vainchtein LD, Rosing H, Thijssen B, Schellens JH, Beijnen JH (2007) Validated assay for the simultaneous determination of the anti-cancer agent gemcitabine and its metabolite 2',2'-difluorodeoxyuridine in human plasma by high-performance liquid chromatography with tandem mass spectrometry. *Rapid Commun Mass Spectrom* 21 (14):2312-2322. doi:10.1002/rcm.3096
21. Khatri A, Williams BW, Fisher J, Brundage RC, Gurvich VJ, Lis LG, Skubitz KM, Dudek AZ, Greeno EW, Kratzke RA, Lamba JK, Kirstein MN (2014) SLC28A3 genotype and gemcitabine rate of infusion affect dFdCTP metabolite disposition in patients with solid tumours. *Br J Cancer* 110 (2):304-312. doi:10.1038/bjc.2013.738
22. Joerger M, Burgers JA, Baas P, Doodeman VD, Smits PH, Jansen RS, Vainchtein LD, Rosing H, Huitema AD, Beijnen JH, Schellens JH (2012) Gene polymorphisms, pharmacokinetics, and hematological toxicity in advanced non-small-cell lung cancer patients receiving cisplatin/gemcitabine. *Cancer Chemother Pharmacol* 69 (1):25-33. doi:10.1007/s00280-011-1670-4
23. Jiang X, Galettis P, Links M, Mitchell PL, McLachlan AJ (2008) Population pharmacokinetics of gemcitabine and its metabolite in patients with cancer: effect of oxaliplatin and infusion rate. *Br J Clin Pharmacol* 65 (3):326-333. doi:10.1111/j.1365-2125.2007.03040.x

24. Beal SL (2001) Ways to fit a PK model with some data below the quantification limit. *J Pharmacokinet Pharmacodyn* 28 (5):481-504. doi:10.1023/a:1012299115260
25. Ciccolini J, Serdjabi C, Peters GJ, Giovannetti E (2016) Pharmacokinetics and pharmacogenetics of Gemcitabine as a mainstay in adult and pediatric oncology: an EORTC-PAMM perspective. *Cancer Chemother Pharmacol* 78 (1):1-12. doi:10.1007/s00280-016-3003-0
26. Mini E, Nobili S, Caciagli B, Landini I, Mazzei T (2006) Cellular pharmacology of gemcitabine. *Ann Oncol* 17 Suppl 5:v7-12. doi:10.1093/annonc/mdj941
27. Rowland M (2012) Microdosing: a critical assessment of human data. *J Pharm Sci* 101 (11):4067-4074. doi:10.1002/jps.23290
28. Burt T, Yoshida K, Lappin G, Vuong L, John C, de Wildt SN, Sugiyama Y, Rowland M (2016) Microdosing and Other Phase 0 Clinical Trials: Facilitating Translation in Drug Development. *Clin Transl Sci* 9 (2):74-88. doi:10.1111/cts.12390

## SUPPLEMENTARY MATERIAL

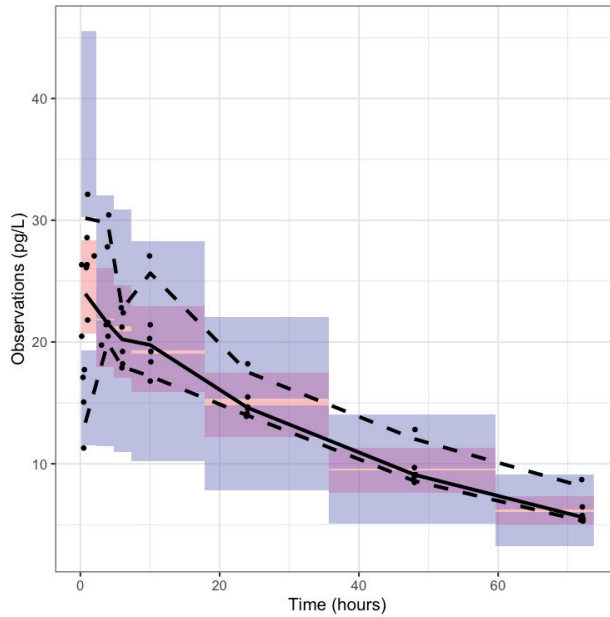


**Supplementary Figure S1.** Visual predictive check of the gemcitabine microdose model. Due to the large range in plasma concentrations a zoomed time interval of 1-8 hours after dosing has been added to the figure. Black dots are the observations, black line is the median of the observations, black dashed lines are the 2.5th and 97.5th percentiles of the observed data, blue shaded areas are the 95th confidence intervals for the 2.5th percentile and the 97.5th percentile of the simulated data, pink shaded area is the 95th confidence interval for the median of the simulated data.

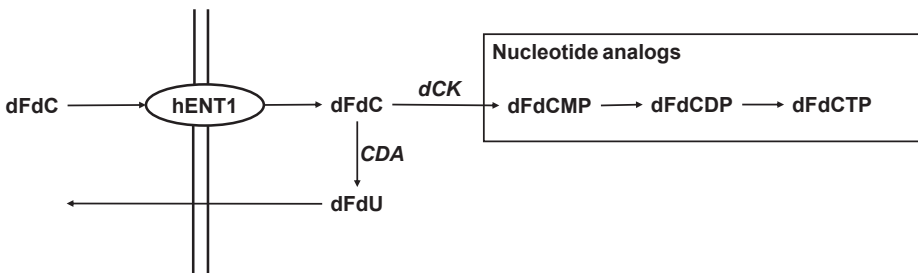


**Supplementary Figure S2.** Visual predictive check of the 2',2'-difluorodeoxyuridine microdose model. Black dots are the observations, black line is the median of the observations, black dashed lines are the 2.5th and 97.5th percentiles of the observed data, blue shaded areas are the 95th confidence intervals for the 2.5th percentile and the 97.5th percentile of the simulated data, pink shaded area is the 95th confidence interval for the median of the simulated data.





**Supplementary Figure S3.** Visual predictive check of the anastrozole microdose model. Black dots are the observations, black line is the median of the observations, black dashed lines are the 2.5th and 97.5th percentiles of the observed data, blue shaded areas are the 95th confidence intervals for the 2.5th percentile and the 97.5th percentile of the simulated data, pink shaded area is the 95th confidence interval for the median of the simulated data.



**Supplementary Figure S4.** Simplified schematic overview of the uptake and metabolism of gemcitabine. Gemcitabine (dFdC) is transported over the cell membrane by the nucleoside transporter (hENT1). Intracellularly dFdC is phosphorylated by deoxycytidine (dCK) into the monophosphate metabolite (dFdCMP) which can be further converted into the active diphosphate (dFdCDP) and triphosphate metabolites (dFdCTP). These phosphate metabolites are the nucleotide analogs. dFdC is metabolised by cytidine deaminase (CDA) to 2, '2-difluorodeoxyuridine (dFdU) [26,26].

**Supplementary Table S1.** Subject demographic characteristics [16-18].

<b>Subject characteristics</b>	<b>Gemcitabine microdose Phase 0</b>	<b>Anastrozole microdose</b>	<b>Anastrozole clinical dose finding</b>
Total number of patients	9	6	6
Gender			
Male	5	6	-
Female	4	-	6
Age, median (range) or $\pm$ SD, years	66 (48-73)	30.2 $\pm$ 8.3	64.2 $\pm$ 6.7
Subject type	Patients with solid tumours	Healthy volunteers	Advanced breast cancer patients

Abbreviation: SD = standard deviation.

**Supplementary Table S2.** Fraction of the observed therapeutic plasma concentrations within two-fold of the extrapolated geometric mean over time.

<b>Time bin (minutes)</b>	<b>Fraction within two-fold of the geometric mean (%)</b>	
	<b>Gemcitabine</b>	<b>dFdU</b>
9.39-23.5	100.0	100.0
23.5-38.5	100.0	100.0
38.5-50.5	75.0	100.0
50.5-68	25.0	100.0
68-75.5	16.7	100.0
75.5-89.5	0.00	100.0
89.5-98.5	12.5	100.0
98.5-113	50.0	70.0
180-360	0.0	20.0
360-602	0.0	0.0
<b>Mean</b>	38.0	75.0

Abbreviation: dFdU = 2',2' difluorodeox





# Chapter 2

**An ultra-sensitive liquid chromatography tandem mass spectrometry method for the simultaneous quantification of  $^2\text{H}_6$ -alectinib and alectinib in human plasma for the support of a microtracer food-effect trial**

*Manuscript in preparation*

Lisa T. van der Heijden

Maida I. Mohmaed Ali

Leon Aardenburg

Jos H. Beijnen

Alwin D.R. Huitema

Hilde Rosing

Matthijs Tibben

## ABSTRACT

A liquid chromatography tandem mass spectrometry (LC-MS/MS) method for the quantification of  $^2\text{H}_6$ -alectinib and alectinib was developed and validated for the support of a pilot microtracer food-effect trial. The aim of the bioanalytical method was the simultaneous quantification of low  $^2\text{H}_6$ -alectinib concentrations and high alectinib concentrations that are present in study samples, using a single sample pretreatment and analysis method. Sample preparation consisted of liquid-liquid extraction with tert-butyl methyl ether (TBME). The final extract was injected on a C18 column (1.7  $\mu\text{m}$  particles, 50 x 2.1 mm ID) with gradient elution. A triple quadrupole mass spectrometer operating in positive method was used for detection and quantification. The validated concentration ranges were from 5 to 400 pg/mL for  $^2\text{H}_6$ -alectinib and from 25 to 2,000 ng/mL for alectinib. The bias was within  $\pm 3.5\%$  and  $\pm 5.1\%$  and precisions  $\leq 5.7\%$  and  $\leq 1.9\%$  for  $^2\text{H}_6$ -alectinib and alectinib, respectively. By correcting for the interference of natural abundant isotopes of alectinib,  $^2\text{H}_6$ -alectinib plasma concentrations between 1 and 5 pg/mL could be quantified, with bias was within  $\pm 15.9\%$  and precision  $\leq 12.5\%$  in the presence of 400 ng/mL or 800 ng/mL alectinib. The method will be used to quantify  $^2\text{H}_6$ -alectinib and alectinib plasma concentrations in patients participating in a pilot microtracer food-effect study.

## 1 INTRODUCTION

Food-effect studies are an important part of clinical drug development for orally dosed drugs [1]. The aim of these studies is to determine the influence of co-administration of food on the pharmacokinetics of the investigational drug. The traditional study design is a randomized, balanced, two-treatment (fed vs. fasting), two-sequence cross-over design with a single dose administration in healthy volunteers [1, 2]. For potentially toxic compounds (e.g., anticancer drugs [1-3]), the traditional study design could give rise to safety concerns. In these situations, a study in patients could be considered [1-3]. However, the traditional study design has its disadvantages for toxic drugs with relative long half-lives. Due to the long wash-out period (five-times the half-life) after the single dose administrations under both fed and fasted conditions, start of treatment is delayed for several days to weeks until after the food-effect study, which can be undesirable. An alternative would be to study the food-effect under steady-state pharmacokinetics. This design would substantially increase the patient burden of the study since patients need to adhere to the food-intervention until steady-state of the investigational drug is reached (five-times the half-life).

There is a need to reduce the patient burden of food-effect studies for toxic drugs with long half-lives, and thereby increase the feasibility of these studies. Microtracers (a stable isotopically labelled drug) could be used to determine the food-effect under steady-state pharmacokinetics of the desired drug. Microtracers are dosed at microgram level (max. 100  $\mu\text{g}$ ) and have been used for the determination of absolute bioavailability [4]. Co-administration of a microtracer with the therapeutic dose would allow the determination of the food-effect on the pharmacokinetics of the microtracer while the treatment of the patient is not interrupted.

A pilot study to demonstrate the feasibility of microtracer food-effect studies was designed with  $^2\text{H}_6$ -alectinib as the microtracer and alectinib as the therapeutic drug. Alectinib is a tyrosine kinase inhibitor (TKI) targeting anaplastic lymphoma kinase (ALK) and is registered for the treatment of non-small cell lung cancer (NSCLC) [5]. The half-life of alectinib is approximately 32 hours [6]. To support the pilot microtracer food-effect study, an ultra-sensitive bioanalytical method of  $^2\text{H}_6$ -alectinib and alectinib in human plasma was developed. While previously accelerated mass spectrometry (AMS) was necessary to measure drug concentration within the  $\text{pg/mL}$  range, recent advances within the bioanalytical field made it possible to quantify increasingly lower drug concentrations with

liquid-chromatography tandem mass spectrometry (LC-MS/MS) [7]. Compared to AMS, LC-MS/MS methods are independent of radioactive labelled compounds. Therefore, LC-MS/MS was chosen for the current bioanalytical method. Previously published methods for the quantification of alectinib were designed for therapeutic drug monitoring (TDM) [8-11]. Our TDM method [10] has a lower limit of quantitation (LLOQ) of 10 ng/mL and we had to increase the sensitivity with a factor of at least 2000 (target LLOQ of 1 to 5 pg/mL) to enable analysis of the patient samples with plasma microtracer. In addition, the method should be able to quantify these low levels of  $^2\text{H}_6$ -alectinib in the presence of high levels of alectinib ( $\geq 400$  ng/mL), a concentration ratio of  $\geq 1:80000$ . Here we describe the development and validation of this ultra-sensitive LC-MS/MS method.



## 2 METHODS

### 2.1 Chemicals

$^2\text{H}_6$ -alectinib was obtained from Clearsynth (Mumbai, India). Alectinib and  $^2\text{H}_8$ -alectinib (internal standard) were purchased from Alsachim (Graffenstaden, France). Acetonitrile, methanol, formic acid, tert-butyl methyl ether (TBME), isopropyl alcohol (IPA), and water (all ULC-MS grade) were acquired from Biosolve (Valkenswaard, the Netherlands). Dimethyl sulfoxide (DMSO) was purchased from Merck (Darmstadt, Germany). Potassium ethylenediaminetetraacetic acid ( $\text{K}_2\text{EDTA}$ ) human plasma from healthy volunteers was supplied by Bioreclamation Inc. (Westbury, New York, USA).

### 2.2 Stocks and working solutions

Stock solutions for both  $^2\text{H}_6$ -alectinib and alectinib were prepared at a concentration of 0.5 mg/mL in DMSO. Stock solutions were diluted with methanol to obtain the concentration range of the working solutions of the calibration standards (250-20,000 pg/mL for  $^2\text{H}_6$ -alectinib and 1250-100,000 ng/mL for alectinib). Working solutions for the quality control (QC) samples were prepared in methanol at concentration level 250, 750, 2500, and 15,000 pg/mL for  $^2\text{H}_6$ -alectinib and 1250, 3750, 15,000, and 75,000 ng/mL for alectinib. All working solutions were stored at  $-20\text{ }^\circ\text{C}$ .

### 2.3 Internal standard

Stock solution of  $^2\text{H}_8$ -alectinib was prepared at a concentration of 1 mg/mL in DMSO. The stock solution was diluted up to a concentration of 5 ng/mL with methanol.

### 2.4 Calibration standards and quality control samples

The working solutions for both analytes were diluted 50-times with  $\text{K}_2\text{EDTA}$  plasma to obtain calibration standards over a concentration range of 5-400 pg/mL for  $^2\text{H}_6$ -alectinib and 25-2,000 ng/mL for alectinib, respectively. The QC samples were obtained by diluting the working solutions 50-times with  $\text{K}_2\text{EDTA}$  human plasma. The concentration levels were 5 pg/mL (lower limit of quantification; LLOQ), 15 pg/mL (Low), 50 pg/mL (Mid), and 300 pg/mL (High) for  $^2\text{H}_6$ -alectinib and 25 ng/mL (LLOQ), 75 ng/mL (Low), 300 ng/mL (Mid), and 1500 ng/mL (High) for alectinib. All calibration standards and QC samples were stored at  $-20\text{ }^\circ\text{C}$ .

## 2.5 Sample preparation

Plasma aliquots of 200  $\mu\text{L}$  were spiked with 20  $\mu\text{L}$  internal standard except the double blank sample. Liquid-liquid extraction was performed by adding 1 mL TBME to each sample. All samples were mixed in an automatic shaker for 5 minutes at 1250 rpm prior to centrifuging (14,000 rpm for 5 minutes). All samples were snap frozen in an ethanol/dry ice bath prior to evaporation under a gentle stream of nitrogen (40  $^{\circ}\text{C}$ ). The samples were reconstituted with 100  $\mu\text{L}$  formic acid-acetonitrile-methanol-water (0.1:25:25:50, v/v/v/v). After reconstitution, the samples were mixed in an automatic shaker for 5 minutes at 1250 rpm prior to centrifuging (14,000 rpm for 5 minutes). Lastly, 65  $\mu\text{L}$  for the supernatant was transferred to vials with inserts for analysis.

## 2.6 Liquid chromatography equipment and conditions

An UPLC pump 1290 Infinity II (Agilent, Santa Clara, CA, USA) was used in combination with a UPLC autosampler 1290 Infinity II (Agilent, Santa Clara, CA, USA) and a column oven 1290 Infinity II (Agilent, Santa Clara, USA). Purge and wash solvent consisted of water-IPA (90:10, v/v). The injection volume was 5  $\mu\text{L}$ . Gradient elution with an Acquity BEH C18 column (1.7  $\mu\text{m}$ , 2.1 X 50 mm) was used for separation. Eluent A was 0.1% formic acid in water (v/v) and eluent B formic acid-acetonitrile-methanol (0.1:50:50, v/v/v). The gradient started at 45% B (0.00-2.00 min) and increased to 100% B (2.00-2.01 min), remained constant at 100% B (2.01-2.50 min), decreased to 45% B (2.50-2.51 min) and equilibrated at 45% B (2.51-3.00 min).

## 2.7 Mass spectrometry equipment and conditions

A Triple Quad 6500<sup>+</sup> mass spectrometer (Sciex, Frammingham, USA) was used for quantification. The system was operating in the positive mode and multiple reaction monitoring (MRM) was used for quantification. The mass transitions of  $m/z$  485.3  $\rightarrow$  396.2 for alectinib [M+2],  $m/z$  489.3  $\rightarrow$  402.3 for  $^2\text{H}_6$ -alectinib, and  $m/z$  491.3  $\rightarrow$  396.3 for  $^2\text{H}_8$ -alectinib were used for quantification. The proposed fragmentation pattern is visualized in Figure 1. MS operating parameters are depicted in Table 1. Data acquisition and processing were executed with Analyst<sup>TM</sup> software (Sciex, version 1.7.2.).

## 2.8 Validation procedures

### 2.8.1 Calibration model and lower limit of quantification

Eight non-zero calibration standards were measured in three separate runs. The concentration range of the calibration standards were from 5 to 400  $\text{pg}/\text{mL}$  for  $^2\text{H}_6$ -alectinib and 25-2,000  $\text{ng}/\text{mL}$  for alectinib. Linear regression was

applied to the area peak ratio of the analytes and the internal standard versus the nominal concentration ( $x$ ) with a weighting factor of  $1/x^2$ . For  $^2\text{H}_6$ -alectinib, two additional calibration levels of 1 and 2 pg/mL were included (<LLOQ1 and <LLOQ2, respectively) in the linear regression to enable quantification of concentrations below 5 pg/mL. The measured concentration of at least 75% of the non-zero calibration standard had to be  $\pm 15\%$  ( $\pm 20\%$  for LLOQ) of the nominal concentration [12, 13]. The LLOQ had to have a signal-to-noise ratio of  $\geq 5:1$  [12, 13].

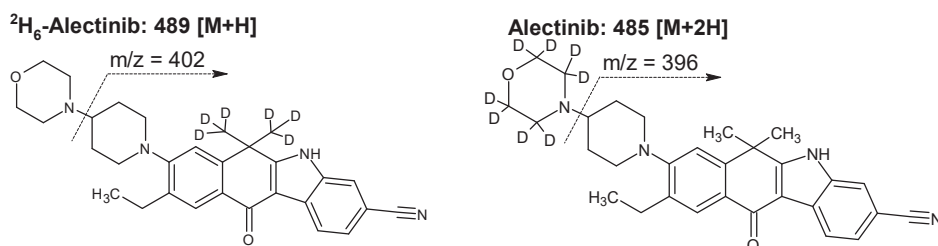


**Figure 1.** Chemical structures of  $^2\text{H}_6$ -alectinib (A) and alectinib (B) including the proposed fragmentation. The position of the deuterium labelling is indicated with the letter D.

**Table 1.** Above: general mass spectrometric parameters. Below: Analyte specific mass spectrometric parameters for alectinib,  $^2\text{H}_6$ -alectinib and  $^2\text{H}_8$ -alectinib.

Mass-spectrometer			
Run duration	3 min		
Ionspray voltage	5500 V		
Nebuliser gas	40 au		
Polarity	Positive		
Turbo gas/heater gas	50 au		
Curtain gas	30 au		
Collision gas	9 au		
Temperature	550 °C		
	Alectinib [M+2]	$^2\text{H}_6$ -alectinib	$^2\text{H}_8$ -alectinib
MRM (m/z)	485.3 $\rightarrow$ 396.2	489.3 $\rightarrow$ 402.3	491.3 $\rightarrow$ 396.3
Collision energy (V)	35	37	35
Collision exit potential (V)	24	24	24
Declustering potential (V)	61	86	61
Entrance potential (V)	10	10	10
Dwell time (msec)	50	50	50

### 2.8.2 Accuracy and precision

Five replicates of the QC samples at LLOQ, Low, Mid, and High concentrations levels for both analytes were prepared for three separate runs. The concentration levels for  $^2\text{H}_6$ -alectinib were 5 pg/mL (LLOQ), 15 pg/mL (Low), 50 pg/mL (Mid), and 300 pg/mL (High) while the concentration levels for alectinib were 25 ng/mL (LLOQ), 75 ng/mL (Low), 300 ng/mL (Mid), and 1,500 ng/mL (High). Calibration standards prepared and analysed in the same analytical run were used for the calculation of the concentrations of the QC samples. Accuracy was defined as the bias of the measured concentration from the nominal concentration. Precision was defined as the coefficient of variation (CV%) of the measured concentrations. Inter-assay bias was specified as the bias of the mean measured concentrations per analytical run compared to the nominal concentration, while inter-assay precision was calculated with one-way ANOVA. The acceptance criteria were  $\pm 15\%$  for accuracy ( $\pm 20\%$  for LLOQ) and  $\leq 15\%$  for precision ( $\leq 20\%$  for LLOQ) [12, 13].

### 2.8.3 Carry-over

Carry-over was determined by injecting two double blank samples directly after the upper limited of quantification (ULOQ). The ULOQ was 400 pg/mL and 2,000 ng/mL for  $^2\text{H}_6$ -alectinib and alectinib, respectively. The peak area at the retention time of both analytes and the internal standard in the double blank was compared to the mean area of the analyte and internal standard in five replicates of LLOQ samples. The peak area in the double should be  $\leq 20\%$  for the analytes and  $\leq 5\%$  for the internal standard [12, 13].

### 2.8.4 Specificity and selectivity

Endogenous interference was investigated in six batches of control  $\text{K}_2\text{EDTA}$  plasma double blank samples (without internal standard) that were spiked at LLOQ and  $<\text{LLOQ}1$  concentration level. The LLOQ was 5 pg/mL for  $^2\text{H}_6$ -alectinib, 25 ng/mL for alectinib and  $<\text{LLOQ}1$  was 1 pg/mL for  $^2\text{H}_6$ -alectinib. Co-eluting peaks at the retention time of the analyte and the internal standard from endogenous interference were evaluated in the double blank samples and compared to the peaks in the LLOQ and  $<\text{LLOQ}1$  samples. Peak present at the retention time of the analytes should be  $\leq 20\%$  and  $\leq 5\%$  for the internal standard [12, 13].

Cross analyte/internal standard interference was determined by spiking the analytes and the internal standard separately to control  $\text{K}_2\text{EDTA}$  human plasma. Analytes were spiked at ULOQ level (400 pg/mL for  $^2\text{H}_6$ -alectinib and 2,000 ng/mL

for alectinib) while the internal standard was spiked at the concentration level used in the bioanalytical method. Interference at the retention times of the analytes and the internal was evaluated and compared to the peak area of the LLOQ samples. Cross analyte/internal standard interference was acceptable when  $\leq 5\%$  of the analytes and  $\leq 20\%$  for the internal standard [12, 13].

### 2.8.5 Matrix factor and recovery

Matrix factor was determined by spiking six batches of control human plasma at Low and High concentrations for both analytes. The Low concentration level was 15 pg/mL and 75 ng/mL and the High concentration level was 300 pg/mL and 1500 pg/mL for  $^2\text{H}_6$ -alectinib and alectinib, respectively. The absolute matrix factor was calculated as the analyte or internal standard peak area in matrix present samples compared to matrix absent samples. The internal standard-normalised matrix factor was calculated by dividing the absolute matrix effect of the analyte with the internal standard, of which the CV% should be  $\leq 15\%$  [12, 13].

### 2.8.6 Isotopic interference correction

The validated calibration range was limited by increasingly high CV% for  $^2\text{H}_6$ -alectinib concentrations below 5 pg/mL, mainly due to expected increasing isotopic interference below this level. The relative isotope interference from alectinib (at clinically relevant steady state concentrations) to  $^2\text{H}_6$ -alectinib increased with decreasing  $^2\text{H}_6$ -alectinib concentrations. It was investigated whether quantification below the LLOQ of 5 pg/mL to a concentration level of 1 pg/mL for  $^2\text{H}_6$ -alectinib was feasible by correcting these low concentrations for the interference of natural abundant isotopes originating from alectinib. A concentration range of 1 to 10 pg/mL of  $^2\text{H}_6$ -alectinib was prepared in human  $\text{K}_2\text{EDTA}$  plasma. All samples including one blank sample were spiked with 800 ng/mL alectinib, representing the steady-state alectinib concentration in patient samples. Samples were processed as described in 2.5 Sample preparation.

Four methods for isotope interference correction were investigated. The first method determined the corrected  $^2\text{H}_6$ -alectinib concentration ( $C_c$ ) by subtracting the concentration determined in the transition window of  $^2\text{H}_6$ -alectinib for the blank sample ( $C_b$ ; containing 800 ng/mL alectinib) from the concentration in the same transition window for the patient sample ( $C_p$ ; Equation 1). The second method calculated the  $C_c$  by subtracting the area ratio of  $^2\text{H}_6$ -alectinib and internal standard in the blank sample ( $AR_b$ ) from the area

ratio of  $^2\text{H}_6$ -alectinib and internal standard in the patient sample ( $AR_p$ ; Equation 2). The third method calculated  $C_c$  by multiplying the difference in  $AR_p$  and  $AR_b$  with the ratio of alectinib area in the patient sample ( $AREA_{ALN,p}$ ) and the blank sample ( $AREA_{ALN,b}$ ; Equation 3). Lastly, in the fourth method the contribution (F) of the interfering natural abundant isotopes originating from alectinib was calculated based on the signal area in the transition window of  $^2\text{H}_6$ -alectinib and this area was then subtracted from the signal area of  $^2\text{H}_6$ -alectinib in the patient sample ( $AREA_{ALN6,p}$ ). Subsequently the corrected  $AREA_{ALN6,p}$  is used to determine the  $C_c$  (Equation 4). This correction factor F represents the average ratio of the response in the transition windows of  $^2\text{H}_6$ -alectinib- and alectinib in samples containing only alectinib. Correction factor F was calculated based on a sample containing only 800 ng/mL alectinib which was injected 10 times.

$$C_c = C_p - C_b \quad (\text{Equation 1})$$

$$C_c = \frac{(AR_p - AR_b) - \text{intercept}}{\text{slope}} \quad (\text{Equation 2})$$

$$C_c = \frac{\left(\frac{AREA_{ALN,p}}{AREA_{ALN,b}}\right) \times (AR_p - AR_b) - \text{intercept}}{\text{slope}} \quad (\text{Equation 3})$$

$$C_c = \frac{\left(\left(\frac{AREA_{ALN6,p} - (AREA_{ALN,p} \times F)}{AREA_{IS,p}}\right) - \text{intercept}\right)}{\text{slope}} \quad (\text{Equation 4})$$

In which  $AREA_{IS,p}$  is the signal area of the internal standard in the patient sample, *intercept* is the intercept of the calibration model for  $^2\text{H}_6$ -alectinib, and *slope* is the slope of the calibration model of  $^2\text{H}_6$ -alectinib.

The verification of interference correction was executed by spiking six batches of control  $\text{K}_2\text{EDTA}$  human plasma with both 400 ng/mL and 800 ng/mL alectinib in duplicate. The two alectinib concentration levels represent two different steady-state levels of alectinib based on the target trough level recommended for therapeutic drug monitoring [14]. One of each sample in the duplicate was spiked with 1 pg/mL  $^2\text{H}_6$ -alectinib (<LLOQ1). The  $^2\text{H}_6$ -alectinib concentrations were corrected with the above-described methods.

### 2.8.7 Stability

Stability of both analytes in several conditions was investigated. The freeze/thaw stability was investigated by letting the samples undergo three freeze/thaw cycles. Thawing was performed unassisted at ambient temperature and the time between thawing and freezing was at least 12 hours. Short-

term stability at ambient temperature was investigated by storing samples at ambient temperature for at least 48 hours. Final extract stability was determined by storing processed samples at nominally 4 °C for at least 48 hours before analysis. Stability of both analytes in human  $\text{K}_2\text{EDTA}$  plasma and working solutions established by storing both samples at nominally -20 °C. All stability experiments were executed in triplicate for Low and High concentration levels.

## 3 RESULTS

### 3.1 Development

#### 3.1.1 Sample preparation

A previously published method for the quantification of alectinib and eight other oral anticancer drugs was used as a starting point for method development [11]. This bioanalytical method used protein precipitation as a sample preparation method resulting in satisfactory sensitivity for therapeutic drug monitoring samples. However, the current method needed to have an ultra-high sensitivity with an increase in sensitivity of 2000-fold to be able to quantify  $^2\text{H}_6$ -alectinib concentration within the pg/mL range. Therefore, the sample preparation method was changed to liquid-liquid extraction with TBME, which resulted in a cleaner extract and lower noise. A concentration step was included by snap freezing the samples, evaporating the TBME with nitrogen (40 °C) and reconstituting the samples with 100  $\mu\text{L}$  formic acid-acetonitrile-methanol-water (0.1:25:25:50, v/v/v/v) resulting in a two-fold increase in concentration. This sample preparation method resulted in sufficient recovery to quantify  $^2\text{H}_6$ -alectinib concentration as low as 1 pg/mL.

#### 3.1.2 Chromatography and mass spectrometry

The chromatography was optimised for  $^2\text{H}_6$ -alectinib from the previously published method [11]. First, ammonium bicarbonate in the mobile phase was switched to 0.1% formic acid to account for the basic characteristics of alectinib. This change in eluent resulted in an improved peak shape for both  $^2\text{H}_6$ -alectinib and alectinib. A shorter column was used in comparison to the published method (50 mm vs 100 mm) to shorten the run time and decrease the pressure of the system. Furthermore, an injection volume of 1 and 2  $\mu\text{L}$  were too small to achieve the desired <LLOQ of 1 pg/mL. Increasing the injection volume to 5  $\mu\text{L}$  resulted in a satisfactory signal at the <LLOQ with a signal-to-noise ratio between 5 and 10. However, the isotope interference of alectinib to the signal  $^2\text{H}_6$ -alectinib was significant (150-200%). To minimise the isotope interference in the calibration standards and QC samples, a ratio between  $^2\text{H}_6$ -alectinib and alectinib was chosen in such a way that the theoretical isotope interference did not exceed 1%. The LLOQ was set at 5 pg/mL mainly due to expected increasing isotope interference below this level. Methods for isotope interference correction were investigated for samples with concentration below LLOQ and for samples with deviant concentrations ratio's between  $^2\text{H}_6$ -alectinib and alectinib (e.g., patient samples). For quantification, the Quadrupole 6500+ was chosen for its high sensitivity. Different mass transitions from the previously published



method [11] were investigated for alectinib to prevent detector saturation caused by the optimized sample recovery. From the two investigated mass transitions,  $m/z$  485.3  $\rightarrow$  396.2 (M+2) and  $m/z$  483.3  $\rightarrow$  381.2 (M+1), the first transition was chosen. For  $^2\text{H}_6$ -alectinib also two mass transition were evaluated:  $m/z$  489.3  $\rightarrow$  402.3 and  $m/z$  489.3  $\rightarrow$  384.3. Both transitions were able to quantify  $^2\text{H}_6$ -alectinib concentrations in the range of 1-1000 pg/mL and both transitions suffered from isotope interference from alectinib. Summation of the transitions resulted in a higher signal. However, the signal-to-noise ratio was consistently higher for the  $m/z$  489.3  $\rightarrow$  402.3 mass transitions and therefore the latter was chosen.

### 3.2 Validation

#### 3.2.1 Calibration model and lower limit of quantification

The method was linear from 5 to 400 pg/mL for  $^2\text{H}_6$ -alectinib and 25 to 2,000 ng/mL for alectinib with  $R \geq 0.999$  and 0.999, respectively. The bias was  $\pm 2.1\%$  (1.1% LLOQ) and  $\pm 2.1\%$  (LLOQ -0.3%) for  $^2\text{H}_6$ -alectinib and alectinib, respectively. Precision was  $\leq 5.2\%$  (4.3% LLOQ) for  $^2\text{H}_6$ -alectinib and  $\leq 2.4\%$  (LLOQ 1.0%) for alectinib. The signal-to-noise ratio for  $^2\text{H}_6$ -alectinib was  $\geq 55$  and for alectinib  $\geq 600$ .

**Table 2.** Assay performance for  $^2\text{H}_6$ -alectinib and alectinib.

Analyte	Nominal conc. (pg/mL)	Intra-assay (n = 3)		Inter-assay (n = 3)	
		Bias (%)	Precision (%)	Bias (%)	Precision (%)
$^2\text{H}_6$ -alectinib	5	$\pm 2.4$	$\leq 5.7$	$\pm 0.5$	*
	15	$\pm 2.8$	$\leq 2.8$	$\pm 1.3$	$\leq 0.9$
	50	$\pm 0.5$	$\leq 1.1$	$\pm 0.1$	$\leq 0.2$
	300	$\pm 3.5$	$\leq 1.2$	$\pm 2.8$	$\leq 1.0$
	(ng/mL)				
Alectinib	25	$\pm 4.0$	$\leq 1.9$	$\pm 3.0$	$\leq 0.9$
	75	$\pm 4.6$	$\leq 1.1$	$\pm 3.6$	$\leq 0.8$
	300	$\pm 5.1$	$\leq 1.2$	$\pm 4.5$	$\leq 0.7$
	1500	$\pm 2.4$	$\leq 1.4$	$\pm 1.6$	$\leq 1.1$

\*No additional variation was found by performing the assay between days (mean square between groups is less than mean square within groups).

#### 3.2.2 Accuracy and precision

Data of accuracy and precision are depicted in Table 2. Representative chromatograms for  $^2\text{H}_6$ -alectinib and alectinib are visualized in Figure 2 and Supplementary Figure S1, respectively. For  $^2\text{H}_6$ -alectinib the intra-assay bias and precision were  $\pm 3.5\%$  and  $\leq 5.7\%$ , respectively over all concentration levels, while the inter-assay bias and precision were  $\pm 2.8\%$  and  $\leq 0.9\%$ , respectively

over all concentration levels. For alectinib, the intra-assay bias and precision was  $\pm 5.1\%$  and  $\leq 1.9\%$ , respectively, over all concentration levels, whereas the inter-assay bias and precision was  $\pm 4.5\%$  and  $\leq 1.1\%$ , respectively, over all concentration levels.

### 3.2.3 Carry-over

The carry-over for both  $^2\text{H}_6$ -alectinib and alectinib was both 0%, whilst the carry-over for the internal standard was  $\leq 0.1\%$  of the LLOQ.

### 3.2.4 Specificity and selectivity

Endogenous interference was negligible for both analytes and the internal standard. The interference of alectinib to  $^2\text{H}_6$ -alectinib was 31.3% and was negligible to the internal standard. The interference of  $^2\text{H}_6$ -alectinib to alectinib and the internal standard and the interference of the internal standard to both analytes was negligible. While the isotope interference from alectinib to  $^2\text{H}_6$ -alectinib did not meet the requirements, the results represent an extreme situation where there is a 400,000-fold differences in concentrations between to two analytes. However, this phenomenon was overcome in the calibration and QC samples, by combining the two analytes within samples with only a 5,000-fold concentration difference. For correct quantification in patient samples, however, several methods were investigated to correct for isotope interference (see section 3.2.6).

### 3.2.5 Matrix effect and recovery

The IS-normalized matrix factor was 0.980 (CV% 3.4) and 1.000 (CV% 0.7) for  $^2\text{H}_3$ -alectinib for the Low and High concentration levels, respectively. For alectinib, the IS-normalized matrix factor was 1.01 (CV% 0.9) and 1.01 (CV% 0.8) for the Low and High concentration levels, respectively. The IS-normalized matrix factor both analytes indicate no ion suppression or ion enhancement. The sample preparation recovery was 102.1-108.4% for  $^2\text{H}_6$ -alectinib and 99.2-101.9% for alectinib. Overall recovery was 99.3-100.1% for  $^2\text{H}_6$ -alectinib and 95.5-97.5% for alectinib.

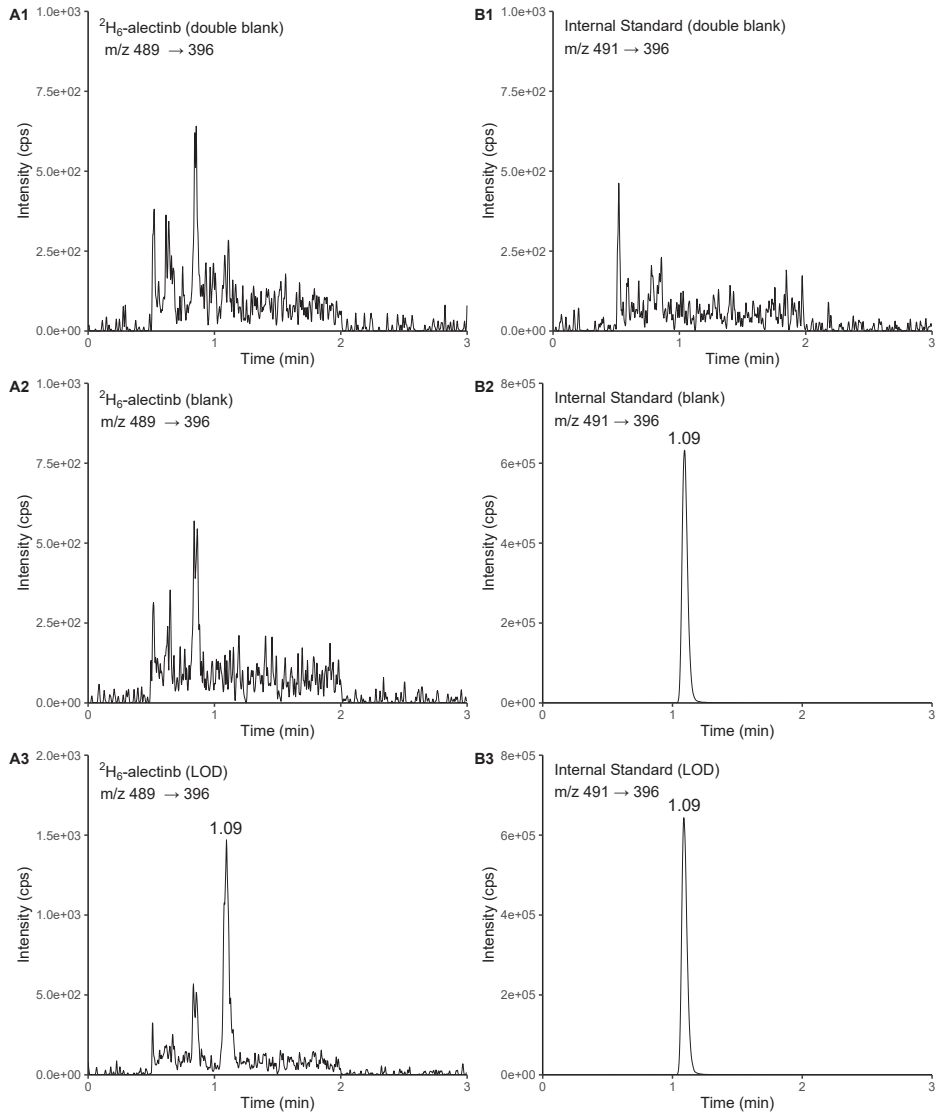


**Figure 2.** Representative LC-MS/MS chromatograms of  $^2\text{H}_6$ -alectinib (A-series) and the internal standard (B-series). The  $^2\text{H}_6$ -alectinib plasma concentration at <LLOQ1, LLOQ, and ULOQ level is 1, 5, and 400 pg/mL, respectively.

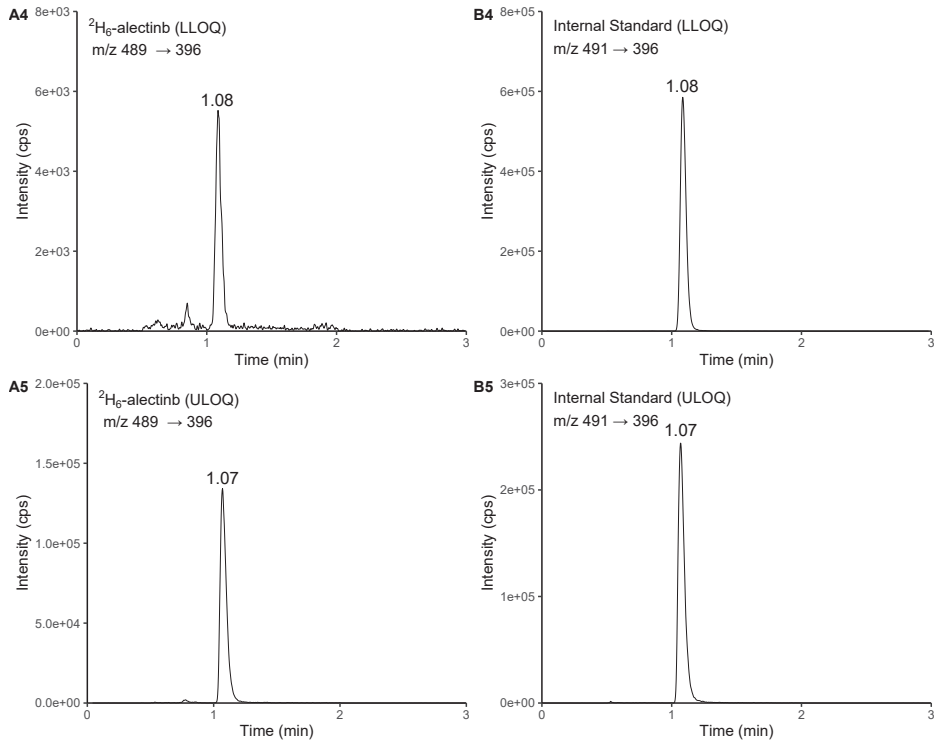


**Figure 2.** Continued.

### 3.2.6 Isotopic interference correction

Results of the isotopic interference correction for  $^2\text{H}_6$ -alectinib concentrations is depicted in Supplementary Table S1. Correction with method 1 resulted in deviations from the nominal concentration of  $\pm 11.3\%$  over a concentration range of 1 to 10 pg/mL with a deviation of  $-4.4\%$  for 1 pg/mL. Method 2 yielded deviations of  $\pm 8.4\%$  for concentrations between 2 and 10 pg/mL and a deviation of  $-20.6\%$  for 1 pg/mL. The deviation of method 3 was within  $\pm 14.4\%$  for concentrations between 1 and 10 pg/mL with a deviation of  $-14.4\%$  for 1 pg/mL. Lastly, method 4 resulted in deviations within  $\pm 14.5\%$  with a deviation of  $-14.5\%$  for 1 pg/mL. Concluding, method 1, method 3, and method 4 were able to correct for isotope interference thereby enabling quantification of  $^2\text{H}_6$ -alectinib concentrations as low as 1 pg/mL within the criteria of the EMA and FDA guidelines [12, 13].

**Table 3.** Verification of the methods for isotope interference correction for the <LLOQ1 (1 pg/mL) of  $^2\text{H}_3$ -alectinib.

Nominal alectinib concentration (ng/mL)		Method 1 (n=6)	Method 2 (n=6)	Method 3 (n=6)	Method 4 (n=6)
400	Mean (pg/mL)	1.22	0.97	0.96	0.97
	Bias (%)	21.8	-3.3	-4.5	-3.2
	Precision (%)	6.7	8.4	9.6	10.6
800	Mean (pg/mL)	1.10	0.85	0.84	1.03
	Bias (%)	9.7	-15.2	-15.9	3.3
	Precision (%)	9.1	11.7	11.9	12.5

Results of the verification of interference correction are given in Table 3. Both method 2, method 3, and method 4 were able to quantify 1 pg/mL of  $^2\text{H}_6$ -alectinib by correction for isotope interference at both tested steady-state concentrations for alectinib (400 and 800 ng/mL) with an acceptable bias ( $\pm 15.2\%$ ,  $\pm 15.9\%$ , and  $\pm 3.3\%$  for method 2, method 3, and method 4, respectively) and good precision ( $\leq 11.7\%$ ,  $\leq 11.9\%$  and  $\leq 12.5\%$  for method 2, method 3, and method 4, respectively). Method 1 also resulted in good precision ( $\leq 9.1\%$ ), but the bias ( $\pm 21.8\%$ ) did not meet the criteria of the EMA and FDA guidelines [12, 13]. A disadvantage of this method is that the noise in these samples is also subtracted, possibly explaining the performance of this method. These results demonstrated the feasibility of isotope correction at different steady-state concentrations of alectinib with method 2, method 3, and method 4 and thereby enabling quantifying  $^2\text{H}_6$ -alectinib plasma concentrations as low as 1 pg/mL. Method 4 has the preference for clinical application over method 2 and method 3 for two reasons. First, method 2 assumes a constant alectinib concentration over all samples collected from the same patient, which is untrue. Second, both method 2 and method 3 are dependent on a predose patient sample which will contain only alectinib. If a predose is unavailable for an individual patient, correction for isotope interference will not be possible for those patient samples.

### 3.2.7 Stability

The results of the stability experiments are presented in Supplementary Table S2. Both  $^2\text{H}_6$ -alectinib and alectinib were stable for three freeze/thaw cycles at  $-20\text{ }^\circ\text{C}$  and ambient temperature. Continuing, both analytes were stable for 2 days at ambient temperature in human  $\text{K}_2\text{EDTA}$  plasma and 44 days at  $-20\text{ }^\circ\text{C}$ . Both analytes were also stable in methanol for 44 days at  $-20\text{ }^\circ\text{C}$ .  $^2\text{H}_6$ -alectinib was stable in the final extract for 7 days when stored nominally at  $4\text{--}8\text{ }^\circ\text{C}$ , while alectinib was stable for 4 days under the same conditions.

## 4 CONCLUSION

An ultra-sensitive bioanalytical method for the simultaneous quantification of  $^2\text{H}_6$ -alectinib in  $\text{K}_2\text{EDTA}$  plasma was developed and validated. The validated concentration range was 5-400 pg/mL for  $^2\text{H}_6$ -alectinib and 25 to 2000 ng/mL for alectinib with an accuracy within  $\pm 3.5\%$  and  $\pm 5.1\%$  and a precision of  $\leq 5.7\%$  and  $\leq 1.9\%$  for  $^2\text{H}_6$ -alectinib and alectinib, respectively. By correcting for isotope interference,  $^2\text{H}_6$ -alectinib plasma concentrations as low as 1 pg/mL were quantified with a bias of  $\pm 15.9\%$  and precision of  $\leq 12.5\%$ .

## REFERENCES

1. European Medicines Agency (EMA) (2012) Guideline on the investigation of drug interactions [https://www.ema.europa.eu/en/documents/scientific-guideline/guideline-investigation-drug-interactions-revision-1\\_en.pdf](https://www.ema.europa.eu/en/documents/scientific-guideline/guideline-investigation-drug-interactions-revision-1_en.pdf). Accessed 14 July 2022
2. US Food and Drug Administration (FDA) (2002) Food effect bioavailability and fed bioequivalence studies <https://www.fda.gov/files/drugs/published/Food-Effect-Bioavailability-and-Fed-Bioequivalence-Studies.pdf>. Accessed 14 July 2022
3. de Las Heras B, Bouyoucef-Cherchalli D, Reeve L, Reichl A, Mandarino D, Flach S, Vidal L, van Brummelen EMJ, Steeghs N (2022) Healthy volunteers in first-in-human oncology drug development for small molecules. *Br J Clin Pharmacol* 88 (4):1773-1784. doi:10.1111/bcp.15092
4. Roosendaal J, Rosing H, Beijnen JH (2020) Stable Isotopically Labeled Intravenous Microdose Pharmacokinetic Trials as a Tool to Assess Absolute Bioavailability: Feasibility and Paradigm to Apply for Protein Kinase Inhibitors in Oncology. *Clin Pharmacol Drug Dev* 9 (5):552-559. doi:10.1002/cpdd.840
5. Kinoshita K, Asoh K, Furuichi N, Ito T, Kawada H, Hara S, Ohwada J, Miyagi T, Kobayashi T, Takanashi K, Tsukaguchi T, Sakamoto H, Tsukuda T, Oikawa N (2012) Design and synthesis of a highly selective, orally active and potent anaplastic lymphoma kinase inhibitor (CH5424802). *Bioorg Med Chem* 20 (3):1271-1280. doi:10.1016/j.bmc.2011.12.021
6. Hirota T, Muraki S, Ieiri I (2019) Clinical Pharmacokinetics of Anaplastic Lymphoma Kinase Inhibitors in Non-Small-Cell Lung Cancer. *Clin Pharmacokinet* 58 (4):403-420. doi:10.1007/s40262-018-0689-7
7. Yamane N, Tozuka Z, Kusama M, Maeda K, Ikeda T, Sugiyama Y (2011) Clinical relevance of liquid chromatography tandem mass spectrometry as an analytical method in microdose clinical studies. *Pharm Res* 28 (8):1963-1972. doi:10.1007/s11095-011-0423-8
8. van Veelen A, van Geel R, Schoufs R, de Beer Y, Stolk LM, Hendriks LEL, Croes S (2021) Development and validation of an HPLC-MS/MS method to simultaneously quantify alectinib, crizotinib, erlotinib, gefitinib and osimertinib in human plasma samples, using one assay run. *Biomed Chromatogr* 35 (12):e5224. doi:10.1002/bmc.5224
9. Zhou L, Wang S, Chen M, Huang S, Zhang M, Bao W, Bao A, Zhang P, Guo H, Liu Z, Xie G, Gao J, Wu Z, Lou Y, Fan G (2021) Simultaneous and rapid determination of 12 tyrosine kinase inhibitors by LC-MS/MS in human plasma: Application to therapeutic drug monitoring in patients with non-small cell lung cancer. *J Chromatogr B Analyt Technol Biomed Life Sci* 1175:122752. doi:10.1016/j.jchromb.2021.122752
10. Mukai Y, Wakamoto A, Hatsuyama T, Yoshida T, Sato H, Fujita A, Inotsume N, Toda T (2021) An Liquid Chromatography-Tandem Mass Spectrometry Method for the Simultaneous Determination of Afatinib, Alectinib, Ceritinib, Crizotinib, Dacomitinib, Erlotinib, Gefitinib, and Osimertinib in Human Serum. *Ther Drug Monit* 43 (6):772-779. doi:10.1097/ftd.0000000000000895

11. Janssen JM, de Vries N, Venekamp N, Rosing H, Huitema ADR, Beijnen JH (2019) Development and validation of a liquid chromatography-tandem mass spectrometry assay for nine oral anticancer drugs in human plasma. *J Pharm Biomed Anal* 174:561-566. doi:10.1016/j.jpba.2019.06.034
12. Agency EEM (2011) Guideline on Bioanalytical Method Validation. Committee for Medicinal Products for Human Use and European Medicines Agency. Accessed 8 May 2022
13. Administration FFaD (2018) Bioanalytical Method Validation. Silver Springs, Maryland: US Food and Drug Administration. Accessed 9 May 2022
14. Groenland SL, Geel DR, Janssen JM, de Vries N, Rosing H, Beijnen JH, Burgers JA, Smit EF, Huitema ADR, Steeghs N (2021) Exposure-Response Analyses of Anaplastic Lymphoma Kinase Inhibitors Crizotinib and Alectinib in Non-Small Cell Lung Cancer Patients. *Clin Pharmacol Ther* 109 (2):394-402. doi:10.1002/cpt.1989



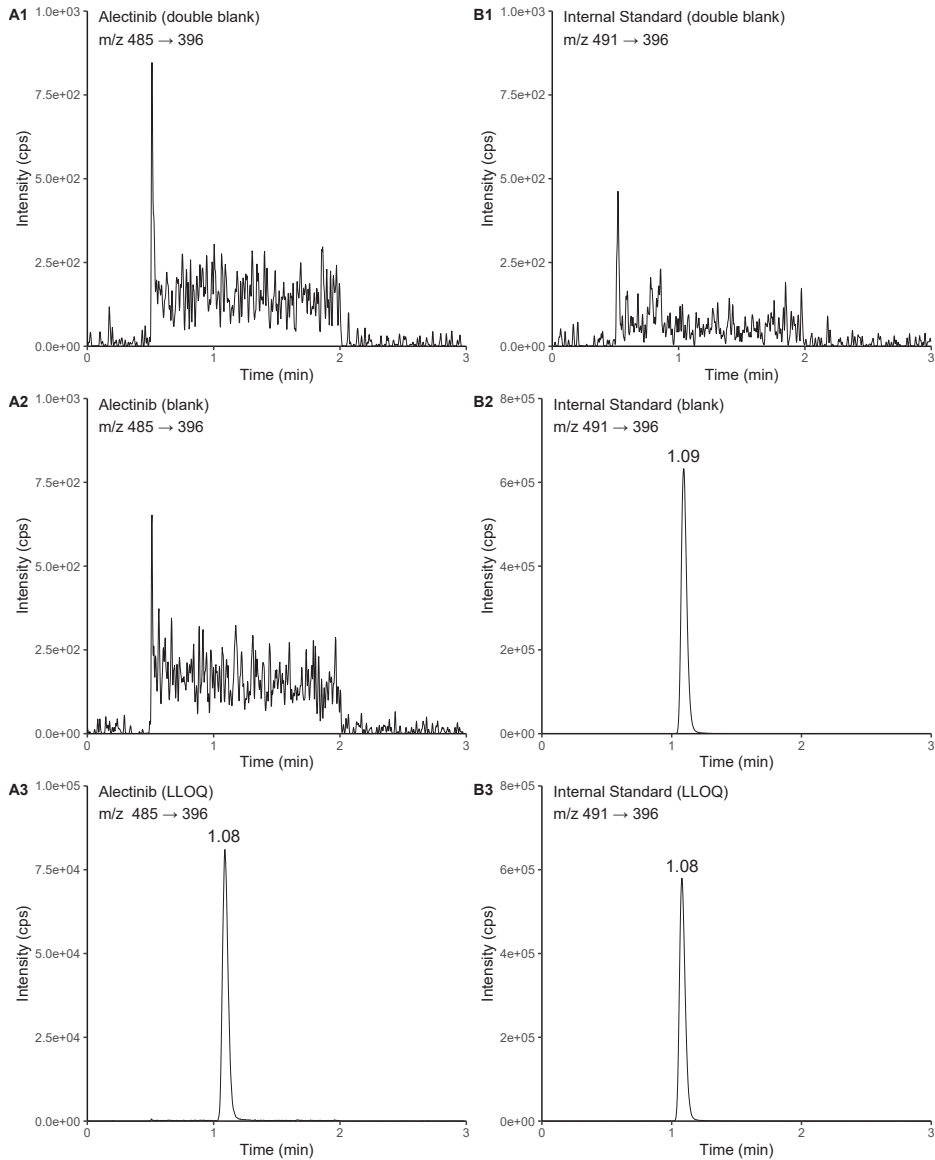
## SUPPLEMENTARY MATERIAL

**Supplementary Table S1.** Performance of the methods of isotope interference correction.

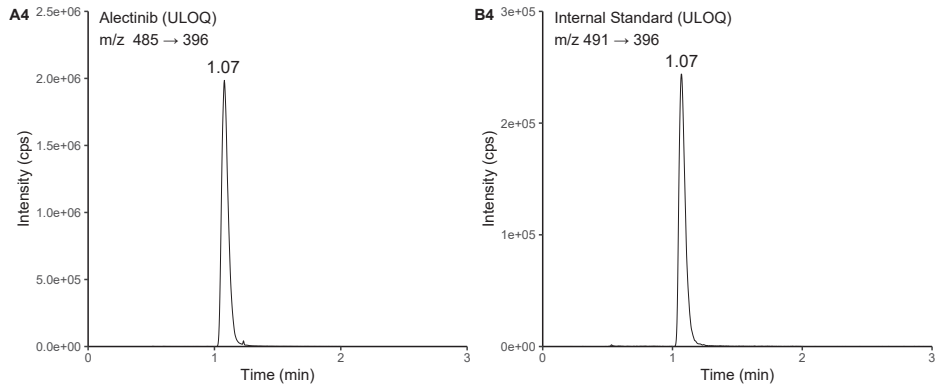
Nom. Conc. (pg/mL)	Deviation from nominal concentration (%)			
	Method 1 (n=1)	Method 2 (n=1)	Method 3 (n=1)	Method 4 (n=1)
1	-4.4	-20.6	-14.4	-14.5%
2	11.3	3.2	3.7	3.6%
3	7.2	2.1	3.4	3.2%
4	-4.3	-8.2	-6.7	-6.8%
5	-5.1	-8.4	-6.9	-6.8%
6	2.1	-0.7	0.3	0.4%
7	4.4	2.4	3.0	2.7%
8	-0.8	-2.5	-2.2	-2.4%
9	1.1	-0.6	-0.6	-0.4%
10	-3.0	-4.2	-3.9	-4.0%

**Supplementary Table S2.** Stability parameters for  $^2\text{H}_6$ -alectinib and alectinib.

Analyte	Matrix	Conditions	Nom. Conc. (ng/mL)	Bias (%)	CV (%)	N
Alectinib	Plasma	3 F/T cycles (-20 °C/ambient)	75	-1.1	1.2	3
		3 F/T cycles (-20 °C, ambient)	1500	-0.9	1.6	3
	Plasma	Ambient, 2 days	75	-4.7	0.2	3
	Plasma	Ambient, 2 days	1500	-1.3	1.4	3
	Plasma	-20 °C, 44 days	75	-1.7	1.8	3
	Plasma	-20 °C, 44 days	1500	-1.6	1.7	3
	Final extract	4-8 °C, 4 days	75	-4.8	1.2	3
	Final extract	4-8 °C, 4 days	1500	-1.8	1.6	3
	MeOH (working)	-20 °C, 44 days	75	-3.6	1.4	3
	MeOH (working)	-20 °C, 44 days	1500	-8.2	0.9	3
$^2\text{H}_6$ -alectinib	Plasma	3 F/T cycles (-20 °C/ambient)	0.015	4.2	3.9	3
		3 F/T cycles (-20 °C, ambient)	0.300	3.1	1.6	3
	Plasma	Ambient, 2 days	0.015	0.7	4.1	3
	Plasma	Ambient, 2 days	0.300	2.4	1.6	3
	Plasma	-20 °C, 44 days	0.015	-0.7	3.7	3
	Plasma	-20 °C, 44 days	0.300	-7.9	2.8	3
	Final extract	4-8 °C, 7 days	0.015	2.9	1.0	3
	Final extract	4-8 °C, 7 days	0.300	3.2	1.0	3
	MeOH (working)	-20 °C, 44 days	0.015	-1.3	2.2	3
	MeOH (working)	-20 °C, 44 days	0.300	-1.6	1.5	3



**Supplementary Figure S1.** Representative LC-MS/MS chromatograms of alectinib (A-series) and the internal standard (B-series). The  $^2\text{H}_6$ -alectinib plasma concentration at LLOQ, and ULOQ level is 25 and 2000 ng/m, respectively.



**Supplementary Figure S1.** Continued.



# Chapter 3

## **The use of microtracers in food-effect trials: An alternative study design for toxic drugs with long half-lives exemplified by the case for alectinib**

*Accepted in Clinical Translational Science.*

Lisa T. van der Heijden  
Neeltje Steeghs  
Jos H. Beijnen  
Alwin D.R. Huitema  
Thomas P.C. Dorlo

## ABSTRACT

The traditional design of food-effect studies has a high patient burden for toxic drugs with long half-lives (e.g., anticancer agents). Microtracers could be used to assess food-effect in patients without influencing their ongoing treatment. The feasibility of a microtracer food-effect study during steady-state of the therapeutic drug was investigated in an *in silico* simulation study with alectinib as example for a relative toxic drug with a long half-life. Microtracer pharmacokinetics were simulated based on a previously published population pharmacokinetic model and used for estimation of a model with and a model without food as a covariate on oral bioavailability of alectinib (assuming a 40% food-effect). Power was defined as the fraction of clinical trials of which a significant ( $p < 0.01$ ) food-effect was identified. The proposed study design of 10 patients on steady state treatment, 10 blood samples collected within 24 hours after administration and an assumed food-effect of 40% had a power of 99.9%. The mean estimated food-effect was 39.8% (80% CI: 31.0-48.6%). The feasibility of microtracer food-effect studies was demonstrated. The design of the microtracer food-effect study allowed estimation of the food-effect with minimal influence on therapeutic treatment and reducing patient burden compared to the traditional study design for toxic drugs with long half-lives.

# 1 INTRODUCTION

Co-administration of food can alter oral drug pharmacokinetics in various ways, by influencing the physiological processes such as gastric emptying time, bile flow, and activity of transporters or enzymes [1]. Furthermore, it can interact with the drug itself, e.g., by influencing solubility [2]. In general, food can have four possible outcomes on the bioavailability of a drug: 1) Delayed absorption, 2) decreased absorption, 3) increased absorption, and 4) no effect on absorption [3].

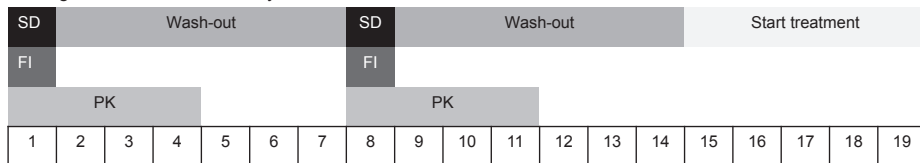
Due to its possible influence on pharmacokinetics, it is essential to study the effect of food intake on drug absorption during drug development [4]. The traditional study design is a randomized, balanced, two-treatment (fed vs. fasting) and two-sequence cross-over design with single dose administration in healthy volunteers [4,5]. It is recommended to use a high-fat, high-caloric meal (800 to 1000 calories of which 50% is fat) since this meal type will have the largest effect on gastro-intestinal physiology and therefore will have maximal effect on the oral bioavailability [3,5].

The above-described study can give rise to safety concerns when the acceptable risk differentiates between healthy volunteers and patients (e.g., anticancer drugs [4,5]) or when exposure could rise higher than expected (e.g., food-drug interaction) [6]. In these situations, conducting food-effect studies in healthy volunteers might be undesirable. Continuing, the study burden of the traditional study design is increased for investigational drugs with long a half-life. An example is alectinib, a tyrosine kinase inhibitor (TKI) selectively targeting anaplastic lymphoma kinase (ALK) [7] with a half-life of approximately 32 hours [8] of which a microtracer is available. A single dose food-effect study for alectinib would consist of two single dose administrations at day 1 and day 8 of the study with a wash-out period of 7 days after the single dose administrations. Alectinib treatment will then be able to start on day 15, effectively delaying treatment with at least 15 days (Figure 1A). Another consequence of the long half-life is the long period of sample collection to capture the complete pharmacokinetics of the drug with non-compartmental analysis (NCA) (e.g., in a food-effect study of alectinib, blood samples were collected up 96 hours after administration [9]).

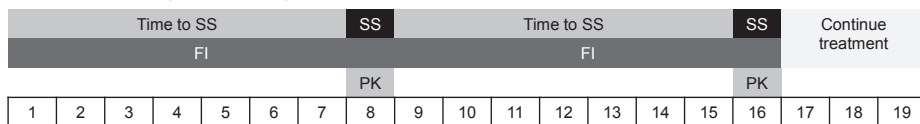
An alternative to the single dose administration would be to study the food-effect at steady-state treatment conditions. In this situation for alectinib, patients have to administer the drug under fasting conditions until steady-state pharmacokinetics is achieved (approximately 7 days [8]), followed by a study day (day 8). The same

procedure is to be repeated but under fed conditions where patients have to administer their twice daily alectinib dose with a standardised meal for days 9 up to 15 and a study day (day 16). This study design requires considerable time investment and commitment of the included patients (Figure 1B).

#### A. Single dose food-effect study



#### B. Food-effect study under steady-state conditions



#### C. SIL microtracer food-effect study

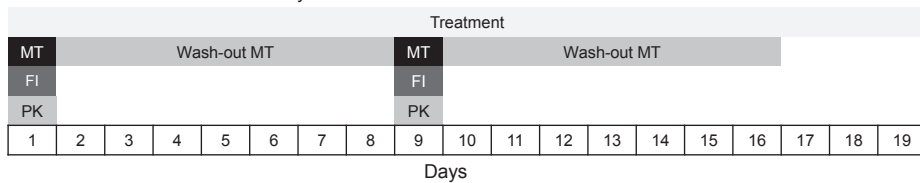


**Figure 1.** Schematic overview of the different study designs for food-effect studies for toxic drugs with long half-lives. For the figure the half-life of alectinib is applied as an example (32 hours).

Abbreviations: FI, food intervention; either fasted conditions or fed conditions. MT = microtracer. SD, single dose. SIL, stable isotopically labelled. SS, steady-state. PK, pharmacokinetic sampling.

Regarding the above-described study designs, there is a need to reduce the patient burden of food-effect studies for toxic drugs with long half-lives. A strategy would be to use microtracers for the determination of food-effect at steady-state. Microtracers are stable isotopically labelled (SIL) drugs that are dosed at a microgram level (max. 100 µg) [10]. These microtracers have originally been used for the determination of the absolute oral bioavailability [10]. Pharmacokinetics of the microtracer could be used for the determination of food-effect, while the therapeutic treatment remains unchanged. To reduce the period of sample collection necessary for the complete capture of alectinib pharmacokinetics with NCA, a population pharmacokinetic approach was used for data analysis [11].



The aim of the current study was to demonstrate the feasibility of a microtracer food-effect study exemplified for an anticancer drug with a relative long half-life. Secondary objectives were to decrease the patient burden of the study and to identify critical aspects of the study design with a sensitivity analysis.

## 2 METHODS

### 2.1 Criteria and proposed study design

Several criteria were defined to reduce the patient burden of the proposed study design for microtracer food-effect studies. The criteria were as follows: (1) The study should consist of maximally two study days where the patient is hospitalized and available for the collection of blood samples, (2) The duration of the hospitalization should not exceed 24 hours, (3) the microtracer should be administrated as a single dose, and (4) the blood sampling schedule should be optimized to reduce the number of samples collected.

The study design was deemed feasible when the following criteria were met: (1) A sample size of approximately 10 patients (max. 15), and (2) power  $\geq 80\%$  to detect a minimal clinically relevant food-effect of 40%. A food-effect of 40% was considered the minimal clinically relevant food-effect due to the previously reported intra-individual variability of 27.0% in alectinib trough levels [12].

The proposed study design is depicted in Figure 1C. Patients who have been treated with alectinib for  $\geq 7$  days (steady-state will co-ingest the microtracer with their therapeutic dose and a standardised meal on study day 1. After a wash-out period of the microtracer of five-times the half-life of alectinib (approximately 7 days), patients will receive the microtracer under fasted conditions (day 9). For drugs with a relative long half-life, population pharmacokinetic analysis is recommended over NCA [11]. With NCA, the Area-Under-the-plasma Concentration-time curve (AUC) is extrapolated to infinity by dividing the last observed concentration by the elimination rate constant. For drugs with long half-lives, such as alectinib (32 hours [8]), the extrapolation to infinity can contribute significantly to AUC calculation relative to the AUC from zero to the last observed concentration. In these cases, population pharmacokinetic analysis is recommended since pharmacokinetic parameters estimates of population pharmacokinetic models are independent of a calculation of the AUC extrapolated to infinity [11]. Blood samples will be collected before administration of the microtracer (predose), and at 0.5, 1, 1.5, 2, 4, and 6 hours to capture the absorption of alectinib (time to maximum concentration is 4-6 hours [8]). To capture the elimination of alectinib, blood samples will be collected at 8, 10, 12, and 24 hours after administration.

## 2.2 Population pharmacokinetic model

Since it is assumed the microtracer (alectinib-d6) has equal pharmacokinetics to alectinib, the population pharmacokinetic model in the assessment report from the European Medicines Agency (EMA) was used [13]. This model was built on pharmacokinetic data from 138 patients with locally advanced or metastatic ALK<sup>+</sup> non-small cell lung cancer (NSCLC). All patients received 600 mg of alectinib bidaily with a meal [14]. The model was a one-compartment model with first-order elimination and sequential absorption [13]. Allometric scaling was included for clearance and volume of distribution with power coefficients of 0.75 for clearance and 1.0 for volume of distribution. The residual error model account for unexplained variability (e.g., bioanalytical variability and model misspecification) consisted of a proportional error and an additive error. The additional error was excluded from the residual error model due to the difference in concentration range between therapeutic alectinib dose and the microtracer (ng/mL vs pg/mL).

Food-effect was included in the model as a covariate on oral bioavailability (F). F was fixed to 1 for microtracer administration with food. As described in 2.1 Criteria and proposed study design, a food-effect of 40% was defined as the minimal clinically relevant food-effect. Therefore, the oral bioavailability was fixed to 0.714 for microtracer administration under fasting conditions. Inter-occasion variability was included in the model on oral bioavailability to account for the variability in oral availability between the two study days. Intra-individual variability was described in the model by the inter-occasion variability and unexplained residual variability. Since the intra-individual variability in alectinib trough levels was reported to be 27.0% [12] and the proportional error was estimated to be 19%, an inter-occasion variability of 8.0% was assumed. Demographic data, model parameter estimates, and the model code are included in the supplementary material.

## 2.3 Clinical trial simulation

Stochastic Simulation and Estimation (SSE) was used to simulate microtracer pharmacokinetics with a food-effect of 40% on bioavailability and perform parameter estimation using two alternative models: 1) A model without food as a covariate on bioavailability, 2) A model with food as a covariate on bioavailability. The SSE was repeated 1000 times for each trial design. For each SSE, bodyweight was (re)sampled from bodyweights from a previous study with NSCLC patients treated with alectinib (median: 77.5 kg, range 49-123 kg) [12]. For each SSE, the difference in Objective Function Value (dOFV) was calculated between the two models. The food-effect was calculated with the following equation:

$$FE = \frac{(F - \theta)}{\theta} \times 100\% \quad (\text{Equation 1})$$

Where  $FE$  is the food-effect and  $\theta$  the estimated oral bioavailability for administration under fasting conditions. The oral bioavailability  $F$  of the microtracer after co-administration with food was fixed to 1. A schematic overview of the clinical trial simulations is visualized in Figure 2.

#### 2.4 Feasibility study

Power was defined as the fraction of clinical trials with significant food effect was found with a p-value of  $<0.01$  ( $dOFV < -6.63$ ). The 80% confidence interval (80% CI) of the estimated food-effect was calculated based on the 1000 study replicates.

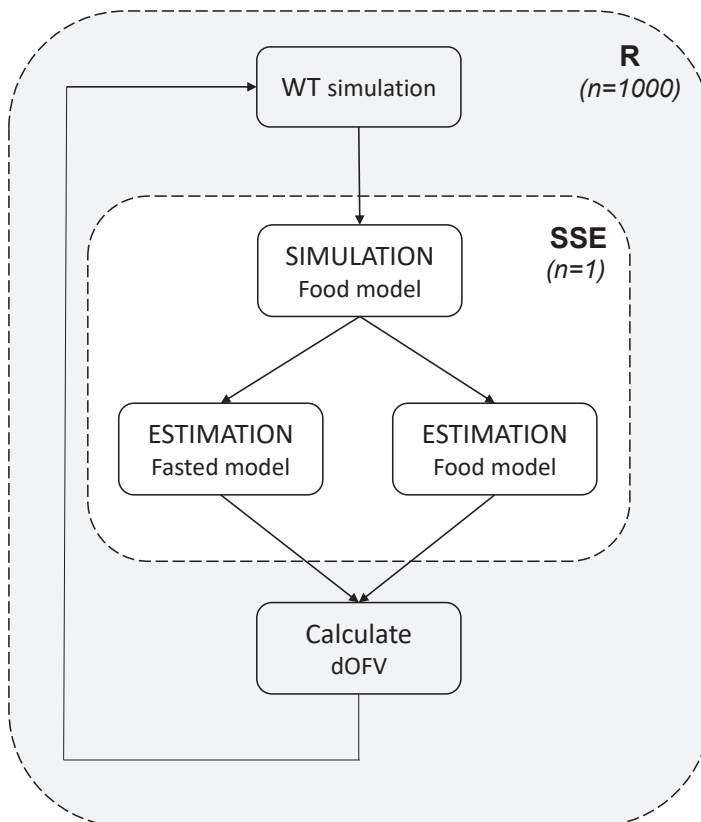


**Figure 2.** Flowchart representing the steps of the Stochastic Simulation and Estimation (SSE) method used. dOFV, difference in Objective Function. SSE, Stochastic Simulation and Estimation. R, programming language R. WT, bodyweight.

### 2.5 Sensitivity analysis

A sensitivity analysis was performed to identify the critical aspects in the design of a microtracer food-effect study. The following aspects of the study design were investigated: Samples size, duration of blood sample collection (8, 10, 12, and 24 h), and number of blood samples collected. For the later samples the following sample schedules were investigated: Predose, 0.5, 1, 1.5, 2, 4, 6, 8, 10, 12, 24 h (11 samples), predose, 0.5, 1, 1.5, 2, 4, 6, 8, 10, 24 h (10 samples), and predose, 0.5, 1, 1.5, 2, 4, 6, 8, 24 h (9 samples). Moreover, the effect of an included patient with an outlier bodyweight (40 kg and 200 kg), the effect size of the food-effect, the effect of the proportional error where investigated, and the effect of inter-occasion variability on oral bioavailability were investigated.

### 2.6 Software

R (version 4.1.2) was used for data preparation, bodyweight sampling, and data analysis. SSE was performed using NONMEM® (version 7.5, ICON Development Solutions, Ellicott City, MD, USA) and Perl-speaks-NONMEM (PsN, version 5.2.6).

## 3 RESULTS

### 3.1 Feasibility study

Figures 3 and 4 provide an overview of the power and estimated food-effect of the study design and the sensitivity study. The proposed study design had a power to reject the null hypothesis that there is no food-effect of 99.9%. The mean estimated food-effect was 39.8% (80% CI: 31.0-48.6%).

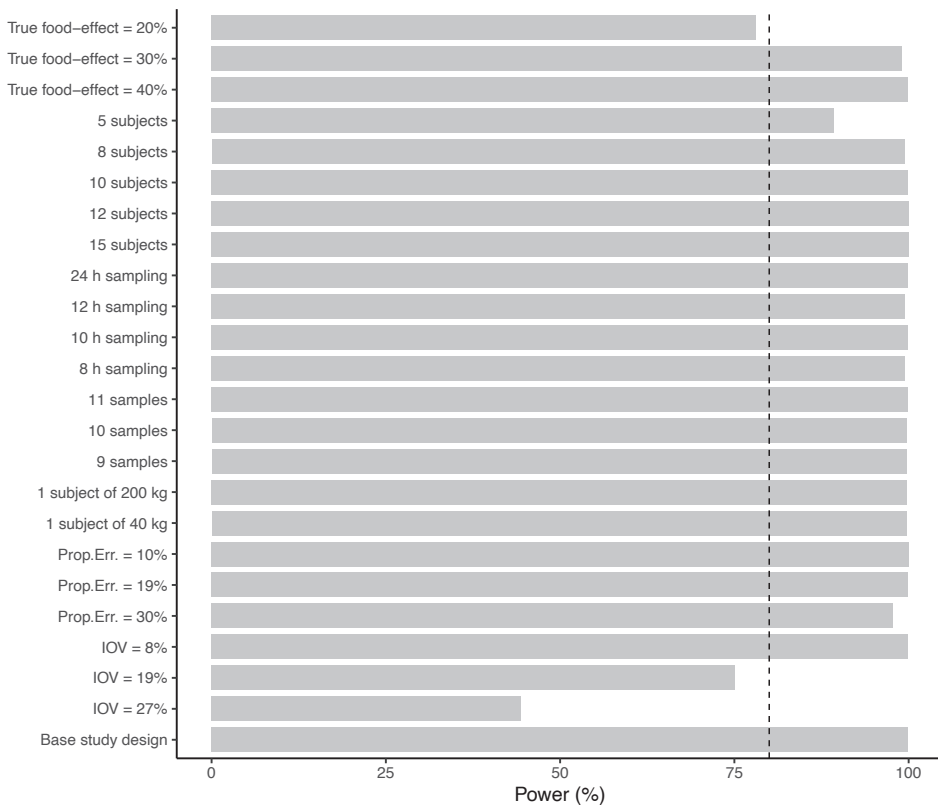


**Figure 3.** Results of the sensitivity analysis on the power of the study design. The base study design consisted of 10 patients, a food-effect of 40%, sample collection at predose, 0.5, 1, 2, 4, 6, 8, 10, 12, and 24 hours after administration of the microtracer, an proportional error of 19%, and no LLOQ. The dashed line represents a power of 80%.

Abbreviations: LLOQ, Lower limit of quantification; IOV, inter-occasion variability; Prop. Err, Proportional error.

### 3.2 Sensitivity analysis

#### 3.2.1 Study design

Changes in the study design demonstrated the robustness of the study in terms of power (see Figure 3) and accurate estimation of the food-effect (see Figure 4). There was no relevant impact of the sample size of included patients on the power and outcome of the study. For a sample size between 5 and 15 patients, the power ranged between 89.3% and 99.9% indicating that sample size was not a critical aspect of the proposed study design (See Supplemental Figure 3). As anticipated, the variability in estimated food-effect decreased with increasing sample size with a sample size of 15 patients having the narrowest confidence interval (80% CI: 32.3-46.5%, see Figure 4).

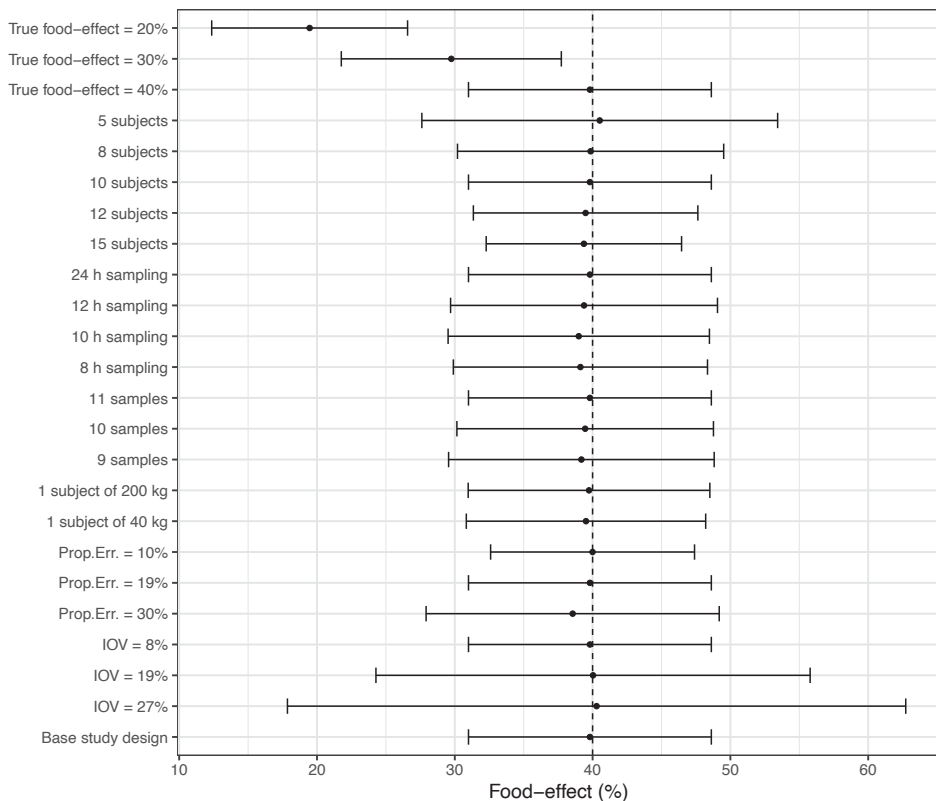


**Figure 4.** Results of the sensitivity analysis on the estimation of the food-effect. The black dots represent the mean food-effect over the clinical trial simulations and the error bars are the 80% confidence intervals. The dashed lines represent the true food-effect of 40%. Abbreviations: LLOQ, Lower limit of quantification; IOV, inter-occasion variability. Prop. Err., Proportional error.

The power was not influenced by the reduction of the duration of blood samples collection (Figure 3). Moving the collection time of the last blood sample from 24 hours to 8 hours after administration of microtracer slightly influenced the estimated food-effect with an estimated food-effect of 39.8% (80% CI: 31.0-48.6%) for 24 h sampling and 39.1% (80% CI: 29.9-48.3%) for 8 h sampling (Figure 4). A similar effect on the estimated food-effect was observed for the removal of samples in the elimination phase (Figure 4). The samples schedule of 10 samples and 9 samples had an estimated food-effect of 39.5% (80% CI: 30.2-48.8%) and 39.2% (80% CI: 29.5-48.8%), respectively, compared to the full blood collection schedule (39.8% (80% CI: 31.0-48.6%)). These results indicate that the hospitalization time could be reduced to 8 hours after administration of the microtracer.

### 3.2.2 Outlier bodyweight

Inclusion of patients with an outlier bodyweight (40 kg or 200 kg) did neither influence the power of the study nor the outcome. The respective estimated food-effect was 39.5% (80% CI: 30.8-48.2%) and 39.7% (80% CI: 30.0-48.5%).

### 3.2.3 Anticipated food-effect

The proposed study design had sufficient power to detect a food-effect of  $\geq 30\%$  (see Figure 3). For an effect-size of 20%, the study design had a power of 78.1% with an estimated food-effect of 19.5% (95% CI: 12.4-26.6%). To detect a food-effect of 20% with a power 80%  $\geq 12$  patients have to be included in the study (see Supplemental Figure S1-S3).

### 3.2.4 Unexplained residual variability

Decreasing the proportional error did not influence the power of the design, but it did influence the precision of the food-effect estimate. An increase of proportional error of 19% to 30% resulted only in a small decrease in power (99.9% vs. 97.7%). However, an increase in the proportional error from 19% to 30% resulted in a decrease in accuracy and precision of the food-effect estimation (39.8% (80% CI: 31.0-48.6%) vs. 38.6% (80% CI: 27.9-49.2%), respectively). However, the differences in the estimated food-effect and the true food-effect were small ( $< 2\%$ ) and were therefore deemed clinically irrelevant.



### 3.2.5 Inter-occasion variability

Inter-occasion variability on oral bioavailability included in the model accounted for the variability in oral bioavailability between the two administrations (with and without food) which cannot be explained by the effect of food. A doubling of the inter-occasion variability from 8%, 16% or 24% resulted in a power of 99.9%, 90%, and 52%, respectively. The variability in estimated food-effect increased with increasing inter-occasion variability: the estimated food-effect was 39.8 (80% CI: 31.0-48.6%), 39.6% (80% CI: 26.0-53.2%), and 39.3% (80% CI: 19.2-59.4%), respectively.

## 4 DISCUSSION

The aim of the current study was to determine the feasibility of a microtracer food-effect study during steady-state of the therapeutic drug and to identify critical aspects of the study design by performing a sensitivity analysis. Alectinib served here as an example. The proposed study design of 10 patients with a parallel food-effect arm, and blood collection at predose, 0.5, 1, 2, 4, 6, 8, 10, 12, and 24 hours after oral administration of 100 µg microtracer (alectinib-d6) had a power of 99.9% to detect an anticipated food-effect of 40% with an estimated food-effect of 39.8% (80% CI: 31.0-48.6%). The sensitivity analysis demonstrated the robustness of the study design. The power of the study was always  $\geq 80\%$  except when the anticipated food-effect was 20%. However, a food-effect of 20% can be considered clinically irrelevant given the high intra-individual variability observed in alectinib trough levels [12]. The high power of the study design was thought due to use of a population pharmacokinetic model instead of NCA as a method of analysis and the cross-over design of the study. Factors that were critical to the study outcome were anticipated food-effect, sample size, and unexplained residual variability.

The sensitivity analysis revealed several critical aspects of the microtracer food-effect study. First, the anticipated food-effect is an important factor in power calculations and therefore the feasibility of a study. The anticipated food-effect of 20% resulted in the lowest power indicating that more patients have to be included to achieve the desirable power of 80% (See supplemental Figure S1). These results demonstrated the importance of defining which food-effect is considered clinically relevant prior to conducting the study. An estimation of a clinically relevant food-effect should be based on (expected) intra-individual variability in pharmacokinetics and the (expected) exposure-response relationship. Food-effect should exceed the intra-individual variability in pharmacokinetics to be clinically relevant for exposure. Continuing, a relatively small food-effect can result in an increase in toxicity for drugs with a small therapeutic window, while a relatively large food-effect is needed to establish the same for drugs with a large therapeutic window. Additionally, minimizing variability in the data is critical. While the parallel study design was robust (e.g., changes in sample collection, inclusion of bodyweight outliers, and sample size minimally influenced the power and the outcome of the study), increasing the unexplained residual variability (proportional error) in the model led to a decrease in accuracy and precision of the estimated food-effect with the 80% CI falling outside a 10% deviation from the true food-effect (80% CI: 27.9-49.2%). Moreover, the inter-occasion variability

on oral bioavailability influenced both the power and estimation of the food-effect. However, inter-occasion variability was not included in the original model. Moreover, it is expected that food will be the main source of variability between the two administrations (with and without food). Therefore, the simulations with increasing inter-occasion variability depict a worst-case scenario. The study design of microtracer food-effect studies, therefore, should be optimised to reduce variability in the data to a minimum, e.g., by standardizing procedures and protocols, training health staff to record dosing and collection times accurately.

The presented study design has several advantages over traditional food-effect studies for toxic drugs with long half-lives that are unsafe in healthy volunteers. The first advantage of microtracer food-effect studies is the ability to study food-effect without influencing therapeutic treatment (Figure 1C). In comparison, the traditional study design [4,5] will either result in treatment delay or treatment interruption which is undesirable and could be unethical (Figure 1A). Studying the food-effect under steady-state conditions (Figure 1B) could be an alternative but would influence treatment by increasing or decreasing therapeutic exposure depending on the food-effect. Furthermore, steady-state conditions also require patients to consume standardized meals for a longer period of time. This not only increases the patient burden of the study but is also sensitive to errors and could possibly result in an underestimation of the food-effect. Secondly, the microtracer food-effect study has limited impact of therapeutic exposure since the microtracer is administered at a maximum dose of 100 µg [10]. No additional side effects are expected. Traditional food-effect studies could influence toxicity and/or efficacy during the study period. Lastly, microtracer food-effect studies are feasible with a reduced hospitalization time and shortened sampling schedule compared to traditional food-effect studies, thereby reducing patient burden.

There are several reasons why the food-effect on the pharmacokinetics of a drug should be investigated. First, food could have a negative effect on efficacy or toxicity. For example, the simultaneous administration of food with nilotinib should be avoided due to the risk of QT prolongation at high peak concentrations [15]. Coadministration with food should also be avoided when exposure is decreased (e.g., capecitabine and afatinib [16]). On the other hand, administration with food could also be an interesting strategy to increase bioavailability of poorly soluble drugs [2,17]. A previous study demonstrated enhanced efficacy while increasing the trough levels of abiraterone by coadministration with food [18]. In addition, food can also play a role in therapy adherence. Studies have shown that adherence to complex dosing regimens could be improved by coupling dosing

with a routine daily activity, such as eating [19,20]. Food can also reduce the variability in bioavailability and thereby resulting in a more consistent exposure (e.g., rivaroxaban) [21]. Furthermore, coadministration with food can be desirable for pharmacodynamic considerations, such as reducing gastrointestinal side effects [21]. Lastly, the food-effect on steady-state pharmacokinetics could be different from the food-effect on single dose pharmacokinetics. For example, the food-effect on lapatinib exposure was smaller at steady-state compared to single dose [22,23]. It is, therefore, not only important to know the maximum magnitude of the food-effect on the pharmacokinetics of a drug but also the food-effect of real-life meals in a real-life context of daily treatment of patients since the food-effect in patients could be different to healthy volunteers due to difference in pharmacokinetics and pharmacodynamics.

## 5 CONCLUSION

The feasibility of microtracer food-effect study for alectinib during steady-state was demonstrated. The design of the microtracer food-effect study allowed estimation of the food-effect of alectinib with minimal influence on therapeutic treatment. Continuing, the feasibility of the study design was also demonstrated with reduced hospitalization time and a reduced number of blood samples, thereby reducing patient burden compared to the traditional food-effect study design. Future microtracer food-effect studies should account for sample size, anticipated effect-size of food-effect, and (unexplained) variability during study design. Lastly, the schedule for the collection of blood samples should be reviewed critically since the feasibility study demonstrated robustness of the estimation of food-effect with a reducing number of blood samples collected after peak concentration.

## REFERENCES

1. Parsad S, Ratain MJ (2017) Food Effect Studies for Oncology Drug Products. *Clin Pharmacol Ther* 101 (5):606-612. doi:10.1002/cpt.610
2. Singh BN, Malhotra BK (2004) Effects of food on the clinical pharmacokinetics of anticancer agents: underlying mechanisms and implications for oral chemotherapy. *Clin Pharmacokinet* 43 (15):1127-1156. doi:10.2165/00003088-200443150-00005
3. Farha M, Masson E, Tomkinson H, Mugundu G (2019) Food Effect Study Design With Oral Drugs: Lessons Learned From Recently Approved Drugs in Oncology. *J Clin Pharmacol* 59 (4):463-471. doi:10.1002/jcph.1351
4. European Medicines Agency (EMA) (2012) Guideline on the investigation of drug interactions [https://www.ema.europa.eu/en/documents/scientific-guideline/guideline-investigation-drug-interactions-revision-1\\_en.pdf](https://www.ema.europa.eu/en/documents/scientific-guideline/guideline-investigation-drug-interactions-revision-1_en.pdf). Accessed 14 July 2022
5. US Food and Drug Administration (FDA) (2002) Food effect bioavailability and fed bioequivalence studies Accessed 14 July 2022
6. de Las Heras B, Bouyoucef-Cherchalli D, Reeve L, Reichl A, Mandarino D, Flach S, Vidal L, van Brummelen EMJ, Steeghs N (2022) Healthy volunteers in first-in-human oncology drug development for small molecules. *Br J Clin Pharmacol* 88 (4):1773-1784. doi:10.1111/bcp.15092
7. Kinoshita K, Asoh K, Furuichi N, Ito T, Kawada H, Hara S, Ohwada J, Miyagi T, Kobayashi T, Takanashi K, Tsukaguchi T, Sakamoto H, Tsukuda T, Oikawa N (2012) Design and synthesis of a highly selective, orally active and potent anaplastic lymphoma kinase inhibitor (CH5424802). *Bioorg Med Chem* 20 (3):1271-1280. doi:10.1016/j.bmc.2011.12.021
8. Hirota T, Muraki S, Ieiri I (2019) Clinical Pharmacokinetics of Anaplastic Lymphoma Kinase Inhibitors in Non-Small-Cell Lung Cancer. *Clin Pharmacokinet* 58 (4):403-420. doi:10.1007/s40262-018-0689-7
9. Morcos PN, Guerini E, Parrott N, Dall G, Blotner S, Bogman K, Sturm C, Balas B, Martin-Facklam M, Phipps A (2017) Effect of Food and Esomeprazole on the Pharmacokinetics of Alectinib, a Highly Selective ALK Inhibitor, in Healthy Subjects. *Clin Pharmacol Drug Dev* 6 (4):388-397. doi:10.1002/cpdd.296
10. Roosendaal J, Rosing H, Beijnen JH (2020) Stable Isotopically Labeled Intravenous Microdose Pharmacokinetic Trials as a Tool to Assess Absolute Bioavailability: Feasibility and Paradigm to Apply for Protein Kinase Inhibitors in Oncology. *Clin Pharmacol Drug Dev* 9 (5):552-559. doi:10.1002/cpdd.840
11. US Food and Drug Administration (FDA). Pharmacokinetics: Guidance of the Industry. (2019). Accessed 12 December 2021
12. Groenland SL, Geel DR, Janssen JM, de Vries N, Rosing H, Beijnen JH, Burgers JA, Smit EF, Huitema ADR, Steeghs N (2021) Exposure-Response Analyses of Anaplastic Lymphoma Kinase Inhibitors Crizotinib and Alectinib in Non-Small Cell Lung Cancer Patients. *Clin Pharmacol Ther* 109 (2):394-402. doi:10.1002/cpt.1989
13. European Medicines Agency (EMA). Alecensa assessment report (2016). Accessed December 12 2021

14. Yang JC, Ou SI, De Petris L, Gadgeel S, Gandhi L, Kim DW, Barlesi F, Govindan R, Dingemans AC, Crino L, Lena H, Popat S, Ahn JS, Dansin E, Golding S, Bordogna W, Balas B, Morcos PN, Zeaiter A, Shaw AT (2017) Pooled Systemic Efficacy and Safety Data from the Pivotal Phase II Studies (NP28673 and NP28761) of Alectinib in ALK-positive Non-Small Cell Lung Cancer. *J Thorac Oncol* 12 (10):1552-1560. doi:10.1016/j.jtho.2017.06.070
15. Boons C, den Hartog YM, Janssen J, Zandvliet AS, Vos RM, Swart EL, Hendrikse NH, Hugtenburg JG (2020) Food-effect study of nilotinib in chronic myeloid leukaemia (NiFo study): Enabling dose reduction and relief of treatment burden. *Eur J Haematol* 105 (2):148-155. doi:10.1111/ejh.13418
16. Omachi F, Kaneko M, Iijima R, Watanabe M, Itagaki F (2019) Relationship between the effects of food on the pharmacokinetics of oral antineoplastic drugs and their physicochemical properties. *J Pharm Health Care Sci* 5:26. doi:10.1186/s40780-019-0155-1
17. Custodio JM, Wu CY, Benet LZ (2008) Predicting drug disposition, absorption/elimination/transporter interplay and the role of food on drug absorption. *Adv Drug Deliv Rev* 60 (6):717-733. doi:10.1016/j.addr.2007.08.043
18. Groenland SL, van Nuland M, Bergman AM, de Feijter JM, Dezentje VO, Rosing H, Beijnen JH, Huitema ADR, Steeghs N (2020) Concomitant intake of abiraterone acetate and food to increase pharmacokinetic exposure: real life data from a therapeutic drug monitoring programme. *Eur J Cancer* 130:32-38. doi:10.1016/j.ejca.2020.02.012
19. Given BA, Spoelstra SL, Grant M (2011) The challenges of oral agents as antineoplastic treatments. *Semin Oncol Nurs* 27 (2):93-103. doi:10.1016/j.soncn.2011.02.003
20. Spoelstra SL, Given BA, Given CW, Grant M, Sikorskii A, You M, Decker V (2013) An intervention to improve adherence and management of symptoms for patients prescribed oral chemotherapy agents: an exploratory study. *Cancer Nurs* 36 (1):18-28. doi:10.1097/NCC.0b013e3182551587
21. Deng J, Zhu X, Chen Z, Fan CH, Kwan HS, Wong CH, Shek KY, Zuo Z, Lam TN (2017) A Review of Food-Drug Interactions on Oral Drug Absorption. *Drugs* 77 (17):1833-1855. doi:10.1007/s40265-017-0832-z
22. Koch KM, Reddy NJ, Cohen RB, Lewis NL, Whitehead B, Mackay K, Stead A, Beelen AP, Lewis LD (2009) Effects of food on the relative bioavailability of lapatinib in cancer patients. *J Clin Oncol* 27 (8):1191-1196. doi:10.1200/jco.2008.18.3285
23. Devriese LA, Koch KM, Mergui-Roelvink M, Matthys GM, Ma WW, Robidoux A, Stephenson JJ, Chu QS, Orford KW, Cartee L, Botbyl J, Arya N, Schellens JH (2014) Effects of low-fat and high-fat meals on steady-state pharmacokinetics of lapatinib in patients with advanced solid tumours. *Invest New Drugs* 32 (3):481-488. doi:10.1007/s10637-013-0055-4

## SUPPLEMENTARY MATERIAL

**Supplementary Table S1.** Demographic data of patients with ALK<sup>+</sup> non-small cell lung cancer who were included in the dataset used for development of the population pharmacokinetic model [14].

Number of patients	138
Median age (range, years)	52 (22-79)
Sex, n (%)	
Male	61 (44)
Female	77 (56)
ECOG PS, n (%)	
0	44 (32)
1	81 (59)
2	13 (9)
Race, n (%)	
White	93 (67)
Asian	36 (26)
Other	4 (3)
Black/African American	1 (0.7)
Multiple	0 (0)
Unknown	3 (2)
American Indian/Alaska native	1 (0.7)
CNS metastases, n (%)	
Yes	84 (61)
No	54 (39)
Histologic subtype, n (%)	
Adenocarcinoma	133 (95)
Other	5 (4)
Prior chemotherapy, n (%)	
Yes	110 (80)
No	28 (20)
Crizotinib + prior therapies	
Crizotinib only	28 (20)
+1 therapy	52 (38)
+2 therapies	16 (12)
+3 therapies	17 (12)
+4 therapies	16 (12)
+5 therapies	4 (3)
≥6 therapies	5 (4)
Smoking status	
Active smoker	3 (2)
Past smoker	39 (28)
Never-smoker	96 (70)

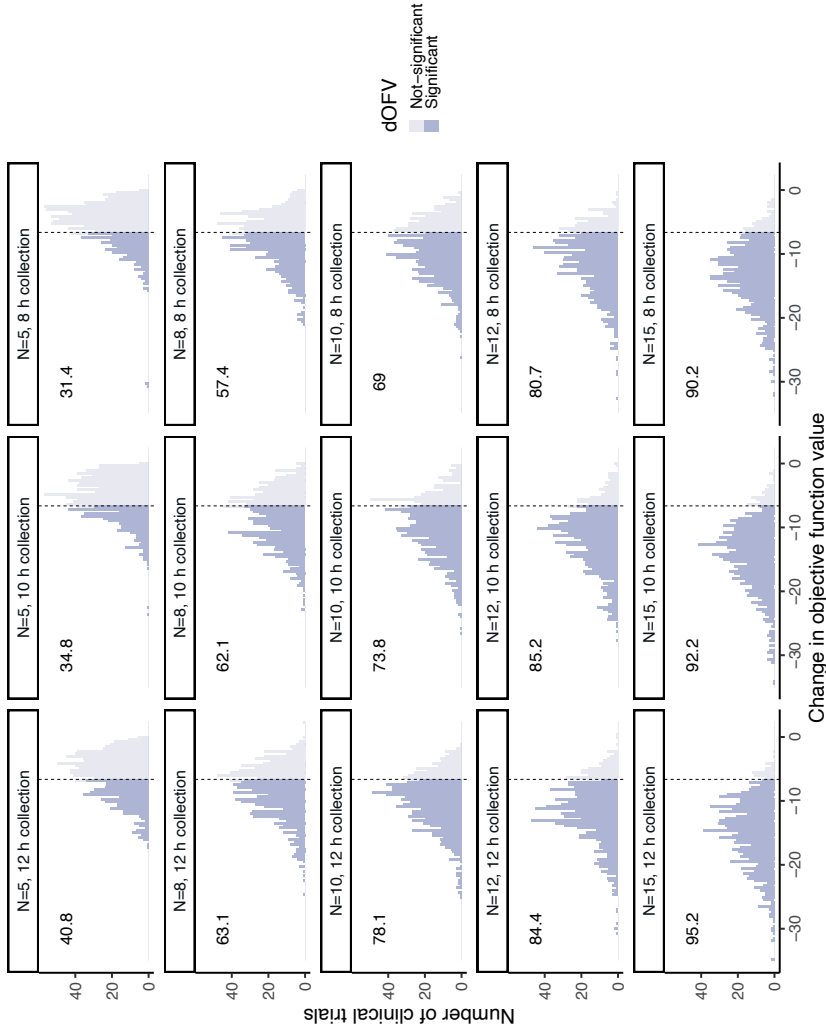
**Supplementary Table S2.** The parameter estimation used for simulation of the microtracer pharmacokinetics.

<b>Fixed effects</b>	<b>Parameter estimate</b>
Cl/F (L/h)	81.9
V/F (L)	4016
Ka (h <sup>-1</sup> )	1.30
D1 (h)	3.44
F (fed conditions)	1
F (fasted conditions)	0.714*
<b>Inter-individual variability</b>	
IIV Cl/F	0.162
IIV Vd/F	0.161
IIV Ka	0.398
IIV D1	0.178
Covariance Cl/F ~ Vd/F	0.0787
IOV	0.0064*
<b>Residual error</b>	
Proportional error	0.0361
Additional error	0 FIXED

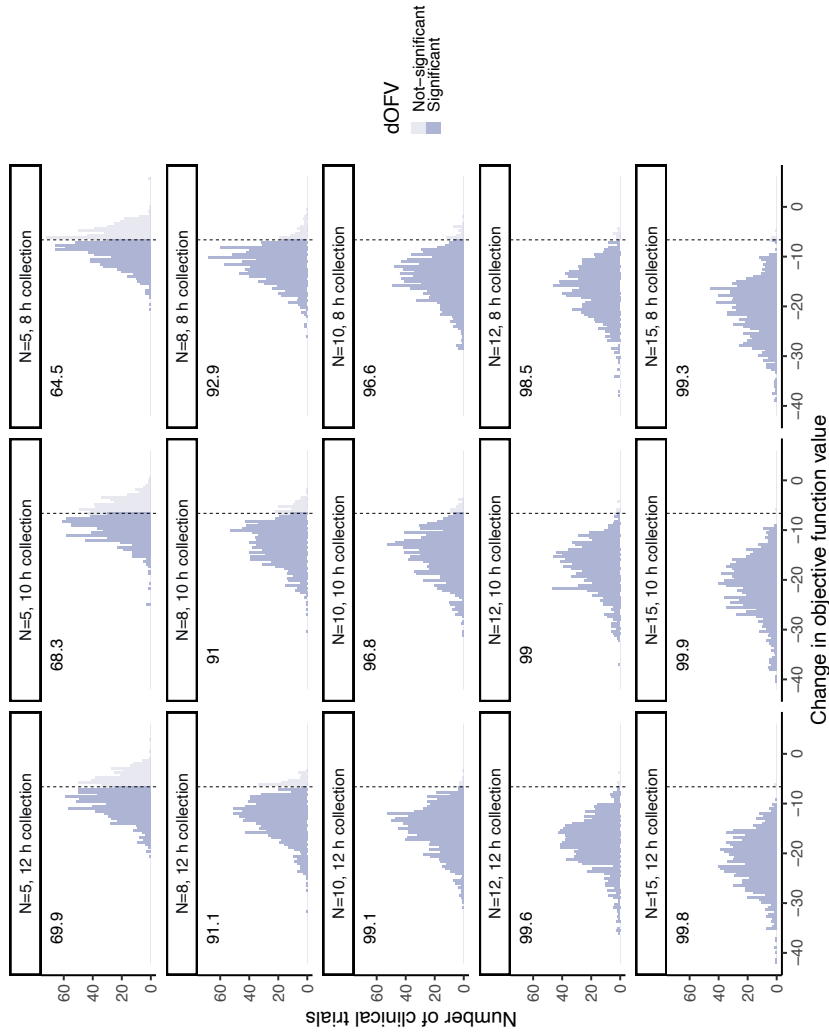
Abbreviations: IIV – inter-individual variability, IOV – inter-occasion variability.

\* These parameters were added to the model for the clinical trial simulation.

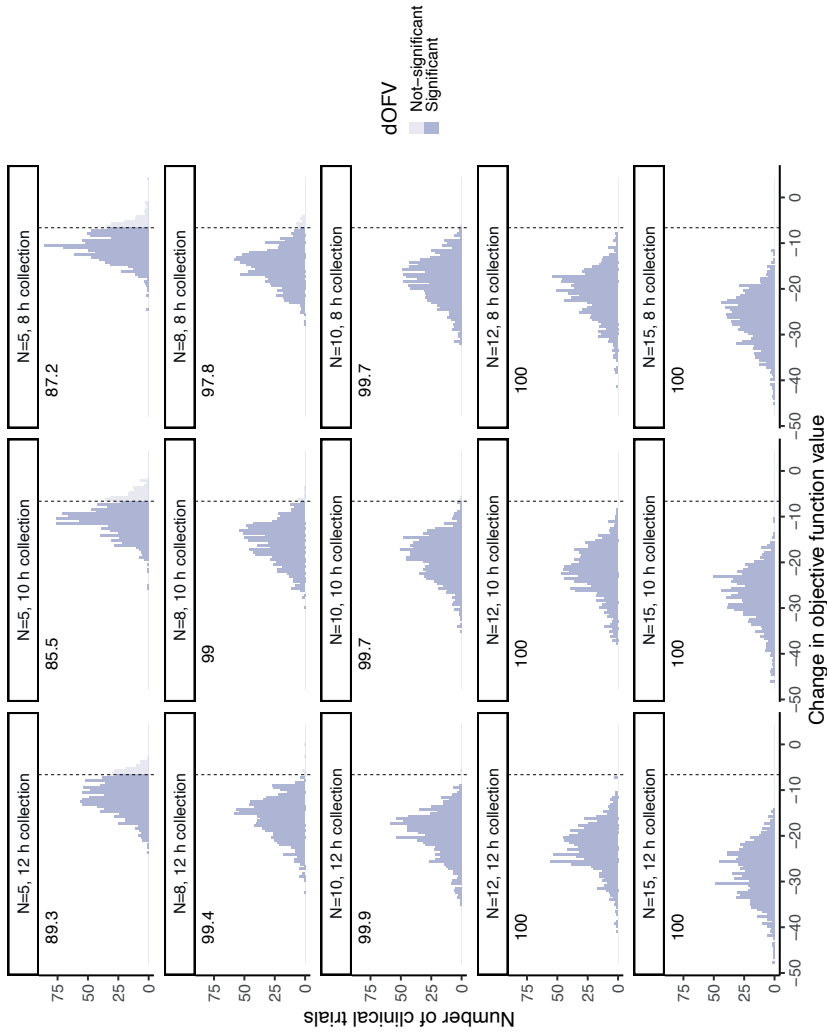




**Supplementary Figure S1.** Power calculation for changing sample sizes and sample collection schedules for a food-effect of 20%. The time of sample collection represents the last sample collected before the collection of the 24 hour sample. The dashed line is de threshold of significance with a value of -6.63. The number is the calculated power. Abbreviation: dOFV, difference in objective function value.



**Supplementary Figure S2.** Power calculation for changing sample sizes and sample collection schedules for a food-effect of 30%. The time of sample collection represents the last sample collected before the collection of the 24 hour sample. The dashed line is de threshold of significance with a value of -6.63. The number is the calculated power. Abbreviation: dOFV, difference in objective function value.



**Supplementary Figure S3.** Power calculation for changing sample sizes and sample collection schedules for a food-effect of 40%. The time of sample collection represents the last sample collected before the collection of the 24 hour sample. The dashed line is de threshold of significance with a value of -6.63. The number is the calculated power. Abbreviation: dOFV difference in objective function value.

**NONMEM code**

```
$SUBROUTINES ADVAN2 TRANS2
```

```
$ABBREVIATED
```

```
REPLACE ETA(OCC_F1)=ETA(5,6) ;Interoccasion variability on bioavailability
```

```
$PK
```

```
; Clearance
```

```
TVCL = THETA(1)*(WT/70)**0.75
```

```
CL = TVCL * EXP(ETA(1))
```

```
;Volume of distribution
```

```
TVV = THETA(2)*(WT/70)**1
```

```
V = TVV * EXP(ETA(2))
```

```
;Absorption parameters
```

```
KA = THETA(3) * EXP(ETA(3)) ;First-order absorption constant
```

```
D1 = THETA(4) * EXP(ETA(4)) ;Zero-order absorption
```

```
;Bioavailability food-effect + interoccasion variability
```

```
F1=THETA(5)*EXP(ETA(OCC_F1)) ;F for occasion 1
```

```
IF(FLAG.EQ.1) F1=THETA(6)*EXP(ETA(OCC_F1)) ;F for occasion 2 with 40% food-effect
```

```
;Elimination rate constant
```

```
K = CL/V
```

```
;Scaling of the model
```

```
S2 = V
```

```
$ERROR
```

```
Y = F*(1+EPS(1))+EPS(2)
```

```
IPRED = F
```

```
REPI = IREP
```

```
$THETA
```

```
(0, 81.9) ;CL (L/h)
```

```
(0, 4016) ;V (L)
```

```
(0, 1.30) ;KA (-h)
```

```
(0, 3.44) ;D1 (h)
```

```
1 FIX ;F for fed conditons
```

```
1 FIX ;F for fasted conditions
```

```
$OMEGA BLOCK(2)
(0, 0.162) ;Cl/F IIV
(0, 0.07865012) (0,0.161) ;Vd IIV

$OMEGA
(0,0.398) ;Ka IIV
(0, 0.178) ;D1 IIV

;IOV
$OMEGA BLOCK(1)
(0, 0.0064) ;IOV F2
$OMEGA BLOCK(1) SAME ;IOV F2

$SIGMA
(0, 0.0361) ;Prop.
0 FIX ;Add (ug/L)
```



# Chapter 4

## **The use of microdosing for in vivo phenotyping of Cytochrome P450: Where do we stand?**

*Submitted*

Lisa T. van der Heijden  
Frans L. Opdam  
Jos H. Beijnen  
Alwin D.R. Huitema

## ABSTRACT

Cytochrome P450 (CYP) enzymes play a central role in the elimination of approximately 80% of all clinically used drugs. Differences in CYP enzyme activity between individuals can contribute to inter-individual variability in exposure and, therefore, treatment outcome. *In vivo* CYP enzyme activity could be determined with phenotyping. Currently, (sub)therapeutic doses are used for *in vivo* phenotyping, which can lead to side effects. The use of microdoses (100 µg) for *in vivo* phenotyping for CYP enzymes could overcome the limitations associated with the use of (sub)therapeutic doses of substrates. The aim of this review is to provide a critical overview of the application of microdosing for *in vivo* phenotyping of CYP enzymes. Based on the currently available evidence, the use of microdosing for *in vivo* phenotyping for subtypes CYP1A2, CYP2C9, CYP2D6, and CYP2E1 is not recommended. Microdosing can be used for the *in vivo* phenotyping of CYP2C19 and CYP3A. The recommended microdose phenotyping test for CYP2C19 is measuring omeprazole  $AUC_{0-24}$  after administration of a single 100 µg dose. CYP3A activity could be best determined with a 0.1-75 µg dose of midazolam and subsequently measuring  $AUC_{\infty}$  or clearance. Moreover, there are two metrics available for midazolam using a limited sampling strategy:  $AUC_{0-10}$  and  $AUC_{2-4}$ .



## 1 INTRODUCTION

Cytochrome P450 (CYP) enzymes are a large superfamily of haem-containing enzymes that are involved in the metabolism of both endogenous and exogenous compounds [1,2]. CYP enzymes play a role in the metabolism of approximately 80% of all clinical drugs [3]. The activity of CYP enzymes is influenced by many factors such as genetics, age, co-administration of exogenous compounds (e.g., drugs or food), and disease state [4-6]. Due to these factors, there is a large variability in CYP enzyme activity between individuals, which might contribute to heterogeneous therapy outcomes [7]. Dosing of drugs based on CYP enzyme activity can result in more predictable therapy outcome, which can potentially be obtained by *in vivo* phenotyping [8-10].

*In vivo* phenotyping would consist of two steps: (1) The administration of a selective substrate (the probe) of the enzyme, and (2) the quantification of the metric representing enzyme activity. The metric is often a pharmacokinetic metric representing clearance (Cl) or a metabolic pathway [11,12]. While there are currently no guidelines regarding the application of phenotyping, recommendations regarding probe and metric selection could be used from the drug-drug interaction guidelines of the European Medicines Agency (EMA) and US Food and Drug Administration (FDA) [13,14]. The major disadvantage of the currently used phenotyping tests is the use of therapeutic or sub-therapeutic doses. Fuhr, *et al* (2007) formulated a list of validated phenotyping procedures of which all are used in the milligram range [11]. These (sub)therapeutic doses can result in side effects or therapeutic effects, such as (mild) sedation for low dose midazolam or hypoglycaemic effect for low dose tolbutamide [11,15-17].

The use of microdosing within the field of *in vivo* phenotyping could overcome the above-described limitations. A microdose has been defined as 1/100<sup>th</sup> of the anticipated therapeutic dose with a maximum of 100 µg [14]. Due to their low dose, microdoses are assumed to be nontoxic and non-pharmacologically active [18]. Originally microdosing has been used to quickly assess the pharmacokinetics of a new drug prior to Phase I clinical trials [19]. In recent years, the application of microdosing has been extended towards drug-drug interaction studies, site of action studies [20] and recently the application in *in vivo* phenotyping studies has been proposed [20,21]. However, there is still much unknown about the application of microdosing for *in vivo* phenotyping.

The aim of this review is to provide a critical overview of the use of microdosing for *in vivo* phenotyping of CYP enzymes. This review will focus on two aspects of *in vivo* microdose phenotyping tests that need to be considered before the test can be investigated for individualised dosing: 1) The sensitivity of the test to detect changes in CYP enzyme activity and 2) the linearity of the phenotyping metric at microdose level to (sub)-therapeutic level. Lastly, recommendations for *in vivo* phenotyping of CYP enzymes at microdose level will be proposed.

## 2 METHODS

### 2.1 Literature search

The literature search was performed in Pubmed and Embase using the following terms: microdose\*, Phase 0, microgram dose, phenotyp\*, drug-drug interactions, drug interactions, human microdosing trials, cytochrome P-450 enzyme. The search was performed on June 23<sup>rd</sup>, 2023. Results were restricted to the English language and studies in humans. Additional studies were selected from review articles and reviewing the reference section of each article (citation snowballing). Initial selection was based on title and abstract, while inclusion was determined by full-text assessment. Continuing, studies were included when pharmacokinetic outcomes of phenotyping and/or drug interactions were available. Microtracer trials were excluded from this review as the total administrated dose exceeds the maximum dose definition of a microdose (>100 µg) [22].

### 2.2 Sensitivity of *in vivo* phenotyping methods

Before a phenotyping test can be used for individualised dosing, the test needs to be validated at the microdose level to ensure that it reflects the enzyme activity in many different settings [11]. A frequently used method to determine the sensitivity of a phenotyping method is to measure the phenotyping metric under three conditions: (1) Baseline (or control) where the metric is quantified in the absence of any factors influencing the enzyme, (2) inhibition where an inhibitor of the enzyme is co-administered with the probe, and (3) induction where an inductor of the enzyme is co-administered with the probe. The phenotyping method is considered sensitive to the respective enzyme activity when the metric significantly changes during inhibition and induction enzyme compared to baseline.

Four different levels of evidence level were defined: A) Similar fold-change in the phenotyping metric at microdose level and therapeutic level for inhibition and induction of the CYP enzyme, B) Significant difference in the metric at microdose level between baseline and inhibition/induction, C) Difference in metric at microdose level between baseline and inhibition/induction but no statistics were performed, D) No significant difference in metric at microdose level between baseline and inhibition/induction. An evidence level of A and B for probe sensitivity indicates that the phenotyping method can be used for *in vivo* phenotyping at microdose level, level C indicates that there is a potential use for the phenotyping method at microdose level, and level D indicates that the probe-metric combination is not suitable for *in vivo* phenotyping at microdose level.

### 2.3 Pharmacokinetic scalability

The scalability of microdose pharmacokinetics was determined by comparing pharmacokinetic parameters of the microdose to the pharmacokinetic parameters of the therapeutic dose. For the area-under-the-concentration-curve (AUC) the value extrapolated to infinity in ng\*h/mL was used, unless otherwise denoted, and presented dose-adjusted to 100 µg. Furthermore, the clearance (Cl) was reported in L/h (apparent Cl for oral administration), volume of distribution ( $V_d$ ) in L (apparent  $V_d$  for oral administration), and half-life ( $t_{1/2}$ ) in hours. Pharmacokinetic data from single microdose studies were completed with literature data from therapeutic pharmacokinetic studies. Microdose pharmacokinetics were considered predictive if the mean observed values of the microdose and of the therapeutic dose were within a two-fold. The two-fold criterion is commonly used criterion of microdose predictability and originates from allometry [23,24]. Two previously reported reviews have reported a predictability of 62% (n=25) and 68% (n=41) for orally administered drugs [22,25].

In this review, four evidence levels of scalability were defined: A) High scalability: All pharmacokinetic parameters of parent and metabolite fell within the two-fold criterion, B) Good scalability: All pharmacokinetic parameters of either parent or metabolite fell within the two-fold criterion, C) Moderate scalability: The metric used for phenotyping fell within the two-fold criterion, D) Poor scalability: None of the pharmacokinetic parameters fell within the two-fold criterion or the metric used for phenotyping falls outside the two-fold criterion. Evidence level A and B indicates that results of *in vivo* phenotyping at microdose level could be extrapolated to therapeutic dose for data interpretation, level C indicates that the results of *in vivo* phenotyping might be extrapolated from microdose level to therapeutic dose level if the respective metric is sensitive to changes in CYP enzyme activity, and D) indicates that the results of *in vivo* phenotyping at microdose level could not be extrapolated to therapeutic dose level. Good scalability allows the use of phenotyping metrics at therapeutic level for comparison with the phenotyping metrics at microdose level. This is relevant since there is more information available of metric performance at different clinical settings at therapeutic level compared to microdose level.

## 3 RESULTS

### 3.1 Included literature

A total of 25 out of 827 retrieved articles were included in the current review. Of these 20 articles, 10 articles reported the sensitivity of 20 *in vivo* microdose phenotyping tests with 8 different probes and for 6 different CYP enzymes [21,26-30]. These articles are summarised in Supplementary Table S1. Continuing, 17 articles were included for the evaluation of scalability of microdose pharmacokinetics to therapeutic level [28,29,31-39]. Details of the comparison between microdose and therapeutic pharmacokinetics are described in Supplementary Table S2 for studies containing both microdose and therapeutic data and Supplementary Table S3 for studies describing only microdose pharmacokinetics. The later studies were completed with studies reporting therapeutic pharmacokinetics. The evidence levels for sensitivity and scalability for each microdose phenotyping test are reported in Table 1.

### 3.2 Cytochrome P450 enzymes

#### 3.2.1 CYP1A2

##### 3.2.1.1 Caffeine

Caffeine is recommended as a probe for CYP1A2 activity by the EMA due to its predominant metabolism by CYP1A2 to paraxanthine at therapeutic levels [13,40]. At microdose levels, the AUC extrapolated to infinity ( $AUC_{\infty}$ ) of caffeine was sensitive to CYP1A2 inhibition, but this effect was smaller compared to the effect at therapeutic level (8.1-fold vs 13.7-fold, respectively) [21,41]. The authors did not report any hypothesis regarding the observed difference, but it could possibly be caused by difference in study design, participant populations, or a concentration-dependent contribution of CYP1A2 to the metabolism of caffeine. Currently, there is no information available about the sensitivity of CYP1A2 induction. The extrapolation of microdose metrics to therapeutic level is complicated due to the difference in effect size between the two dosing levels despite the linear pharmacokinetics (0.25-250 mg) [21,41-43]. Therefore, sensitivity data of the  $AUC_{\infty}$  of a caffeine microdose to induction needs to be obtained before clinical application (Table 1).

#### 3.2.2 CYP2C9

##### 3.2.2.1 Glibenclamide

Glibenclamide is predominantly metabolized by CYP2C9 into its two main metabolites: 4'-hydroxy glibenclamide and 3'-hydroxy glibenclamide [44]. There is no information available about sensitivity of phenotyping metrics to inhibition or induction of CYP2C9. However, a genotyping study reported difference in  $AUC_{\infty}$  and  $t_{1/2}$  of a glibenclamide microdose between genotypes indicating a possible use

as a microdose phenotyping probe [33]. The pharmacokinetics of glibenclamide was moderate to poorly scalable from 10 µg to 2.5 mg [33,44,45]. Taken together, sensitivity of metrics at microdose level during enzyme inhibition and induction needs to be established before clinical application (Table 1).

#### 3.2.2.2 Losartan

The major metabolic route for losartan is its metabolism by CYP2C9 into the E3174 metabolite [46]. There is no information available about the sensitivity of phenotyping metrics at microdose level. The scalability of losartan pharmacokinetics over a dosing range of 100 µg to 50 mg was considered good in both healthy volunteers and hypertensive patients (See supplementary Table 2) [47]. Before losartan can be used for *in vivo* phenotyping at microdose level the sensitivity of the phenotyping metric to changes in CYP2C9 needs to be investigated at microdose level.

#### 3.2.2.3 Tolbutamide

Tolbutamide is a recommended probe by the EMA due to its predominant metabolism by CYP2C9 to 4'-hydroxy tolbutamide [13,48]. The AUC<sub>∞</sub> of tolbutamide appears to be sensitive to CYP2C9 inhibition at microdose level since inhibition resulted in an increase in AUC<sub>∞</sub> of 1.8-fold but the change from baseline was not significant [21]. This was attributed to use of moderate CYP2C9 inhibitors (ketoconazole and fluvoxamine) [21]. There is no information available about the sensitivity of AUC<sub>∞</sub> to CYP2C9 induction at microdose level. Continuing, the pharmacokinetics was good scalable over a dosing range of 25 µg to 125 mg [49]. Summarising, sensitivity studies at microdose level needs to be performed before tolbutamide could be considered as a CYP2C9 probe at microdose level.

#### 3.2.2.4 Warfarin

S-warfarin is recommended as a probe for CYP2C9 activity at therapeutic level by the EMA [13]. Currently, there is no evidence available if phenotyping metrics for S-warfarin are sensitivity at microdose level. A microdose genotyping study did not find any significant differences in warfarin pharmacokinetics between different genotypes, indicating that warfarin might not be a sensitive probe for CYP2C9 activity at microdose level [33]. The authors reported quantification of racemic warfarin instead of (S)-warfarin and an incomplete capture of the pharmacokinetics as possible causes of this result [33]. Furthermore, the pharmacokinetics of warfarin were moderately scalable from microdose level to therapeutic level (Supplementary Table S3) [31,33,50,51]. In conclusion, sensitivity studies at microdose level need to be performed before a warfarin microdose could be used for *in vivo* phenotyping (Table 1).

### 3.2.3 CYP2C19

#### 3.2.3.1 Lansoprazole

The predominant metabolic pathway for lansoprazole is its 5-hydroxylation by CYP2C19 to 5'-hydroxy lansoprazole [52]. Currently, there is no sensitivity information at microdose level available but results from a pharmacogenetic-pharmacokinetic study suggests the possible sensitivity of lansoprazole  $AUC_{\infty}$  to changes in CYP2C19 activity [33]. The pharmacokinetics of lansoprazole demonstrated non-linearity over a dosing range of 50  $\mu\text{g}$  to 30 mg (evidence level D) [33,53]. Concluding, sensitivity studies at microdose studies are needed before the application of lansoprazole as a microdose probe (Table 1).

#### 3.2.3.2 Omeprazole

Due to omeprazole's good selectivity for CYP2C19 and its tolerability, it is recommended as a CYP2C19 probe by the EMA at therapeutic level [13]. At microdose level the  $AUC_{0-24}$  is sensitive to inhibition and induction of CYP2C19 [26]. The effect size at microdose level on  $AUC_{0-24}$  during both inhibition and induction of the enzyme was similar to therapeutic level (evidence level A; Table 1) [26]. Furthermore, the pharmacokinetics of omeprazole was non-linear over a dosing range of 100  $\mu\text{g}$  to 20 mg (evidence level D) [26]. This non-linearity was attributed to metabolic saturation [26]. Taken together, a microdose of 100  $\mu\text{g}$  omeprazole is suitable as an *in vivo* phenotyping trope of CYP2C19 (Table 1).

### 3.2.4 CYP2D6

#### 3.2.4.1 Yohimbine

Yohimbine has been investigated as a probe for CYP2D6. At microdose level yohimbine  $AUC_{\infty}$ , Cl/F and metabolic ratio of yohimbine to 11-hydroxy yohimbine seemed to be sensitive to inhibition and induction of CYP2D6 [54,55]. While the fold-difference in pharmacokinetic parameters at microdose was smaller compared to the therapeutic dose and no statistical tests were conducted. The pharmacokinetic parameters of yohimbine were not well scalable from microdose to therapeutic dose, while the metabolic ratio of yohimbine to 11-hydroxy yohimbine was well scalable (Supplementary Table S2) [54]. This was credited to the high variability in yohimbine pharmacokinetics [54]. Concluding, sensitivity to changes in CYP2D6 activity needs to be established at microdose level before yohimbine could be considered as a microdose probe.

**Table 1.** Overview of probes and metrics available for in vivo phenotyping of Cytochrome P450 enzymes and the evidence level for their application.

Enzyme	Probe	Dose (µg)	Route of ad.	Metric	Evidence level	
					Sens.	PK
<b>CYP1A2</b>	Caffeine	25	PO	AUC <sub>∞</sub>	B	B
<b>CYP2C9</b>	Glibenclamide	10	PO	AUC <sub>∞</sub>	NA	C/D
	Losartan	100	PO	AUC <sub>∞</sub>	NA	B
	Tolbutamide	25	PO	AUC <sub>∞</sub>	D	B
	Warfarin	10-100	PO	AUC <sub>∞</sub>	NA	C
<b>CYP2C19</b>	Lansoprazole	50-70	PO	AUC <sub>∞</sub>	NA	D
				Cl/F	NA	D
				AUC 5-OH/LSP	NA	D
Omeprazole	100	PO	AUC <sub>0-24</sub>	A/B	C/D	
<b>CYP2D6</b>	Yohimbine	50	PO	AUC <sub>∞</sub>	C/D	A/B
				AUC YH/11-OH YH	C/D	A/B
				Cl/F	A/C	A/B
<b>CYP2E1</b>	Chlorzoxazone	2.5-50	PO	AUC <sub>∞</sub>	NA	A/B
				Cl/F	NA	A/B
<b>CYP3A4</b>	Apixaban	25	PO	AUC <sub>∞</sub>	A/B	B/C
				Cl/F	A/B	B/C
	Edoxaban	25	PO	AUC <sub>∞</sub>	B	C
				Cl/F	B	C
	Midazolam	75	PO	AUC 1-OH/MDZ	C/D	A/B
				AUC <sub>0-10</sub>	B	A/B
		10	PO	AUC <sub>2-4</sub>	B	A/B
	0.1-75	PO	AUC <sub>∞</sub>	A/B	A/B	
			Cl/F	A/B	A/B	
	3-10	PO	Cl <sub>met</sub>	B	A/B	
Rivaroxaban			25	PO	AUC <sub>∞</sub>	B
	Cl/F	B			NA	



Comment	Recommendation
Only evidence for inhibition	Data is needed about performance of AUC <sub>∞</sub> during enzyme induction
No information about sensitivity	Sensitivity studies at microdose level need to be performed
No information about sensitivity	Sensitivity studies at microdose level need to be performed
Only evidence for inhibition	Sensitivity studies at microdose level need to be performed
No information about sensitivity	Sensitivity studies at microdose level need to be performed
Difference in enzyme activity between genotypes	Sensitivity studies at microdose level need to be performed
	Suitable for <i>in vivo</i> phenotyping at microdose level
	Sensitivity studies at microdose level need to be performed
	Sensitivity studies at microdose level need to be performed
	Use limited due to affinity for P-gp
No effect of voriconazole	Use limited due to affinity for P-gp
No effect of voriconazole	
Only evidence for inhibition	Not suitable for <i>in vivo</i> phenotyping
Only evidence for inhibition	Suitable for <i>in vivo</i> phenotyping at microdose level
Only evidence for inhibition	Suitable for <i>in vivo</i> phenotyping at microdose level
Dependent on perpetrator dose and route of administration	Suitable for <i>in vivo</i> phenotyping at microdose level
No effect with cyclosporine with or without fluconazole	Suitable for <i>in vivo</i> phenotyping at microdose level
	Suitable for <i>in vivo</i> phenotyping at microdose level
Only evidence for inhibition	Use limited due to affinity for P-gp
Only evidence for inhibition	Use limited due to affinity for P-gp

**Table 1.** Continued.

Enzyme	Probe	Dose ( $\mu\text{g}$ )	Route of ad.	Metric	Evidence level	
					Sens.	PK
	Quinidine	100	PO	$\text{AUC}_{\infty}$	NA	B
AUC 3-OH/QND				NA	B	
AUC N-OX/QND				NA	B	
	Verapamil	100	PO	$\text{AUC}_{\infty}$	NA	A/B
AUC NVP/VPN				NA	A/B	

Abbreviations:  $\text{AUC}_{\infty}$ , area-under-the-concentration-time-curve extrapolated to infinity;  $\text{AUC}_{0-24}$ , AUC from 0 to 24 hours;  $\text{AUC}_{0-10}$ , AUC from 0 to 10 hours;  $\text{AUC}_{2-4}$ , AUC from 2 to 4 hours; AUC YH/11-OH YH, AUC N-OX/QND, AUC of N-oxide quinidine divided by quinidine; AUC NVP/VPN, AUC of norverapamil divided by verapamil; AUC of yohimbine divided by 11-hydroxy yohimbine;

### 3.2.5 CYP2E1

#### 3.2.5.1 Chlorzoxazone

The metabolic ratio of 6'-hydroxy chlorzoxazone and chlorzoxazone is a commonly used metric for CYP2E1 activity [56,57]. At this moment, there is no data available over the sensitivity of the metabolic ratio to perpetrators of CYP2E1 at microdose level. However, chlorzoxazone pharmacokinetics was linear over a dose range from 25  $\mu\text{g}$  to 5 mg [58]. However, sensitivity studies should be performed before the use of chlorzoxazone as a microdose phenotyping test.

### 3.2.6 CYP3A

#### 3.2.6.1 Apixaban

CYP3A is the predominant enzyme in the metabolism of apixaban [59,60]. Both apixaban  $\text{AUC}_{\infty}$  and Cl/F are sensitive to both inhibition and induction of CYP3A4 [27,61-63]. However, these results are complicated since apixaban is also a substrate for P-glycoprotein (P-gp) which is visible in the increase in  $\text{AUC}_{\infty}$  after co-administration with rifampicin (a CYP3A4 inducer and P-gp inhibitor; Supplementary table S1) [27]. The pharmacokinetics of apixaban was moderately scalable over a dosing range of 25  $\mu\text{g}$  to 10 mg [27,61,63]. While apixaban  $\text{AUC}_{\infty}$  and Cl/F and are sensitive to changes in CYP3A activity, the interpretation of the metrics was complicated by the affinity of apixaban for P-gp.

Comment	Recommendation
	Sensitivity studies at microdose level need to be performed
	Sensitivity studies at microdose level need to be performed
	Sensitivity studies at microdose level need to be performed
	Sensitivity studies at microdose level need to be performed
	Sensitivity studies at microdose level need to be performed

AUC 1-OH/MDZ, AUC of 1'-hydroxy midazolam divided by midazolam; AUC 3-OH/QND, AUC of 3-hydroxy quinidine divided by quinidine; AUC 5-OH/LSP, AUC of 5-hydroxy lansoprazole divided by lansoprazole; Cl/F, apparent clearance; NA, not available; PK, pharmacokinetics; PO, oral administration; Route of Ad., route of administration; Sens., sensitivity.

### 3.2.6.2 Edoxaban

Edoxaban is predominantly metabolized by CYP3A into several different metabolites [64,65]. While edoxaban AUC<sub>∞</sub> and Cl/F are sensitive to changes in CYP3A activity (evidence level B), the phenotype interpretation is complicated by edoxaban's affinity for P-gp [27,61]. Continuing, AUC<sub>∞</sub> and Cl/F were insensitive to CYP3A inhibition by voriconazole [27,61]. The pharmacokinetics of edoxaban was moderately scalable over a dosing range of 50 µg to 60 mg [27,61,66]. Concluding, the clinical application of edoxaban as a microdose phenotyping probe is limited by its affinity to P-gp.

### 3.2.6.3 Midazolam

Midazolam is a highly selective probe for CYP3A activity due to its selective metabolism by CYP3A to its main metabolite 1'-hydroxy midazolam [67]. Furthermore, midazolam is a recommended CYP3A probe by the EMA [13]. Of the available phenotyping metrics AUC<sub>∞</sub> and Cl/F had the best evidence for sensitivity (Supplementary Table S1) [7,5,8,9]. The metabolic ratio of 1'-hydroxy midazolam/midazolam is thought to give a more accurate estimation of CYP3A activity and is, therefore, the metric of preference [13].

**Table 2.** Overview of the bioanalytical methods used for the quantification of drug concentrations in the support of in vivo phenotyping of Cytochrome P450 enzymes at microdose level.

Compound	Matrix	Sample volume ( $\mu\text{L}$ )	Internal standard	Sample preparation
Apixaban	Plasma	100	$^{13}\text{C}^2\text{H}_8$ -apixaban	SPE
$^{14}\text{C}$ -caffeine	Plasma	190	Caffeine	PP
Chlorzoxazone <sup>#</sup>	Plasma	500	$^3\text{H}_2$ -chlorzoxazone	LLE
Dextromethorphan <sup>#</sup>	Urine	100	n.r.	LLE
Edoxaban	Plasma	100	$^2\text{H}_6$ -edoxaban	SPE
Glibenclamide	Plasma	200	n.r.	SPE
Lansoprazole <sup>#</sup>	Plasma	100	n.r.	LLE
Losartan	Plasma	1000	Candesartan	LLE
$^{14}\text{C}$ -midazolam	Plasma	190	Midazolam	PP
$^{14}\text{C}$ -midazolam	Plasma	500	Midazolam	LLE
Midazolam <sup>#</sup>	Plasma	250	$^2\text{H}_5$ -midazolam	SPE
Midazolam <sup>#</sup>	Plasma	1000	N-ethyloxazepam	LLE
Midazolam	Plasma	750	Rosuvastatin	SPE
Omeprazole	Plasma	300	Lansoprazole	LLE
Omeprazole	Plasma	100	$^2\text{H}_3$ -omeprazole	PPE
Quinidine <sup>#</sup>	Plasma	500	$^3\text{H}_2$ -Quinidine	PP
Rivaroxaban	Plasma	100	$^{13}\text{C}_6$ -rivaroxaban	SPE
$^{14}\text{C}$ -Tolbutamide	Plasma	190	Tolbutamide	PP
Yohimbine	Plasma	25	$^{13}\text{C}^2\text{H}_3$ -yohimbine	LLE
$^{14}\text{C}$ -warfarin	Plasma	500	Warfarin	LLE
Warfarin	Plasma	200	n.r.	SPE
Verapamil <sup>#</sup>	Plasma	500	$^2\text{H}_6$ -verapamil hydroxide	PP

Abbreviations: LLE: Liquid-Liquid Extraction; LLOQ, Lower Limit of Quantification; n.r., not reported; PP: Protein precipitation; SPE = Solid Phase Extraction

<sup>#</sup> Simultaneous quantification of metabolite

Quantification method	Run time (min)	LLOQ (pg/mL)	EMA/FDA <sup>¶</sup>	Ref.
LC-MS/MS	4.5	2.5	Yes	[73,61]
HPLC-AMS	30	5.21	No	[21]
LC-MS/MS	5.5	2.5	Yes	[58]
LC-MS/MS	n.r.	10	No	[33]
LC-MS/MS	4.5	2.5	Yes	[73,61]
LC-MS/MS	n.r.	1	No	[33]
LC-MS/MS	n.r.	10	No	[33]
LC-MS/MS	n.r.	50	No	[74]
HPLC-AMS	30	5.75	No	[21]
HPLC-AMS	NA	0.1 <sup>§</sup>	No	[31]
UHPLC-MS/MS	2.5	0.05	Yes	[75]
Gas chromatography	NA	10	No	[76]
LC-MS/MS	6.5	5-200	No	[29]
LC-MS/MS	2.5	34	No	[26,77]
LC-MS/MS	NA	10	Yes	[78]
LC-MS/MS	4.5	5	No	[71]
LC-MS/MS	4.5	2.5	Yes	[73,61]
HPLC-AMS	30	5.84	No	[21]
LC-MS/MS	3	5	Yes	[54]
HPLC-AMS	20	10 <sup>§</sup>	No	[31]
LC-MS/MS	n.r.	50,000	No	[33]
LC-MS/MS	4.5	1	No	[71]

<sup>§</sup> Lowest measured concentration

<sup>¶</sup> Validated according the guidelines of the European Medicines Agency (EMA) and/or US Food and Drug Administration (FDA) [79,80]

Surprisingly, the metabolic ratio was not sensitive to CYP3A induction [28]. The authors did not comment on this result but concluded that the metabolic ratio determined 30 min after administration correlated well with midazolam Cl/F (Spearman correlation;  $p < 0.005$ ) [13]. Moreover, two metrics that are determined with limited sampling strategies,  $AUC_{0-10}$  and  $AUC_{2-4}$  were investigated. Both of these metrics were found to be sensitive to changes in CYP3A activity at microdose level. Overall, the pharmacokinetics of midazolam can be considered as good scalable over a wide range of doses (0.003-7.5 mg). Concluding, midazolam  $AUC_{\infty}$  and Cl/F are both suitable for *in vivo* phenotyping of CYP3A at microdose level (Table 1).

#### 3.2.6.4 Rivaroxaban

Rivaroxaban is a substrate for both CYP3A and P-gp [68]. The  $AUC_{\infty}$  and Cl/F of rivaroxaban were sensitive to CYP3A inhibition [27,61]. Both  $AUC_{\infty}$  and Cl/F were insensitive to CYP3A4 induction with rifampicin (Supplementary Table S1), probably due to affinity of rivaroxaban for P-gp [27] and a relatively small contribution of CYP3A to the metabolism of rivaroxaban (18% of a dose) [69]. The pharmacokinetics of rivaroxaban were moderately scalable from a dose of 25  $\mu$ g to 20 mg [27,61,36]. In conclusion, the application of rivaroxaban as a microdose phenotyping probe for CYP3A is limited by its affinity for P-gp (Table 1).

#### 3.2.6.5 Quinidine

Quinidine is predominantly metabolized by CYP3A4 and CYP2D6 [70]. There is currently no information about the sensitivity of microdose phenotyping metric for quinidine. Quinidine pharmacokinetics were considered good scalable (0.1-10 mg), while its metabolite quinidine N-oxide was not well scalable (Supplementary Table 2) [71]. Before its application as an *in vivo* phenotyping probe, sensitivity to changes to CYP3A activity at microdose level should be established (Table 1).

#### 3.2.6.6 Verapamil

Verapamil is a substrate for both CYP3A and CYP2C8 enzymes [72]. It is currently unclear if any of the phenotyping metrics of verapamil are sensitive to changes in CYP3A activity. Verapamil had highly scalable pharmacokinetics from a dose of 100  $\mu$ g to 16 mg [71]. Continuing, the metabolic ratio for the main metabolite norverapamil and verapamil was good scalable over the same dosing range [71]. Preferably sensitivity studies should be performed at microdose level before the use of verapamil as *in vivo* microdose phenotyping probe (Table 1).

## 4 DISCUSSION

The suitability of microdosing for *in vivo* phenotyping of CYP enzymes was determined. Sensitivity to changes in enzyme activity (e.g., inhibition/induction) was reported for 7 probes of 5 different CYP enzymes. Metrics of 6 out of 7 probes, were sensitive to changes in CYP enzyme activity. Information about linearity between microdose and therapeutic dose was available for 14 probes, of which 7 demonstrated linear pharmacokinetics. Several recommendations can be made regarding the above-described literature regarding the use of microdosing for the *in vivo* phenotyping for CYP enzymes. Microdosing for *in vivo* phenotyping of CYP1A2, CYP2C9, and CYP2E1 is currently not recommended. For these three enzymes, sensitivity of the probes at microdose levels needs to be established, before their uses could be recommended. However, microdosing can be used for the *in vivo* phenotyping of CYP2C19 and CYP3A4. For CYP2C19 the recommended microdose phenotyping test is the omeprazole  $AUC_{0-24}$  after a 100  $\mu\text{g}$  dose. CYP3A activity could be best determined with an oral 0.1-75  $\mu\text{g}$  dose of midazolam and the midazolam  $AUC_{\infty}$  or Cl. Moreover, there are two metrics available that are determined with a limited sampling strategy:  $AUC_{0-10}$  and  $AUC_{2-4}$ .

There are currently no guidelines on *in vivo* phenotyping of CYP enzymes. However, recommended probes and metrics in the drug-drug interaction guidelines from the EMA and FDA could be used [13,14]. Characteristics of a validated probe are listed in these guidelines, but the use of microdosing for *in vivo* phenotyping is not discussed. Based on the found literature, several recommendations can be defined for the extension of probe validation to microdose level. First, sensitivity of a probe at microdose level seems to be more relevant than linear pharmacokinetics. This is illustrated by omeprazole and tolbutamide (see Table 1). For omeprazole,  $AUC_{0-24}$  is sensitive to changes in CYP2C19 while its pharmacokinetics is not linear, while for tolbutamide the pharmacokinetics is linear, but the phenotyping metric is not sensitive to changes in enzyme activity. Therefore, validation studies need to be performed where the investigational probe is administered as a microdose alone, together with a strong inhibitor of the enzyme, and with a strong inductor of the enzyme. Perpetrators should be chosen based on their strength of inhibition or induction of the enzyme in question [13,14]. Moreover, the dose [81], duration of exposure [14,81,82] and time of administration of the perpetrator [14,81], should be chosen in such a way that the inhibition or induction of the enzyme is maximised. If the probe is meant to be used in a phenotyping cocktail, drug-drug interactions studies at microdose level should be conducted making sure that the individual probes in the cocktail do not influence each other metrics.

The ultimate aim of *in vivo* phenotyping is contribution to individualised dosing by explaining (in part) the variability in drug clearance. There are indications of the clinical relevance of *in vivo* phenotyping. Simvastatin dosing could be improved when CYP3A activity was taken into account [8], accounting for CYP3A phenotype in the dose calculation of irinotecan improved the predictability of the pharmacokinetic and toxicity profile [9] and midazolam Cl was found to be highly correlated with sunitinib exposure and explained a large proportion in the observed inter-patient variability in pharmacokinetics [10]. A second study reported a significant correlation between the metabolic ratio of midazolam and sunitinib but concluded that it did not predict variability in sunitinib clearance sufficiently to be useful in clinical dosing strategy [83]. Of these four studies, only the first study used a microdose for phenotyping [8]. Another study used a microdose cocktail to investigate the influence of renal impairment on the pharmacokinetics of the probes [84]. Lastly, microdosing could also be used to investigate time course of indication or inhibition [85,86].

The clinical application of microdose *in vivo* phenotyping for clinical dosing strategies is enabled by recent advances within the field of bioanalysis. Innovations made it possible to use relatively simple equipment as liquid chromatography tandem mass spectrometry (LC-MS/MS) for the quantification of extreme low plasma concentrations instead of accelerated mass spectrometry (AMS) (see Table 2). The advantages of LC-MS/MS over AMS are the fast data acquisition, the independency of radioactive isotopes and the higher accessibility in laboratories [74]. Another crucial aspect for clinical application is a suitable pharmaceutical formulation for microdose phenotyping test. At present, therapeutic formulations are adjusted such as the dilution of intravenous infusions or dissolving and dilution or oral formulations. However, commercially available microdose formulations are desired to increase the reliability of the administered dose and to increase the accessibility of microdose phenotyping. Furthermore, patient burden of *in vivo* microdose phenotyping tests should be minimised. Limited sampling strategies could reduce the number of blood samples necessary for phenotyping as well as reducing the time spend at the clinic. Single-time concentrations or parent over metabolite concentrations could be investigated [87] or maximum posteriori Bayesian estimation using population pharmacokinetic models could be investigated [88,89]. Moreover, oral administration would be preferable as well as less invasive sample collection methods such as volumetric absorptive microsampling (VAMS) from a finger prick instead of venepuncture.



## 5 CONCLUSION

In this review we questioned whether microdoses could be used for in vivo phenotyping of CYP enzymes. Based on literature, in vivo phenotyping with microdoses is in its infancy. For most CYP enzymes, the use of microdoses for in vivo phenotyping cannot be recommended yet. For most probes information is lacking regarding its sensitivity to changes in enzyme activity at microdose level. However, for phenotyping of CYP2C19, a microdose of 100  $\mu\text{g}$  omeprazole can be administered orally and the  $\text{AUC}_{0-24}$  determined, while for CYP3A4 an oral 0.1-75  $\mu\text{g}$  can be administered and the  $\text{AUC}_{\infty}$  or  $\text{Cl}$  calculated. Furthermore, a midazolam  $\text{AUC}_{0-10}$  or midazolam  $\text{AUC}_{2-4}$  can be considered as metric. For clinical application, more studies are needed regarding the sensitivity of probes at microdose level, the use of in vivo phenotypes in dosing strategies, limited sampling strategies and less invasive sampling methods.

## REFERENCES

1. Rendic S, Guengerich FP (2015) Survey of Human Oxidoreductases and Cytochrome P450 Enzymes Involved in the Metabolism of Xenobiotic and Natural Chemicals. *Chem Res Toxicol* 28 (1):38-42. doi:10.1021/tx500444e
2. Guengerich FP, Waterman MR, Egli M (2016) Recent Structural Insights into Cytochrome P450 Function. *Trends Pharmacol Sci* 37 (8):625-640. doi:10.1016/j.tips.2016.05.006
3. Ingelman-Sundberg M (2004) Human drug metabolising cytochrome P450 enzymes: properties and polymorphisms. *Naunyn Schmiedebergs Arch Pharmacol* 369 (1):89-104. doi:10.1007/s00210-003-0819-z
4. Zanger UM, Schwab M (2013) Cytochrome P450 enzymes in drug metabolism: regulation of gene expression, enzyme activities, and impact of genetic variation. *Pharmacol Ther* 138 (1):103-141. doi:10.1016/j.pharmthera.2012.12.007
5. Hohmann N, Haefeli WE, Mikus G (2016) CYP3A activity: towards dose adaptation to the individual. *Expert Opin Drug Metab Toxicol* 12 (5):479-497. doi:10.1517/17425255.2016.1163337
6. Eichelbaum M, Ingelman-Sundberg M, Evans WE (2006) Pharmacogenomics and individualized drug therapy. *Annu Rev Med* 57:119-137. doi:10.1146/annurev.med.56.082103.104724
7. Song Y, Li C, Liu G, Liu R, Chen Y, Li W, Cao Z, Zhao B, Lu C, Liu Y (2021) Drug-Metabolizing Cytochrome P450 Enzymes Have Multifarious Influences on Treatment Outcomes. *Clin Pharmacokinet* 60 (5):585-601. doi:10.1007/s40262-021-01001-5
8. Stoll F, Burhenne J, Lausecker B, Weiss J, Thomsen T, Haefeli WE, Mikus G (2013) Reduced exposure variability of the CYP3A substrate simvastatin by dose individualization to CYP3A activity. *J Clin Pharmacol* 53 (11):1199-1204. doi:10.1002/jcph.161
9. van der Bol JM, Mathijssen RH, Creemers GJ, Planting AS, Loos WJ, Wiemer EA, Friberg LE, Verweij J, Sparreboom A, de Jong FA (2010) A CYP3A4 phenotype-based dosing algorithm for individualized treatment of irinotecan. *Clin Cancer Res* 16 (2):736-742. doi:10.1158/1078-0432.Ccr-09-1526
10. de Wit D, Gelderblom H, Sparreboom A, den Hartigh J, den Hollander M, König-Quartel JM, Hessing T, Guchelaar HJ, van Erp NP (2014) Midazolam as a phenotyping probe to predict sunitinib exposure in patients with cancer. *Cancer Chemother Pharmacol* 73 (1):87-96. doi:10.1007/s00280-013-2322-7
11. Fuhr U, Jetter A, Kirchheiner J (2007) Appropriate phenotyping procedures for drug metabolizing enzymes and transporters in humans and their simultaneous use in the "cocktail" approach. *Clin Pharmacol Ther* 81 (2):270-283. doi:10.1038/sj.clpt.6100050
12. Streetman DS, Bertino JS, Jr., Nafziger AN (2000) Phenotyping of drug-metabolizing enzymes in adults: a review of in-vivo cytochrome P450 phenotyping probes. *Pharmacogenetics* 10 (3):187-216. doi:10.1097/00008571-200004000-00001
13. European Medicines Agency (EMA) (2012) Guideline on the investigation of drug interactions. Accessed 12 August 2022
14. US Food and Drug Administration (FDA) (2006) Guidance for the industry, investigators and reviewers: exploratory IND studies. . *Biotechnol Law Rep* 25:167-174

15. Donzelli M, Derungs A, Serratore MG, Noppen C, Nezic L, Krahenbuhl S, Haschke M (2014) The basel cocktail for simultaneous phenotyping of human cytochrome P450 isoforms in plasma, saliva and dried blood spots. *Clin Pharmacokinet* 53 (3):271-282. doi:10.1007/s40262-013-0115-0
16. Chainuvati S, Nafziger AN, Leeder JS, Gaedigk A, Kearns GL, Sellers E, Zhang Y, Kashuba AD, Rowland E, Bertino JS, Jr. (2003) Combined phenotypic assessment of cytochrome p450 1A2, 2C9, 2C19, 2D6, and 3A, N-acetyltransferase-2, and xanthine oxidase activities with the "Cooperstown 5+1 cocktail". *Clin Pharmacol Ther* 74 (5):437-447. doi:10.1016/S0009-9236(03)00229-7
17. Doroshenko O, Rokitta D, Zadoyan G, Klement S, Schlafke S, Dienel A, Gramatte T, Luck H, Fuhr U (2013) Drug cocktail interaction study on the effect of the orally administered lavender oil preparation silexan on cytochrome P450 enzymes in healthy volunteers. *Drug Metab Dispos* 41 (5):987-993. doi:10.1124/dmd.112.050203
18. Marchetti S, Schellens JH (2007) The impact of FDA and EMEA guidelines on drug development in relation to Phase 0 trials. *Br J Cancer* 97 (5):577-581. doi:10.1038/sj.bjc.6603925
19. Garner RC, Lappin G (2006) The phase 0 microdosing concept. *Br J Clin Pharmacol* 61 (4):367-370. doi:10.1111/j.1365-2125.2006.02575.x
20. Hohmann N, Haefeli WE, Mikus G (2015) Use of microdose phenotyping to individualise dosing of patients. *Clin Pharmacokinet* 54 (9):893-900. doi:10.1007/s40262-015-0278-y
21. Croft M, Keely B, Morris I, Tann L, Lappin G (2012) Predicting drug candidate victims of drug-drug interactions, using microdosing. *Clin Pharmacokinet* 51 (4):237-246. doi:10.2165/11597070-000000000-00000
22. Lappin G, Noveck R, Burt T (2013) Microdosing and drug development: past, present and future. *Expert Opin Drug Metab Toxicol* 9 (7):817-834. doi:10.1517/17425255.2013.786042
23. Lappin G, Garner RC (2008) The utility of microdosing over the past 5 years. *Expert Opin Drug Metab Toxicol* 4 (12):1499-1506. doi:10.1517/17425250802531767
24. Rowland M (2007) Commentary on ACCP position statement on the use of microdosing in the drug development process. *J Clin Pharmacol* 47 (12):1595-1596; author reply 1597-1598. doi:10.1177/0091270007310548
25. van Nuland M, Rosing H, Huitema ADR, Beijnen JH (2019) Predictive Value of Microdose Pharmacokinetics. *Clin Pharmacokinet* 58 (10):1221-1236. doi:10.1007/s40262-019-00769-x
26. Park GJ, Bae SH, Park WS, Han S, Park MH, Shin SH, Shin YG, Yim DS (2017) Drug-drug interaction of microdose and regular-dose omeprazole with a CYP2C19 inhibitor and inducer. *Drug Des Devel Ther* 11:1043-1053. doi:10.2147/dddt.S131797
27. Mikus G, Foerster KI, Schaumaeker M, Lehmann ML, Burhenne J, Haefeli WE (2020) Application of a microdosed cocktail of 3 oral factor Xa inhibitors to study drug-drug interactions with different perpetrator drugs. *Br J Clin Pharmacol*. doi:10.1111/bcp.14277
28. Eap CB, Buclin T, Cucchia G, Zullino D, Hustert E, Bleiber G, Golay KP, Aubert AC, Baumann P, Telenti A, Kerb R (2004) Oral administration of a low dose of midazolam (75 microg) as an in vivo probe for CYP3A activity. *Eur J Clin Pharmacol* 60 (4):237-246. doi:10.1007/s00228-004-0762-z

29. Maeda K, Ikeda Y, Fujita T, Yoshida K, Azuma Y, Haruyama Y, Yamane N, Kumagai Y, Sugiyama Y (2011) Identification of the rate-determining process in the hepatic clearance of atorvastatin in a clinical cassette microdosing study. *Clin Pharmacol Ther* 90 (4):575-581. doi:10.1038/clpt.2011.142
30. Carls A, Jedamzik J, Witt L, Hohmann N, Burhenne J, Mikus G (2014) Systemic exposure of topical erythromycin in comparison to oral administration and the effect on cytochrome P450 3A4 activity. *Br J Clin Pharmacol* 78 (6):1433-1440. doi:10.1111/bcp.12497
31. Lappin G, Kuhnz W, Jochemsen R, Kneer J, Chaudhary A, Oosterhuis B, Drijfhout WJ, Rowland M, Garner RC (2006) Use of microdosing to predict pharmacokinetics at the therapeutic dose: experience with 5 drugs. *Clinical pharmacology and therapeutics* 80 (3):203-215. doi:10.1016/j.clpt.2006.05.008
32. Halama B, Hohmann N, Burhenne J, Weiss J, Mikus G, Haefeli WE (2013) A nanogram dose of the CYP3A probe substrate midazolam to evaluate drug interactions. *Clinical pharmacology and therapeutics* 93 (6):564-571. doi:10.1038/clpt.2013.27
33. Ieiri I, Fukae M, Maeda K, Ando Y, Kimura M, Hirota T, Nakamura T, Iwasaki K, Matsuki S, Matsuguma K, Kanda E, Deguchi M, Irie S, Sugiyama Y (2012) Pharmacogenomic/pharmacokinetic assessment of a four-probe cocktail for CYPs and OATPs following oral microdosing. *International journal of clinical pharmacology and therapeutics* 50 (10):689-700. doi:10.5414/cp201763
34. Prueksaritanont T, Tatosian DA, Chu X, Railkar R, Evers R, Chavez-Eng C, Lutz R, Zeng W, Yabut J, Chan GH, Cai X, Latham AH, Hehman J, Stypinski D, Brejda J, Zhou C, Thornton B, Bateman KP, Fraser I, Stoch SA (2017) Validation of a microdose probe drug cocktail for clinical drug interaction assessments for drug transporters and CYP3A. *Clin Pharmacol Ther* 101 (4):519-530. doi:10.1002/cpt.525
35. Kiene K, Hayasi N, Burhenne J, Uchitomi R, Sunderhauf C, Schmid Y, Haschke M, Haefeli WE, Krahenbuhl S, Mikus G, Inada H, Huwyler J (2019) Microdosed midazolam for the determination of cytochrome P450 3A activity: Development and clinical evaluation of a buccal film. *Eur J Pharm Sci* 135:77-82. doi:10.1016/j.ejps.2019.05.010
36. Brings A, Lehmann ML, Foerster KI, Burhenne J, Weiss J, Haefeli WE, Czock D (2019) Perpetrator effects of ciclosporin (P-glycoprotein inhibitor) and its combination with fluconazole (CYP3A inhibitor) on the pharmacokinetics of rivaroxaban in healthy volunteers. *Br J Clin Pharmacol* 85 (7):1528-1537. doi:10.1111/bcp.13934
37. Hohmann N, Mikus G, Haefeli WE, Schwenger V, Gattuso G, Barreca D, Weiss J (2019) A follow-up report on potential drug interactions with clemastines: Two single case experiments show no effect on CYP3A-dependent midazolam clearance. *Eur J Pharm Sci* 133:54-58. doi:10.1016/j.ejps.2019.03.013
38. Hohmann N, Reinhard R, Schnaidt S, Witt L, Carls A, Burhenne J, Mikus G, Haefeli WE (2016) Treatment with rilpivirine does not alter plasma concentrations of the CYP3A substrates tadalafil and midazolam in humans. *J Antimicrob Chemother* 71 (8):2241-2247. doi:10.1093/jac/dkw125
39. Woolsey SJ, Beaton MD, Choi YH, Dresser GK, Gryn SE, Kim RB, Tirona RG (2016) Relationships between Endogenous Plasma Biomarkers of Constitutive Cytochrome P450 3A Activity and Single-Time-Point Oral Midazolam Microdose Phenotype in Healthy Subjects. *Basic & clinical pharmacology & toxicology* 118 (4):284-291. doi:10.1111/bcpt.12492

40. Jeppesen U, Loft S, Poulsen HE, Brßen K (1996) A fluvoxamine-caffeine interaction study. *Pharmacogenetics* 6 (3):213-222. doi:10.1097/00008571-199606000-00003
41. Culm-Merdek KE, von Moltke LL, Harmatz JS, Greenblatt DJ (2005) Fluvoxamine impairs single-dose caffeine clearance without altering caffeine pharmacodynamics. *Br J Clin Pharmacol* 60 (5):486-493. doi:10.1111/j.1365-2125.2005.02467.x
42. Perera V, Gross AS, Ku H, McLachlan AJ (2011) Pharmacokinetics of caffeine in plasma and saliva, and the influence of caffeine abstinence on CYP1A2 metrics. *J Pharm Pharmacol* 63 (9):1161-1168. doi:10.1111/j.2042-7158.2011.01326.x
43. Amchin J, Zarycranski W, Taylor KP, Albano D, Klockowski PM (1999) Effect of venlafaxine on CYP1A2-dependent pharmacokinetics and metabolism of caffeine. *J Clin Pharmacol* 39 (3):252-259
44. Lilja JJ, Niemi M, Fredrikson H, Neuvonen PJ (2007) Effects of clarithromycin and grapefruit juice on the pharmacokinetics of glibenclamide. *Br J Clin Pharmacol* 63 (6):732-740. doi:10.1111/j.1365-2125.2006.02836.x
45. Rambiritch V, Naidoo P, Maharaj B, Pillai G (2016) Population pharmacokinetic modeling of glibenclamide in poorly controlled South African type 2 diabetic subjects. *Clin Pharmacol* 8:83-92. doi:10.2147/CPAA.S102676
46. Sica DA, Gehr TW, Ghosh S (2005) Clinical pharmacokinetics of losartan. *Clin Pharmacokinet* 44 (8):797-814. doi:10.2165/00003088-200544080-00003
47. KMRPAG (2009) Microdosing vs. Therapeutic Dosing for Evaluation of Pharmacokinetic Data: A Comparative Study. *J Young Pharmacists* 1 (4):4
48. Bi YA, Mathialagan S, Tylaska L, Fu M, Keefer J, Vildhede A, Costales C, Rodrigues AD, Varma MVS (2018) Organic Anion Transporter 2 Mediates Hepatic Uptake of Tolbutamide, a CYP2C9 Probe Drug. *J Pharmacol Exp Ther* 364 (3):390-398. doi:10.1124/jpet.117.245951
49. Uchida S, Yamada H, Li XD, Maruyama S, Ohmori Y, Oki T, Watanabe H, Umegaki K, Ohashi K, Yamada S (2006) Effects of Ginkgo biloba extract on pharmacokinetics and pharmacodynamics of tolbutamide and midazolam in healthy volunteers. *J Clin Pharmacol* 46 (11):1290-1298. doi:10.1177/0091270006292628
50. Frymoyer A, Shugarts S, Browne M, Wu AH, Frassetto L, Benet LZ (2010) Effect of single-dose rifampin on the pharmacokinetics of warfarin in healthy volunteers. *Clin Pharmacol Ther* 88 (4):540-547. doi:10.1038/clpt.2010.142
51. Chan E, McLachlan AJ, Pegg M, MacKay AD, Cole RB, Rowland M (1994) Disposition of warfarin enantiomers and metabolites in patients during multiple dosing with rac-warfarin. *Br J Clin Pharmacol* 37 (6):563-569. doi:10.1111/j.1365-2125.1994.tb04305.x
52. Pearce RE, Rodrigues AD, Goldstein JA, Parkinson A (1996) Identification of the human P450 enzymes involved in lansoprazole metabolism. *J Pharmacol Exp Ther* 277 (2):805-816
53. Mainz D, Borner K, Koeppe P, Kotwas J, Lode H (2002) Pharmacokinetics of lansoprazole, amoxicillin and clarithromycin after simultaneous and single administration. *J Antimicrob Chemother* 50 (5):699-706. doi:10.1093/jac/dkf172
54. Vay M, Sauter M, Mikus G, Burhenne J (2019) Quantification of microdosed oral yohimbine and its major metabolite in human plasma in the picogram range. *Bioanalysis* 11 (16):1459-1467. doi:10.4155/bio-2019-0129

55. Elbe A, Foerster KI, Blank A, Rose P, Burhenne J, Haefeli WE, Mikus G (2022) Evaluation of CYP2C19 activity using microdosed oral omeprazole in humans. *Eur J Clin Pharmacol* 78 (6):975-987. doi:10.1007/s00228-022-03304-3
56. Lucas D, Ferrara R, Gonzalez E, Bodenez P, Albores A, Manno M, Berthou F (1999) Chlorzoxazone, a selective probe for phenotyping CYP2E1 in humans. *Pharmacogenetics* 9 (3):377-388. doi:10.1097/00008571-199906000-00013
57. Guengerich FP, Kim DH, Iwasaki M (1991) Role of human cytochrome P-450 IIE1 in the oxidation of many low molecular weight cancer suspects. *Chem Res Toxicol* 4 (2):168-179. doi:10.1021/tx00020a008
58. Witt L, Suzuki Y, Hohmann N, Mikus G, Haefeli WE, Burhenne J (2016) Ultrasensitive quantification of the CYP2E1 probe chlorzoxazone and its main metabolite 6-hydroxychlorzoxazone in human plasma using ultra performance liquid chromatography coupled to tandem mass spectrometry after chlorzoxazone microdosing. *J Chromatogr B Analyt Technol Biomed Life Sci* 1027:207-213. doi:10.1016/j.jchromb.2016.05.049
59. Wang L, Zhang D, Raghavan N, Yao M, Ma L, Frost CE, Maxwell BD, Chen SY, He K, Goosen TC, Humphreys WG, Grossman SJ (2010) In vitro assessment of metabolic drug-drug interaction potential of apixaban through cytochrome P450 phenotyping, inhibition, and induction studies. *Drug Metab Dispos* 38 (3):448-458. doi:10.1124/dmd.109.029694
60. Raghavan N, Frost CE, Yu Z, He K, Zhang H, Humphreys WG, Pinto D, Chen S, Bonacorsi S, Wong PC, Zhang D (2009) Apixaban metabolism and pharmacokinetics after oral administration to humans. *Drug Metab Dispos* 37 (1):74-81. doi:10.1124/dmd.108.023143
61. Mikus G, Foerster KI, Schaumaeker M, Lehmann ML, Burhenne J, Haefeli WE (2019) Microdosed Cocktail of Three Oral Factor Xa Inhibitors to Evaluate Drug-Drug Interactions with Potential Perpetrator Drugs. *Clin Pharmacokinet* 58 (9):1155-1163. doi:10.1007/s40262-019-00749-1
62. Frost CE, Byon W, Song Y, Wang J, Schuster AE, Boyd RA, Zhang D, Yu Z, Dias C, Shenker A, LaCreta F (2015) Effect of ketoconazole and diltiazem on the pharmacokinetics of apixaban, an oral direct factor Xa inhibitor. *Br J Clin Pharmacol* 79 (5):838-846. doi:10.1111/bcp.12541
63. Vakkalagadda B, Frost C, Byon W, Boyd RA, Wang J, Zhang D, Yu Z, Dias C, Shenker A, LaCreta F (2016) Effect of Rifampin on the Pharmacokinetics of Apixaban, an Oral Direct Inhibitor of Factor Xa. *Am J Cardiovasc Drugs* 16 (2):119-127. doi:10.1007/s40256-015-0157-9
64. Mikkaichi T, Yoshigae Y, Masumoto H, Imaoka T, Rozehnal V, Fischer T, Okudaira N, Izumi T (2014) Edoxaban transport via P-glycoprotein is a key factor for the drug's disposition. *Drug Metab Dispos* 42 (4):520-528. doi:10.1124/dmd.113.054866
65. Bathala MS, Masumoto H, Oguma T, He L, Lowrie C, Mendell J (2012) Pharmacokinetics, biotransformation, and mass balance of edoxaban, a selective, direct factor Xa inhibitor, in humans. *Drug Metab Dispos* 40 (12):2250-2255. doi:10.1124/dmd.112.046888
66. Parasrampur DA, Mendell J, Shi M, Matsushima N, Zahir H, Truitt K (2016) Edoxaban drug-drug interactions with ketoconazole, erythromycin, and cyclosporine. *Br J Clin Pharmacol* 82 (6):1591-1600. doi:10.1111/bcp.13092

67. Arendt RM, Greenblatt DJ, Garland WA (1984) Quantitation by gas chromatography of the 1- and 4-hydroxy metabolites of midazolam in human plasma. *Pharmacology* 29 (3):158-164. doi:10.1159/000138007
68. Mueck W, Kubitzka D, Becka M (2013) Co-administration of rivaroxaban with drugs that share its elimination pathways: pharmacokinetic effects in healthy subjects. *Br J Clin Pharmacol* 76 (3):455-466. doi:10.1111/bcp.12075
69. Rohr BS, Foerster KI, Blank A, Burhenne J, Mahmoudi M, Haefeli WE, Mikus G (2022) Perpetrator Characteristics of Azole Antifungal Drugs on Three Oral Factor Xa Inhibitors Administered as a Microdosed Cocktail. *Clin Pharmacokinet* 61 (1):97-109. doi:10.1007/s40262-021-01051-9
70. Marcsisin SR, Jin X, Bettger T, McCulley N, Sousa JC, Shanks GD, Tekwani BL, Sahu R, Reichard GA, Sciotti RJ, Melendez V, Pybus BS (2013) CYP450 phenotyping and metabolite identification of quinine by accurate mass UPLC-MS analysis: a possible metabolic link to blackwater fever. *Malar J* 12:214. doi:10.1186/1475-2875-12-214
71. Maeda K, Takano J, Ikeda Y, Fujita T, Oyama Y, Nozawa K, Kumagai Y, Sugiyama Y (2011) Nonlinear pharmacokinetics of oral quinidine and verapamil in healthy subjects: a clinical microdosing study. *Clinical pharmacology and therapeutics* 90 (2):263-270. doi:10.1038/clpt.2011.108
72. Tracy TS, Korzekwa KR, Gonzalez FJ, Wainer IW (1999) Cytochrome P450 isoforms involved in metabolism of the enantiomers of verapamil and norverapamil. *Br J Clin Pharmacol* 47 (5):545-552. doi:10.1046/j.1365-2125.1999.00923.x
73. Foerster KI, Huppertz A, Müller OJ, Rizos T, Tilemann L, Haefeli WE, Burhenne J (2018) Simultaneous quantification of direct oral anticoagulants currently used in anticoagulation therapy. *J Pharm Biomed Anal* 148:238-244. doi:10.1016/j.jpba.2017.10.011
74. Yamane N, Tozuka Z, Kusama M, Maeda K, Ikeda T, Sugiyama Y (2011) Clinical relevance of liquid chromatography tandem mass spectrometry as an analytical method in microdose clinical studies. *Pharm Res* 28 (8):1963-1972. doi:10.1007/s11095-011-0423-8
75. Burhenne J, Halama B, Maurer M, Riedel KD, Hohmann N, Mikus G, Haefeli WE (2012) Quantification of femtomolar concentrations of the CYP3A substrate midazolam and its main metabolite 1'-hydroxymidazolam in human plasma using ultra performance liquid chromatography coupled to tandem mass spectrometry. *Analytical and bioanalytical chemistry* 402 (7):2439-2450. doi:10.1007/s00216-011-5675-y
76. Eap CB, Bouchoux G, Powell Golay K, Baumann P (2004) Determination of picogram levels of midazolam, and 1- and 4-hydroxymidazolam in human plasma by gas chromatography-negative chemical ionization-mass spectrometry. *J Chromatogr B Analyt Technol Biomed Life Sci* 802 (2):339-345. doi:10.1016/j.jchromb.2003.12.014
77. Vittal S, Ganneboina R, Layek B, Trivedi RK, Hotha KK, Bharathi DV, Mullangi R (2009) Highly sensitive method for the determination of omeprazole in human plasma by liquid chromatography-electrospray ionization tandem mass spectrometry: application to a clinical pharmacokinetic study. *Biomed Chromatogr* 23 (4):390-396. doi:10.1002/bmc.1129
78. Mahmoudi M, Foerster KI, Burhenne J, Weiss J, Mikus G, Haefeli WE (2021) Application of Microdosed Intravenous Omeprazole to Determine Hepatic CYP2C19 Activity. *J Clin Pharmacol* 61 (6):789-798. doi:10.1002/jcph.1789

79. US Food and Drug Administration (FDA). FDA Guidance for Industry Bioanalytical Method Validation (2001). Silver Spring, Maryl US Food Drug Adm
80. European Medicines Agency (EMA), Guideline on Bioanalytical Method Validation. Committe for Medicinal Prodsuts for Human Use and European Medicines Agency., Londen. (2011).
81. Rohr BS, Mikus G (2020) Proposal of a Safe and Effective Study Design for CYP3A-Mediated Drug-Drug Interactions. *J Clin Pharmacol* 60 (10):1294-1303. doi:10.1002/jcph.1622
82. Templeton I, Peng CC, Thummel KE, Davis C, Kunze KL, Isoherranen N (2010) Accurate prediction of dose-dependent CYP3A4 inhibition by itraconazole and its metabolites from in vitro inhibition data. *Clin Pharmacol Ther* 88 (4):499-505. doi:10.1038/clpt.2010.119
83. Kloth JS, Klümpen HJ, Yu H, Eechoute K, Samer CF, Kam BL, Huitema AD, Daali Y, Zwinderman AH, Balakrishnar B, Bennink RJ, Wong M, Schellens JH, Mathijssen RH, Gurney H (2014) Predictive value of CYP3A and ABCB1 phenotyping probes for the pharmacokinetics of sunitinib: the ClearSun study. *Clin Pharmacokinet* 53 (3):261-269. doi:10.1007/s40262-013-0111-4
84. Tatosian DA, Yee KL, Zhang Z, Mostoller K, Paul E, Sutradhar S, Larson P, Chhibber A, Wen J, Wang YJ, Lassman M, Latham AH, Pang J, Crumley T, Gillespie A, Marricco NC, Marenco T, Murphy M, Lasseter KC, Marbury TC, Tweedie D, Chu X, Evers R, Stoch SA (2021) A Microdose Cocktail to Evaluate Drug Interactions in Patients with Renal Impairment. *Clin Pharmacol Ther* 109 (2):403-415. doi:10.1002/cpt.1998
85. Nassar YM, Hohmann N, Michelet R, Gottwalt K, Meid AD, Burhenne J, Huisinga W, Haefeli WE, Mikus G, Kloft C (2022) Quantification of the Time Course of CYP3A Inhibition, Activation, and Induction Using a Population Pharmacokinetic Model of Microdosed Midazolam Continuous Infusion. *Clin Pharmacokinet* 61 (11):1595-1607. doi:10.1007/s40262-022-01175-6
86. Katzenmaier S, Markert C, Riedel KD, Burhenne J, Haefeli WE, Mikus G (2011) Determining the time course of CYP3A inhibition by potent reversible and irreversible CYP3A inhibitors using A limited sampling strategy. *Clin Pharmacol Ther* 90 (5):666-673. doi:10.1038/clpt.2011.164
87. Nguyen TT, Bénech H, Delaforge M, Lenuzza N (2016) Design optimisation for pharmacokinetic modeling of a cocktail of phenotyping drugs. *Pharm Stat* 15 (2):165-177. doi:10.1002/pst.1731
88. Merlé Y, Mentré F (1995) Bayesian design criteria: computation, comparison, and application to a pharmacokinetic and a pharmacodynamic model. *J Pharmacokinet Biopharm* 23 (1):101-125. doi:10.1007/bf02353788
89. Combes FP, Retout S, Frey N, Mentré F (2013) Prediction of shrinkage of individual parameters using the bayesian information matrix in non-linear mixed effect models with evaluation in pharmacokinetics. *Pharm Res* 30 (9):2355-2367. doi:10.1007/s11095-013-1079-3
90. Mendell J, Chen S, He L, Desai M, Parasramupria DA (2015) The effect of rifampin on the pharmacokinetics of edoxaban in healthy adults. *Clin Drug Investig* 35 (7):447-453. doi:10.1007/s40261-015-0298-2



91. Hohmann N, Kocheise F, Carls A, Burhenne J, Weiss J, Haefeli WE, Mikus G (2016) Dose-Dependent Bioavailability and CYP3A Inhibition Contribute to Non-Linear Pharmacokinetics of Voriconazole. *Clin Pharmacokinet* 55 (12):1535-1545. doi:10.1007/s40262-016-0416-1
92. Saari TI, Laine K, Leino K, Valtonen M, Neuvonen PJ, Olkkola KT (2006) Effect of voriconazole on the pharmacokinetics and pharmacodynamics of intravenous and oral midazolam. *Clin Pharmacol Ther* 79 (4):362-370. doi:10.1016/j.clpt.2005.12.305
93. Chen M, Nafziger AN, Bertino JS, Jr. (2006) Drug-metabolizing enzyme inhibition by ketoconazole does not reduce interindividual variability of CYP3A activity as measured by oral midazolam. *Drug Metab Dispos* 34 (12):2079-2082. doi:10.1124/dmd.106.011742
94. Chung E, Nafziger AN, Kazierad DJ, Bertino JS, Jr. (2006) Comparison of midazolam and simvastatin as cytochrome P450 3A probes. *Clin Pharmacol Ther* 79 (4):350-361. doi:10.1016/j.clpt.2005.11.016
95. Lee J, Yoon SH, Yi S, Kim AH, Kim B, Lee S, Yu KS, Jang IJ, Cho JY (2019) Quantitative prediction of hepatic CYP3A activity using endogenous markers in healthy subjects after administration of CYP3A inhibitors or inducers. *Drug Metab Pharmacokinet* 34 (4):247-252. doi:10.1016/j.dmpk.2019.04.002
96. Derungs A, Donzelli M, Berger B, Noppen C, Krähenbühl S, Haschke M (2016) Effects of Cytochrome P450 Inhibition and Induction on the Phenotyping Metrics of the Basel Cocktail: A Randomized Crossover Study. *Clin Pharmacokinet* 55 (1):79-91. doi:10.1007/s40262-015-0294-y
97. Hohmann N, Kocheise F, Carls A, Burhenne J, Haefeli WE, Mikus G (2015) Midazolam microdose to determine systemic and pre-systemic metabolic CYP3A activity in humans. *Br J Clin Pharmacol* 79 (2):278-285. doi:10.1111/bcp.12502
98. Huppertz A, Ott C, Bruckner T, Foerster KI, Burhenne J, Weiss J, Zorn M, Haefeli WE, Czock D (2019) Prolonged-Release Tacrolimus Is Less Susceptible to Interaction With the Strong CYP3A Inhibitor Voriconazole in Healthy Volunteers. *Clin Pharmacol Ther* 106 (6):1290-1298. doi:10.1002/cpt.1529
99. Fuchs I, Hafner-Blumenstiel V, Markert C, Burhenne J, Weiss J, Haefeli WE, Mikus G (2013) Effect of the CYP3A inhibitor ketoconazole on the PKR-mediated induction of CYP3A activity. *Eur J Clin Pharmacol* 69 (3):507-513. doi:10.1007/s00228-012-1388-1

## SUPPLEMENTARY MATERIAL

**Supplementary Table S1.** Overview of sensitivity information of Cytochrome P450 probes at microdose level versus therapeutic level.

<b>CYP enzyme</b>	<b>Probe</b>	<b>Metric</b>	<b>Microdose (µg)</b>	<b>Route of Ad.</b>	<b>Perpetrators<sup>#</sup></b>
<b>CYP1A2</b>	Caffeine	AUC <sub>∞</sub>	25	PO	Ketoconazole 400 mg Fluvoxamine 100 mg
<b>CYP2C9</b>	Tolbutamide	AUC <sub>∞</sub>	25	PO	Ketoconazole 400 mg Fluvoxamine 100 mg
<b>CYP2C19</b>	Omeprazole	AUC <sub>0-24</sub>	100	PO	Fluconazole 50 mg Rifampicin 150 mg
		AUC <sub>∞</sub>	100	PO	Fluconazole 400/200 mg Rifampicin 600 mg
		Cl/F	100	PO	Fluconazole 400/200 mg Rifampicin 600 mg
<b>CYP2D6</b>	Yohimbine	AUC <sub>∞</sub>	50	PO	Fluconazole 400/200 mg Paroxetine 20 mg
		AUC <sub>∞</sub> YH/11-OH	50	PO	Rifampicin 600 mg Paroxetine 50 mg
		Cl/F	50	PO	Fluconazole 400/200 mg Paroxetine 20 mg
<b>CYP3A4</b>	Apixaban	AUC <sub>∞</sub>	25	PO	Rifampicin 600 mg
					Cobicistat 150 mg
					Fluconazole 400 mg
					Isavuconazole 600 mg
					Itraconazole 200 mg
					Ketoconazole 400 mg
					Posaconazole 600 mg
Rifampicin 600 mg					
Voriconazole 200/400 mg					
Voriconazole 400 mg					

Microdose level		Therapeutic level		Evidence level	Ref.
Fold-difference	P-value	Fold-difference	P-value		
8.1	<0.01	13.7	<0.01	B	[21,41]
1.8	>0.05	NA	NA	D	[21]
4.07	NA	4.33	NA	A	[26]
0.16	NA	0.15	NA	A	[26]
12.9	<0.05	8.2	<0.05	B	[55]
0.17	<0.05	0.09	<0.05	B	[55]
0.08	<0.05	0.12	<0.05	B	[55]
5.8	<0.05	11.3	<0.05	B	[55]
1.13-1.14	NA	NA	NA	D	[55]
3.9 (EM)	NA	6.7 (EM)	NA	C	[54]
5.7 (IM)		6.2 (EM)		C	
0.8 (PM)		0.7 (PM)		A	
0.71-0.74	NA	NA	NA	C	[55]
2.0 (EM)	NA	6.7 (EM)	NA	C	[54]
2.4 (IM)		5.3 (IM)		C	
1.0 (PM)		0.94 (PM)		D	
0.88	NA	NA	NA	C	[55]
0.18 (EM)	NA	0.15 (EM)	NA	A	[54]
0.17 (IM)	NA	0.16 (IM)	NA	A	
1.25 (PM)	NA	1.45 (PM)	NA	C	
1.35-1.40	NA	NA	NA	C	[55]
1.7	<0.01	NA	NA	B	[27]
1.1	>0.05	NA	NA	D	[69]
1.3	<0.05	NA	NA	B	[69]
1.4	<0.05	NA	NA	B	[69]
1.6-1.9	<0.0001	2.0	NA	A	[61,62,69]
1.6	<0.05	NA	NA	B	[69]
1.3	<0.05	0.48	NA	B	[27,63]
1.3	<0.05	NA	NA	B	[27]
1.2	<0.05	NA	NA	B	[69]

**Supplementary Table S1.** Continued.

<b>CYP enzyme</b>	<b>Probe</b>	<b>Metric</b>	<b>Microdose (µg)</b>	<b>Route of Ad.</b>	<b>Perpetrators<sup>#</sup></b>		
		Cl/F	25	PO	Cobicistat 150 mg Fluconazole 400 mg Isavuconazole 200 mg Itraconazole 200 mg Ketoconazole 400 mg Posaconazole 300 mg Rifampicin 600 mg Voriconazole 200/400 mg Voriconazole 400 mg		
<b>CYP3A4</b>	Edoxaban	AUC <sub>∞</sub>	25-50	PO	Ketoconazole 400 mg		
				PO	Cobicistat 150 mg Rifampicin 600 mg Voriconazole 200/400 mg		
			50	PO	Fluconazole 400 mg Isavuconazole 600 mg Itraconazole 200 mg Posaconazole 600 mg Voriconazole 400 mg		
				25-50	PO	Ketoconazole 400 mg	
					PO	Cobicistat 150 mg Rifampicin 600 mg Voriconazole 200/400 mg Fluconazole 400 mg Isavuconazole 600 mg Itraconazole 200 mg Posaconazole 600 mg Voriconazole 400 mg	
		Cl/F	25-50	PO	Ketoconazole 400 mg		
				PO	Cobicistat 150 mg Rifampicin 600 mg Voriconazole 200/400 mg Fluconazole 400 mg Isavuconazole 600 mg Itraconazole 200 mg Posaconazole 600 mg Voriconazole 400 mg		
			AUC	75	PO	Ketoconazole 400 mg	
				$\frac{1 - OH\ MDZ}{MDZ}$	75	PO	Rifampicin 450 mg
				AUC <sub>0-10</sub>	33	PO	Itraconazole 200 mg Rifampicin 600 mg

Microdose level		Therapeutic level		Evidence level	Ref.
Fold-difference	P-value	Fold-difference	P-value		
0.60	<0.05	NA	NA	B	[27]
0.91	>0.05	NA	NA	D	[69]
0.75	<0.05	NA	NA	B	[69]
0.71	<0.05	NA	NA	B	[69]
0.53-0.61	<0.0001	0.50	NA	A	[61,62,69]
0.62	<0.05	NA	NA	B	[69]
0.75	<0.05	2.1	NA	B	[27,63]
0.75	<0.05	NA	NA	B	[27]
0.81	<0.05				[69]
2.1-2.3	<0.0001	1.8	NA	B	[61,66,69]
1.7	<0.005	NA	NA	B	[27]
1.9	<0.005	0.65	NA	B	[27,90]
1.3	>0.05	NA	NA	D	[27]
1.1	>0.05	NA	NA	D	[69]
1.5	<0.05	NA	NA	B	[69]
1.9	<0.05	NA	NA	B	[69]
2.1	<0.05	NA	NA	B	[69]
1.3	<0.05	NA	NA	B	[69]
0.43-0.48	<0.0001	0.53	NA	B	[61,66,69]
0.6	<0.01	NA	NA	B	[27]
0.53	<0.005	1.5	NA	B	[27,90]
0.79	>0.05	NA	NA	D	[27]
0.87	>0.05	NA	NA	D	[69]
0.66	<0.05	NA	NA	B	[69]
0.54	<0.05	NA	NA	B	[69]
0.48	<0.05	NA	NA	B	[69]
0.79	<0.05	NA	NA	B	[69]
0.2	NA	NA	NA	C	[28]
1.1	NA	0.39-2.9	NA	D	[28]
1.7	<0.05	NA	NA	B	[29]
1.1	>0.05	NA	NA	D	[29]

**Supplementary Table S1.** Continued.

<b>CYP enzyme</b>	<b>Probe</b>	<b>Metric</b>	<b>Microdose (µg)</b>	<b>Route of Ad.</b>	<b>Perpetrators<sup>#</sup></b>
		AUC <sub>2-4</sub>	3	PO	Erythromycin 1000 mg Erythromycin 250 mg
			10	PO	Cobicistat 150 mg Itraconazole 400 mg Fluconazole 400 mg Ketoconazole 400 mg Posaconazole 300 mg Isavuconazole 600 mg Rifampicin 600 mg Voriconazole 200/400 mg Voriconazole 400 mg
		AUC <sub>∞</sub>	1	IV	Voriconazole 400 mg Voriconazole 400 mg IV Voriconazole 50 mg Voriconazole 50 mg IV
			0.1	PO	Ketoconazole 400 mg
			0.3	PO	Ketoconazole 400 mg
Midazolam		AUC <sub>∞</sub>	3	PO	Voriconazole 400 mg Voriconazole 400 mg IV Voriconazole 50 mg Voriconazole 50 mg IV
			10	PO	Clarithromycin 1000 mg Itraconazole 200 mg Rifampicin 600 mg
			25	PO	Ketoconazole 400 mg Fluvoxamine 100 mg
			30	PO	Ciclosporin 100 mg Ciclosporin 100 mg Fluconazole 400 mg
			75	PO	Ketoconazole 400 mg Rifampicin 450 mg
		Cl/F	0.1	PO	Ketoconazole 400 mg
			0.3	PO	Ketoconazole 400 mg
			30	PO	Ciclosporin 100 mg Ciclosporin 100 mg Fluconazole 400 mg
			75	PO	Ketoconazole 400 mg Rifampicin 450 mg

Microdose level		Therapeutic level		Evidence level	Ref.
Fold-difference	P-value	Fold-difference	P-value		
5.0	<0.05	NA	NA	B	[30]
1.7	<0.05	NA	NA	B	[30]
8.8	<0.0001	NA	NA	B	[27]
3.7	<0.05	NA	NA	B	[81]
4.3	<0.05	NA	NA	B	[81]
8.4	<0.05	NA	NA	B	[81]
2.5	<0.05	NA	NA	B	[81]
1.9	<0.05	NA	NA	B	[81]
1.3	<0.05	NA	NA	D	[27]
8.2	<0.0001	8.3	<0.001	A	[27,86]
5.3	<0.05	NA	NA	B	[81]
2.02	<0.0001	3.5	<0.001	B	[91,92]
2.16	<0.001	NA	NA	B	[91]
0.98	0.7944	NA	NA	D	[91]
0.96	0.6039	NA	NA	D	[91]
19.5	NA	9.5	<0.0001	B	[32,93,94]
10.9	NA	9.5	<0.0001	A	[32,93,94]
6.95	<0.0001	9.4	<0.001	B	[91,92]
3.94	<0.0001	NA	NA	B	[91]
1.84	0.0027	NA	NA	B	[91]
1.14	0.1995	NA	NA	D	[91]
4.84	NA	5.8-6.5	NA	B	[34]
7.04	NA	9.9-11.2	NA	B	[34,95]
0.94	NA	0.05-1.2	NA	D	[28,34,94,96]
12.8	<0.01	NA	NA	B	[21]
1.5	NA	NA	NA	C	[36]
4.8	NA	NA	NA	C	[36]
6.5	<0.05	9.5	<0.0001	B	[28,93,94]
0.4	<0.05	0.05	<0.05	B	[28]
0.05	NA	0.07-0.11	<0.0001	B	[32,93,94]
0.05	NA	0.07-0.11	<0.0001	B	[32,93,94]
0.7	NA	NA	NA	C	[36]
0.2	NA	NA	NA	C	[36]
0.15	<0.05	0.11	<0.0001	A	[28,32,93]
8.5	<0.05	16.9	<0.05	B	[28]

**Supplementary Table S1.** Continued.

<b>CYP enzyme</b>	<b>Probe</b>	<b>Metric</b>	<b>Microdose (µg)</b>	<b>Route of Ad.</b>	<b>Perpetrators<sup>#</sup></b>
		$Cl_{met}$	3	PO	Erythromycin 1000 mg Erythromycin 250 mg
			10	PO	Cobicistat 150 mg Fluconazole 400 mg Itraconazole 400 mg Isavuconazole 600 mg Ketoconazole 400 mg Rifampicin 600 mg Posaconazole 600 mg Voriconazole 200/400 mg Voriconazole 400 mg
	Rivaroxaban	$AUC_{\infty}$	25	PO	Cobicistat 150 mg Fluconazole 400 mg Isavuconazole 200 mg Itraconazole 200 mg Ketoconazole 400 mg Posaconazole 600 mg Rifampicin 600 mg Voriconazole 200/400 mg Voriconazole 400 mg
		Cl/F	25	PO	Cobicistat 150 mg Fluconazole 400 mg Isavuconazole Itraconazole 200 mg Ketoconazole 400 mg Posaconazole 300 mg Rifampicin 600 mg Voriconazole 200/400 mg Voriconazole 400 mg

Abbreviations:  $AUC_{\infty}$ , area-under-the-concentration-time-curve extrapolated to infinity;  $AUC_{0-24}$ , AUC from 0 to 24 hours;  $AUC_{0-10}$ , AUC from 0 to 10 hours;  $AUC_{2-4}$ , AUC from 2 to 4 hours; Cl/F, apparent clearance;  $Cl_{met}$ , metabolic clearance;



Microdose level		Therapeutic level		Evidence level	Ref.
Fold-difference	P-value	Fold-difference	P-value		
0.18	<0.05	NA	NA	B	[30]
0.58	<0.05	NA	NA	B	[30]
0.11	<0.0001	NA	NA	B	[27]
0.22	<0.05	NA	NA	B	[81]
0.27	<0.05	NA	NA	B	[81]
0.52	<0.05	NA	NA	B	[81]
0.11	<0.05	NA	NA	B	[81]
0.77	<0.05	NA	NA	B	[27]
0.40	<0.05	NA	NA	B	[81]
0.16	0.0009	NA	NA	B	[27]
0.19	<0.05	NA	NA	B	[81]
2.0	<0.001	NA	NA	B	[27]
1.3	<0.05	NA	NA	B	[81]
1.1	>0.05	NA	NA	D	[81]
1.5	<0.05	NA	NA	B	[81]
2.3	<0.0001	2.6	NA	A	[61,68,81]
1.4	<0.05	NA	NA	B	[81]
1.3	>0.05	NA	NA	D	[27]
1.3	<0.05	NA	NA	B	[27]
1.2	<0.05	NA	NA	N	[81]
0.5	<0.05	NA	NA	B	[27]
0.79	<0.05	0.71	NA	B	[81,68]
0.88	>0.05	NA	NA	D	[81]
0.68	<0.05	NA	NA	B	[81]
0.43	<0.0001	0.39	NA	A	[61,68,81]
0.73	<0.05	NA	NA	B	[81]
0.76	>0.05	NA	NA	D	[27]
0.76	<0.05	NA	NA	B	[27]
0.86	<0.05	NA	NA	B	[81]

AUC<sub>∞</sub> 1-OH MDZ/MDZ, AUC of 1-hydroxy midazolam divided by midazolam; AUC<sub>∞</sub> YH/11-OH, AUC of yohimbine divided 11-hydroxy yohimbine.

**Supplementary Table S2.** Pharmacokinetic parameters of drugs from trials in which both microdose and therapeutic doses were administered.

<b>CYP enzyme</b>	<b>Probe</b>	<b>Microdose (<math>\mu\text{g}</math>)</b>	<b>Therapeutic dose (mg)</b>	<b>Route of Ad.</b>
<b>CYP2C9</b>	Losartan	100	50	PO
<b>CYP2C19</b>	Omeprazole	100	20	PO
<b>CYP2D6</b>	Yohimbine	50	5	PO

Microdose PK	Therapeutic PK	Evidence level	Ref.
$C_{\max} = 0.88$ $T_{\max} = 1.45$ $AUC = 3.62$ $t_{1/2} = 3.31$	$C_{\max} = 0.86$ $T_{\max} = 1.4$ $AUC = 3.41$ $t_{1/2} = 3.41$	B	[47]
$C_{\max} = 0.88$ $T_{\max} = 1.45$ $AUC = 3.62$ $t_{1/2} = 3.31$	$C_{\max} = 0.83$ $T_{\max} = 1.35$ $AUC = 3.48$ $t_{1/2} = 3.17$	B	[47] <sup>#</sup>
$AUC = 2.59$ $t_{1/2} = 1.21$	$AUC = 8.24$ $t_{1/2} = 2.40$	D	[26]
$C_{\max} = 4.48$ $T_{\max} = 0.86$ $AUC = 264$ $Cl/F = 379$ $V/F = 26.1$	$C_{\max} = 1.87$ $T_{\max} = 3.0$ $AUC = 258$ $Cl/F = 388$ $V/F = 90.8$	C	[55]
5-OH omeprazole $AUC = 107$	5-OH omeprazole $AUC = 130$		
$C_{\max} = 0.15$ $T_{\max} = 0.36$ $AUC = 0.15$ $t_{1/2} = 0.68$ $Cl/F = 669$ $V/F = 810$	$C_{\max} = 0.35$ $T_{\max} = 0.36$ $AUC = 0.32$ $t_{1/2} = 0.64$ $Cl/F = 308$ $V/F = 313$	B	[54] <sup>§</sup>
<b>11-OH yohimbine</b> $AUC = 8.7$ $AUC\ YH/11-OH\ YH = 0.02$	<b>11-OH yohimbine</b> $AUC = 9.6$ $AUC\ YH/11-OH\ YH = 0.03$		
$C_{\max} = 0.53$ $T_{\max} = 0.75$ $AUC = 0.912$ $t_{1/2} = 0.64$ $Cl/F = 110$ $V/F = 226$	$C_{\max} = 1.06$ $T_{\max} = 0.75$ $AUC = 1.57$ $t_{1/2} = 0.96$ $Cl/F = 63.5$ $V/F = 115$	B	[54] <sup>¶</sup>
<b>11-OH yohimbine</b> $AUC = 4.12$ $AUC\ YH/11-OH\ YH = 0.10$	<b>11-OH yohimbine</b> $AUC = 7.52$ $AUC\ YH/11-OH\ YH = 0.21$		

**Supplementary Table S2.** Continued.

<b>CYP enzyme</b>	<b>Probe</b>	<b>Microdose (<math>\mu\text{g}</math>)</b>	<b>Therapeutic dose (mg)</b>	<b>Route of Ad.</b>
-------------------	--------------	---	------------------------------	---------------------

<b>CYP2E1</b>	Chlorzoxazone	2.5	2.5	PO
---------------	---------------	-----	-----	----

		5	2.5	PO
--	--	---	-----	----

		25	2.5	PO
--	--	----	-----	----

Microdose PK	Therapeutic PK	Evidence level	Ref.
$C_{\max} = 4.38$ $T_{\max} = 1.42$ $AUC = 30.5$ $t_{1/2} = 5.85$ $Cl/F = 3.3$ $V/F = 28.4$	$C_{\max} = 3.96$ $T_{\max} = 1.42$ $AUC = 40.9$ $t_{1/2} = 6.59$ $Cl/F = 2.4$ $V/F = 24.5$	A	[54] <sup>y</sup>
<b>11-OH yohimbine</b>	<b>11-OH yohimbine</b>		
$AUC = 8.8$ $AUC\ YH/11-OH = 3.53$	$AUC = 11.7$ $AUC\ YH/11-Oh = 3.50$		
$C_{\max} = 1.6$ $AUC = 2.64$ $t_{1/2} = 1.02$ $Cl/F = 37.9$ $V/F = 55.5$	$C_{\max} = 2.1$ $AUC = 3.23$ $t_{1/2} = 1.27$ $Cl/F = 31.0$ $V/F = 56.9$	B	[58]
$C_{\max} = 1.6$ $AUC = 2.64$ $t_{1/2} = 1.02$ $Cl/F = 37.9$ $V/F = 55.5$	$C_{\max} = 1.5$ $AUC = 2.13$ $t_{1/2} = 1.14$ $Cl/F = 46.9$ $V/F = 77.2$	B	[58]
$C_{\max} = 1.00$ $C_{\max}\ MR = 0.033$ $AUC = 2.37$ $t_{1/2} = 1.00$ $Cl/F = 42.1$ $V/F = 60.7$	$C_{\max} = 2.1$ $C_{\max}\ MR = 0.027$ $AUC = 3.23$ $t_{1/2} = 1.27$ $Cl/F = 31.0$ $V/F = 56.9$	A	[58]
$C_{\max} = 1.00$ $C_{\max}\ MR = 0.033$ $AUC = 2.37$ $t_{1/2} = 1.00$ $Cl/F = 42.1$ $V/F = 60.7$	$C_{\max} = 1.5$ $C_{\max}\ MR = 0.041$ $AUC = 2.13$ $t_{1/2} = 1.14$ $Cl/F = 46.9$ $V/F = 77.2$	A	[58]
$C_{\max} = 2.4$ $C_{\max}\ MR = 0.020$ $AUC = 3.41$ $t_{1/2} = 1.05$ $Cl/F = 29.28$ $V/F = 44.4$	$C_{\max} = 2.1$ $C_{\max}\ MR = 0.027$ $AUC = 3.23$ $t_{1/2} = 1.27$ $Cl/F = 31.0$ $V/F = 56.9$	A	[58]

**Supplementary Table S2.** Continued.

<b>CYP enzyme</b>	<b>Probe</b>	<b>Microdose (<math>\mu\text{g}</math>)</b>	<b>Therapeutic dose (mg)</b>	<b>Route of Ad.</b>
		50	2.5	PO
			5	PO
<b>CYP3A4</b>	Midazolam	0.1	1	PO
			3	PO
		0.3	1	PO
			3	PO
		1	1	PO
			3	PO

Microdose PK	Therapeutic PK	Evidence level	Ref.
$C_{\max} = 2.4$ $C_{\max} \text{ MR} = 0.020$ $AUC = 3.41$ $t_{1/2} = 1.05$ $Cl/F = 29.28$ $V/F = 44.4$	$C_{\max} = 1.5$ $C_{\max} \text{ MR} = 0.041$ $AUC = 2.13$ $t_{1/2} = 1.14$ $Cl/F = 46.9$ $V/F = 77.2$	B	[58]
$C_{\max} = 1.74$ $C_{\max} \text{ MR} = 0.029$ $AUC = 2.49$ $t_{1/2} = 1.10$ $Cl/F = 40.2$ $V/F = 63.8$	$C_{\max} = 2.1$ $C_{\max} \text{ MR} = 0.027$ $AUC = 3.23$ $t_{1/2} = 1.27$ $Cl/F = 31.0$ $V/F = 56.9$	A	[58]
$C_{\max} = 1.74$ $C_{\max} \text{ MR} = 0.029$ $AUC = 2.49$ $t_{1/2} = 1.10$ $Cl/F = 40.2$ $V/F = 63.8$	$C_{\max} = 1.5$ $C_{\max} \text{ MR} = 0.041$ $AUC = 2.13$ $t_{1/2} = 1.14$ $Cl/F = 46.9$ $V/F = 77.2$	A	[58]
$AUC = 1.07$ $t^{1/2} = 1.52$ $Cl = 93.0$ $V = 225$	$AUC = 0.944$ $t^{1/2} = 4.54$ $Cl = 106.2$ $V = 445$	C	[32]
$AUC = 1.07$ $t^{1/2} = 1.52$ $Cl = 93.0$ $V = 225$	$AUC = 1.06$ $t^{1/2} = 4.11$ $Cl = 94.2$ $V = 353$	C	[32]
$AUC = 1.10$ $t^{1/2} = 3.54$ $Cl = 91.2$ $V = 376$	$AUC = 0.944$ $t^{1/2} = 4.54$ $Cl = 106.2$ $V = 445$	B	[32]
$AUC = 1.10$ $t^{1/2} = 3.54$ $Cl = 91.2$ $V = 376$	$AUC = 1.06$ $t^{1/2} = 4.11$ $Cl = 94.2$ $V = 353$	B	[32]
$AUC = 0.970$ $t^{1/2} = 3.11$ $Cl = 103.2$ $V = 382$	$AUC = 0.944$ $t^{1/2} = 4.54$ $Cl = 106.2$ $V = 445$	B	[32]
$AUC = 0.970$ $t^{1/2} = 3.11$ $Cl = 103.2$ $V = 382$	$AUC = 1.06$ $t^{1/2} = 4.11$ $Cl = 94.2$ $V = 353$	B	[32]

**Supplementary Table S2.** Continued.

<b>CYP enzyme</b>	<b>Probe</b>	<b>Microdose (<math>\mu\text{g}</math>)</b>	<b>Therapeutic dose (mg)</b>	<b>Route of Ad.</b>
			1	IV
		3	1	PO
			3	PO
		30	1	PO
			3	PO
			1	PO
			3	PO



Microdose PK	Therapeutic PK	Evidence level	Ref.
AUC = 3.79 $t_{1/2}$ = 3.55 Cl = 26.34 $Cl_{met}$ = 15.18 V = 83.5 Ae (1-OH MDZ) = 59.9	AUC = 3.9 $t_{1/2}$ = 4.02 Cl = 25.68 $Cl_{met}$ = 16.68 V = 73.5 Ae (1-OH MDZ) = 61.2	A	[97]
AUC = 1.11 $t_{1/2}$ = 3.68 Cl = 90.6 V = 373	AUC = 0.944 $t_{1/2}$ = 4.54 Cl = 106.2 V = 445	B	[32]
AUC = 1.11 $t_{1/2}$ = 3.68 Cl = 90.6 V = 373	AUC = 1.06 $t_{1/2}$ = 4.11 Cl = 94.2 V = 353	B	[32]
AUC = 0.887 $t_{1/2}$ = 3.26 Cl = 112.8 $Cl_{met}$ = 77.16 V = 413 Ae (1-OH MDZ) = 69.4	AUC = 0.813 $t_{1/2}$ = 3.96 Cl = 123.0 $Cl_{met}$ = 71.94 V = 469 Ae (1-OH MDZ) = 67.5	A	[97]
F = 23.4 AUC = 1.05 $t_{1/2}$ = 3.93 Cl = 95.4 V = 344	F = 20.9 AUC = 0.944 $t_{1/2}$ = 4.54 Cl = 106.2 V = 445	B	[32]
AUC = 1.05 $t_{1/2}$ = 3.93 Cl = 95.4 V = 344	AUC = 1.06 $t_{1/2}$ = 4.11 Cl = 94.2 V = 353	B	[32]
AUC = 1.05 $t_{1/2}$ = 4.53 Cl = 95.4 V = 383	AUC = 0.944 $t_{1/2}$ = 4.54 Cl = 106.2 V = 445	B	[32]
AUC = 1.05 $t_{1/2}$ = 3.93 Cl = 95.4 V = 344	AUC = 1.06 $t_{1/2}$ = 4.11 Cl = 94.2 V = 353	B	[32]

**Supplementary Table S2.** Continued.

CYP enzyme	Probe	Microdose ( $\mu\text{g}$ )	Therapeutic dose (mg)	Route of Ad.
		75	7.5	PO
		100	7.5	IV
				PO
	Quinidine	100	1	PO
			10	PO
			100	PO

Microdose PK	Therapeutic PK	Evidence level	Ref.
AUC = 0.91 $t_{1/2} = 1.7$ Cl = 128 V = 276 <b>1-OH MDZ</b>	AUC = 0.89 $t_{1/2} = 2.2$ Cl = 129 V = 383 <b>1-OH MDZ</b>	A	[28]
AUC = 0.24 $t_{1/2} = 1.3$ Cl = 516 V = 878	AUC = 0.43 $t_{1/2} = 2.0$ Cl = 258 V = 713		
AUC = 4.53 $t_{1/2} = 4.87$ Cl = 21.2	AUC = 4.68 $t_{1/2} = 2.55$ Cl = 20.4	B	[31]
$t_{1/2} = 4.87$ F = 22.8%	$t_{1/2} = 3.31$ F = 20.9%	B	[31]
AUC = 2.46 $t_{1/2} = 1.01$	AUC <sub>t</sub> = 6.195 $t_{1/2} = 2.12$	D	[26]
AUC = 0.813 $t_{1/2} = 5.07$ <b>3-OH QND</b>	AUC = 1.05 $t_{1/2} = 5.73$ <b>3-OH QND</b>	B	[71]
AUC <sub>0-12</sub> = 0.116 AUC $\frac{3-OH QND}{QND} = 0.19$ <b>QND N-oxide</b> AUC <sub>0-12</sub> = 0.701 AUC $\frac{QND N-oxide}{QND} = 1.1$	AUC <sub>0-12</sub> = 0.157 AUC $\frac{3-OH QND}{QND} = 0.20$ <b>QND N-oxide</b> AUC <sub>0-12</sub> = 2.27 AUC $\frac{QND N-oxide}{QND} = 2.9$		
AUC = 0.813 $t_{1/2} = 5.07$ <b>3-OH QND</b>	AUC = 1.48 $t_{1/2} = 5.24$ <b>3-OH QND</b>	B	[71]
AUC <sub>0-12</sub> = 0.116 AUC $\frac{3-OH QND}{QND} = 0.19$ <b>QND N-oxide</b> AUC <sub>0-12</sub> = 0.701 AUC $\frac{QND N-oxide}{QND} = 1.1$	AUC <sub>0-12</sub> = 0.212 AUC $\frac{3-OH QND}{QND} = 0.19$ <b>QND N-oxide</b> AUC <sub>0-12</sub> = 1.88 AUC $\frac{QND N-oxide}{QND} = 1.7$		
AUC = 0.813 $t_{1/2} = 5.07$ <b>3-OH QND</b>	AUC = 2.08 $t_{1/2} = 5.59$ <b>3-OH QND</b>		[71]
AUC <sub>0-12</sub> = 0.116 AUC $\frac{3-OH QND}{QND} = 0.19$ <b>QND N-oxide</b> AUC <sub>0-12</sub> = 0.701 AUC $\frac{QND N-oxide}{QND} = 1.1$	AUC <sub>0-12</sub> = 0.441 AUC $\frac{3-OH QND}{QND} = 0.28$ <b>QND N-oxide</b> AUC <sub>0-12</sub> = 2.27 AUC $\frac{QND N-oxide}{QND} = 1.4$		

**Supplementary Table S2.** Continued.

CYP enzyme	Probe	Microdose ( $\mu\text{g}$ )	Therapeutic dose (mg)	Route of Ad.
	Verapamil	100	3	PO
			80	PO
			16	PO

**Abbreviations:** AUC, Area-under-the-concentration-time-curve extrapolated to infinity; Cl/F, apparent clearance;  $C_{\text{max}}$ , maximum concentration; MR, metabolic ratio; route of Ad., route of administration;  $t_{1/2}$ , half-life; QND N-oxide, quinidine N-oxide; 3-OH QND, 3-hydroxy quinidine, YH, yohimbine; 11-OH YH, 11-hydroxy yohimbine.

**Supplementary Table S3.** Pharmacokinetic parameters of drugs from microdose trials in which no therapeutic dose was administered. Microdose pharmacokinetics were compared to pharmacokinetic of the therapeutic dose as described in literature.

CYP enzyme	Probe	Microdose ( $\mu\text{g}$ )	Therapeutic dose (mg)	Route of Ad.
<b>CYP1A2</b>	Caffeine	25	100	PO
			200	PO
			250	PO

Microdose PK	Therapeutic PK	Evidence level	Ref.
AUC = 0.139 $t_{1/2} = 2.48$	AUC = 0.165 $t_{1/2} = 3.29$	A	[71]
<b>Norverapamil</b> AUC <sub>0-12</sub> = 0.285 AUC $\frac{NVPN}{VPN} = 2.2$ AUC = 0.139 $t_{1/2} = 2.48$	<b>Norverapamil</b> AUC <sub>0-12</sub> = 0.35 AUC $\frac{NVPN}{VPN} = 2.3$ AUC = 0.32 $t_{1/2} = .3.21$	B	[71]
<b>Norverapamil</b> AUC <sub>0-12</sub> = 0.285 AUC $\frac{NVPN}{VPN} = 2.2$ AUC = 0.139 $t_{1/2} = 2.48$	<b>Norverapamil</b> AUC <sub>0-12</sub> = 0.538 AUC $\frac{NVPN}{VPN} = 1.8$ AUC = 0.238 $t_{1/2} = 3.04$	A	[71]
<b>Norverapamil</b> AUC <sub>0-12</sub> = 0.285 AUC $\frac{NVPN}{VPN} = 2.2$	<b>Norverapamil</b> AUC <sub>0-12</sub> = 0.441 AUC $\frac{NVPN}{VPN} = 1.9$		

# Hypertensive patients

\$ Extensive metabolizers

‡ Intermediate metabolizers

‡ Poor metabolizers

Microdose PK	Therapeutic PK	Evidence level	Ref.
C <sub>max</sub> = 2.4 T <sub>max</sub> = 0.58 AUC = 10.76 $t_{1/2} = 4.1$	C <sub>max</sub> = 1.5 T <sub>max</sub> = 1.0 AUC = 15.50 $t_{1/2} = 5.5$	B	[21,42]
C <sub>max</sub> = 2.4 T <sub>max</sub> = 0.58 AUC = 10.76 $t_{1/2} = 4.1$	C <sub>max</sub> = 2.5 T <sub>max</sub> = 1.2 AUC = 24.35 $t_{1/2} = 6.1$	D	[21,43]
C <sub>max</sub> = 2.4 T <sub>max</sub> = 0.58 AUC = 10.76 $t_{1/2} = 4.1$	C <sub>max</sub> = 2.3 T <sub>max</sub> = 1.1 AUC = 18.52 $t_{1/2} = 4.9$	B	[21,41]

**Supplementary Table S3.** Continued.

<b>CYP enzyme</b>	<b>Probe</b>	<b>Microdose (<math>\mu\text{g}</math>)</b>	<b>Therapeutic dose (mg)</b>	<b>Route of Ad.</b>
<b>CYP2C9</b>	Glibenclamide	10	0.875	PO
			2.5	PO
	Tolbutamide	25	125	PO
	Warfarin	10	7.5	PO
100		5	PO	
<b>CYP2C19</b>	Lansoprazole	50-70	30	PO
<b>CYP3A4</b>	Apixaban	25	10	PO

Microdose PK	Therapeutic PK	Evidence level	Ref.
$C_{\max} = 1.3$ $T_{\max} = 4.0$ AUC = 8.39 $t_{1/2} = 2.37$	$C_{\max} = 5.0$ $T_{\max} = 1.3$ AUC = 15.2 $t_{1/2} = 2.4$	C	[33,44]
$C_{\max} = 1.3$ $T_{\max} = 4.0$ AUC = 8.39 $t_{1/2} = 2.37$ Cl/F = 12.6	$C_{\max} = 6.3$ $T_{\max} = 2.1$ AUC = 55.06 $t_{1/2} = 5.09$ Cl/F = 1.94	D	[33,45]
$C_{\max} = 14.9$ AUC = 167.3 $t_{1/2} = 8.13$	$C_{\max} = 13.0$ AUC = 143.0 $t_{1/2} = 7.70$	B	[21,49]
AUC <sub>0-12</sub> = 47.77 AUC <sub>0-12</sub> = 56.35 AUC = 571 $t_{1/2} = 274$ V = 67.3	AUC <sub>0-12</sub> = 68.00 AUC = 416 $t_{1/2} = 48.6$ V = 17.9	C	[33,50]
AUC <sub>0-12</sub> = 0.13-0.18 $t_{1/2} = 1.26$	AUC <sub>0-12</sub> = 12.17 $t_{1/2} = 1.46$	D	[33,53]
AUC <sub>0-12</sub> = 0.12-0.17 $t_{1/2} = 0.97$	AUC <sub>0-12</sub> = 12.17 $t_{1/2} = 1.46$	D	[33,53]
AUC = 25.54 $t_{1/2} = 6.80$ Cl/F = 3.92	AUC = 17.95 $t_{1/2} = 13.91$ Cl/F = 5.57	C	[61,63]
AUC = 21.36 $t_{1/2} = 6.32$ Cl/F = 4.68	AUC = 17.95 $t_{1/2} = 13.91$ Cl/F = 5.57	C	[27,63]
AUC = 31.09 $t_{1/2} = 8.37$ Cl/F = 53.6	AUC = 17.95 $t_{1/2} = 13.91$ Cl/F = 5.57	B	[27,63]
AUC = 25.09 $t_{1/2} = 5.85$ Cl/F = 3.98	AUC = 17.95 $t_{1/2} = 13.91$ Cl/F = 5.57	C	[27,63]
$C_{\max} = 3.7$ $T_{\max} = 1$ AUC = 29.86 $t_{1/2} = 5.63$ Cl/F = 3.35 V = 28.3	$C_{\max} = 1.5$ $T_{\max} = 3$ AUC = 17.95 $t_{1/2} = 13.91$ Cl/F = 5.57 V = 20.39	C	[63,69]

**Supplementary Table S3.** Continued.

<b>CYP enzyme</b>	<b>Probe</b>	<b>Microdose (<math>\mu\text{g}</math>)</b>	<b>Therapeutic dose (mg)</b>	<b>Route of Ad.</b>
	Edoxaban	25	10	PO
		50	10	PO
	Midazolam	1	7.5	PO
		3	7.5	PO
		10	7.5	PO
		25	7.5	PO



Microdose PK	Therapeutic PK	Evidence level	Ref.
AUC = 2.39 $t_{1/2} = 5.42$ Cl/F = 43.7 V/F = 341	AUC = 2.75 $t_{1/2} = 11.86$ Cl/F = 38.9 V/F = 666	C	[61,66]
AUC = 1.89 $t_{1/2} = 5.47$ Cl/F = 52.9 V/F = 373	AUC = 2.75 $t_{1/2} = 11.86$ Cl/F = 38.9 V/F = 666	C	[27,66]
AUC = 2.59 $t_{1/2} = 5.60$ Cl/F = 38.6 V/F = 297	AUC = 2.75 $t_{1/2} = 11.86$ Cl/F = 38.9 V/F = 666	C	[27,66]
AUC = 2.45 $t_{1/2} = 5.19$ Cl/F = 40.9 V/F = 302	AUC = 2.75 $t_{1/2} = 11.86$ Cl/F = 38.9 V/F = 666	C	[27,66]
$C_{\max} = 0.264$ $T_{\max} = 1$ AUC = 1.72 $t_{1/2} = 4.92$ Cl/F = 58.1	$C_{\max} = 0.408$ $T_{\max} = 1.02$ AUC = 2.75 $t_{1/2} = 11.86$ Cl/F = 38.9	C	[66,69]
AUC = 0.608 $t^{1/2} = 2.29$ V = 543 Cl = 164.4 $AUC_{0.5-24} \frac{MDZ}{1-OH MDZ} = 2.5$	AUC = 0.89 $t^{1/2} = 2.2$ V = 383 Cl = 129 $AUC \frac{MDZ}{1-OH MDZ} = 2.1$	A	[28,75]
AUC = 0.97 $t^{1/2} = 2.32$ V = 344 Cl = 103.0 $AUC_{0.5-24} \frac{MDZ}{1-OH MDZ} = 2.2$	AUC = 0.89 $t^{1/2} = 2.2$ V = 383 Cl = 129 $AUC \frac{MDZ}{1-OH MDZ} = 2.1$	A	[28,75]
AUC = 0.604 $t^{1/2} = 2.49$ V = 596 Cl = 165.7 $AUC_{0.5-24} \frac{MDZ}{1-OH MDZ} = 2.1$	AUC = 0.89 $t^{1/2} = 2.2$ V = 383 Cl = 129 $AUC \frac{MDZ}{1-OH MDZ} = 2.1$	A	[28,75]
AUC = 1.97 $t^{1/2} = 5.8$	AUC = 0.89 $t^{1/2} = 2.2$	C	[28,34]
AUC = 1.76 $t^{1/2} = 4.01$	AUC = 0.89 $t^{1/2} = 2.2$	B	[21,28]

**Supplementary Table S3.** Continued.

CYP enzyme	Probe	Microdose ( $\mu\text{g}$ )	Therapeutic dose (mg)	Route of Ad.
		30	7.5	PO
			3	PO
			7.5	PO
			7.5	PO <sup>†</sup>
			7.5	PO
		30	7.5	PO
			3	PO
		100	7.5	PO

Microdose PK	Therapeutic PK	Evidence level	Ref.
AUC = 1.08	AUC = 0.89	A	[28,75]
$t^{1/2} = 3.95$	$t^{1/2} = 2.2$		
V = 526	V = 383		
Cl = 92.22	Cl = 129		
$AUC_{0.5-24} \frac{MDZ}{1-OH MDZ} = 2.4$	$AUC \frac{MDZ}{1-OH MDZ} = 2.1$		
$Cl_{met} = 38.4$	$Cl_{met} = 32.58$	B	[98,99]
AUC = 3.53	AUC = 0.89	D	[28,35,99]
$t^{1/2} = 3.25$	$t^{1/2} = 2.2$		
Cl = 0.0283	Cl = 129		
$Cl_{met} = 14.4$	$Cl_{met} = 32.58$		
<b>1-OH MDZ</b>	<b>1-OH MDZ</b>		
AUC = 0.763	AUC = 0.43		
$t^{1/2} = 4.02$	$t^{1/2} = 2.0$		
$AUC \frac{MDZ}{1-OH MDZ} = 4.86$	$AUC \frac{MDZ}{1-OH MDZ} = 2.1$		
AUC = 4.217	AUC = 0.89	D	[28,35,99]
$t^{1/2} = 3.96$	$t^{1/2} = 2.2$		
Cl = 0.0237	Cl = 129		
$Cl_{met} = 13.8$	$Cl_{met} = 32.58$		
<b>1-OH MDZ</b>	<b>1-OH MDZ</b>		
AUC = 0.923	AUC = 0.43		
$t^{1/2} = 4.12$	$t^{1/2} = 2.0$		
$AUC \frac{MDZ}{1-OH MDZ} = 4.79$	$AUC \frac{MDZ}{1-OH MDZ} = 2.1$		
AUC = 1.66	AUC = 0.89	C	[28,36]
$t^{1/2} = 5.9$	$t^{1/2} = 2.2$		
Cl = 60.4	Cl = 129		
V = 514	V = 383		
AUC = 883	AUC = 0.89	D	[28,37,53]
$Cl_{met} = 43.2$	$Cl_{met} = 32.6$	C	
$AUC_{2-4} = 0.325$	$AUC_{2-4} = 0.373$	B	[38,99]
$Cl_{met} = 17.4$	$Cl_{met} = 32.6$		
AUC = 0.686	AUC = 0.89	A	[28,75]
$t^{1/2} = 3.30$	$t^{1/2} = 2.2$		
V = 694	V = 383		
Cl = 145.8	Cl = 129		
$AUC \frac{MDZ}{1-OH MDZ} = 2.0$	$AUC \frac{MDZ}{1-OH MDZ} = 2.1$		
Cl = 112	Cl = 129	B	[28,39]

**Supplementary Table S3.** Continued.

<b>CYP enzyme</b>	<b>Probe</b>	<b>Microdose (<math>\mu\text{g}</math>)</b>	<b>Therapeutic dose (mg)</b>	<b>Route of Ad.</b>
	Rivaroxaban	25	20	PO

**Abbreviations:** AUC, Area-under-the-concentration-curve;  $\text{AUC}_{0-12}$ , AUC from 0 to 12 hours;  $\text{Cl}/F$ , apparent clearance;  $C_{\text{max}}$ , maximum concentration  $\text{Cl}_{\text{met}}$ , metabolic clearance;

Microdose PK	Therapeutic PK	Evidence level	Ref.
AUC = 14.81	AUC = 10.44	C	[36,27,61]
$t_{1/2}$ = 4.90	$t_{1/2}$ = 9.3		
Cl = 6.78	Cl = 9.6	C	
V = 47.7	V = 128		
AUC = 13.80		C	
$t_{1/2}$ = 5.00			
Cl = 7.26		C	
V = 35			
AUC = 14.74			
$t_{1/2}$ = 5.02			
Cl = 6.78			
V = 33			
AUC = 15.97			
$t_{1/2}$ = 4.70			
Cl = 6.24			
V = 29			
$C_{max}$ = 3288	$C_{max}$ = 1175	C	[36,81]
$T_{max}$ = 0.6	$T_{max}$ = 2.0		
AUC = 14.5	AUC = 10.44		
$t_{1/2}$ = 4.7	$t_{1/2}$ = 9.3		
Cl/F = 6.9	Cl/F = 9.6		
V/F = 35.8	V/F = 128		

MDZ, midazolam;  $t_{1/2}$ , half-life;  $T_{max}$  = time to maximum concentration; V/F, apparent volume of distribution; 1-OH MDZ, 1-hydroxy midazolam





# Part 2

**Dose finding of targeted agents  
in combination therapy**





# Chapter 5

## **Safety of the triple combination lapatinib, binimetinib, and vinorelbine for RAS mutated metastatic colorectal cancer patients: A preliminary analysis of the first dose levels from the RASTRIC Phase I/II clinical trial**

*Interim analysis*

Maarten A. Huisman  
Lisa T. van der Heijden  
Sander Mertens  
Helena M. Klein Wolterink  
Marijke Linschoten  
Manon N.G.J.A. Braat  
Miangela M. Lacle  
Geert W.J. Frederix  
Sjoerd G. Elias  
Frans L. Opdam  
Henk M.W. Verheul

Miriam Koopman  
Arco J. Teske  
Johannes L. Bos  
Filip Y.F.L. de Vos  
Hilde H. Nienhuis  
Lot A. Devriese  
Heleen A. Crommelin  
Eelke H. Gort  
Hugo J.G. Snippert  
Alwin D.R. Huitema  
Jeanine M.L. Roodhart

## ABSTRACT

**Background:** Treatment options for patients with metastatic RAS-mutated colorectal cancer (CRC) are limited. Promising results were observed for triple therapy consisting of MEK inhibitors, pan-HER inhibitors, and a microtubule targeting agent (MTA) in patient derived organoids. Triple therapy of binimetinib (MEK inhibitor), lapatinib (pan-HER inhibitor), and vinorelbine (MTA) was investigated in a Phase I/II trial (RASTRIC study).

**Methods:** The main objective was to determine safety and the Recommended Phase 2 Dose of this triple therapy. Patients with RAS mutated CRC were treated with escalating doses of binimetinib twice daily (BID), lapatinib once daily (QD), starting at 15 mg BID and 750 mg QD, respectively, and vinorelbine 17.5 mg/m<sup>2</sup> weekly in an intermittent schedule during two out of three weeks.

**Results:** At data cut-off (February 2022), 14 patients were included across the first four dose levels. Dose-limiting adverse events were reported in 3 out of 14 patients, including diarrhoea (n=3), decreased neutrophil count (n=1), dehydration (n=1), and febrile neutropenia (n=1). Most frequent toxicities were diarrhoea (n=10), rash (n=11), and anaemia (n=4). A dose of 1000 mg lapatinib QD, 30 mg binimetinib 30 mg BID, and 17.5 mg/m<sup>2</sup> vinorelbine was tolerable. Pharmacokinetic data (PK) showed a direct dose-exposure relationship for binimetinib but not for lapatinib, consistent with their relative increase in toxicity. No drug-drug interactions were observed.

**Conclusion:** The dose of lapatinib 1000mg QD, binimetinib 30mg BID and vinorelbine 17,5 mg/m<sup>2</sup> in a rest week schedule was safe and well tolerated. No relevant PK interactions were found. Subsequent dose levels are ongoing to optimise vinorelbine dose and treatment schedule to define the recommended phase 2 dose.

## 1 INTRODUCTION

The RAS-RAF-MEK-ERK pathway, or Mitogen Activated Protein Kinase-(MAPK) pathway, is of vital importance for growth and survival in colorectal carcinomas (CRC). Around half of all metastatic CRC (mCRC) patients have a mutation in the RAS gene. Compared to mCRC patients with RAS/BRAF wildtype, these patients have fewer available treatment options and a worse overall prognosis [1]. Targeting RAS has been found challenging for many years [2] but recently targeting of the G12C and G12D KRAS mutations have become possible [3,4]. Despite promising results, these treatments are available only for a subset of KRAS mutations. Moreover, resistance to treatment remains an issue [5] Therefore, for most patients with RAS-mutated mCRC, there is a dire need of effective therapy to improve prognosis.

The possibility of such an effective therapy might lie in combining multiple drugs targeting both upstream and downstream of the mutated gene. This double inhibition approach has proved to more effective than targeting MAPK components as single agent [6]. Combining selective BRAF V600E inhibitors with EGFR targeting antibodies improved efficacy and could overcome resistance which is now applied as standard treatment in BRAF-mutated CRC [7,8]. Similarly, combining KRAS G12C inhibitors with EGFR targeting is more effective than monotherapy [9]. However, early Phase trials combining EGFR-targeting pan-HER with MEK inhibitors to target RAS-mutated colorectal cancer has led to disappointing results [10–12].

One explanation for the lack of effect as observed in these clinical trials is the observation that in patient-derived organoids (PDOs), the double targeting strategy was cytostatic rather than cytotoxic [13]. Even at high dose, these combinations did not result in a killing effect when observed with brightfield microscopy, while a (almost) complete metabolic shutdown was observed, and thus seen as ‘dead’ in classical ATP-based screening assays. Using a microscopy based screen, we identified that adding microtubule targeting agents (MTA) to the double targeting strategy has a synergistic killing effect [14] We predicted that the combination of pan-HER inhibitor lapatinib, MEK-inhibitor binimetinib and MTA vinorelbine could have a good balance between efficacy and safety based on available safety data [15–17].

Indeed, we found this triple combination to be effective in 23/25 predominantly RAS-mutated PDOs and safe and effective in a xenotransplant mouse model [14]. Lapatinib is a tyrosine kinase inhibitor targeting the ERBB-family, comprised of amongst others HER2 and EGFR [18] and is routinely used in combination with MTA vinorelbine in HER2+ breast cancer patients [16]. Binimetinib is one of the first developed MEK-inhibitors [17] and is widely used in BRAF V600E mutant CRC patients [8]. However, safety of this triple combination has not been tested in humans before.

Therefore, in this RASTRIC Phase 1 dose-escalation trial, we investigate the safety and pharmacokinetics of the triple combination of lapatinib, binimetinib and vinorelbine in colorectal cancer patients for whom no effective palliative treatment was available. Here we present the results of the first interim analysis with regards to initial pharmacokinetics and preliminary safety of the first four dose levels. The RASTRIC trial is currently ongoing and additional dose levels are being evaluated.

## 2 METHODS

### 2.1 Study design and treatment

This study is an ongoing open-label Phase 1 dose-escalation trial with a 3+3 design to test the safety and efficacy of a combination of lapatinib, binimetinib, and vinorelbine. The study is conducted in the University Medical Center Utrecht in Utrecht, the Netherlands.

To find the optimal combination of doses for this triplet, we prioritized to escalate binimetinib first, lapatinib second, and vinorelbine third, since the combination of lapatinib and vinorelbine had already been established [19–21]. We started with a rest week schedule, with a three-week-cycle consisting of two treatment weeks with lapatinib and binimetinib 5 days on and 2 days off with vinorelbine infusion every third day of lapatinib of that week, and one week without study drugs (representation of the schedule in Figure 1, lower left panel). In treatment weeks, patients took oral doses of lapatinib once daily in the morning before breakfast and oral doses of binimetinib twice daily 12 hours apart. On the third day of binimetinib and lapatinib treatment, patients received intravenous dose of vinorelbine at the clinical ward in the morning. Additional dose levels evaluating different treatment schedules are currently ongoing.

### 2.2 Patients

Patients with mCRC are included if they have a proven RAS mutation after failure of standard chemotherapeutic regimens including at least 5-FU/capecitabine-oxaliplatin and irinotecan based standard treatment (unless contra-indications for either oxaliplatin or irinotecan). Other inclusion criteria are WHO performance status of 0-1, willing and able to undergo a biopsy of a metastasis lesion, adequate bone marrow-, kidney-, and liver function.

Exclusion criteria are symptomatic or untreated leptomeningeal disease, symptomatic brain metastasis, history of interstitial lung disease or pneumonitis, significant cardiovascular disease, history of retinal vein occlusion, incapacity to ingest oral drugs or known malabsorption, ileostomy, and prior therapy containing targeted drug combinations known to interfere with EGFR, HER2, HER3, HER4 or MAPK- and PI3K-pathway components. Further exclusion criteria are serum albumin <30g/L, serum LDH >2x ULN and a left ventricular ejection fraction <50%. The study protocol provides a full list of all inclusion and exclusion criteria.

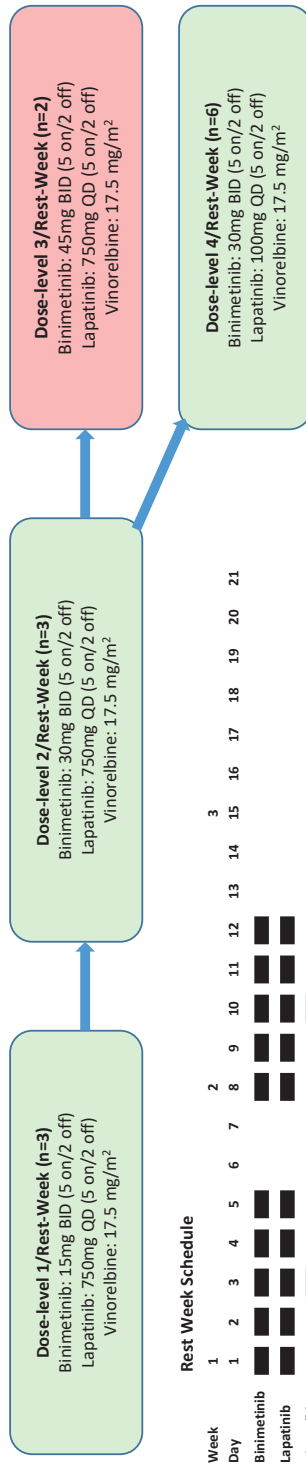


**Figure 1.** Graphical representation of dose-escalation and treatment schedule.

### 2.3 Safety and efficacy assessments

The primary endpoint of this trial is the incidence of dose-limiting toxicity (DLT) resulting in a recommended phase 2 regimen (RP2R). All patients who received at least one administration of all three trial drugs are included in the safety population. Adverse events are graded using CTCAE version 5.0 and are monitored continuously. All patients in the study are discussed at least weekly by a Phase 1 team consisting of medical oncologists and research nurses and pharmacists.

DLT is defined as an adverse event of predefined severity occurring during the first complete treatment cycle of three weeks, or longer if a delay occurs during treatment, and determined to be at least probably related to lapatinib, binimetinib or vinorelbine. DLT definitions included grade 3 or higher non-haematological adverse events, grade 4 or higher haematological adverse events, any retinal vein occlusion or retinopathy of grade 2 or higher, a drop in LVEF below 45% or grade 2 or higher toxicity occurring beyond 21 days, which in the judgement of the investigator was a DLT.

To assess disease-activity, CT scans are performed at baseline and every 6 weeks post-baseline until progression of disease according to RECIST 1.1, or withdrawal of patient's consent. Patients are evaluable if they have received two cycles of trial treatment and at least one response outcome post baseline.

### 2.4 Adverse event management

Prophylactic schedules are used to limit the occurrence and severity of diarrhoea and skin toxicity. In the event of unformed or frequent stools, standard supportive care for diarrhoea involved the administration of loperamide, with an initial dose of 4 mg followed by 2 mg every four hours or after each loose stool.

Starting from dose level 4, we adjusted our approach to diarrhoea treatment based on results from the CONTROL trial, which tested several prophylactic regimens for the HER2-targeting drug, neratinib [22]. Our schedule included a daily dose of budesonide 9 mg during the first and second treatment cycles, along with the standard prophylactic dosage of loperamide.

For skin toxicity, patients are encouraged to avoid sunlight, if possible, use sunscreen SPF  $\geq 30$  and thick alcohol-free emollient cream on dry areas. At first symptoms of rash, additional measures were taken to prevent severe rash from developing: prescription of doxycycline and class 3 topical steroids (e.g., betamethasone 1 mg/g) on affected skin lesions.

## 2.5 Pharmacokinetic assessments

In the first four dose levels presented in this interim analysis, blood samples were obtained from all patients on day 1 of cycle 1 before and 0.5, 1, 2, 6, 8, and 24 h after administration of the first dose for pharmacokinetic analysis. On day 3 of cycle 1, blood samples were collected before and 1, 2, 6, 8, and 24 h after administration of the first dose.

Plasma concentrations of lapatinib and vinorelbine were quantified with previously reported validated liquid-chromatography tandem mass spectrometry (LC-MS/MS) methods [23,24]. Binimetinib plasma concentrations were quantified as follows: binimetinib was extracted from plasma with protein precipitation with acetonitrile. An Acquity BEH C18 Column (50 x 2.1 mm, 1.7  $\mu$ m particle size) was used for liquid chromatography. Detection was performed with an TQ6500+ tandem mass spectrometer equipped with a turbo ion spray interface operating in positive ion mode. The transition  $m/z$  441.9 to 379.9 was monitored for the detection of binimetinib. A stable isotope-labelled internal standard was used. The lower limit of quantification was 10.0 ng/mL and the upper limit of quantification was 1000 ng/mL.

Pharmacokinetic parameters were calculated in R using a validated script for non-compartmental pharmacokinetic analyses (version 4.2.1).

## 2.6 Patient-Derived Organoid (PDO) culture and drug screens

To evaluate if pharmacokinetic observations in this trial correspond to levels used in preclinical drug screens, drug screens were performed on CRC PDOs from a biobank established and characterized previously according to ethical principles and regulation [25,26]. All organoids were established after ethical committee approved informed consent forms were signed by patients [25].

The method of our drug screen is written in detail in our previous work [14]. In short: organoids were plated in 384 well plates 5-7 day after seeding. Drugs were added using a Tecan D300e Digital Dispenser. After 72 hours of incubation, organoids were imaged in the presence of 10 $\mu$ g/mL Hoechst. Afterwards an imaging pipeline was used to assess organoid survival per well.

## 2.7 Ethical considerations and regulation

The study protocol and all amendments were reviewed and accepted by the Medical Research Ethics Committee associated with the UMC Utrecht (NedMec) and the Dutch competent authority (CCMO). The study is conducted in full



conformance with the principles of the declaration of Helsinki, guidelines for Good Clinical Practice and local legislation, taking priority for whichever afforded the greater protection for our participants. The trial was registered with the European Clinical Trials Database (EudraCT) under identifier: 2019-004987-23.

## 3 RESULTS

This trial is still ongoing and in this interim analysis, the data of the finished dose levels 1-4 are presented. Consequently, the data cut-off of this interim analysis is February 2022.

### 3.1 Patient Characteristics

In dose level 1-4, a total of 14 mCRC patients were included. An overview of patient characteristics can be found in Table 1. Patients were heavily pretreated, all patients received treatment lines containing a fluoropyrimidine, oxaliplatin and irinotecan. Most patients had a liver metastasis, and almost all had a pathogenic KRAS mutation. One patient was included that had a KRAS wildtype amplification which was considered as causing an aberrant increase of KRAS activity.

### 3.2 Dose Administration and Escalation

A diagram of the dose levels in this trial is given in Figure 1. Binimetinib dosing was initiated at 15 mg BID and escalated to 30 mg and 45 mg after dose level 1 and 2 were cleared with manageable toxicity. The 45 mg dose was not tolerated by both patients in this dose level, both not able to complete the first cycle due to diarrhoea despite adequate prophylactic treatment (grade 3 and grade 2 diarrhoea, with the latter not being able to complete 75% of prescribed cycle 1 dose), no third patient was included in this dose level.

Dose level 4 was then initiated, where the lapatinib dose was escalated to 1000 mg QD. The first patient in this dose level had a DLT of grade 3 diarrhoea and febrile neutropenia grade 3. The dose level was expanded to include a total of six patients, but no other patients experienced a DLT. The subsequent patients received a more stringent prophylactic diarrhoea protocol, with daily loperamide on treatment days given to prevent severe diarrhoea. The following patients had manageable toxicity in this dose level with no higher diarrhoea grade than 2 in 4 patients.

**Table 1.** Descriptive characteristics of the study population, median (range) or N (%)

<b>Characteristic</b>	<b>Total (N=14)</b>
Median Age in years (Range)	55 (31-67)
Female Sex - N (%)	8 (57)
WHO Performance Score - N (%)	
0	4 (29)
1	10 (71)
Median prior lines (Range)	3 (2-4)
Type of therapy - N (%)	
Fluoropyrimidine	14 (100)
Oxaliplatin	14 (100)
Irinotecan	14 (100)
Anti-VEGF	9 (64)
Anti-EGF	1 (7)
KRAS G12C inhibitor	1 (7)
Primary Tumour Location - N (%)	
Left	11 (79)
Right	1 (7)
Rectum	2 (14)
Metastatic laesion site - N (%)	
Lymph Node	7 (50)
Liver	13 (93)
Lung	12 (86)
Bone	5 (36)
Peritoneal	3 (21)
Other	5 (36)
Number of metastatic sites - N (%)	
1	1 (7)
2	5 (36)
3	3 (21)
≥ 4	5 (36)
Molecular status - N (%)	
KRAS codon 12 mutation	9 (64)
KRAS codon 13 mutation	2 (14)
Non-exon 2 KRAS mutation	2 (14)
KRAS WT amplification	1 (7)
BRAF mutation	0 (0)

### 3.3 Safety

Treatment-related adverse events of any grade occurred in all 14 patients evaluable for safety during the first treatment cycle (Table 2). The most common adverse events were rash (maculopapular or papulopustular), diarrhoea, and anaemia in respectively 79%, 71%, and 29% of patients. Three patients experienced a grade 3 or higher adverse event during the first cycle: diarrhoea in 2 patients and a neutrophil count decrease in 1 patient. Adverse events lead to treatment discontinuation in 12% of patients, and dose reduction in 18%. All other patients were discontinued from treatment due to progressive disease.

### 3.4 Pharmacokinetic analysis

Pharmacokinetic parameters of lapatinib and binimetinib on day 1 and day 3 of cycle 1 and of vinorelbine on day 3 of cycle 1 are summarized in Table 3. Area under the plasma-concentration-time curve from time 0 to 8 h ( $AUC_{0-8}$ ) was calculated for binimetinib and  $AUC$  from time 0 to 24 h ( $AUC_{0-24}$ ) for lapatinib and vinorelbine.

Lapatinib pharmacokinetics were characterized by a large interindividual variability (see Figure 2A-B). Maximum concentration ( $C_{max}$ ) and  $AUC_{0-24}$  were relatively constant over the different dose levels, except dose level 1 for cycle 1, indicating that there was no dose-linearity between the 750 and 1000 mg doses. The  $AUC_{0-24}$  between day 1 and day 3 of cycle 1 increased approximately 1.1 to 2.7-fold after multiple dosing, which is consistent with previous studies [10]. The time to reach the maximum concentration ( $T_{max}$ ) ranged between 2.5-6.0 h suggesting a highly variable absorption rate of lapatinib between patients. One patient in dose level 3 never reached a true  $C_{max}$  for day 3 (see Figure 2B), but rather reached a plateau during the period of sample collection.

The pharmacokinetics of binimetinib were characterized by a fast absorption ( $T_{max}$  range: 0.8-2.2) and a short half-life (mean: 3.4 h, range: 1.7-9.0 h, see Figure 2C-D). Both  $C_{max}$  and  $AUC_{0-8}$  demonstrated dose-proportional increase, suggesting dose-linearity. There was no increase in  $C_{max}$  and  $AUC$  between day 1 and day 3 indicating no accumulation of binimetinib, which is consistent with the short half-life of binimetinib.

We observed low interindividual variability for the pharmacokinetics of vinorelbine ( $CV\% \leq 25.6$ ). The  $AUC_{0-24}$  was relatively constant over the different dose-levels consistent with the observed low variability in the data (see Figure 2E).

### 3.4.1 Drug interaction

The AUC of the three drugs is depicted together per dose level in Figure 3. An increase of 1.6-fold in lapatinib  $AUC_{0-24}$  between dose level 1 and 2 could be observed. However, exposure of the three drugs is in line with the observed exposure for monotherapy.

### 3.4.2 Association pharmacokinetics and toxicity

The  $AUC_{0-8}$  of binimetinib was higher for patients who experienced a DLT compared to patients who did not experience a DLT (geometric mean (CV%): 1400 ng/mL\*h (47.1) vs 826 ng/mL\*h (54.2), respectively). Patients who experienced a DLT also had a slightly higher lapatinib  $AUC_{0-24}$  (7825 ng/mL\*h (42.5) vs 6681 ng/mL\*h (40.8), respectively). The  $AUC_{0-24}$  of vinorelbine was similar between patients with a DLT and patients without a DLT (88.9 ng/mL\*h (15.6) vs 87.6 ng/mL\*h (19.3), respectively).

## 3.5 Determining optimal dosing based on organoid drug screens

Our earlier research demonstrated the synergistic impact of using a microtubule targeting agent in combination with a pan-HER inhibitor and a MEK inhibitor [14]. To evaluate if the observed PK parameters for the specific mix of lapatinib, binimetinib, and vinorelbine correspond to levels needed *in vitro* to elicit efficacy, drug screening tests were performed before the trial was started. The aim was to evaluate efficacy *in vitro* at an optimal dose range for this combination therapy, using *in vitro* drug concentrations similar to serum concentrations achieved in patients, which we call “achievable” (as seen in Figure 4 and boxes in 4A and 4B). Then, the aim was to evaluate if the drug concentrations found in our study are within this range so that a potential biological effect may be expected.

We conducted these drug screenings on four unique patient-derived organoids (PDOs) harbouring a KRAS mutation from a biobank established earlier [25].

The screening results, both with and without vinorelbine for P9T, are exemplified in Figure 4A and B. The boxes indicate the range of drug concentrations for lapatinib (301 to 3219 ng/mL) and binimetinib (122 to 1297 ng/mL). The nine achievable drug concentrations falling within these ranges were summarized for the four patient-derived organoids (PDOs) in screenings with and without vinorelbine at 77 ng/mL, as illustrated in Figure 4C. For binimetinib, a steady state  $C_{max}$  (maximum serum concentration) of 654 ng/mL was measured for the 45 mg twice-daily dose after 15 days in combination with encorafenib [27]. For lapatinib, the steady state  $C_{max}$  for the daily dose of 1200 mg was 1.39 ng/mL [28]. Lastly, the concentration at 30 min after administration for intravenously administered vinorelbine at 20 mg/m<sup>2</sup> was 647 ng/ml [29].

**Table 2.** Summary of treatment-related adverse events during the first treatment cycle

<b>Toxicities leading to:</b>	<b>Dose-level 1 (n=3)</b>		<b>Dose-level 2 (n=3)</b>	
DLT	0 (0)		0 (0)	
Dose discontinuation	0 (0)		0 (0)	
Dose interruption	0 (0)		0 (0)	
Dose reduction	0 (0)		1 (33)	
<b>Highest related adverse events grade per patient* during safety period – amount of patient (percentage of dose level/total)</b>				
	<b>Dose-level 1 (n=3)</b>		<b>Dose-level 2 (n=3)</b>	
	Grade 1 or 2	Grade ≥3	Grade 1 or 2	Grade ≥3
<b>Highest grade related toxicity</b>	3 (100)	0 (0)	3 (100)	0 (0)
<b>Rash</b>	3 (100)	0 (0)	3 (100)	0 (0)
<b>Diarrhoea</b>	0 (0)	0 (0)	3 (100)	0 (0)
<b>Anaemia</b>	1 (33)	0 (0)	2 (67)	0 (0)
<b>CPK increased</b>	1 (33)	0 (0)	0 (0)	0 (0)
<b>Nausea</b>	1 (33)	0 (0)	1 (33)	0 (0)
<b>Abdominal distension</b>	3 (100)	0 (0)	1 (33)	0 (0)
<b>Hypokalaemia</b>	2 (67)	0 (0)	1 (33)	0 (0)
<b>Neutrophil count decreased</b>	0 (0)	0 (0)	0 (0)	0 (0)
<b>AST increased</b>	0 (0)	0 (0)	1 (33)	0 (0)
<b>Fatigue</b>	0 (0)	0 (0)	0 (0)	0 (0)
<b>Hypoalbuminaemia</b>	0 (0)	0 (0)	1 (33)	0 (0)
<b>Hypomagnesaemia</b>	1 (33)	0 (0)	1 (33)	0 (0)
<b>Hypophosphatemia</b>	0 (0)	0 (0)	1 (33)	0 (0)
<b>Vomiting</b>	0 (0)	0 (0)	1 (33)	0 (0)
<b>Dehydration</b>	0 (0)	0 (0)	0 (0)	0 (0)
<b>Lymphocyte count decreased</b>	1 (33)	0 (0)	0 (0)	0 (0)
<b>ALT increased</b>	0 (0)	0 (0)	1 (33)	0 (0)
<b>Dry skin</b>	0 (0)	0 (0)	1 (33)	0 (0)
<b>Dyspepsia</b>	0 (0)	0 (0)	0 (0)	0 (0)
<b>Hyperglycemia</b>	0 (0)	0 (0)	0 (0)	0 (0)
<b>Hyperphosphatemia</b>	1 (33)	0 (0)	1 (33)	0 (0)
<b>LDH increased</b>	0 (0)	0 (0)	0 (0)	0 (0)
<b>Mucositis oral</b>	0 (0)	0 (0)	0 (0)	0 (0)
<b>Febrile neutropenia</b>	0 (0)	0 (0)	0 (0)	0 (0)
<b>White blood cell decreased</b>	0 (0)	0 (0)	0 (0)	0 (0)

\* Only adverse events grade 1 or 2 occurring in >1 patient or any event grade 3 or higher is listed in this table.

<b>Dose-level 3 (n=2)</b>		<b>Dose-level 4 (n=6)</b>		<b>All dose levels (n=14)</b>	
	2 (100)		1 (17)		3 (21)
	0 (0)		1 (17)		1 (7)
	1 (50)		2 (33)		3 (21)
	1 (50)		1 (17)		3 (21)

<b>Dose-level 3 (n=2)</b>		<b>Dose-level 4 (n=6)</b>		<b>All dose levels (n=14)</b>		
Grade 1 or 2	Grade ≥3	Grade 1 or 2	Grade ≥3	Any grade	Grade 1 or 2	Grade ≥3
0 (0)	2 (100)	5 (83)	1 (17)	14 (100)	11 (79)	3 (21)
1 (50)	0 (0)	4 (67)	0 (0)	11 (79)	11 (79)	0 (0)
1 (50)	1 (50)	4 (67)	1 (17)	10 (71)	8 (57)	2 (14)
1 (50)	0 (0)	0 (0)	0 (0)	4 (29)	4 (29)	0 (0)
1 (50)	0 (0)	1 (17)	0 (0)	3 (21)	3 (21)	0 (0)
1 (50)	0 (0)	0 (0)	0 (0)	3 (21)	3 (21)	0 (0)
0 (0)	0 (0)	0 (0)	0 (0)	4 (29)	4 (29)	0 (0)
0 (0)	0 (0)	1 (17)	0 (0)	4 (29)	4 (29)	0 (0)
1 (50)	0 (0)	0 (0)	1 (17)	2 (14)	1 (7)	1 (7)
1 (50)	0 (0)	0 (0)	0 (0)	2 (14)	2 (14)	0 (0)
1 (50)	0 (0)	1 (17)	0 (0)	2 (14)	2 (14)	0 (0)
0 (0)	0 (0)	1 (17)	0 (0)	2 (14)	2 (14)	0 (0)
0 (0)	0 (0)	0 (0)	0 (0)	2 (14)	2 (14)	0 (0)
0 (0)	0 (0)	1 (17)	0 (0)	2 (14)	2 (14)	0 (0)
1 (50)	0 (0)	2 (33)	0 (0)	4 (29)	4 (29)	0 (0)
0 (0)	0 (0)	0 (0)	1 (17)	1 (7)	0 (0)	1 (7)
0 (0)	1 (50)	0 (0)	0 (0)	2 (14)	1 (7)	1 (7)
0 (0)	0 (0)	0 (0)	0 (0)	1 (7)	1 (7)	0 (0)
1 (50)	0 (0)	0 (0)	0 (0)	2 (14)	2 (14)	0 (0)
1 (50)	0 (0)	0 (0)	0 (0)	1 (7)	1 (7)	0 (0)
0 (0)	0 (0)	1 (17)	0 (0)	1 (7)	1 (7)	0 (0)
0 (0)	0 (0)	0 (0)	0 (0)	2 (14)	2 (14)	0 (0)
1 (50)	0 (0)	0 (0)	0 (0)	1 (7)	1 (7)	0 (0)
0 (0)	0 (0)	1 (17)	0 (0)	1 (7)	1 (7)	0 (0)
0 (0)	0 (0)	0 (0)	1 (17)	1 (7)	0 (0)	1 (7)
0 (0)	0 (0)	0 (0)	0 (0)	0 (0)	0 (0)	0 (0)

**Table 3.** Pharmacokinetic parameters of lapatinib, binimetinib and vinorelbine.

Dose level	1	2	3
<b>Lapatinib QD</b>	750 mg (5/2)	750 mg (5/2)	750 mg (5/2)
<b>Binimetinib BID</b>	15 mg (5/2)	30 mg (5/2)	45 mg (5/2)
<b>Vinorelbine Q3W</b>	17.5 mg/m <sup>2</sup>	17.5 mg/m <sup>2</sup>	17.5 mg/m <sup>2</sup>
<b>Lapatinib</b>	<b>Cycle 1 Day 1</b>		
<b>Geometric mean (CV%)</b>	n=3	n=3	n=2
<b>C<sub>max</sub> (ng/mL)</b>	754 (34.3)	1242 (47.5)	1570 (22.7)
<b>t<sub>max</sub> (h)</b>	2.5	2.6	6.0
<b>AUC<sub>0-24</sub> (ng/mL*h)</b>	4290 (32.2)	7033 (41.9)	9062 (29.4)
<b>Lapatinib</b>	<b>Cycle 1 Day 3</b>		
<b>Geometric mean (CV%)</b>	n=3	n=3	n=1
<b>C<sub>max</sub> (ng/mL)</b>	1031 (46.5)	1394 (53.2)	1085
<b>t<sub>max</sub> (h)</b>	3.4	3.5	-
<b>AUC<sub>0-24</sub> (ng/mL*h)</b>	6736 (45.0)	7934 (15.8)	6916
<b>Binimetinib</b>	<b>Cycle 1 Day 1</b>		
<b>Geometric mean (CV%)</b>	n=3	n=3	n=2
<b>C<sub>max</sub> (ng/mL)</b>	156 (24.6)	376 (20.9)	514 (30.7)
<b>t<sub>max</sub> (h)</b>	1.0	0.8	1.4
<b>AUC<sub>0-8</sub> (ng/mL*h)</b>	432 (18.9)	882 (6.4)	1650 (19.0)
<b>Binimetinib</b>	<b>Cycle 1 Day 3</b>		
<b>Geometric mean (CV%)</b>	n=3	n=3	n=1
<b>C<sub>max</sub> (ng/mL)</b>	123 (120)	236 (23.5)	276
<b>t<sub>max</sub> (h)</b>	1.5	1.3	2.2
<b>AUC<sub>0-8</sub> (ng/mL*h)</b>	473 (78.9)	940 (12.5)	1569
<b>Vinorelbine</b>	<b>Cycle 1 Day 3</b>		
<b>Geometric mean (CV%)</b>	n=3	n=3	n=1
<b>AUC<sub>0-24</sub> (ng/mL*h)</b>	94.01 (11.8)	88.58 (12.0)	92.34

Abbreviations: C<sub>max</sub>, peak plasma concentration; CV%; coefficient of variation; t<sub>max</sub>, time of maximum plasma concentration; AUC<sub>0-8</sub>, area under the plasma concentration-time curve from time zero to 8 hours after administration;



<b>4</b>			
1000 mg (5/2)			
30 mg (5/2)			
17.5 mg/m <sup>2</sup>			
	<b>All 750 mg doses</b>	<b>All 1000 mg doses</b>	
n=6	n=8	n=6	
1070 (38.0)	1092 (47.1)	1070 (38.0)	
4.3	3.2	4.3	
5860 (41.4)	6225 (46.1)	5860 (41.4)	
	<b>All 750 mg doses</b>	<b>All 1000 mg doses</b>	
n=6	n=7	n=6	
1490 (45.6)	1182 (43.4)	1490 (43.4)	
5.1	3.5	5.1	
9143 (39.2)	7253 (28.3)	9143 (39.2)	
	<b>All 15 mg doses</b>	<b>All 30 mg doses</b>	<b>All 45 mg doses</b>
n=6	n=3	n=12	n=2
327 (59.1)	156 (24.6)	342 (47.4)	514 (30.7)
1.1	1.0	1.0	1.4
1062 (38.5)	432 (18.9)	998 (31.8)	1650 (19.0)
	<b>All 15 mg doses</b>	<b>All 30 mg doses</b>	<b>All 45 mg doses</b>
n=6	n=3	n=9	n=1
332 (39.7)	123 (120)	296 (37.9)	276
1.8	1.5	1.7	2.2
1408 (33.5)	473 (78.9)	1230 (34.3)	1569
	<b>All patients</b>		
n=5	n=12		
83.34 (25.6)	87.96 (17.7)		

AUC<sub>0-24</sub>, area under the plasma concentration-time curve from time zero to 24 hours after administration; 5/2, 5 days on/2 days off.

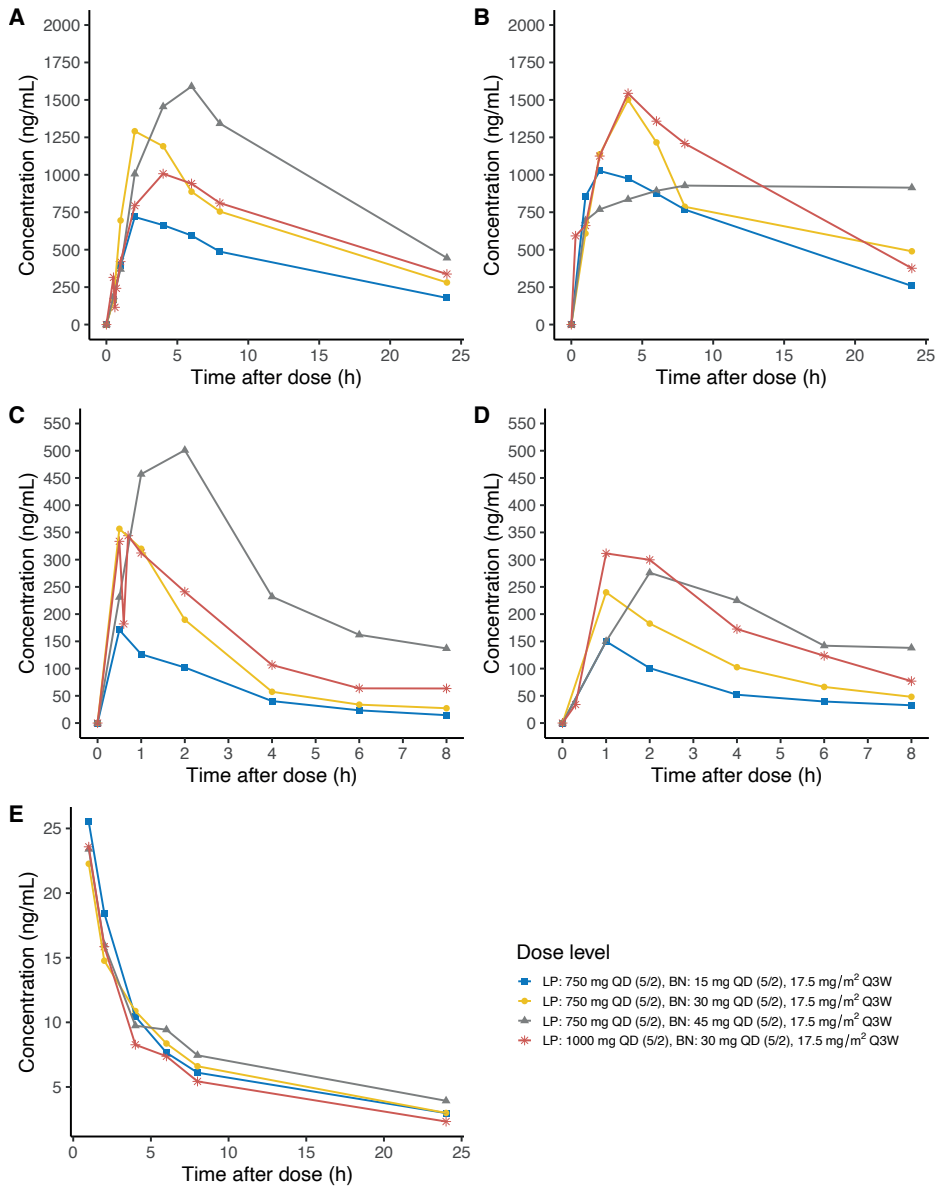


**Figure 2.** Plasma-concentration-time curves per dose level for lapatinib (A and B), binimetinib (C and D), and vinorelbine (E) for day 1 of cycle 1 or day 3 for cycle 2, respectively.

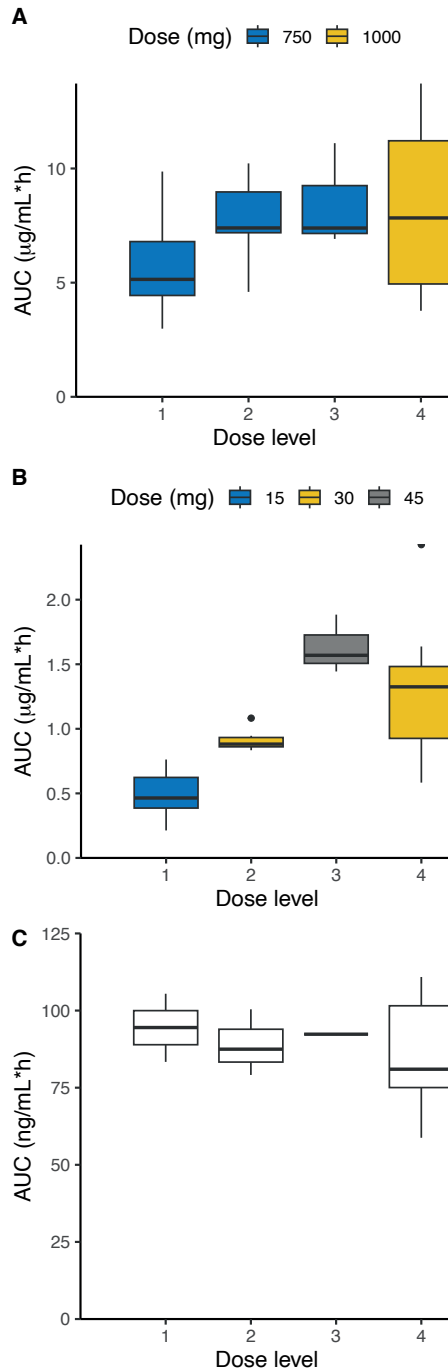


**Figure 3.** Area under the plasma concentration time curve (AUC) per dose level for lapatinib (A), binimetinib (B) and vinorelbine (C).

**B** Percentage survival per condition for P9T PDO drug screen with 72h lapatinib, binimetinib and vinorelbine (60nM fixed)

3.1	-2.1	7.6	14.1	6.7	4.6	1.5	1.5	-1.9
15.9	10.8	4.9	2.1	7.9	-2.2	-0.3	6.5	0.3
88.5	58.9	51.7	19.4	15.4	15.9	9.6	8.5	9.4
99.5	93.3	81.6	83.6	62.4	44.0	16.8	24.7	10.5
105.3	97.9	93.0	77.9	84.1	56.7	38.5	13.0	11.7
105.9	94.1	95.5	97.4	75.8	64.4	54.6	30.7	17.2
104.0	103.7	96.5	93.3	76.5	83.1	61.3	40.0	22.2
104.9	99.3	95.7	90.1	82.9	80.1	63.3	39.6	28.7
	97.6	98.4	91.4	83.1	85.9	80.5	63.0	36.3

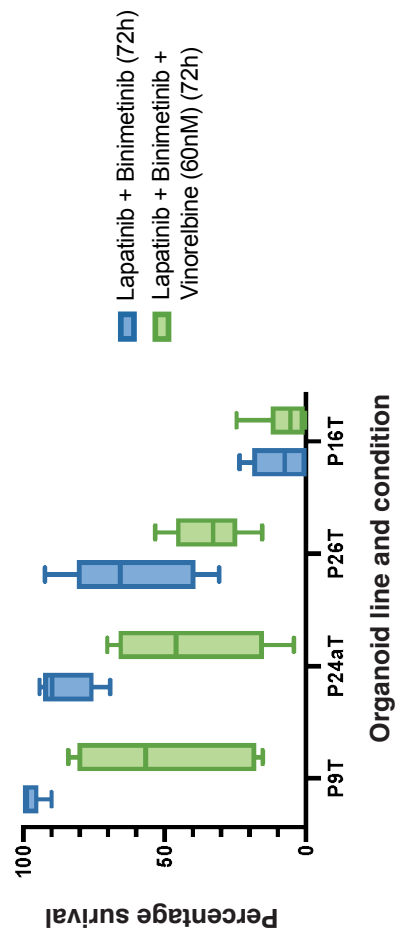
Binimetinib

**A** Percentage survival per condition for P9T PDO drug screen with 72h lapatinib and binimetinib

31.4	20.0	13.7	10.1	5.8	2.3	1.6	-0.9	-2.0
108.9	103.6	91.8	91.5	85.1	85.6	78.0	93.7	77.8
106.8	103.2	103.2	96.7	99.5	90.0	85.3	87.4	90.6
110.7	105.9	93.7	93.8	98.9	95.4	87.0	76.5	87.2
95.0	105.5	104.4	104.2	100.1	104.3	89.6	91.3	88.8
102.2	100.8	99.8	105.7	94.7	100.9	93.6	93.1	88.7
102.2	93.4	105.1	94.5	91.4	103.2	94.0	95.3	79.1
97.3	99.1	111.3	100.9	100.4	99.1	99.2	91.7	87.0
	99.7	99.0	98.2	98.3	100.6	95.4	91.7	82.4

Binimetinib

**C** PDO survival for 4 different organoids at 9 clinically achievable dose conditions for double combination drugs screen with and without vinorelbine (60nM)



◀ **Figure 4.** Results of preclinical drug screens were used to create an estimate of achievable killing dose for different KRAS mutated organoids. **A & B)** Results of a microscopy-based drug screen showing percentage survival per condition for P9T PDO with a matrix of descending doses of lapatinib (columns) and ascending doses of binimetinib (rows) with and without vinorelbine at 77 ng/mL. Doses for lapatinib were (from low to high): 8.6, 27.5, 92.9, 301, 985, 3219, 10534, and 34423 ng/mL. Dose for binimetinib were (from low to high): 11.3, 36.3, 122, 397, 1297, 4240, 13878, and 45352 ng/mL. Boxes show range of approximate  $C_{max}$  found in literature and three doses below. The intersect of these two boxes represent 9 approximate achievable dose conditions represented in C. **C)** Boxplot summarizing survival results in the 9 achievable dose conditions shown for P9T in the bold box in A and B. Data is shown for KRAS mutated PDOs P9T, P24aT, P26T and P16T without and with vinorelbine 77 ng/mL doses (blue and green respectively). All 4 PDO lines had KRAS-mutations.

The observed drug concentration in the current study fell within the ranges of the above predefined drug concentrations. For lapatinib, plasma concentrations of all dose levels fell within the predefined range, with the observed concentrations ranging from 298-2480 ng/mL. For binimetinib, the minimum observed concentration of the first dose level fell outside the predefined range (11.9 ng/mL), while all observed concentrations from the other dose levels fell within the predefined range (20.7-679 ng/mL). Vinorelbine concentrations ranged from 4.2 to 38.4 ng/mL. However, the first vinorelbine sample collected was 1 h after administration. Considering the fast initial drop in vinorelbine plasma concentrations (Figure 2E) it is possible that a concentration of 77 ng/mL was achieved.

## 4 DISCUSSION

Our preliminary findings show that lapatinib, binimetinib and vinorelbine can be combined with manageable toxicity at approximately 67% of the single agent dose. The fourth dose level consisting of 1000 mg lapatinib QD, 30 mg binimetinib BID and 17.5 mg/m<sup>2</sup> vinorelbine once weekly at a 5 days on/2 days off schedule during two weeks with one rest week was safe in 5 out of 6 patients. One patient experienced a DLT, while the five other patient in this dose level experienced grade 2 or lower toxicities. We successfully mitigated adverse events, which often limit the applicability of MEK- and pan-HER inhibitors, by implementing two relatively novel measures. First, our study design incorporated the 5 days on/2 days off schedule and prophylactic skin care regimens used in previous trials combining MEK- and pan-HER inhibitors [10,12]. Second, during our study we adopted an extensive prophylactic protocol tested in the CONTROL trial, which aimed to reduce diarrhoea in breast cancer patients receiving neratinib [22]. This approach effectively decreased the frequency and severity of diarrhoea. Thanks to these measures, we achieved clinically relevant drug levels.

Dose-escalation of binimetinib was limited due to dose-limiting diarrhoea in patients receiving 45 mg BID. While this binimetinib dose is used in the BEACON combination, which combines BRAF V600E, EGFR, and MEK inhibitors [8], this dose was found to be intolerable in the current triple therapy with lapatinib and vinorelbine. Pharmacokinetics of binimetinib depicted a linear dose-exposure relationship, which was consistent with previous studies [17]. Moreover, patients with DLTs had a 1.7-fold higher binimetinib exposure compared to patients without DLTs, suggesting an exposure-toxicity relationship. Conversely, lapatinib pharmacokinetics showed no dose-exposure relationship and were characterized by large inter-individual variability, which was consistent with literature [15]. Furthermore, patients with a DLT had a 1.2-fold higher lapatinib exposure compared to patients without a DLT, which is very small when considering the large inter-individual variability. Previous studies, however, reported a dose-toxicity relationship for lapatinib and diarrhoea over a dose range of 500 to 1600 mg[15].

Treatment-related adverse events of the triple therapy were largely similar to the combination therapy of MEK and pan-HER inhibitors [10–12]. The incidence of skin toxicity and diarrhoea was slightly lower compared to the combination therapy (79% vs 90% for skin toxicity and 71% vs 82% for diarrhoea, respectively [10–12], which might be due to the prophylactic protocols for skin toxicity and diarrhoea in

the current study. Both diarrhoea and skin toxicity are well known class-effects of both pan-HER inhibitors and MEK inhibitors [12,15,30–34]. Currently, it is unclear which drug class contributes more to toxicity. The exposure-toxicity relationships observed in the current study, suggests binimetinib might contribute more to the incidence of DLTs in the triple therapy. However, this data is limited, and a more extensive exposure-toxicity analysis needs to be performed before more definite conclusions can be drawn. The third most common treatment-related adverse event, anaemia, was not previously reported as part of the combination therapy. However, anaemia is a well-known adverse event of vinorelbine. Other well-known adverse events of vinorelbine were also observed in the current study, such as decreased neutrophil count and febrile neutropenia. These adverse events could not be explained by variability in vinorelbine exposure.

Several options can be considered regarding the further dose-optimisation of triple therapy with lapatinib, binimetinib, and vinorelbine. First, the observed exposure of lapatinib, binimetinib, and vinorelbine corresponded well with the observed effective concentrations in PDOs. While binimetinib dose could not be escalated to 45 mg BID, skin biopsies obtained from patients receiving 30 mg BID demonstrated inhibition of downstream MAPK activity marker pERK, indicating sufficient activity for the 30 mg dose level. Therefore, binimetinib dose was thought to be optimal for the current combination therapy. Second, co-administration with food could be considered for lapatinib. Lapatinib exposure increased with 167% when co-administrated with a low-fat breakfast and 325% with a high-fat breakfast [35]. Using this strategy, lapatinib dose could be decreased while maintaining similar exposure. Co-administration with food has already been implemented for abiraterone [36]. Third, dose increase for vinorelbine could be considered. Lastly, continuous dosing of lapatinib and binimetinib with weekly administration of vinorelbine could be considered.

## 5 CONCLUSION

Safety and pharmacokinetic results of the first four dose levels of the triple therapy with lapatinib, binimetinib and vinorelbine were described. Lapatinib 100 mg QD and binimetinib 30 mg BID in a 5 days on/2 days off schedule with weekly administrations of vinorelbine 17.5 mg/m<sup>2</sup> for two consecutive weeks followed by a rest week was found to be safe with manageable toxicity in mCRC patients. Most common treatment-related adverse events were skin toxicity, diarrhoea, and anaemia. Dose increase for vinorelbine or continuous dosing for lapatinib and binimetinib could be considered for future dose levels.



## REFERENCES

1. Li Z-N, Zhao L, Yu L-F, Wei M-J (2020) BRAF and KRAS mutations in metastatic colorectal cancer: future perspectives for personalized therapy. *Gastroenterol Rep (Oxf)* 15;8(3):192–205.
2. Cox AD, Fesik SW, Kimmelman AC, Luo J, Der CJ (2014) Drugging the undruggable RAS: Mission possible? *Nat Rev Drug Discov* 13(11):828–51.
3. Ostrem JM, Peters U, Sos ML, Wells JA, Shokat KM (2013) K-Ras(G12C) inhibitors allosterically control GTP affinity and effector interactions. *Nature* 28;503(7477):548–51.
4. Mao Z, Xiao H, Shen P, Yang Y, Xue J, Yang Y, et al (2022) KRAS(G12D) can be targeted by potent inhibitors via formation of salt bridge. *Cell Discov* 25;8(1):5.
5. Liu J, Kang R, Tang D (2022) The KRAS-G12C inhibitor: activity and resistance. *Cancer Gene Ther* 29(7):875–8.
6. Sun C, Hobor S, Bertotti A, Zecchin D, Huang S, Galimi F, et al (2014) Intrinsic resistance to MEK inhibition in KRAS mutant lung and colon cancer through transcriptional induction of ERBB3. *Cell Rep*. 10;7(1):86–93.
7. Russo M, Crisafulli G, Sogari A, Reilly NM, Arena S, Lamba S, et al (2019) Adaptive mutability of colorectal cancers in response to targeted therapies. *Science* 20;366(6472):1473–80.
8. Van Cutsem E, Huijberts S, Grothey A, Yaeger R, Cuyle P-J, Elez E, et al (2019) Binimetinib, Encorafenib, and Cetuximab Triplet Therapy for Patients With BRAF V600E-Mutant Metastatic Colorectal Cancer: Safety Lead-In Results From the Phase III BEACON Colorectal Cancer Study. *J Clin Oncol* 10;37(17):1460–9.
9. Yaeger R, Weiss J, Pelster MS, Spira AI, Barve M, Ou S-HI, et al (2023) Adagrasib with or without Cetuximab in Colorectal Cancer with Mutated KRAS G12C. *N Engl J Med* 388(1):44–54.
10. Huijberts SCFA, van Geel RMJM, van Brummelen EMJ, Opdam FL, Marchetti S, Steeghs N, et al (2020) Phase I study of lapatinib plus trametinib in patients with KRAS-mutant colorectal, non-small cell lung, and pancreatic cancer. *Cancer Chemother Pharmacol* 85(5):917–30.
11. van Brummelen EMJ, Huijberts S, van Herpen C, Desar I, Opdam F, van Geel R, et al (2021) Phase I Study of Afatinib and Selumetinib in Patients with KRAS-Mutated Colorectal, Non-Small Cell Lung, and Pancreatic Cancer. *Oncologist* 26(4):290-e545.
12. van Geel RMJM, van Brummelen EMJ, Eskens FALM, Huijberts SCFA, de Vos FYFL, Lolkema MPJK, et al (2020) Phase 1 study of the pan-HER inhibitor dacomitinib plus the MEK1/2 inhibitor PD-0325901 in patients with KRAS-mutation-positive colorectal, non-small-cell lung and pancreatic cancer. *Br J Cancer* 122(8):1166–74.
13. Verissimo CS, Overmeer RM, Ponsioen B, Drost J, Mertens S, Verlaan-Klink I, et al (2016) Targeting mutant RAS in patient-derived colorectal cancer organoids by combinatorial drug screening. *eLife* 5.
14. Mertens S, Huismans MA, Verissimo CS, Ponsioen B, Overmeer R, Proost N, et al (2023) Drug-repurposing screen on patient-derived organoids identifies therapy-induced vulnerability in KRAS-mutant colon cancer. *Cell Rep* 42(4):112324.

15. Burris HA, Hurwitz HI, Dees EC, Dowlati A, Blackwell KL, O'Neil B, et al (2005) Phase I safety, pharmacokinetics, and clinical activity study of lapatinib (GW572016), a reversible dual inhibitor of epidermal growth factor receptor tyrosine kinases, in heavily pretreated patients with metastatic carcinomas. *J Clin Oncol* 23(23):5305–13.
16. Thallinger C, Lang I, Kuhar CG, Bartsch R, Singer CF, Petruzelka L, et al (2016) Phase II study on the efficacy and safety of Lapatinib administered beyond disease progression and combined with vinorelbine in HER-2/neu- positive advanced breast cancer: results of the CECOG LaVie trial. *BMC Cancer* 16:121.
17. Bendell JC, Javle M, Bekaii-Saab TS, Finn RS, Wainberg ZA, Laheru DA, et al (2017) A phase 1 dose-escalation and expansion study of binimetinib (MEK162), a potent and selective oral MEK1/2 inhibitor. *Br J Cancer* 116(5):575–83.
18. Xia W, Mullin RJ, Keith BR, Liu L-H, Ma H, Rusnak DW, et al (2002) Anti-tumor activity of GW572016: a dual tyrosine kinase inhibitor blocks EGF activation of EGFR/erbB2 and downstream Erk1/2 and AKT pathways. *Oncogene* 21(41):6255–63.
19. Chew HK, Somlo G, Mack PC, Gitlitz B, Gandour-Edwards R, Christensen S, et al (2012) Phase I study of continuous and intermittent schedules of lapatinib in combination with vinorelbine in solid tumors. *Ann Oncol* 23(4):1023–9.
20. Stravodimou A, Voutsadakis IA (2019) A Systematic Review and Meta-analysis of the Combination of Vinorelbine and Lapatinib in Patients With Her2-positive Metastatic Breast Cancer. *Anticancer Res* 39(7):3295–301.
21. Brain E, Isambert N, Dalenc F, Diéras V, Bonnetterre J, Rezai K, et al (2012) Phase I study of lapatinib plus vinorelbine in patients with locally advanced or metastatic breast cancer overexpressing HER2. *Br J Cancer* 106(4):673–7.
22. Barcenas CH, Hurvitz SA, Di Palma JA, Bose R, Chien AJ, Iannotti N, et al (2020) Improved tolerability of neratinib in patients with HER2-positive early-stage breast cancer: the CONTROL trial. *Ann Oncol* 31(9):1223–30.
23. Herbrink M, de Vries N, Rosing H, Huitema ADR, Nuijen B, Schellens JHM, et al (2016) Quantification of 11 therapeutic kinase inhibitors in human plasma for therapeutic drug monitoring using liquid chromatography coupled with tandem mass spectrometry. *Ther Drug Monit* 38(6):649–56.
24. van der Heijden LT, Gebretensae A, Thijssen B, van Andel L, Nijstad AL, Wang Y, et al (2022) A highly sensitive bioanalytical method for the quantification of vinblastine, vincristine, vinorelbine and 4-O-deacetylvinorelbine in human plasma using LC-MS/MS. *J Pharm Biomed Anal* 215:114772.
25. van de Wetering M, Francies HE, Francis JM, Bounova G, Iorio F, Pronk A, et al (2015) Prospective derivation of a living organoid biobank of colorectal cancer patients. *Cell* 161(4):933–45.
26. Ubink I, Bolhaqueiro ACF, Elias SG, Raats DAE, Constantinides A, Peters NA, et al (2019) Organoids from colorectal peritoneal metastases as a platform for improving hyperthermic intraperitoneal chemotherapy. *Br J Surg* 106(10):1404–14.
27. European Medicines Agency (EMA). Mektovi SmPC (2018) [https://www.ema.europa.eu/en/documents/product-information/mektovi-epar-product-information\\_en.pdf](https://www.ema.europa.eu/en/documents/product-information/mektovi-epar-product-information_en.pdf) Accessed 21 July 2023
28. Burris HA, Taylor CW, Jones SF, Koch KM, Versola MJ, Arya N, et al (2009) A phase I and pharmacokinetic study of oral lapatinib administered once or twice daily in patients with solid malignancies. *Clin Cancer Res* 15(21):6702–8.

29. Khayat D, Rixe O, Brunet R, Goupil A, Bugat R, Harousseau J-L, et al (2004) Pharmacokinetic linearity of i.v. vinorelbine from an intra-patient dose escalation study design. *Cancer Chemother Pharmacol* 54(3):193–205.
30. Takahashi T, Boku N, Murakami H, Naito T, Tsuya A, Nakamura Y, et al (2012) Phase I and pharmacokinetic study of dacomitinib (PF-00299804), an oral irreversible, small molecule inhibitor of human epidermal growth factor receptor-1, -2, and -4 tyrosine kinases, in Japanese patients with advanced solid tumors. *Invest New Drugs* 30(6):2352–63.
31. O'Neil BH, Goff LW, Kauh JSW, Strosberg JR, Bekaii-Saab TS, Lee R-M, et al (2011) Phase II study of the mitogen-activated protein kinase 1/2 inhibitor selumetinib in patients with advanced hepatocellular carcinoma. *J Clin Oncol* 29(17):2350–6.
32. LoRusso P, Venkatakrishnan K, Chiorean EG, Noe D, Wu J-T, Sankoh S, et al (2014) Phase 1 dose-escalation, pharmacokinetic, and cerebrospinal fluid distribution study of TAK-285, an investigational inhibitor of EGFR and HER2. *Invest New Drugs* 32(1):160–70.
33. Infante JR, Fecher LA, Falchook GS, Nallapareddy S, Gordon MS, Becerra C, et al (2012) Safety, pharmacokinetic, pharmacodynamic, and efficacy data for the oral MEK inhibitor trametinib: a phase 1 dose-escalation trial. *Lancet Oncol* 13(8):773–81.
34. Marshall J, Hwang J, Eskens FALM, Burger H, Malik S, Uttenreuther-Fischer M, et al (2013) A Phase I, open-label, dose escalation study of afatinib, in a 3-week-on/1-week-off schedule in patients with advanced solid tumors. *Invest New Drugs* 31(2):399–408.
35. Koch KM, Reddy NJ, Cohen RB, Lewis NL, Whitehead B, Mackay K, et al (2009) Effects of food on the relative bioavailability of lapatinib in cancer patients. *J Clin Oncol* 27(8):1191–6.
36. Groenland SL, van Nuland M, Bergman AM, de Feijter JM, Dezentje VO, Rosing H, et al (2020) Concomitant intake of abiraterone acetate and food to increase pharmacokinetic exposure: real life data from a therapeutic drug monitoring programme. *Eur J Cancer* 130:32–8.



# Chapter 6

## **Quantification of the exposure-toxicity relationship of combined MEK and pan-HER inhibitors in patients with KRAS mutated tumours**

*Interim analysis*

Lisa T. van der Heijden  
Emilie van Brummelen  
Maarten Huismans  
Jeanine Roodhart  
Thomas P.C. Dorlo  
Jos H. Beijnen  
Frans L. Opdam  
Alwin D.R. Huitema

## ABSTRACT

**Aim:** For patients with Kirsten rat sarcoma viral oncogene homolog (KRAS) mutated (m) tumours, the combination of MEK and pan-HER inhibitors provides a promising treatment option based on preclinical research. Dose-escalation of this combination therapy was limited by toxicity. Insight in the relationship between exposure and toxicity could help in determining the optimal doses. Therefore, a pharmacokinetic (PK)-toxicodynamic (TOX) model was developed to quantify the relationship between exposure to MEK and pan-HER inhibitors and the occurrence of dose-limiting toxicities (DLTs).

**Methods:** PK and TOX data of 118 patients was used for the development of the PK-TOX model. PK was linked to toxicity using an effect compartment model, representing latent damage. Normalised plasma concentrations of MEK and pan-HER inhibitors were used as input in the effect compartment, to account for inter-drug differences in plasma concentrations. Development of a DLT was modelled using a logistic regression model based on the latent variable to account for cumulative toxic effects.

**Results:** The final PK-TOX model described the relationship between the latent variable and the probability of DLT. The probability of developing a DLT during the first 28 days of treatment was related to normalised cumulative exposure. The relative contribution of MEK inhibitors on overall toxicity compared to pan-HER inhibitor was estimated at 7.6-fold (relative standard error: 1.3%). The maximum estimated probability of DLT increased from 6% in week 1 to 17% in week 4, corresponding to an observed incidence of 22%.

**Conclusion:** Relationship between pan-HER and MEK inhibitor exposure and the probability of DLT was quantified. The PK-TOX model was able to discriminate between the impact of exposure of pan-HER and MEK inhibitors on the probability of developing DLTS. Based on our findings, exposure optimisation of MEK inhibitors should be prioritised for safety.

# 1 INTRODUCTION

Persistent activation of the Ras-Raf-MEK-ERK mitogen-activated-protein-kinase (MAPK) signalling pathway is frequently observed in human cancers and is associated with sustained malignant cell growth and proliferation. Often, mutations in the Kirsten rat sarcoma viral oncogene homolog (KRAS) protein underlie this persistent pathway activation. Mutations in the *KRAS* gene occur as frequently as 45% in colorectal cancer (CRC), 35% in non-small cell lung cancer (NSCLC) and 90% in pancreatic cancer (PC) [1]. Targeting the *KRAS* protein or other proteins in the MAPK pathway provides an attractive treatment option for these groups of patients. However, attempts to inhibit *KRAS*-induced cell growth with Raf, MEK, or ERK inhibitors have not resulted in sustained clinical responses so far [2-5]. Hence, a high unmet medical need exists for patients with *KRAS* mutant (*KRAS*m) tumours.

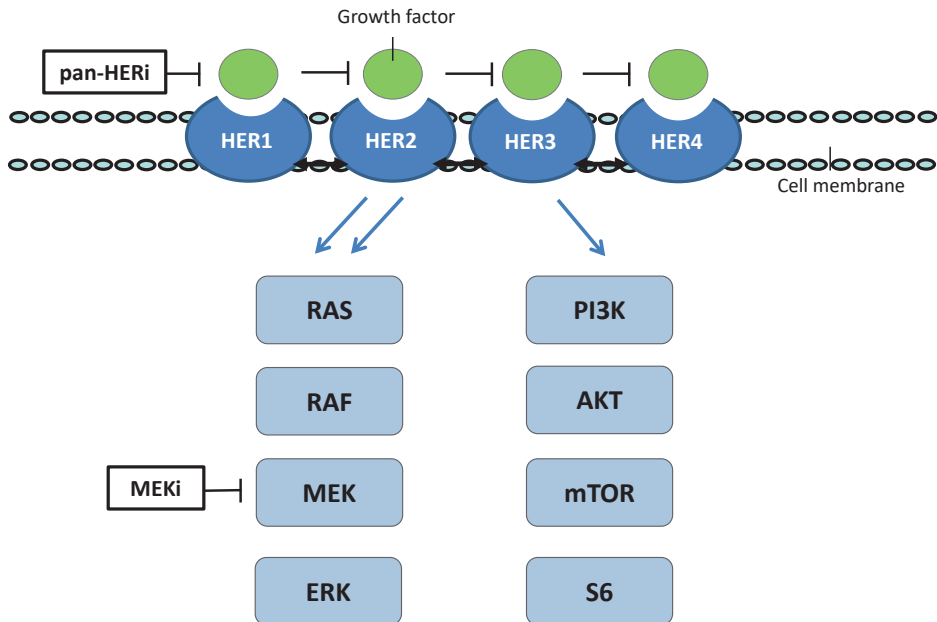


**Figure 1.** Schematic overview of the mitogen-activated protein kinase (MAPK) and phosphoinositide 3-kinase (PI3K) pathway

Preclinical experiments have shown that combined inhibition of MEK and multiple (pan-) human epidermal growth factor receptors (HER-1, HER-2, HER-3, HER-4) can lead to complete suppression of cell growth of *KRAS*m cell lines [5].

The underlying mechanism is that upon MEK inhibition, overexpression of HER, in particular HER-2 and HER-3, occurs which re-activates not only the MAPK-pathway but also the phosphoinositide 3-kinase (PI3K)-AKT pathway (Figure 1) [6]. This resistance mechanism can be overcome by combining MEK and pan-HER inhibitors [7]. Based on this preclinical evidence, three clinical trials were conducted in which different combinations of MEK and pan-HER inhibitors were administered [8-10]. The best clinical response in these studies was stable disease, indicating that in humans this combination inhibited growth but was not cytotoxic [8-10]. Subsequent preclinical studies with patient-derived organoids demonstrated strong cytotoxic effects when MEK and pan-HER inhibitors were combined with a microtubule-targeting agent, such as vinorelbine [11]. Currently, a clinical trial testing the safety and efficacy of this triple therapy combination is in progress [12].

Results from these studies indicated that toxicities limit dose-escalation and clinical use of these agents, which was previously also reported for the combination of MEK and HER-1 (EGFR) inhibitors [13]. Frequently observed dose-limiting toxicities (DLTs) included diarrhoea, nausea, skin toxicity, dehydration and liver damage, which is in line with the known safety profiles of single agent use [14-19]. Particularly skin toxicity and diarrhoea are well known class-effects of both MEK and HER inhibitors. In previous (single agent) phase I studies, skin toxicity occurred in about 70% of the patients on MEK as well as HER inhibitors, and diarrhoea occurred in 80% of patients on MEK inhibitors versus 50% on HER inhibitors. With the combination therapy, >90% of patients experienced skin toxicity and >82% diarrhoea, which was dose-limiting in 4% and 6% of the patients, respectively [8-10], while the incidence of skin toxicity and diarrhoea in the interim analysis of the triple therapy study was 79% and 71%, respectively. In addition, nausea and fatigue are known overlapping toxicities (40%-50% on MEK or HER inhibitors as single agents [14,18,20-23]), which was reflected in the data of the combination therapy as well, where approximately 40% of patients experienced nausea and fatigue. [8-10,12]

Upon the occurrence of a DLT, dose-reduction of either or both drugs is required to manage toxicity for the individual patient. However, due to the overlap in the type of toxicities related to MEK and pan-HER inhibitors, it is difficult to decide which of the drugs in the combination should be administered at a reduced dose. To investigate whether it is more rational to prioritise escalation of MEK or pan-HER inhibitor doses in combination therapy, the here reported pharmacokinetic (PK)-toxicodynamic (TOX) model was developed. We aimed to relate the exposure



to the MEK inhibitors selumetinib, trametinib, mirdametinib, binimetinib, and pan-HER inhibitors afatinib, lapatinib and dacomitinib to the probability of encountering DLTs. Ultimately, this could provide supportive evidence for dose- and schedule-selection for dose-escalation trials of these and comparable drug combinations.

## 2 METHODS

### 2.1 Clinical studies

In three separate clinical studies, patients with KRAS<sup>m</sup> colorectal cancer, non-small cell lung cancer and pancreatic cancer were treated with one of the MEK inhibitors selumetinib, trametinib or mirdametinib in a dual combination with one of the pan-HER inhibitors afatinib, lapatinib or dacomitinib, respectively [8-10]. Doses were escalated according to pre-specified criteria, starting with 20-50% of the recommended monotherapy doses for each agent up to 75%-100% of the monotherapy doses. In a fourth study, patients with KRAS<sup>m</sup> colorectal cancer were treated with lapatinib, binimetinib and vinorelbine [12]. In this study, dose-escalation of binimetinib was prioritized starting at 33% of the recommended monotherapy dose up to 100% of the monotherapy dose, while lapatinib dose-escalation was conducted secondly with two dose levels. Dose-escalation was limited by the occurrence of dose-limiting toxicities (DLTs) during the first 28 days of treatment (21 days for the triple therapy study). Pre-defined criteria for DLTs were given in the study protocols and were consistent throughout the three studies, graded according to Common Terminology Criteria for Adverse Events version 4.0. DLTs were defined as severe neutropenia, anaemia or thrombopenia (grade 3 for > 5 days or grade 4), grade  $\geq 3$  nausea, vomiting or diarrhoea in the presence of maximal supportive care, grade  $\geq 2$  neuropathy, severe liver enzyme elevations (aspartate aminotransferase (AST), alanine aminotransferase (ALT)), > 10% decrease in left-ventricular ejection fraction, significant treatment delay (> 7 days of delay or administration of <75% of planned doses in cycle 1), any other non-haematological toxicity grade  $\geq 3$ , or any grade 2 toxicity which was considered a DLT in the judgement of the investigator. The dual therapy studies were conducted at the Netherlands Cancer Institute and three other hospitals in the Netherlands according to good clinical practice (GCP) guidelines and were registered at ClinicalTrials.gov as NCT02039336, NCT02450656, NCT02230553. The triple therapy study was conducted at the University Medical Center Utrecht and was registered at EU trial register under EudraCT Number 2019-004987-23. All patients signed informed consent prior to start according to the Declaration of Helsinki.

### 2.2 PK data

The occurrence of DLTs was evaluated at minimum at day 1, 2, 8, 15, 21 and 28 and in case of DLT at additional time points. Plasma concentration levels were measured in venous blood obtained by extensive pharmacokinetic sampling on day 1 (predose and 7 or 8 times postdose) and single pre-dose sampling on day

2, 4, 7, 15, 21 and 28 for the dual therapy studies. For the triple therapy study, venous blood was obtained on day 1 and day 3 (predose and 5 or 6 times postdose). A combined validated assay was used to determine total drug concentrations administered in the dual therapy studies in the Good Laboratory Practice Certified (GLP) Bioanalytical Laboratory of the Netherlands Cancer Institute. Lower and upper limits of quantifications (LLOQs-ULOQs) were 0.5 – 50 ng/mL for dacomitinib, trametinib and afatinib, 5 – 500 ng/mL for mirdametininib and selumetinib and 50 – 5,000 ng/mL for lapatinib. For samples obtained during the triple therapy study, total drug concentrations were quantified with separate validated assay in the GLP Bioanalytical Laboratory of the Netherlands Cancer Institute. The limits of quantifications were 50-1,000 ng/mL for lapatinib, 10-1,000 ng/mL for binimetininib, and 0.0250-10 ng/mL for vinorelbine. Concentrations below the LLOQ were included in the dataset as LLOQ/2 for any post-dose timepoint or as 0 if the time since the last administration exceeded five times the half-life of the compound.

### 2.3 Model development and evaluation

For each compound, a PK model was developed based on the measured drug concentrations, taking into account all dose-interruptions based on real intake data from patient diaries and electronic patient dossiers. The PK models were accepted if successful minimization was reached, parameters and relative standard errors (RSE) could be estimated and weighted residuals were within acceptable ranges and without trends. Visual model evaluation was performed by visual predictive checks and by several other goodness-of-fit plots. These PK models were integrated in the TOX model using the individual parameter estimate as input according to the sequential individual PK parameters (IPP) modelling approach [24]. For each drug, plasma concentrations were normalized to the mean weekly AUC of the Recommend Phase 2 Dose established in the individual studies to account for inter-drug differences in the expected plasma concentrations and to allow a pooled analysis of all four trials. For example, the recommended Phase 2 dose for dacomitinib was 15 mg QD dosed in a 21 days on 7 days off dosing schema. The average week AUC is therefore the average weekly dose (78.75 mg) divided by dacomitinib clearance (21.16 L/h), resulting in an AUC of 3.14 mg/mL\*h (see Table S2).

The normalized concentration-time data of each compound was used as input in an effect compartment, representing a latent variable accounting for the cumulative toxic effects of the combinations, which was subsequently linked to the probability of DLT (Figure 2). This was based on the null hypothesis that

each compound contributed equally to the probability of toxicity. Subsequently, a scaling factor was evaluated for the MEK inhibitor exposure to account for differences between classes (pan-HER inhibitor versus MEK inhibitor) in their contribution to overall probability of DLT.

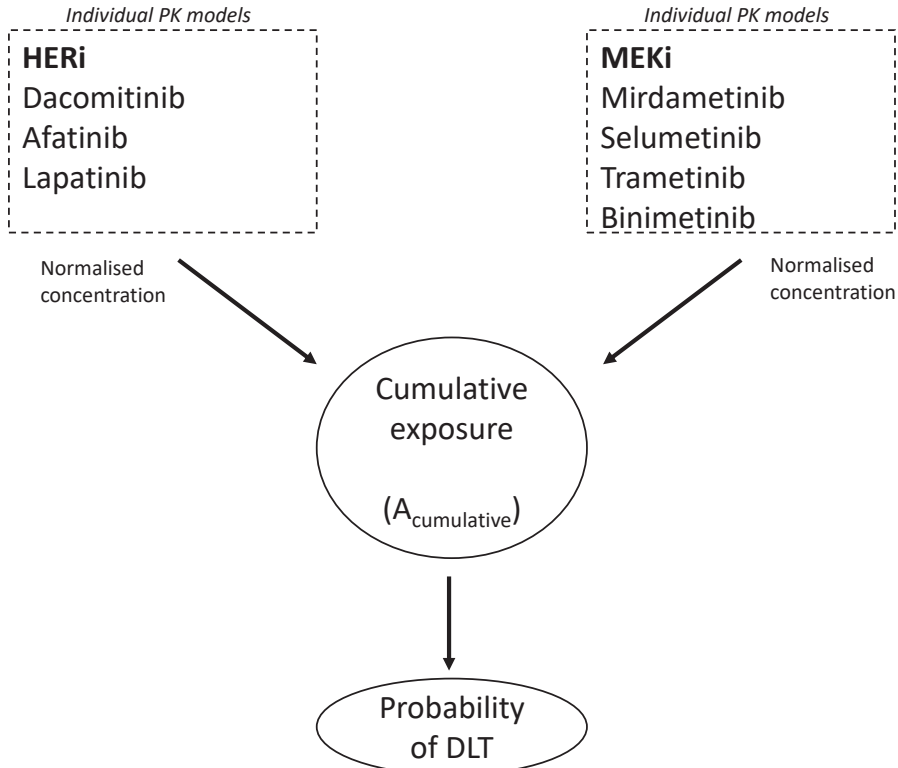


**Figure 2.** Schematic presentation of the pharmacokinetic (PK) – toxicodynamic (TOX) model for MEK and pan-HER inhibitors (i). DLT, dose-limiting toxicity.

The probability of a DLT was modelled using the following equations:

$$\frac{dA_{cumulative}}{dt} = C_{HER} + S * C_{MEK}$$

$$f = B_0 + B_1 * (A_{cumulative}/1000)$$

$$P_{DLT} = \frac{\exp(f)}{1 + \exp(f)}$$

Where  $dA_{cumulative}$  represents the effect compartment, being a latent variable accounting for the cumulative toxic effects of MEK and pan-HER inhibitors over time (dt),  $C_{HER} + S * C_{MEK}$  represents the normalized concentration of MEK and pan-HER inhibitors in the central compartment with a scaling factor (S) on MEK concentration,  $f$  is a linear function of  $A_{cumulative}$  with  $B_0$  as intercept and  $B_1$  as the slope of the exposure-toxicity relationship.  $P_{DLT}$  is the probability of DLT as a function of logit-transformed  $f$ , in line with common probability estimations.

First-order elimination (representing recovery of the latent cumulative toxicity effects) from the effect compartment was initially included in the model. The PK-TOX models were evaluable only if successful minimization was reached with plausible and precise parameter estimates. Models were considered significantly improved in case of decreases in objective function values (OFVs) meeting the significance level of  $p < 0.01$  (with 1 degree of freedom this corresponds to a decrease in OFV  $> 6.6$ ) with lower or equal relative standard errors to the parameter estimates [25-27]. The PK-TOX model was considered successful if all of the above requirements were met and if it could be applied on the data of the four clinical studies as well as the combined data. For model-evaluation, the cumulative exposure and the maximum probability per week of treatment was extracted from the model output. This was plotted together with the observed number of patients with and without DLT for every week of treatment.

#### 2.4 Extrapolation to a new dose level

The final PK-TOX model was used to predict the probability of DLTs of a new dose level in the ongoing clinical trial investigating the triple therapy. Patients in this dose level will receive 1000 mg lapatinib QD and 30 mg binimetinib BID in a 5 days on 2 days off regimen for 3 weeks. Vinorelbine was administered on day 3 and 10 of treatment. The final PK models for lapatinib and binimetinib were used to obtain PK parameter for 1000 typical patients. These PK parameters were used in the integrated PK-TOX model for the prediction of the probability of a DLT for these 1000 typical patients during the first 21 days of treatment.

#### 2.5 Software

Model estimations were performed using NONMEM (version 7.5.0, ICON Development Solutions, Ellicott City, MD, USA) together with Pirana (version 3.0.0) as graphical interface [28]. R (version 4.1.2) was used for data processing

and graphical presentations [29]. For the PK modelling the first order conditional estimation option with interaction (FOCE-I) was used. Individual Bayesian parameter estimates were generated using the POSTHOC option of NONMEM. For the modelling of probability of DLT, FOCE was used in combination with the LAPLACE and LIKELIHOOD options.

## 3 RESULTS

### 3.1 Clinical data

Description of the clinical data is provided in Table 1. A total of 118 patients were included in the data analysis for both the PK analysis and the PK-TOX analysis. In this population, 26 patients experienced a DLT and 31 DLTs were reported, indicating that some patients experienced multiple DLTs. The most common DLTs were diarrhoea (8.5%), followed by dehydration (3.4%), and increased ALT/AST (2.5%) and skin rash (2.5%). These DLTs are well known toxicities of MEK inhibition and pan-HER inhibition. One patient receiving the triple therapy with lapatinib, binimetinib, and vinorelbine had decreased neutrophil count and febrile neutropenia, which could be attributed to vinorelbine. No other patients experienced vinorelbine-associated DLTs. It was considered rational to merge the PK and TOX data from four trials based on the known similarities in toxicities within the class of MEK inhibitors (selumetinib, trametinib, mirdametinib, binimetinib) and HER inhibitors (afatinib, dacomitinib, lapatinib) [8-10,12].

### 3.2 PK-TOX model

Parameter estimates of the PK models for each of the seven drugs can be found in Table S1. Estimation of the first-order elimination rate from the effect compartment (recovery rate,  $K_e$ ) resulted in negative and very low estimates. Therefore, the elimination from the effect compartment was omitted from the model and the effect compartment can be interpreted as a latent variable accounting for the cumulative toxic effects of pan-HER inhibitors and MEK inhibitors.

### 3.3 Contribution of MEK and pan-HER inhibition to toxicity

Parameter estimates of the relationship between the latent variable for cumulative toxicity and the probability of DLT assuming equal contribution of MEK and HER inhibitors were  $-4.42$  (RSE: 6.3%) for  $B_0$  and  $141$  (RSE: 32%) for  $B_1$ . A steep exposure-toxicity relationship with a sharp increase in the probability of DLT already at low exposures was identified, which is in accordance with the clinical observation of occurrence of DLT already at low dose levels. The latent variable for cumulative damage in the clinical studies was on average  $6 \text{ h}^{-1}$  [range:  $0\text{-}25 \text{ h}^{-1}$ ]. At the mean of the latent variable, the estimated probability of DLT was 3%, whereas at the maximum of the latent variable the estimated probability of DLT was 29%.

**Table 1.** Descriptive clinical data of the four dose-escalation studies.

<b>Study</b>	<b>1 [8]</b>	<b>2 [10]</b>	<b>3 [9]</b>	<b>4 [12]</b>	<b>All studies</b>
<b>PK data</b>					
Number of patients (n=)	41	34	26	17	118
Pan-HER inhibitor	Dacomitinib	Lapatinib	Afatinib	Lapatinib	-
Dose (mg/day)	15, 30	500, 750	20, 30	750, 1000	-
PK samples (n=)	649	428	490	211	1778
MEK inhibitor	Mirdame- tinib	Trame- tinib	Selum- tinib	Binime- tinib	-
Dose (mg/day)	4, 6, 8, 10, 12	1, 1.5, 2	50, 100,	15, 30, 45	-
PK samples (n=1)	649	428	490	211	1778
<b>TOX data</b>					
DLT (n, (%))	9 (22)	6 (18)	8 (31)	8 (47)	31 (26)
Decreased appetite	0 (0)	0 (0)	1 (3.8)	0 (0)	1 (0.8)
Decreased neutrophil count	0 (0)	0 (0)	0 (0)	1 (5.9)	1 (0.8)
Dehydration	1 (2.4)	0 (0)	2 (7.7)	1 (5.9)	4 (3.4)
Diarrhoea	1 (2.4)	2 (5.9)	3 (12)	4 (24)	10 (8.5)
Dyspnoea	1 (2.4)	0 (0)	0 (0)	0 (0)	1 (0.8)
Fatigue	2 (4.9)	0 (0)	0 (0)	0 (0)	2 (1.7)
Febrile neutropenia	0 (0)	0 (0)	0 (0)	1 (5.9)	1 (0.8)
Increased AST/ALT	2 (4.9)	1 (2.9)	0 (0)	1 (5.9)	3 (2.5)
Mucositis	0 (0)	0 (0)	1 (3.8)	0 (0)	1 (0.8)
Nausea	0 (0)	1 (2.9)	1 (3.8)	0 (0)	2 (1.7)
Neuropathy	1 (2.4)	0 (0)	0 (0)	0 (0)	1 (0.8)
Skin rash	1 (2.4)	2 (5.9)	0 (0)	0 (0)	3 (2.5)

Abbreviations: DLT, dose-limiting toxicity; PK, pharmacokinetics; TOX, toxicity.

To assess the relative contributions of MEK and pan-HER inhibitors, a scaling factor (S) was applied to the normalised MEK concentrations. The scaling factor was estimated at 7.6 (RSE: 1.3%) indicating that the relative contribution of normalised exposure of MEK inhibitors to the latent damage variable is higher compared to the normalised exposure of pan-HER inhibitors, suggesting optimisation of MEK inhibitor exposure should be prioritised for safety. The parameter estimates and the corresponding relationship between the amount in the effect compartment and the probability of a DLT with a scaling factor of 7.6 for the contribution of MEK inhibitors are shown in Table 2 and Figure 3. The normalized cumulative exposure was on average 20 h<sup>-1</sup> [range: 0-70 h<sup>-1</sup>]. The probability of a DLT was 2.6% at the average value of the latent variable and 18% at the maximum observed latent variable.



**Table 2.** Parameter estimates for the combined model of MEK and pan-HER inhibitors.

Parameters	Estimate	RSE (%)	95% CI
Intercept ( $B_0$ )	-4.49	6.2%	-5.1 to -4.0
Slope ( $B_1$ )	42.5	28	16.0 to 62.3
Scaling factor	7.6	1.3	7.5 to 7.8

Abbreviations: 95% CI, 95% confidence interval; RSE, relative standard error.

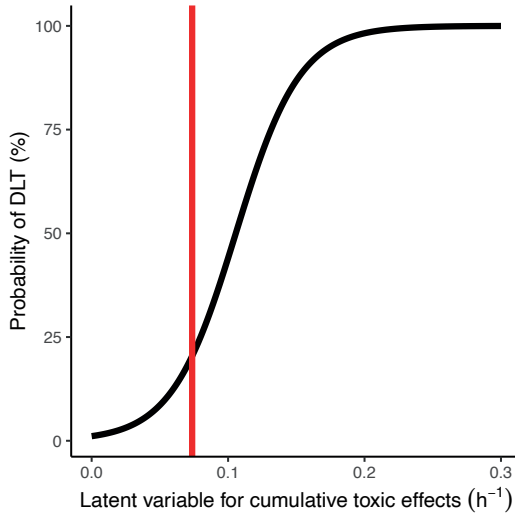


**Figure 3.** Relationship between the latent variable for cumulative toxic effects ( $h^{-1}$ ) and the predicted probability of dose-limiting toxicity (DLT) for the combined model with the maximum observed normalized cumulative exposure indicated by the red line.

Figure 4 illustrates the normalized cumulative exposure with  $S=7.6$  per week of treatment and the corresponding predicted probability for DLT as well as the observed incidence of DLTs. With an increase of the normalised cumulative exposure, also the incidence of DLT increase from 2.5% in the first week of treatment (Week 1), to 7.8% in week 2, and 10% in week 3 followed by 3.7% in week 4. This corresponds with an increasing maximum predicted probability per week from 6.0% in week 1 to 14% in week 2, 20.3% in week 4 and 17% in week 4, corresponding to an observed incidence of 22%. The DLT period in the lapatinib-binimetinib-vinorelbine study was shorter (21 days versus 28 days).

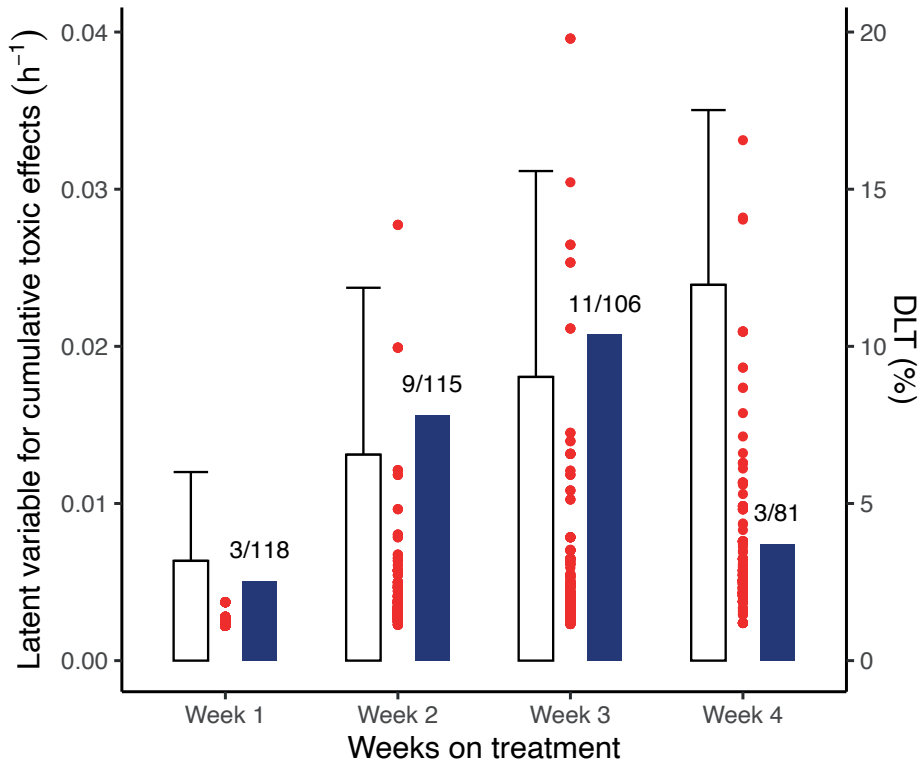


**Figure 4.** The latent variable for cumulative toxic effects of MEK and pan-HER inhibitors (left y-axis) per week of treatment (white bars) with the corresponding observed incidence of DLTs (%) (blue bars) and the predicted individual probability of DLT (%) (right y-axis).

Subsequently, the scaling factor  $S$  was estimated separately for the different studies. No significant differences were found for the scaling factor  $S$  between the different studies. Lastly, a scaling factor for the relative contribution of vinorelbine to the probability of a DLT was considered since one patient had vinorelbine-associated DLTs. A scaling factor of the relative contribution of vinorelbine to the probability of a DLT was estimated. However, the parameter was unidentifiable and was therefore excluded from the model. The parameter unidentifiability might be explained by the small inter-individual variability in vinorelbine pharmacokinetics ( $RSE\% \leq 16$ ) and that only one patient experienced a DLT which could be attributed to vinorelbine. Moreover, preclinical studies investigating the triple therapy reported no additional toxicities from the triple therapy with a microtubule targeting agent compared to the combination therapy with pan-HER and MEK inhibitors [11].

### 3.4 Extrapolation to a new dose level

The probability of experiencing a DLT within the first 21 days of treatment was predicted for 1000 typical patients receiving 1000 mg lapatinib QD and 30 mg binimetinib BID in a 5 days on 2 days off regimen for 3 weeks. The maximum predicted probability of experiencing a DLT was 2.7% within the first week of treatment, 6.7% within the second week of treatment, and 15.4% within the third week of treatment. Generally, in Phase I clinical trials, a maximum probability of 16.7% is considered acceptable [30]. Based on the extrapolation, it is expected that the new dose level will result in acceptable toxicity.

## 4 DISCUSSION

The relationship between exposure and toxicity was described by a PK-TOX model which related the latent variable for cumulative toxicity of MEK and pan-HER inhibitors to the probability of DLT using a logistic regression model. This model was applied to the following combinations of pan-HER and MEK inhibitors: afatinib-selumetinib, lapatinib-trametinib, dacomitinib-mirdametinib, and lapatinib-binimetinib.

With this model, we provide a novel approach to combine pharmacokinetic and toxicodynamic data from different clinical studies that investigate the same concept. We used a unique set of extensive PK and toxicity data from four clinical trials, of which one is still ongoing. Based on the similarities in toxicities within the class of MEK inhibitors and pan-HER inhibitors [8-10,12], and on the comparable trial design, data collection and data handling procedures, it was considered rational to merge the PK and toxicity data from the four trials. Dose finding in all four studies, according to a rule-based design, proved to be complicated due to occurrence of toxicity at relatively low dose levels. The nature of DLTs in the different studies were similar and consistent mainly with diarrhoea, nausea, skin toxicity, liver damage and dehydration. Taken together, it was considered a rational approach to combine data to be able to quantify the relationship between drug exposure and toxicity and to assess contribution of drug class and/or individual drugs on toxicity. This model may assist in rational dose finding of this combination by predicting the maximum probability of DLT for dose levels and prioritising dose levels on their probabilities of DLTs as described for the new dose level for the ongoing triple therapy study.

Importantly, there may be a discrepancy between the plasma levels and the tissue levels. In particular, the pan-HER inhibitors have a large volume of distribution (see Table S1) which may mean that more drug is distributed to the tissues with the potential of inducing damage. This is not reflected by our PK-TOX model and may lead to an underestimation of the effects of HER inhibition when there is a poor correlation between plasma exposure and tissue exposure. Furthermore, this model does not differentiate between free and protein-bound fraction. Plasma concentrations were generated from the PK model which is based on measured total (bound and unbound) fraction. Although all drugs have extensive protein binding (in the range of >95%-99.9%) it is unsure if the use of total drug concentrations affects the ability of the model to discriminate between the effects of MEK and pan-HER inhibitors.

A scaling factor was used to discriminate between the influence of drugs class on probability of DLT. Other descriptive PK-TOX models for dual combinations have been described [31,32], but the distinction between effects of two classes of drugs has not been addressed earlier. The relative contribution of MEK inhibitors to the probability was estimated to be 7.6 (RSE%: 1.6) suggesting normalised exposure of MEK inhibitors affect the probability of DLT relatively more than the normalised exposure to pan-HER inhibitors. Estimating the scaling factor for the individual studies, resulted in scaling factors ranging from 2.95 to 12.6, suggesting inter-compound variability regarding the relative contribution to the probability of DLT. However, the dOFV was small and parameter precision decreased. Taken together, that the results suggest that normalised exposure of MEK inhibitors contribute more to the probability of a DLT compared to normalised exposure of pan-HER inhibitors.

Clinical implementation of these findings requires some caution [33]. First of all, DLTs were modelled as binary outcome while in practice this is a gradual process. However, the binary approach is in line with clinical trial practice, as it guides dose finding in the rule-based design of the studies. Although the model could be refined by defining toxicity as any toxicity that results in clinical interventions or treatment interruptions, for the scope of this study we aimed to select the most relevant toxicities by using DLTs as primary toxicity parameter. Secondly, MEK inhibitors were escalated over a larger dose range compared to pan-HER inhibitors (Table 1), which could have resulted an underestimation of the effect of pan-HER inhibitors on the probability of DLT. Lastly, the external validity of this model is unclear since only our internal dataset was available. Emerging data from the ongoing trials may help in establishing the robustness of the model. To test external validity, also data from other trials should be incorporated if feasible in the future.

The ultimate goal of this model was to develop an algorithm that could explain how exposure to MEK, or pan-HER inhibitors relates to toxicity to assist dose finding in combination trials. In the combined PK-TOX model, the relative contribution to the probability of DLT was higher of MEK inhibitors compared to pan-HER inhibitors. This suggest that there is a class-specific impact on toxicity of MEK inhibitors versus pan-HER implying that exposure optimisation of MEK inhibitors should be prioritised before pan-HER inhibitors for safety.

Our model confirmed and quantified our clinical finding that the dose range in which MEK and pan-HER inhibitors can be safely combined is narrow. Generally, a maximum probability of DLT of 16.7% is accepted for Phase I clinical trials [30]. Although this incidence was not exceeded in the three clinical trials, our predictions show that the probability increased steeply with higher cumulative normalized exposure. This may also be a consequence of the fact that the dose-escalation started at 20-50% of the recommended single agent doses, and no information on lower dose-levels could be included. A better prediction of the dose-toxicity relationship could be obtained by including data from trials with these combinations in lower doses.

## **5 CONCLUSION**

Based on our findings, the probability of DLT is relatively more dependent on exposure to MEK inhibitors compared to HER inhibitors. There seems to be inter-compound variability regarding the relative contribution of MEK inhibitors to the probability of DLT. These results suggest that exposure optimisation of MEK inhibitors should be prioritised for safety. However, in view of efficacy, it should be considered that inhibition of MEK forms the basis for the responsive upregulation of HER proteins [5]. Therefore, maintenance of clinical effective plasma concentration should be an aim when dose reductions are being considered.

## **ACKNOWLEDGEMENTS**

Our gratefulness goes out to all patients who participated in the clinical studies.

## REFERENCES

1. Downward J (2003) Targeting RAS signalling pathways in cancer therapy. *Nat Rev Cancer* 3 (1):11-22. doi:10.1038/nrc969
2. Migliardi G, Sassi F, Torti D, Galimi F, Zanella ER, Buscarino M, Ribero D, Muratore A, Massucco P, Pisacane A, Risio M, Capussotti L, Marsoni S, Di Nicolantonio F, Bardelli A, Comoglio PM, Trusolino L, Bertotti A (2012) Inhibition of MEK and PI3K/mTOR suppresses tumor growth but does not cause tumor regression in patient-derived xenografts of RAS-mutant colorectal carcinomas. *Clin Cancer Res* 18 (9):2515-2525. doi:10.1158/1078-0432.Ccr-11-2683
3. Adjei AA, Cohen RB, Franklin W, Morris C, Wilson D, Molina JR, Hanson LJ, Gore L, Chow L, Leong S, Maloney L, Gordon G, Simmons H, Marlow A, Litwiler K, Brown S, Poch G, Kane K, Haney J, Eckhardt SG (2008) Phase I pharmacokinetic and pharmacodynamic study of the oral, small-molecule mitogen-activated protein kinase kinase 1/2 inhibitor AZD6244 (ARRY-142886) in patients with advanced cancers. *J Clin Oncol* 26 (13):2139-2146. doi:10.1200/jco.2007.14.4956
4. Jänne PA, Shaw AT, Pereira JR, Jeannin G, Vansteenkiste J, Barrios C, Franke FA, Grinsted L, Zazulina V, Smith P, Smith I, Crinò L (2013) Selumetinib plus docetaxel for KRAS-mutant advanced non-small-cell lung cancer: a randomised, multicentre, placebo-controlled, phase 2 study. *Lancet Oncol* 14 (1):38-47. doi:10.1016/s1470-2045(12)70489-8
5. Sun C, Hobor S, Bertotti A, Zecchin D, Huang S, Galimi F, Cottino F, Prahallad A, Grernrum W, Tzani A, Schlicker A, Wessels LF, Smit EF, Thunnissen E, Halonen P, Lieftink C, Beijersbergen RL, Di Nicolantonio F, Bardelli A, Trusolino L, Bernards R (2014) Intrinsic resistance to MEK inhibition in KRAS mutant lung and colon cancer through transcriptional induction of ERBB3. *Cell Rep* 7 (1):86-93. doi:10.1016/j.celrep.2014.02.045
6. Huang L, Fu L (2015) Mechanisms of resistance to EGFR tyrosine kinase inhibitors. *Acta Pharm Sin B* 5 (5):390-401. doi:10.1016/j.apsb.2015.07.001
7. Verissimo CS, Overmeer RM, Ponsioen B, Drost J, Mertens S, Verlaan-Klink I, Gerwen BV, van der Ven M, Wetering MV, Egan DA, Bernards R, Clevers H, Bos JL, Snippert HJ (2016) Targeting mutant RAS in patient-derived colorectal cancer organoids by combinatorial drug screening. *Elife* 5. doi:10.7554/eLife.18489
8. van Geel R, van Brummelen EMJ, Eskens F, Huijberts S, de Vos F, Lolkema M, Devriese LA, Opdam FL, Marchetti S, Steeghs N, Monkhorst K, Thijssen B, Rosing H, Huitema ADR, Beijnen JH, Bernards R, Schellens JHM (2020) Phase 1 study of the pan-HER inhibitor dacomitinib plus the MEK1/2 inhibitor PD-0325901 in patients with KRAS-mutation-positive colorectal, non-small-cell lung and pancreatic cancer. *Br J Cancer* 122 (8):1166-1174. doi:10.1038/s41416-020-0776-z
9. van Brummelen EMJ, Huijberts S, van Herpen C, Desar I, Opdam F, van Geel R, Marchetti S, Steeghs N, Monkhorst K, Thijssen B, Rosing H, Huitema A, Beijnen J, Bernards R, Schellens J (2021) Phase I Study of Afatinib and Selumetinib in Patients with KRAS-Mutated Colorectal, Non-Small Cell Lung, and Pancreatic Cancer. *Oncologist* 26 (4):290-e545. doi:10.1002/onco.13631

10. Huijberts S, van Geel R, van Brummelen EMJ, Opdam FL, Marchetti S, Steeghs N, Pulleman S, Thijssen B, Rosing H, Monkhorst K, Huitema ADR, Beijnen JH, Bernards R, Schellens JHM (2020) Phase I study of lapatinib plus trametinib in patients with KRAS-mutant colorectal, non-small cell lung, and pancreatic cancer. *Cancer Chemother Pharmacol* 85 (5):917-930. doi:10.1007/s00280-020-04066-4
11. Mertens S, Huismans MA, Verissimo CS, Ponsioen B, Overmeer R, Proost N, van Tellinghen O, van de Ven M, Begthel H, Boj SF, Clevers H, Roodhart JML, Bos JL, Snippert HJG (2023) Drug-repurposing screen on patient-derived organoids identifies therapy-induced vulnerability in KRAS-mutant colon cancer. *Cell Rep* 42 (4):112324. doi:10.1016/j.celrep.2023.112324
12. Utrecht UMC (2020) A Dose-Escalating Phase I/II Study in Patients with RAS-Mutated Metastatic Colorectal Cancer to Investigate Safety and Clinical Activity of the Triple Combination of: MEK-inhibitor binimetinib, Pan-EGFR inhibitor lapatinib and the Microtubule Targeting Agent (MTA) vinorelbine. Accessed 7 June 2023
13. Ko AH, Bekaii-Saab T, Van Ziffle J, Mirzoeva OM, Joseph NM, Talasz A, Kuhn P, Tempero MA, Collisson EA, Kelley RK, Venook AP, Dito E, Ong A, Ziyeh S, Courtin R, Linetskaya R, Tahiri S, Korn WM (2016) A Multicenter, Open-Label Phase II Clinical Trial of Combined MEK plus EGFR Inhibition for Chemotherapy-Refractory Advanced Pancreatic Adenocarcinoma. *Clin Cancer Res* 22 (1):61-68. doi:10.1158/1078-0432.Ccr-15-0979
14. Takahashi T, Boku N, Murakami H, Naito T, Tsuya A, Nakamura Y, Ono A, Machida N, Yamazaki K, Watanabe J, Ruiz-Garcia A, Imai K, Ohki E, Yamamoto N (2012) Phase I and pharmacokinetic study of dacomitinib (PF-00299804), an oral irreversible, small molecule inhibitor of human epidermal growth factor receptor-1, -2, and -4 tyrosine kinases, in Japanese patients with advanced solid tumors. *Invest New Drugs* 30 (6):2352-2363. doi:10.1007/s10637-011-9789-z
15. O'Neil BH, Goff LW, Kauh JS, Strosberg JR, Bekaii-Saab TS, Lee RM, Kazi A, Moore DT, Learoyd M, Lush RM, Sebt SM, Sullivan DM (2011) Phase II study of the mitogen-activated protein kinase 1/2 inhibitor selumetinib in patients with advanced hepatocellular carcinoma. *J Clin Oncol* 29 (17):2350-2356. doi:10.1200/jco.2010.33.9432
16. LoRusso P, Venkatakrishnan K, Chiorean EG, Noe D, Wu JT, Sankoh S, Corvez M, Sausville EA (2014) Phase 1 dose-escalation, pharmacokinetic, and cerebrospinal fluid distribution study of TAK-285, an investigational inhibitor of EGFR and HER2. *Invest New Drugs* 32 (1):160-170. doi:10.1007/s10637-013-9988-x
17. Burris HA, 3rd, Hurwitz HI, Dees EC, Dowlati A, Blackwell KL, O'Neil B, Marcom PK, Ellis MJ, Overmoyer B, Jones SF, Harris JL, Smith DA, Koch KM, Stead A, Mangum S, Spector NL (2005) Phase I safety, pharmacokinetics, and clinical activity study of lapatinib (GW572016), a reversible dual inhibitor of epidermal growth factor receptor tyrosine kinases, in heavily pretreated patients with metastatic carcinomas. *J Clin Oncol* 23 (23):5305-5313. doi:10.1200/jco.2005.16.584
18. Infante JR, Fecher LA, Falchook GS, Nallapareddy S, Gordon MS, Becerra C, DeMarini DJ, Cox DS, Xu Y, Morris SR, Peddareddigari VG, Le NT, Hart L, Bendell JC, Eckhardt G, Kurzrock R, Flaherty K, Burris HA, 3rd, Messersmith WA (2012) Safety, pharmacokinetic, pharmacodynamic, and efficacy data for the oral MEK inhibitor trametinib: a phase 1 dose-escalation trial. *Lancet Oncol* 13 (8):773-781. doi:10.1016/s1470-2045(12)70270-x



19. Marshall J, Shapiro GI, Uttenreuther-Fischer M, Ould-Kaci M, Stopfer P, Gordon MS (2013) Phase I dose-escalation study of afatinib, an ErbB family blocker, plus docetaxel in patients with advanced cancer. *Future Oncol* 9 (2):271-281. doi:10.2217/fon.12.195
20. Marshall J, Hwang J, Eskens FA, Burger H, Malik S, Uttenreuther-Fischer M, Stopfer P, Ould-Kaci M, Cohen RB, Lewis NL (2013) A Phase I, open-label, dose escalation study of afatinib, in a 3-week-on/1-week-off schedule in patients with advanced solid tumors. *Invest New Drugs* 31 (2):399-408. doi:10.1007/s10637-012-9890-y
21. Chien AJ, Munster PN, Melisko ME, Rugo HS, Park JW, Goga A, Auerback G, Khanafshar E, Ordovas K, Koch KM, Moasser MM (2014) Phase I dose-escalation study of 5-day intermittent oral lapatinib therapy in patients with human epidermal growth factor receptor 2-overexpressing breast cancer. *J Clin Oncol* 32 (14):1472-1479. doi:10.1200/jco.2013.52.1161
22. LoRusso PM, Krishnamurthi SS, Rinehart JJ, Nabell LM, Malburg L, Chapman PB, DePrimo SE, Bentivegna S, Wilner KD, Tan W, Ricart AD (2010) Phase I pharmacokinetic and pharmacodynamic study of the oral MAPK/ERK kinase inhibitor PD-0325901 in patients with advanced cancers. *Clin Cancer Res* 16 (6):1924-1937. doi:10.1158/1078-0432.Ccr-09-1883
23. Banerji U, Camidge DR, Verheul HM, Agarwal R, Sarker D, Kaye SB, Desai IM, Timmer-Bonte JN, Eckhardt SG, Lewis KD, Brown KH, Cantarini MV, Morris C, George SM, Smith PD, van Herpen CM (2010) The first-in-human study of the hydrogen sulfate (Hyd-sulfate) capsule of the MEK1/2 inhibitor AZD6244 (ARRY-142886): a phase I open-label multicenter trial in patients with advanced cancer. *Clin Cancer Res* 16 (5):1613-1623. doi:10.1158/1078-0432.Ccr-09-2483
24. Zhang L, Beal SL, Sheiner LB (2003) Simultaneous vs. sequential analysis for population PK/PD data I: best-case performance. *J Pharmacokinet Pharmacodyn* 30 (6):387-404. doi:10.1023/b:jopa.0000012998.04442.1f
25. Boeckman A, Sheiner L, Beal S. NONMEM Users Guide. University of California at San Francisco; 2013. .
26. Wählby U, Bouw MR, Jonsson EN, Karlsson MO (2002) Assessment of type I error rates for the statistical sub-model in NONMEM. *J Pharmacokinet Pharmacodyn* 29 (3):251-269. doi:10.1023/a:1020254823597
27. Duffull SB, Wright DF, Winter HR (2011) Interpreting population pharmacokinetic-pharmacodynamic analyses - a clinical viewpoint. *Br J Clin Pharmacol* 71 (6):807-814. doi:10.1111/j.1365-2125.2010.03891.x
28. Keizer RJ, Karlsson MO, Hooker A (2013) Modeling and Simulation Workbench for NONMEM: Tutorial on Pirana, PsN, and Xpose. *CPT Pharmacometrics Syst Pharmacol* 2 (6):e50. doi:10.1038/psp.2013.24
29. R Core Team. R: A language and environment for statistical computing. R Foundation for Statistical Computing [Internet]. Vienna, Austria. 2021. Available from: <http://www.r-project.org/>.
30. van Brummelen EM, Huitema AD, van Werkhoven E, Beijnen JH, Schellens JH (2016) The performance of model-based versus rule-based phase I clinical trials in oncology : A quantitative comparison of the performance of model-based versus rule-based phase I trials with molecularly targeted anticancer drugs over the last 2 years. *J Pharmacokinet Pharmacodyn* 43 (3):235-242. doi:10.1007/s10928-016-9466-0

31. Kathman SJ, Williams DH, Hodge JP, Dar M (2009) A Bayesian population PK-PD model for ispinesib/docetaxel combination-induced myelosuppression. *Cancer Chemother Pharmacol* 63 (3):469-476. doi:10.1007/s00280-008-0760-4
32. Liu P, Mould DR (2014) Population pharmacokinetic-pharmacodynamic analysis of voriconazole and anidulafungin in adult patients with invasive aspergillosis. *Antimicrob Agents Chemother* 58 (8):4727-4736. doi:10.1128/aac.02809-13
33. Tuntland T, Ethell B, Kosaka T, Blasco F, Zang RX, Jain M, Gould T, Hoffmaster K (2014) Implementation of pharmacokinetic and pharmacodynamic strategies in early research phases of drug discovery and development at Novartis Institute of Biomedical Research. *Front Pharmacol* 5:174. doi:10.3389/fphar.2014.00174

## SUPPLEMENTARY MATERIAL

**Supplementary Table S1.** Final parameter estimates of the population pharmacokinetic models of the three pan-HER inhibitors and four MEK inhibitors.

Structural model parameters [unit]		Estimate	RSE%	Estimate
Lapatinib		Population estimate		Between-subject variability
Ke	[h <sup>-1</sup> ]	0.0387	9.4	0.285
Vd	[L]	790	8.2	0.291
Ka	[h <sup>-1</sup> ]	2.9	5.1	0.102
K12	[h <sup>-1</sup> ]	0.0312	14.5	-
K21	[h <sup>-1</sup> ]	0.00159	17.6	-
Trametinib		Theta		
Ke	[h <sup>-1</sup> ]	0.0150	20.8	0.462
Vd	[L]	247	11.4	0.082
Ka	[h <sup>-1</sup> ]	2.17	12.6	0.249
K12	[h <sup>-1</sup> ]	0.703	17.2	-
K21	[h <sup>-1</sup> ]	0.151	0.0863	-
Binimetinib		Theta		
CL	[L/h]	17.9	8.7	0.105
Vd	[L]	12.2	36.2	2.06
Ka	[h <sup>-1</sup> ]	0.589	13.0	-
Q	[L/h]	15.9	14.0	-
V <sub>p</sub>	[L]	112	15.2	-
Dacomitinib		Theta		
Ke	[h <sup>-1</sup> ]	0.0129	10.6	0.229
Vd	[L]	1949	8.4	0.196
Ka	[h <sup>-1</sup> ]	0.769	12.3	0.484
K12	[h <sup>-1</sup> ]	0.0256	38.9	-
K21	[h <sup>-1</sup> ]	0.0276	43.0	-
Mirdametinib		Theta		
Ke	[h <sup>-1</sup> ]	0.229	13.6	0.323
Vd	[L]	18.9	8.7	0.097
Ka	[h <sup>-1</sup> ]	5.2	11.0	0.170
K12	[h <sup>-1</sup> ]	0.633	10.8	-
K21	[h <sup>-1</sup> ]	0.151	7.8	-
K13	[h <sup>-1</sup> ]	0.0620	22.6	-
K31	[h <sup>-1</sup> ]	0.00102	36.3	-

**Supplementary Table S1.** Continued.

Structural model parameters [unit]		Estimate	RSE%	Estimate
Afatinib		Parameters were fixed based on literature model (Freiwald <i>et al.</i> 2014 [1])		
		Theta		
Cl	[L*h <sup>-1</sup> ]	42.3	-	-
Vd	[L]	456	-	-
Ka	[h <sup>-1</sup> ]	0.252	-	0.432
K23	[h <sup>-1</sup> ]	0.17	-	-
K32	[h <sup>-1</sup> ]	0.0685	-	-
ALAG	[h]	0	-	-
F1	-	1	-	0.179
Weight on CL	Weight fixed to: 75 kg (power function)	0.595	-	-
Creatinin on CL	Creatinin clearance fixed to: 79 ml/min (< 120 mL/min vs ≥120 mL/min)	0.0048	-	-
Female	Female decrease versus male	0.871	-	-
Weight on Vd	Weight fixed to: 75 kg (power function)	0.899	-	-
Dose ≤70 mg	YES (dose-dependent power function)	0.485	-	-
Selumetinib		Parameters were fixed based on literature model (Patel <i>et al.</i> 2017 [2])		
		Theta		
Cl	[L/h]	13.5	-	0.0700
Vd	[L]	32.6	-	0.201
Ka	[h <sup>-1</sup> ]	3.7	-	-
K23	[h <sup>-1</sup> ]	0.252	-	0.295
K32	[h <sup>-1</sup> ]	0.149	-	0.295
ALAG1	[h]	0.319	-	0.165
F1	-	1	-	-
D1	[h <sup>-1</sup> ]	0.622	-	0.171
Vd (3)	[L]	55	-	0.388
BSA on CL	BSA mean 1.95 (power function)	0.923	-	-
ALT on CL	ALT fixed to: 20 (power function)	0.187	-	-
BSA on Vd (2)	BSA mean:1.95 (power function)	1.24	-	-
Age on Vd (2)	Age mean: 65 (power function)	0.327	-	-
Vinorelbine				
CL	[L/h]	133	9.4	-
Vd	[L]	822	12.8	0.205
Q	[L/h]	362	9.0	-
Vp	[L]	1240	7.7	-

**Supplementary Table S1.** Continued.

Abbreviations: ALAG, lag time; ALT, Alanine aminotransferase; BSA, body surface area; CL, clearance; D1, duration of administration in compartment 1; F1, oral bioavailability; K12, rate constant from compartment 1 to compartment 2; K13, rate constant from compartment 1 to compartment 3; K21, rate constant from compartment 2 to compartment 1; K23, rate constant from compartment 2 to compartment 3; K31, rate constant from compartment 3 to compartment 1; K32, rate constant from compartment 3 to compartment 2; Ka, absorption rate constant, Ke, elimination rate constant; Vd, central volume of distribution.

**REFERENCES:**

1. Freiwald M, Schmid U, Fleury A, Wind S, Stopfer P, Staab A. Population pharmacokinetics of afatinib, an irreversible ErbB family blocker, in patients with various solid tumors. *Cancer Chemother Pharmacol.* 2014;73(4):759-770. doi:10.1007/s00280-014-2403-2.
2. Patel Y, Daryani V, Patel P, et al. Population Pharmacokinetics of Selumetinib and Its Metabolite N-desmethyl-selumetinib in Adult Patients With Advanced Solid Tumors and Children With Low-Grade Gliomas. *CPT Pharmacometrics Syst Pharmacol.* 2017;6(5):305-314. doi:10.1002/psp4.12175.

**Supplementary Table S2.** Overview of the recommended Phase 2 Dose for the different MEK and pan-HER inhibitors and the corresponding average week exposure.

Study	RP2D	Drug	Average week dose (mg)	Cl (L/h)	Average AUC <sub>week</sub> (mg/mL*h)
1	Dacomitinib 15 mg QD + mirdametininib 6 mg BID (21/7)	Dacomitinib	78.75	25.2	3.13
		Mirdametininib	63	4.33	14.6
2	Afatinib 20 mg QD + selumetinib 25 mg BID (21/7)	Afatinib	105	42.3	2.48
		Selumetinib	262.5	13.5	19.4
3	Lapatinib 750 mg QD + trametinib 1 mg BID	Lapatinib	5250	30.6	172
		Trametinib	7	3.71	1.89
4	Lapatinib 1000 mg QD + binimetininib 30 mg BID (5/2)*	Lapatinib	5000	30.6	163
		Binimetininib	300	17.9	16.8

Abbreviations: (5/2), 5 days on, 2 days off; (21/7), 21 days on 7 days off; AUC<sub>week</sub>, area-under-the-concentration-time-curve over a week; BID, bidaily weekly dosing; CL, clearance; RP2D, recommended Phase 2 Dose; QD, once daily dosing.

## REFERENCES:

- van Geel, R., et al. (2020). Phase 1 study of the pan-HER inhibitor dacomitinib plus the MEK1/2 inhibitor PD-0325901 in patients with KRAS-mutation-positive colorectal, non-small-cell lung and pancreatic cancer. *Br J Cancer* 122(8): 1166-1174.
- van Brummelen, E. M. J., et al. (2021). Phase I Study of Afatinib and Selumetinib in Patients with KRAS-Mutated Colorectal, Non-Small Cell Lung, and Pancreatic Cancer. *Oncologist* 26(4): 290-e545.
- Huijberts, S., et al. (2020). Phase I study of lapatinib plus trametinib in patients with KRAS-mutant colorectal, non-small cell lung, and pancreatic cancer. *Cancer Chemother Pharmacol* 85(5): 917-930.
- Utrecht Medical Center. A Dose-Escalating Phase I/II Study in Patients with RAS-Mutated Metastatic Colorectal Cancer to Investigate Safety and Clinical Activity of the Triple Combination of: MEK-inhibitor binimetininib, Pan-EGFR inhibitor lapatinib and the Microtubule Targeting Agent (MTA) vinorelbine [Internet]. *Clinicaltrialsregister.eu* [Citer 2023 June 12]. Available from: <https://www.clinicaltrialsregister.eu/ctr-search/trial/2019-004987-23/NL>









# Part 3

**Dose finding of oral docetaxel  
for patients with metastatic  
castration resistant  
prostate cancer**



# Chapter 7

## **Dose optimization of oral docetaxel in combination with ritonavir for patients with metastatic castration resistant prostate cancer**

*Manuscript in preparation*

Lisa T. van der Heijden  
Marit A.C. Vermunt  
Thomas P.C. Dorlo  
Jos H. Beijnen  
Alwin D.R. Huitema

## ABSTRACT

Patients with metastatic castration resistant prostate cancer (mCRPC) have a lower docetaxel exposure compared to patients with other advanced solid tumours when treated with the same dose. A lower exposure could influence treatment outcomes such as efficacy and toxicity. The current study aimed to find a dose resulting for oral docetaxel with ritonavir in a similar exposure to the recommended Phase 2 dose (RP2D) of the combination in other solid tumours using an update of a previously published population pharmacokinetic model the combination of for oral docetaxel and ritonavir. Data from 23 mCRPC patients were pooled with data from 149 patients with other solid tumours. mCRPC was tested as a binary covariate on ritonavir clearance and oral bioavailability and on docetaxel intrinsic clearance and oral bioavailability. Oral docetaxel exposure defined as the area-under-the-plasma concentration time curve for 1 week (AUC1wk) was simulated over different docetaxel-ritonavir dose levels in a bidaily once weekly dosing scheme. mCRPC patients had a 2.3-fold higher ritonavir clearance (RSE%: 7.1) and a 1.5-fold higher docetaxel intrinsic clearance (RSE%: 14.6). A morning dose of 30 mg docetaxel and 200 mg ritonavir with an evening dose of 20 mg docetaxel and 200 mg ritonavir (denoted as 30-20/200-200) and 30-30/200-100 in mCRPC patients had an AUC1wk similar to the RP2D in patients with other solid tumours (simulated AUC1wk 1.80 [1.13-2.80] mg/L\*h and 1.80 [1.14-2.81] mg/L\*h vs 1.77 [1.12-2.81] mg/L\*h, respectively). The RP2D for mCRPC patients (30-20/200-100) had a similar exposure to doses 20-20/200-200, 20-30/200-100, and 20-30/100-200 despite having different pharmacokinetic profiles. Its clinical relevance is currently unknown.

## 1 INTRODUCTION

Docetaxel is a well-established treatment of several solid tumours including non-small cell-lung cancer (NSCLC), breast cancer, head and neck cancer, gastric cancer and prostate cancer. It is most commonly administered as a 3-weekly 1-hour intravenous infusion. Oral administration of docetaxel could reduce the patient burden associated with intravenous administration due to its administration at home and avoidance of infusion reactions due to additives such as polysorbate 80 and ethanol in the intravenous formulation [1].

Oral administration of docetaxel is, however, hampered by a high first-pass effect and poor water solubility. The high first-pass metabolism is caused by docetaxel's high affinity for drug transporters such as P-glycoprotein (P-gp) and metabolism by Cytochrome P450 (CYP) 3A [2]. The first pass effect could be decreased by co-administering oral docetaxel with the CYP3A and a P-gp inhibitor ritonavir, which was demonstrated in a proof-of-concept study [3]. The development of two solid dispersion pharmaceutical formulations for oral use: ModraDoc001 capsule (10 mg docetaxel, freeze-dried), and ModraDoc006 tablet (10 mg docetaxel, spray dried) improved the water solubility of docetaxel [4-6].

Clinical trials in patients with advanced solid tumours have a defined recommended Phase 2 dose (RP2D) for the ModraDoc006 tablets for bidaily once weekly administration in a morning dose of 30 mg docetaxel co-administered with 100 mg ritonavir (r) and an evening dose of 20 mg docetaxel in combination with 100 mg ritonavir, denoted as ModraDoc006/r 30-20/100-100 [4,7,8]. However, a different RP2D might be required for patients with metastatic castration resistant prostate cancer (mCRPC). mCRPC patients demonstrated a lower area-under-the-plasma concentration time curve (AUC) for both intravenous docetaxel (1.8-fold) [9] and oral docetaxel (2.4-fold)[10] than in patients with other solid tumours. Furthermore, a lower docetaxel exposure after intravenous administration in mCRPC patients was associated with 2.2-fold lower odds for the development of neutropenia [9] and might affect efficacy of the treatment. The defined RP2D for the bidaily once weekly regimen for mCRPC patients (30-20/200-100) contains a higher ritonavir dose compared to the RP2D for other solid tumours (30-20/100-100) but the associated exposure was lower than the latter (0.367 mg/L\*h vs 0.894 mg/L\*h) [10]. The observed difference in docetaxel pharmacokinetics might be caused by an altered metabolism via CYP3A or an upregulated hepatic uptake, resulting in a higher clearance and lower exposure [11,12].

There is a need for dose optimisation for oral docetaxel in the mCRPC populations. The aim of the current study was to find a dose of oral docetaxel and ritonavir with a similar exposure, AUC over 1 week ( $AUC_{1wk}$ ), to the RP2D (30-20/100-100) in patients with other solid tumours using an update of a previously published population pharmacokinetic model for dose simulations [13]. The model was updated with data from a recent Phase I trial in mCRPC patients [12]. The objectives were two-fold. The first objective was to quantify the difference in pharmacokinetics between the two patient populations (mCRPC vs other solid tumours). The influence of mCRPC on docetaxel clearance and bioavailability was investigated for this. The second objective was to perform dose simulations with the final updated model to identify dose regimens for mCRPC with a similar  $AUC_{1wk}$  to the RP2D in other solid tumours.

## 2 METHODS

### 2.1 Clinical studies

The population pharmacokinetics of both intravenous and oral docetaxel with and without ritonavir was described in a previously published population pharmacokinetic analysis [13]. For the current analysis, the data regarding the oral administration of docetaxel, administered as drinking solution, ModraDoc001 capsules or ModraDoc006 tablets, were included. Pharmacokinetic data was obtained from patients with advanced solid tumours who were included in several clinical trials [3-5,7,14,15,8]. No patients with prostate cancer were included in these studies. This dataset was updated with all the available pharmacokinetic data from a dose-escalation study in mCRPC patients [12]. An overview of the data included from the different clinical studies is provided in Table 1. A summary of the individual clinical studies is described in the sections below.

#### 2.1.1 Study 1

This proof-of-concept study investigated ritonavir as a boosting agent for oral docetaxel. Intravenous docetaxel formulation (Taxotere®) was orally ingested as a drinking solution at a single dose of 10 or 100 mg docetaxel in combination with ritonavir soft gel capsules (Norvir; Abbott, Illinois, USA) at a dose of 100 mg. The study is described in detailed by Oostendorp., *et al* [3].

#### 2.1.2 Study 2

A dose-escalation study of orally administered docetaxel in combination with ritonavir was executed. The docetaxel-ritonavir combination was administrated at a once-weekly schedule. Three different oral docetaxel formulations were included in the study: the intravenous docetaxel formulation ingested as a drinking solution, ModraDoc001 capsule formulation, and ModraDoc006 tablet formulation. The formulation of ritonavir was switched during the execution of the study by the manufacturer from a soft gel capsule to a tablet formulation (Norvir; Abbott, Illinois, USA). Oral docetaxel was administered in doses of 20-80 mg in combination with 100 or 200 mg ritonavir. Pharmacokinetic data was obtained during cycle 1, 2 and 3 of treatment (1 cycle corresponds to 1 week). The study is described in detail by Moes., *et al* [4], Koolen., *et al* [14] and Marchetti., *et al* [15].

**Table 1.** Overview of the included oral docetaxel data per study.

	<b>Study 1 [3]</b>	<b>Study 2 [4,14,15]</b>
<b>Number of patients</b>		
Total	25	89
ModraDoc001 capsule	-	68
ModraDoc006 tablet	-	10
Docetaxel drinking solution	25	11
<b>Docetaxel</b>		
Dose (mg/day)	10, 100	20, 30, 40, 60, 80
Dosing time (hours)	t=0, t=1	t=0
Formulation	Drinking solution	Drinking solution ModraDoc001 ModraDoc006
PK data	Yes	Yes
<b>Ritonavir</b>		
Dose (mg/day)	0, 100	0, 100, 200
Dosing times (hours)	t=0, t=1	t=0
Ritonavir formulation	Capsules	Capsules Tablets
PK data	No	Yes

### 2.1.3 Study 3

In this dose-escalation study, a weekly bi-daily dosing schedule of oral docetaxel was administered as either ModraDoc001 capsules or ModraDoc006 tablets (both with 10 mg docetaxel). Docetaxel and ritonavir were administered at t = 0 and t = 7 hours. The total daily doses of docetaxel were 40-80 mg and ritonavir 200 mg. Pharmacokinetic data were obtained during cycle 1, 2 and 3 of treatment. The study is described in detail by de Weger., *et al* [7].

### 2.1.4 Study 4

A crossover study was performed to compare the exposure of different oral docetaxel formulations simultaneously administered with ritonavir. Docetaxel was administered at a dose of 40 mg in combination with a 100 or 200 mg ritonavir dose. Pharmacokinetic data was obtained during cycle 1, 2, and 3 of treatment. A detailed description of the study was published by Moes., *et al* [5].



Study 3 [7]	Study 4 [5]	Study 5 [12]
29	6	23
17	6	-
12	-	23
-	-	-
40, 50, 60, 80 t=0, 7 ModraDoc001 ModraDoc006	40 t=0 ModraDoc001	40, 50 t=0,7 ModraDoc006
Yes	Yes	Yes
200 t=0, 7 Tablets	100, 200 t=0 Tablets	200, 300, 400 t=0,7 Tablets
Yes	Yes	Yes

### 2.1.5 Study 5

A dose-escalation study was executed to establish the safety, pharmacokinetics and RP2D for mCRPC patients. Oral docetaxel was administered as ModraDoc006 tablets (with 10 mg docetaxel per tablet) at a total weekly dose of 40 or 50 mg in combination with 200, 300 or 400 mg ritonavir. Docetaxel and ritonavir were administered at  $t = 0$  and  $t = 7$  hours. Pharmacokinetic data was obtained in cycles 1 and 2 of treatment. The study has been described in detail by Vermunt., *et al* [12].

### 2.2 Population pharmacokinetic model

A previously developed semi-mechanistic population pharmacokinetic model for intravenous and oral docetaxel and ritonavir was used [13]. The model consisted of two linked models for ritonavir and docetaxel (see Figure 1). Stochastic approximation expectation maximization (SAEM) was used to avoid local minima in the parameter estimation [16].

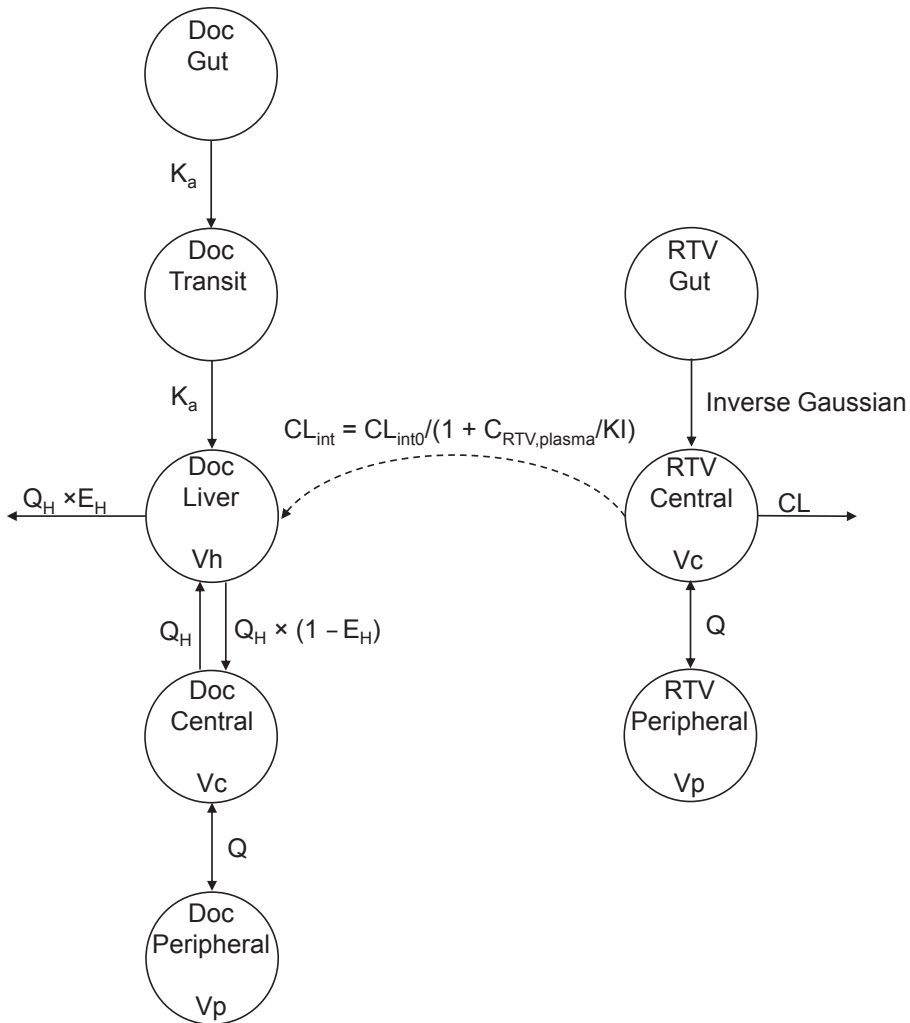


**Figure 1.** Schematic overview of the integrated docetaxel-ritonavir model. CL, clearance;  $CL_{int}$ , intrinsic clearance of docetaxel;  $CL_{int0}$ , uninhibited intrinsic clearance of docetaxel;  $C_{RTV,plasma}$ , ritonavir plasma concentration, Doc, Docetaxel;  $E_H$ , hepatic extraction ratio;  $K_a$ , first-order absorption rate constant;  $KI$ , inhibition constant of ritonavir on docetaxel metabolism;  $Q$ , intercompartment distribution;  $Q_H$ , hepatic blood flow; RTV, ritonavir;  $V_c$ , central volume of distribution;  $V_h$ , hepatic volume of distribution;  $V_p$ , peripheral volume of distribution.

### 2.2.1 Ritonavir

Ritonavir pharmacokinetics was described by a two-compartmental model with linear elimination (see Figure 1). Absorption of ritonavir was described with an inverse Gaussian density input function (Equation 1) [17]. The model included relative bioavailability of the second ritonavir dose compared to the first dose ( $F_{2nd/1st}$ ) and a relative bioavailability of the tablet formulation compared to the soft gel capsule ( $F_{tablet}$ ). Between subject variability (BSV) was included for the variability of mean absorption time, clearance, central volume of distribution,  $F_{2nd/1st}$  and  $F_{tablet}$ . Inter-occasion variability (IOV) was included on the mean absorption time and the variability of mean absorption time. Residual error was described with a proportional error model.

$$N_{in} = A_D \left[ \frac{MAT}{2\pi \times CV^2 \times t^3} \right]^{1/2} \times \exp\left(-\frac{(t-MAT)^2}{2CV^2 \times MAT \times t}\right) \quad (\text{Equation 1})$$

In which  $N_{in}$  is the incoming influx transport,  $A_D$  is the dose,  $MAT$  the mean absorption time,  $CV$  the variation in the mean absorption time, and  $t$  is time.

### 2.2.2 Docetaxel

Oral docetaxel pharmacokinetics was described by a two-compartment model (see Figure 1). Absorption was described by a first order absorption rate constant and one transit compartment to the liver compartment. A well-stirred liver model was used to describe the overall metabolism of docetaxel by CYP3A and the influence of ritonavir on CYP3A. Docetaxel hepatic intrinsic clearance was described as a function of the uninhibited intrinsic clearance and the ritonavir plasma concentration and an inhibition constant of CYP3A by ritonavir ( $KI$ ) (see Equations 2-4).

$$Cl_{int}(t) = \frac{Cl_{int0}}{(1 + C_{RTV,plasma}(t))/KI} \quad (\text{Equation 2})$$

$$E_H(t) = \frac{Cl_{int}(t) \times fu}{Q_H + Cl_{int}(t) \times fu} \quad (\text{Equation 3})$$

$$F_H(t) = 1 - E_H(t) \quad (\text{Equation 4})$$

In which  $Cl_{int}$  is the uninhibited intrinsic docetaxel clearance,  $Cl_{int0}$  is the intrinsic docetaxel clearance,  $C_{RTV,plasma}$  is the ritonavir plasma concentration,  $E_H$  is the hepatic extraction fraction,  $fu$  is the free fraction of docetaxel in plasma which was fixed to 4.6% [18],  $Q_H$  is the hepatic blood flow which was fixed to 80 L/h [19], and  $F_H$  is the hepatic bioavailability. The volume of the liver compartment was assumed to be 1 L [20].

Gut bioavailability of docetaxel ( $F_g$ ) was described by a function of the relative bioavailability of the ModraDoc006 tablets compared to the ModraDoc001 capsules ( $F_{formulation}$ ), the relative bioavailability of docetaxel with and without ritonavir ( $F_{ritonavir}$ ), and lastly the relative bioavailability of the second dose versus the first dose ( $F_{2nd/1st}$ ) (Equation 5).

$$F_G = F_{formulation} \times F_{ritonavir} \times F_{2nd/1st} \quad (\text{Equation 5})$$

BSV was included on the absorption rate for both the ModraDoc tablet and capsule formulation, and the drinking solution, intrinsic clearance, central volume of distribution,  $F_{2nd/1st}$  and the bioavailability of the drinking solution. Inter-occasion variability was included in the model to describe the within-day and between-day variability in bioavailability and absorption rate constant.

### 2.3 Covariate analysis

The influence of mCRPC on the pharmacokinetics of oral docetaxel and ritonavir was investigated. The hypothesis behind the observed difference in pharmacokinetics was either an altered metabolism via CYP3A and/or an upregulated hepatic uptake, leading to a higher clearance and lower exposure [11]. Hence, mCRPC was tested as a binary covariate on ritonavir clearance, docetaxel intrinsic clearance, and bioavailability according to Equation 6.

$$P_i = P_{pop} \times \theta_{covariate} \quad (\text{Equation 6})$$

In which,  $P_i$  is the respective pharmacokinetic parameter for patient  $i$ ,  $P_{pop}$  is the typical value of the respective pharmacokinetic parameter for the population, and  $\theta_{covariate}$  is the theta representing the effect of mCRPC on the respective pharmacokinetic parameter. mCRPC was retained in the model as a covariate when the drop in Objective Function Value (dOFV, equal to minus two times the log-likelihood) exceeded 3.841 ( $P < 0.05$  based on  $\chi^2$  distribution with one degree of freedom), which was considered statistically significant for hierarchical models. Model performance was evaluated with visual predictive checks ( $n = 1000$ ).

### 2.4 Simulations

Simulation studies were executed for the ModraDoc006 tablet and ritonavir tablet combination (ModraDoc006/r), as mCRPC patients exclusively received this formulation [12]. Oral docetaxel plasma concentrations were simulated for 16 bidaily once weekly dosing regimens where oral docetaxel is co-administrated

with ritonavir at  $t = 0$  hours and  $t = 7$  hours. The 16 dosing regimens were variations of the following daily once weekly doses of docetaxel (40, 50, 60 mg) and ritonavir (200, 300, 400 mg), taking into account the availability of 10 mg docetaxel tablets and 100 mg ritonavir tablets. Variations in docetaxel and ritonavir doses were simulated with the aim of finding a dose with a similar exposure in mCRPC patients compared to the simulated exposure of the RP2D (30-20/100-100) in patients with other solid tumours [7]. The area-under-the-plasma concentration-time curve for 1 week ( $AUC_{1wk}$ ) corresponding to the exposure during a single cycle was used to compare the dosing regimens for mCRPC patients to the RP2D for patients with other solid tumours. For each dosing regimen, plasma concentrations were simulated for 1000 patients.

## 2.5 Software

NONMEM (version 7.5, ICON Development Solutions, Ellicott City, MD, USA) was used for model estimation. Parameter precision was obtained using the \$COVARIANC option of NONMEM. Perl-speaks-NONMEM (PsN, version 5.2.6) was used to obtain visual predictive checks. R (version 4.1.2) was used for data preparation and visualisation of the data.

### 3 RESULTS

Data from 23 mCRPC patients were pooled with the dataset of 149 patients with other solid tumours. A total of 735 ritonavir and 735 docetaxel plasma concentrations were obtained from the mCRPC patients of which 5 concentrations were below the lower limit of quantification (LLOQ) of each drug. These concentrations <LLOQ were excluded from the dataset because it was only 0.7% of the total amount of plasma concentrations obtained from mCRPC patients.

Final parameter estimates of the ritonavir model and the docetaxel model are depicted in Table 2 and Table 3, respectively.

#### 3.1 Ritonavir

Inclusion of mCRPC as a binary covariate on ritonavir clearance significantly improved the model (dOFV: 22,  $p < 0.001$ ). Ritonavir clearance was 2.3-fold (RSE%: 7.1) higher for mCRPC patients compared to patients with other solid tumours. mCRPC as a binary covariate on bioavailability did not improve the model fit and was therefore not included in the model. Peak ritonavir concentrations increased more than dose-proportional causing them to be underestimated by the model. Therefore, cumulative ritonavir dose was included as a power function on F (See Equation 7):

$$F_{RTV} = 1 * \left( \frac{\text{cumulative dose}}{100} \right)^{\theta} \times e^{\eta} \quad (\text{Equation 7})$$

In which  $F_{RTV}$  is the ritonavir bioavailability,  $\theta$  is the effect size of cumulative ritonavir dose which is normalised by the minimal administered dose (100 mg), and  $\eta$  is the between subject variability is assumed to be distributed following  $N(0, \omega^2)$ .

The estimated effect of the cumulative ritonavir dose on bioavailability was 0.666 (RSE%: 13.6) with a dOFV of 55 ( $p < 0.001$ ). The underestimation of peak concentrations visually improved (Figure S1). Individual predicted concentrations provided a good description of observed concentrations (Figure S1 B). Covariance between clearance, central volume of distribution, and bioavailability were estimated to account for correction between these parameters for simulations. The prediction corrected visual predicted check (see Figure S2) shows that the model predicts the model adequately.

**Table 2.** Parameter estimates of ritonavir in the final model.

Parameter	Units	Estimate	RSE (%) <sup>d</sup>	Shrinkage (%)
Population parameter				
CL <sub>RTV</sub>	L/h	7.57	7.7	-
V <sub>c,RTV</sub>	L	46.8	9.6	-
MAT	h	5.33	5.85	-
CV	%	92.4	1.02	-
Q <sub>RTV</sub>	L/h	3.41	4.33	-
V <sub>p,RTV</sub>	L	19.9	9.1	-
F <sub>2nd/1st</sub>	-	1.55	8.4	-
F <sub>tablet</sub>	-	1.06	8.3	-
mCRPC-CL	-	2.29	7.1	-
θ <sub>RTV,dose</sub>	-	0.666	13.6	-
Between subject variability				
CL <sub>RTV</sub> <sup>a</sup>	CV%	8.3	106.2	12
V <sub>c,RTV</sub> <sup>b</sup>	CV%	71.9	13.8	9
F <sup>c</sup>	CV%	65.3%	12.0	2
F <sub>2nd/st</sub>	CV%	37.4%	28.4	15
CV	CV%	12.2%	64.7	51
Inter-occasion variability				
MAT	CV%	51.8	9.7	30
CV	CV%	22.4	15.6	9
Residual unexplained variability				
Prop. Err.	CV%	35.4	2.2	13

Abbreviations: θ<sub>RTV,dose</sub>, Effect of ritonavir dose on bioavailability; CL<sub>RTV</sub>, ritonavir clearance; CV, variability in mean absorption time; F<sub>2nd/1st</sub>, relative bioavailability of the second ritonavir dose versus the first dose; F<sub>tablet</sub>, relative bioavailability of the ritonavir tablet versus the capsule; mCRPC-CL, the fold difference in ritonavir clearance for patients with metastatic castration resistant prostate cancer versus patients with other solid tumours; MAT, mean absorption time; Prop. Err., proportional error; Q<sub>RTV</sub>, ritonavir inter-compartmental clearance; V<sub>c,RTV</sub>, ritonavir central volume of distribution; V<sub>p,RTV</sub>, ritonavir peripheral volume of distribution.

<sup>a</sup> Correlation was estimated between CL<sub>RTV</sub> and V<sub>c,RTV</sub>, F, and F<sub>2nd/1st</sub> of 0.0314, -0.03, and 0.0164, respectively.

<sup>b</sup> Correlation was estimated between V<sub>c,RTV</sub> and F, and F<sub>2nd/1st</sub> of 0.126 and 0.131, respectively.

<sup>c</sup> Correlation was estimated between F and F<sub>2nd/1st</sub> of -0.129.

<sup>d</sup> Relative standard errors were obtained from the successful covariance step.

### 3.2 Docetaxel

The addition of the data obtained from mCRPC patients resulted in a drop in  $KI$  of 1.7-fold and an increase in peripheral volume of 1.5-fold. These changes in parameter estimates were presumably caused by the difference in doses and pharmacokinetics between the two patient populations. The  $KI$  was fixed to 186 ng/mL (the value obtained from the SAEM estimation of the original model by Yu., *et al*) [13] because it was assumed that disease type would not influence the affinity of ritonavir to CYP3A. Inclusion of mCRPC as a binary covariate on the intrinsic clearance of docetaxel resulted in a significant drop in OFV of 20 ( $p < 0.001$ ). The intrinsic docetaxel clearance was 1.5-fold (RSE%: 14.6) higher for mCRPC. Inclusion of mCRPC and ritonavir dose on  $F_{gut}$  and ritonavir dose on the absorption rate constant of docetaxel did not improve model fit. Incorporation of BSV on peripheral volume resulted in a significant drop in OFV of 64. Figures 2 and 3 depict the graphical evaluations of the model, indicating a general adequate description of the data. In the structural model a bias was visible for higher docetaxel concentration which could not be improved. However, this bias was not visible in the individual predicted concentrations versus observed concentrations or the conditional weighted residuals versus population predictions or time after dose (Figure 2) neither in de prediction corrected visual predictive check (Figure 3). The model described the different dose levels well (Figure S3), especially considering the small number of patients per dose level ( $n \leq 6$ ).

### 3.3 Simulations

The comparison of exposure of oral docetaxel in combination with ritonavir administered at different bidaily once weekly doses in mCRPC patients and the RP2D in patients with other solid tumours (30-20/100-100) is shown in Figure 4 and Table 4. The RP2D of other solid tumours resulted in a 1.9-fold lower simulated exposure in mCRPC patients compared to other solid tumours ( $AUC_{1wk}$  median [interquartile range]: 0.922 [0.579-1.47] mg/L\*h vs 1.77 [1.12-2.81] mg/L\*h, respectively). Simulated doses regimens of 30-20/200-200 and 30-30/200-100 resulted in similar exposures as the simulated exposure of the RP2D in other solid tumours ( $AUC_{1wk}$  1.80 [1.13-2.80] mg/L\*h and 1.80 [1.14-2.81] mg/L\*h vs 1.77 [1.12-2.81] mg/L\*h, respectively). Moreover, the simulated dose regimens of 20-20/200-200, 30-20/200-100, 20-30/200-100, and 20-30/100-200 all resulted in a similar exposure in mCRPC ( $AUC_{1wk}$ : 1.50 [0.952-2.35] mg/L\*h, 1.44 [0.900-2.31] mg/L\*h, 1.54 [0.971-2.43] mg/L\*h, and 1.47 [0.929-2.28] mg/L\*h, respectively) despite differences in administered docetaxel (40-50 mg) and ritonavir doses (300-400 mg). While these doses regimens



have similar simulated AUCs, the simulated pharmacokinetic curve as well as the simulated inhibition of docetaxel intrinsic clearance differs between the dose levels (see Figure 5), which was due to difference in docetaxel doses and difference in inhibition of docetaxel intrinsic clearance by ritonavir.

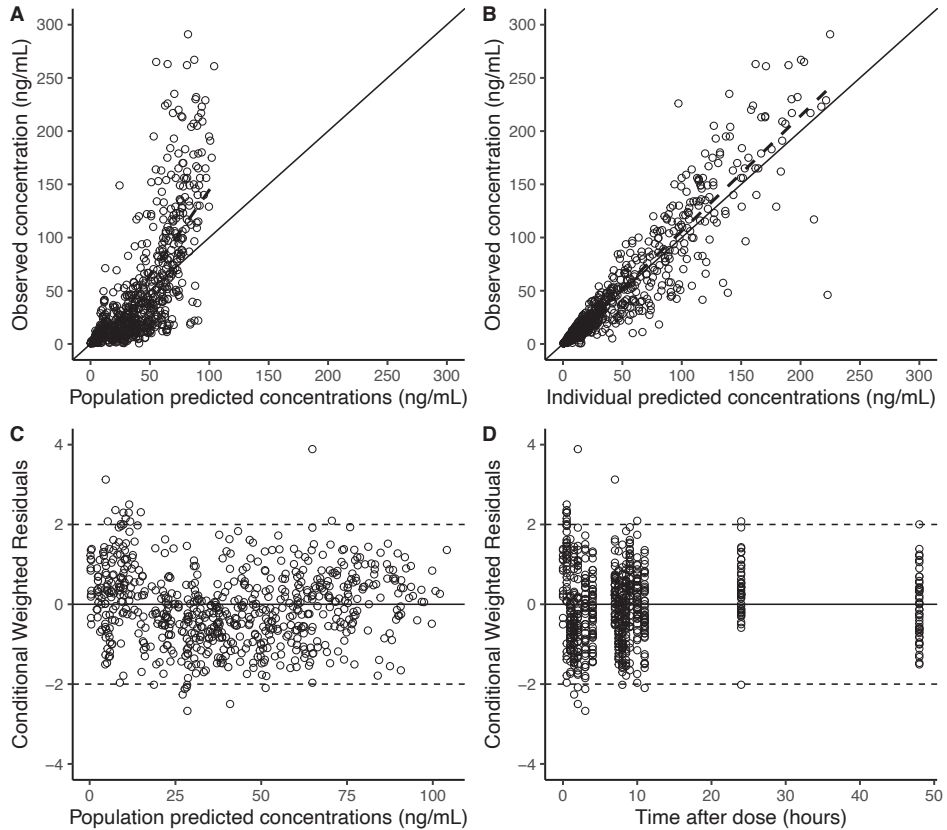


**Figure 2.** Diagnostic plots for the final docetaxel model. A, Population predicted concentrations versus observed concentration; B, Individual predicted concentrations versus observed concentrations. The solid line is the line of unity. The dashed line is the trend line in the data. C, Population predicted concentrations versus conditional weight residuals, D, Time after dose versus conditional weighted residuals.

**Table 3.** Parameter estimates of docetaxel in the final model.

Parameter
Population parameter
First-order $K_a$ ModraDoc001 capsule
First-order $K_a$ ModraDoc006 tablet
First-order $K_a$ drinking solution
$CL_{int0}$
KI
$V_{cDOC}$
$Q_{DOC}$
$V_{pDOC}$
$F_{ritonavir}$
$F_{2nd/1st,DOC}$
$F_{formulation,ModraDoc001}$
$F_{formulation,ModraDoc006}$
$F_{formulation,drinking\ solution}$
mCRPC- $CL_{int0}$
Between subject variability
$K_a$ ModraDoc001 & ModraDoc006
$K_a$ drinking solution
$CL_{int0}$
$V_{cDOC}$
$V_{pDOC}$
$F_g$ ModraDoc001 & ModraDoc006
$F_g$ drinking solution
Within subject variability
Between day variability on $K_a$ ModraDoc001 & ModraDoc006
Between day variability on $K_a$ drinking solution
Within day variability on $K_a$ ModraDoc001 & ModraDoc006
Between day variability on $F_g$ ModraDoc001 & ModraDoc006
Between day variability on $F_g$ drinking solution
Within day variability on $F_g$ ModraDoc001 & ModraDoc006
Residual unexplained variability
Prop. Err.
Abbreviations: $CL_{int0}$ , uninhibited intrinsic clearance; CV%, coefficient of variation; DOC, docetaxel; $F_{2nd/1st}$ , doc, gut bioavailability of the second dose relative to the first dose; $F_{formulation,drinking\ solution}$ , gut bioavailability of drinking solution without ritonavir coadministration; $F_{formulation,ModraDoc001}$ , gut bioavailability of ModraDoc001 without ritonavir coadministration; $F_{formulation,ModraDoc006}$ , gut bioavailability of ModraDoc006 without ritonavir coadministration; $F_g$ , gut bioavailability; Fritonavir, gut bioavailability in combination with ritonavir relative to without; $k_a$ , absorption rate constant; KI, inhibition constant; mCRPC- $CL_{int0}$ , the effect of metastatic castration resistant prostate cancer on docetaxel intrinsic clearance; $Q_{DOC}$ , intercompartment clearance 1; RSE, relative standard error; $V_{cDOC}$ , volume of distribution of central compartment; $V_{pDOC}$ , volume of distribution of peripheral compartment.

Units	Estimate	RSE (%)	Shrinkage (%)
h <sup>-1</sup>	1.45	6.7	-
h <sup>-1</sup>	0.977	8.0	-
h <sup>-1</sup>	1.92	16.8	-
L/h	1980 FIX <sup>a</sup>	-	-
ng/mL	186 FIX	-	-
L	133	6.1	-
L/h	32.4	4.1	-
L	863	7.9	-
-	3.35	23.3	-
-	1.24	5.4	-
-	0.211	23.1	-
-	0.230	24.1	-
-	0.325	25.1	-
-	1.54	14.6	-
CV%	31.4	32.3	42
CV%	75.2	35.6	61
CV%	38.5	34.9	28
CV%	49.9	19.2	24
CV%	43.7	30.6	30
CV%	50.3	22.9	23
CV%	72.0	28.4	42
CV%	41.0	21.4	34
CV%	54.1	25.1	71
CV%	49.9	22.6	54
CV%	25.9	14.8	39
CV%	32.2	41.4	72
CV%	22.9	31.2	60
CV%	36.6	4.0	12

<sup>a</sup>Parameter was fixed in the previously published model after estimating it on intravenous docetaxel [13]

<sup>b</sup> Correlation was estimated between  $CL_{int0}$  and  $V_{c,DOC}$ ,  $V_{p,DOC}$  and  $F_g$  ModraDoc001 & ModraDoc006 of 0.0018, 0.0602, and 0.0732, respectively.

<sup>c</sup> Correlation was estimated between  $V_{c,DOC}$  and  $V_{p,DOC}$ , and  $F_g$  ModraDoc001 & ModraDoc006 of 0.111 and 0.0429, respectively.

<sup>d</sup> Correlation was estimated between  $V_{p,DOC}$  and  $F_g$  ModraDoc001 & ModraDoc006 of 0.18 and 0.166, respectively.

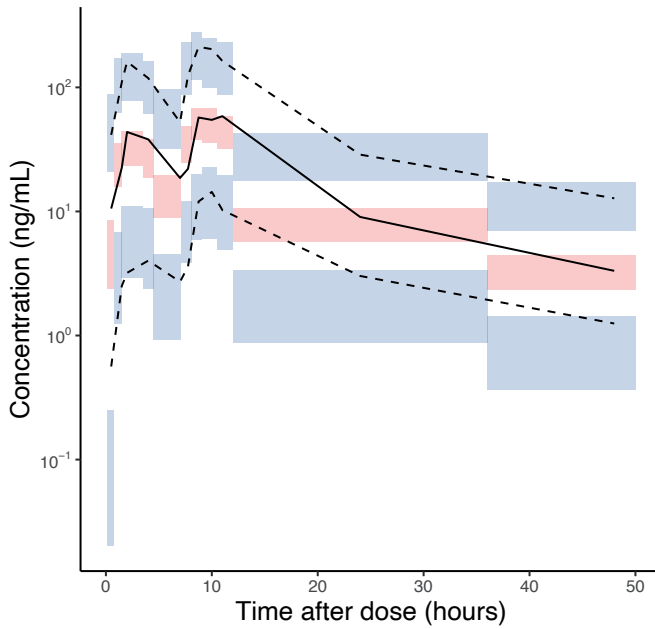


**Figure 3.** Prediction corrected visual predictive checks for docetaxel ( $n = 1,000$ ). Solid lines and red areas represent the median observed values and simulated 95% confidence interval. Dashed lines and purple areas represent the 10% and 90% percentiles of the observed values and 95% confidence intervals of the simulated percentiles.

**Table 4.** Simulated area-under-the-plasma concentration-time-curve over 1 week of ModraDoc006/r for different bidaily once weekly doses of oral docetaxel with ritonavir.

Population	Dose (mg)	Simulated AUC <sub>1wk</sub> (mg/L*h) median [IOR]	Reported AUC <sub>inf</sub> (mg/L*h) <sup>¶</sup>	Comment
No-mCRPC	30-20/100-100	1.77 [1.12-2.81]	1.42 (n=16) <sup>#</sup> [7]	RP2D
mCRPC	20-20/100-100	0.791 [0.495-1.25]	-	-
	20-20/200-100	1.20 [0.757-1.87]	0.526 (cycle 1), 0.590 (cycle 2) <sup>§</sup> (n=3) [12]	-
	20-20/100-200	1.09 [0.685-1.70]	-	-
	20-20/200-200	1.50 [0.952-2.35]	-	-
	20-30/100-100	1.05 [0.659-1.65]	-	-
	20-30/200-100	1.54 [0.971-2.43]	-	-
	20-30/100-200	1.47 [0.929-2.28]	-	-
	20-30/200-200	1.98 [1.23-3.06]	-	-
	30-20/100-100	0.922 [0.579-1.47]	0.399 (cycle 1) 0.524, (cycle 2) <sup>§</sup> (n=5) [12]	-
	30-20/200-100	1.44 [0.900-2.31]	1.34 (cycle 1),1.69 (cycle 2) <sup>§</sup> (n=6) [12]	RP2D
	30-20/100-200	1.25 [0.786-1.95]	-	-
	30-20/200-200	1.80 [1.13-2.80]	1.55 (cycle 1), 1.82 (cycle 2) <sup>§</sup> (n=6) [12]	-
	30-30/100-100	1.19 [0.742-1.88]	-	-
	30-30/200-100	1.80 [1.14-2.81]	-	-
30-30/100-200	1.64 [1.03-2.56]	-	-	
30-30/200-200	2.24 [1.43-3.52]	-	-	

Abbreviations: AUC<sub>1wk</sub>, area-under-the-plasma concentration-time-curve over 1 week; mCRPC, metastatic castration-resistant prostate cancer; IOR, Interquartile range; RP2D, recommended Phase 2 dose.

<sup>¶</sup> Reported area-under-the-plasma concentration-time curve extrapolated to infinity was calculated with non-compartmental analysis

<sup>#</sup> Reported mean area-under-the-plasma concentration-time-curve extrapolated to infinity of the first cycle.

<sup>§</sup> Reported the mean area-under-the-plasma concentration-time-curve extrapolated to infinity of the first and second cycle.

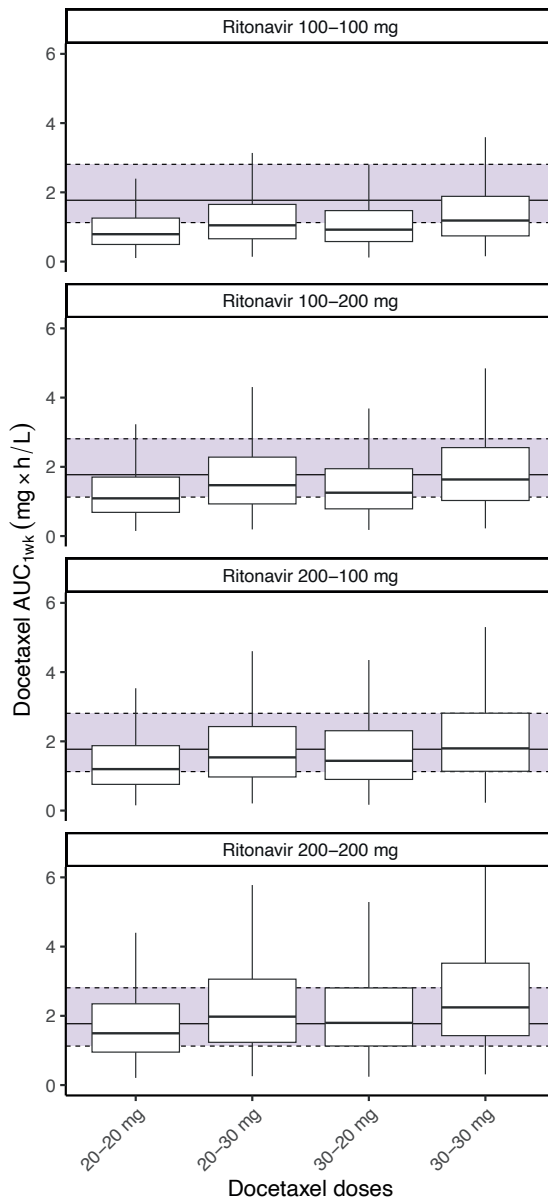


**Figure 4.** Comparison of the simulated docetaxel exposures between ModraDoc006 with ritonavir dosing regimens in mCRPC with the recommended Phase 2 dose in patients with other solid tumours (30-20/100-100). The boxplots depict the median and interquartile range of the simulated 1-week time area under the plasma concentration-time curve ( $AUC_{1wk}$ ). The horizontal solid line represents the median exposure of the recommended Phase 2 dose in other solid tumours, whereas the dashed lines represent the 25<sup>th</sup> and 75<sup>th</sup> percentiles. The purple area covers the interquartile range of the  $AUC_{1wk}$  of the recommended Phase 2 dose in other solid tumours.

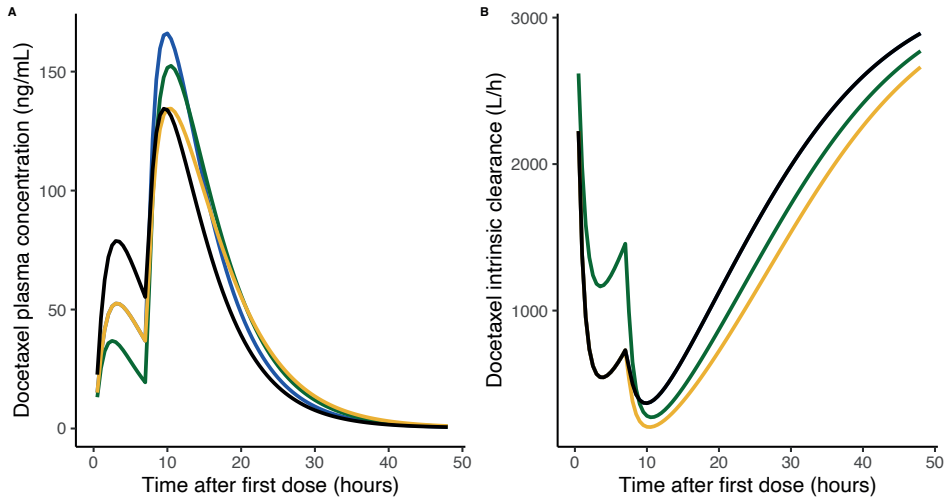


**Figure 5.** Simulation of population plasma concentrations of oral docetaxel (A) and docetaxel intrinsic clearance (L/h) for patients with metastatic castration resistant prostate cancer. The black line corresponds to a dose of 30-20/200-100, the blue line corresponds to a dose of 20-30/200-100, the green line corresponds to a dose of 20-30/100-200, and the yellow line corresponds to a dose of 20-20/200-200. In B the yellow line falls below the black line for the first dose.

## 4 DISCUSSION

In the current study, the differences in pharmacokinetics of ritonavir and oral docetaxel between mCRPC patients and patients with other solid tumours were quantified. mCRPC had a 2.3-fold higher ritonavir clearance (RSE%: 7.1) and a 1.5-fold (RSE%: 14.6) higher intrinsic clearance of docetaxel. Dose finding was performed to find a bidaily once weekly oral docetaxel dose in combination with ritonavir for patients with mCRPC which results in a similar  $AUC_{1wk}$  compared to the RP2D (30-20/100-100) in patients with other solid tumours [7]. The simulated  $AUC_{1wk}$  of the different dose levels are in similar range to the observed mean  $AUC_{inf}$  in the clinical studies (see Table 4). Especially,  $AUC_{1wk}$  of dose levels 30-20/200-100 and 30-20/200-200 correspond well to the clinical observations. For 30-20/100-100 and 20-20/200-100, the reported  $AUC_{inf}$  is lower than the median simulated  $AUC_{1wk}$  but fell inside the simulated range (0.117-7.41 mg/L\*h and 0.151-8.89 mg/L\*h, respectively for a 1000 typical patients). There are two limitations regarding this comparison. First, the reported mean  $AUC_{inf}$  are obtained from non-compartmental analysis based on the trapezium rule with extrapolation to infinity, which might not capture the true peak concentration well. Second, the number of patients per dose level is small ( $\leq 6$ ), while the pharmacokinetics of oral docetaxel demonstrates high inter-patient variability especially during absorption. Taking these considerations into account, the model predicts the  $AUC_{1wk}$  adequately for the different dose levels. Therefore, the simulated median  $AUC_{1wk}$  of the simulated dose regimens can be considered appropriate estimated of the expected exposure in mCRPC patients, particularly for mutual comparison.

Dose regimens of 30-20/200-200 and 20-30/200-100 in mCRPC patients resulted in similar simulated  $AUC_{1wk}$  to the RP2D in patients with other solid tumours with their median values within the interquartile range of each other. However, 30-20/200-200 was associated with dose-limiting toxicities (DLTs) in mCRPC patients [12] and therefore 30-20/200-100 was defined as the RP2D for mCRPC patients. This could indicate that there are pharmacodynamic differences between mCRPC patients and patients with other solid tumours. Four dose regimens (20-20/200-200, 20-30/100-200, 20-30/200-100, and 30-20/200-100) had a similar simulated  $AUC_{1wk}$  but their pharmacokinetic profiles differed (Figure 5). The different pharmacokinetics profiles were partly caused by differences in inhibition of docetaxel intrinsic clearance by ritonavir. Administration of two consecutive doses of 200 mg leads to the most pronounced inhibition of intrinsic clearance, which resulted in a slower



elimination of docetaxel, compared to 200 mg followed by 100 mg ritonavir. Consecutive doses of 100 mg and 200 mg ritonavir resulted in a small initial inhibition of intrinsic clearance followed by a steep decrease in intrinsic clearance (Figure 5B). These difference in pharmacokinetic profiles might influence efficacy and/or toxicity of ModraDoc006/r treatment.

In the current analysis, the inhibition constant of CYP3A by ritonavir (KI) was fixed to 186 ng/mL. Estimation of KI resulted in a drop of 1.7-fold in KI and an increase in the peripheral volume of 1.5-fold, while the other parameter remained constant. It was concluded that the KI was difficult to estimate due to the skewed distribution of data between the two patient populations. In general, mCRPC patients had lower plasma concentrations of both ritonavir and docetaxel despite receiving higher doses compared to patients with other solid tumour with only one dose level (30-20/100-100) administered to both patient populations. Therefore, the model tried to describe both groups of data with a higher peripheral distribution to account for relative low plasma concentration associated with the relative higher doses of mCRPC patients, while the KI decreased to account for the higher plasma concentration of patients with other solid tumours who received relative lower doses. Therefore, KI was fixed under the assumption that disease type would not influence the affinity of ritonavir to CYP3A. Despite this limitation, the model was able to describe the plasma concentrations in mCRPC patients well and the dose simulations resulted in reasonable estimations of exposure.

The RP2D established for patients with other solid tumours resulted in a 1.9-fold lower exposure in mCRPC patients, which is higher than the found 1.5-fold difference in docetaxel intrinsic clearance indicating that a decrease in exposure of ritonavir contributes to the observed differences in docetaxel pharmacokinetics between mCRPC and other solid tumour patients, possibly due to less inhibition of docetaxel intrinsic clearance. Currently, there are two hypotheses regarding the observed difference in docetaxel pharmacokinetics between mCRPC patients and patients with other solid tumours. The first hypothesis assumes a higher CYP3A activity in mCRPC patients due to their hormone status. However, this hypothesis is unlikely since two published phenotyping studies and one yet to be published phenotyping study reported no significant difference in CYP3A activity between the two patient groups [11,21]. The second hypothesis assumes an increased hepatic uptake of docetaxel due to a higher expression of hepatic drug transporters. Preclinical studies have reported an upregulated hepatic transporter organic anion transporter 2

(OAT2) which was associated with an increased hepatic and CYP3A exposure of docetaxel and lower plasma exposure in castrated rats [11]. OAT2 expression seems to be regulated by liver receptor homolog 1 (Lrh-1). Expression of Lrh-1 was found to be associated with both OAT2 expression as well as docetaxel exposure [22]. While the exact relationship between Lrh-1 and prostate cancer remains to be elucidated, androgens such as testosterone seems to be involved [23-27].

## 5 CONCLUSION

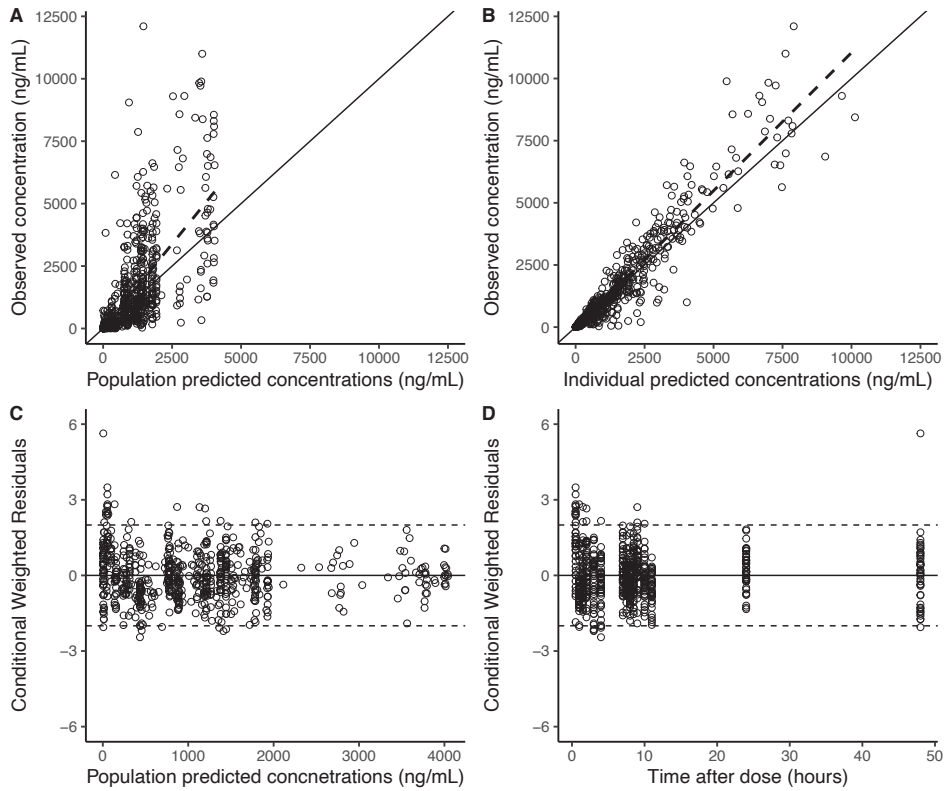
mCRPC was successfully incorporated in a previously published pharmacokinetic model for oral docetaxel and ritonavir. Inclusion of mCRPC as a covariate on ritonavir clearance and docetaxel intrinsic clearance significantly improved the model. mCRPC patients had a 2.5-fold (RSE%: 7.1) higher ritonavir clearance and 1.5-fold (RSE%: 18.5) higher docetaxel intrinsic clearance versus patients with other solid tumours. Compared to the RP2D for patients with other solid tumours (30-20/100-100), dose regimens for mCRPC patients of 30-20/200-200 and 30-30/200-100 resulted in a similar exposure. The RP2D for mCRPC patients (30-20/200-100) had similar exposure to the simulated doses 20-20/200-200, 20-30/200-100 and 20-30/100-200. The shape of the pharmacokinetic profile differed though. While differences in pharmacokinetic profiles could influence efficacy and toxicity, it is currently unknown if these dose regimens differ in their clinical outcomes.

## REFERENCES

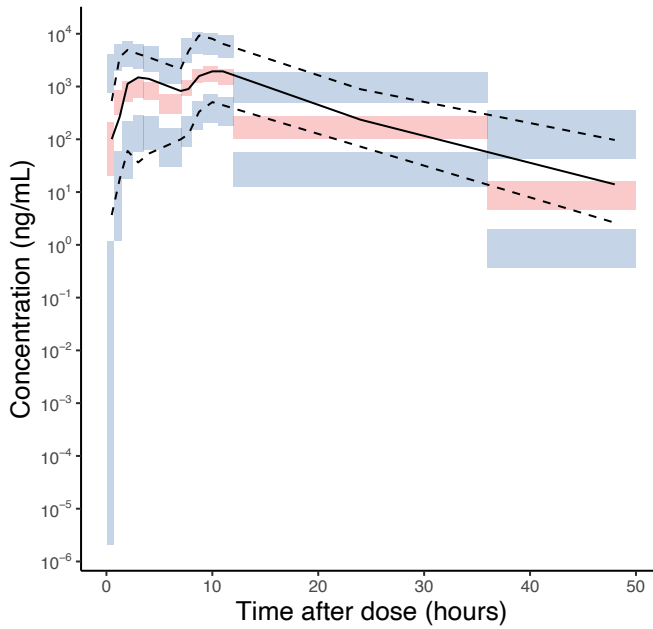
1. ten Tije AJ, Verweij J, Loos WJ, Sparreboom A (2003) Pharmacological effects of formulation vehicles: implications for cancer chemotherapy. *Clin Pharmacokinet* 42 (7):665-685. doi:10.2165/00003088-200342070-00005
2. Bardelmeijer HA, Ouwehand M, Buckle T, Huisman MT, Schellens JH, Beijnen JH, van Tellingen O (2002) Low systemic exposure of oral docetaxel in mice resulting from extensive first-pass metabolism is boosted by ritonavir. *Cancer Res* 62 (21):6158-6164
3. Oostendorp RL, Huitema A, Rosing H, Jansen RS, Ter Heine R, Keessen M, Beijnen JH, Schellens JH (2009) Coadministration of ritonavir strongly enhances the apparent oral bioavailability of docetaxel in patients with solid tumors. *Clin Cancer Res* 15 (12):4228-4233. doi:10.1158/1078-0432.Ccr-08-2944
4. Moes JJ, Koolen SL, Huitema AD, Schellens JH, Beijnen JH, Nuijen B (2011) Pharmaceutical development and preliminary clinical testing of an oral solid dispersion formulation of docetaxel (ModraDoc001). *Int J Pharm* 420 (2):244-250. doi:10.1016/j.ijpharm.2011.08.041
5. Moes JJ, Stuurman FE, Hendriks JJ, Marchetti S, Huitema AD, Beijnen JH, Schellens JH, Nuijen B (2013) Pharmacokinetic evaluation of three oral formulations of docetaxel boosted with ritonavir: two single-drug formulations vs. a fixed-dose combination tablet. *Drug Deliv Transl Res* 3 (3):243-251. doi:10.1007/s13346-012-0127-6
6. Sawicki E, Beijnen JH, Schellens JH, Nuijen B (2016) Pharmaceutical development of an oral tablet formulation containing a spray dried amorphous solid dispersion of docetaxel or paclitaxel. *Int J Pharm* 511 (2):765-773. doi:10.1016/j.ijpharm.2016.07.068
7. de Weger VA, Stuurman FE, Hendriks J, Moes JJ, Sawicki E, Huitema ADR, Nuijen B, Thijssen B, Rosing H, Keessen M, Mergui-Roelvink M, Beijnen JH, Schellens JHM, Marchetti S (2017) A dose-escalation study of bi-daily once weekly oral docetaxel either as ModraDoc001 or ModraDoc006 combined with ritonavir. *Eur J Cancer* 86:217-225. doi:10.1016/j.ejca.2017.09.010
8. de Weger VA, Stuurman FE, Koolen SLW, Moes JJ, Hendriks J, Sawicki E, Thijssen B, Keessen M, Rosing H, Mergui-Roelvink M, Huitema ADR, Nuijen B, Beijnen JH, Schellens JHM, Marchetti S (2019) A Phase I Dose Escalation Study of Once-Weekly Oral Administration of Docetaxel as ModraDoc001 Capsule or ModraDoc006 Tablet in Combination with Ritonavir. *Clin Cancer Res* 25 (18):5466-5474. doi:10.1158/1078-0432.Ccr-17-2299
9. de Vries Schultink AHM, Crombag MBS, van Werkhoven E, Otten HM, Bergman AM, Schellens JHM, Huitema ADR, Beijnen JH (2019) Neutropenia and docetaxel exposure in metastatic castration-resistant prostate cancer patients: A meta-analysis and evaluation of a clinical cohort. *Cancer Med* 8 (4):1406-1415. doi:10.1002/cam4.2003
10. Vermunt MAC, van der Heijden LT, Hendriks J, Schinkel AH, de Weger VA, van der Putten E, van Triest B, Bergman AM, Beijnen JH (2021) Pharmacokinetics of docetaxel and ritonavir after oral administration of ModraDoc006/r in patients with prostate cancer versus patients with other advanced solid tumours. *Cancer Chemother Pharmacol* 87 (6):855-869. doi:10.1007/s00280-021-04259-5

11. Franke RM, Carducci MA, Rudek MA, Baker SD, Sparreboom A (2010) Castration-dependent pharmacokinetics of docetaxel in patients with prostate cancer. *J Clin Oncol* 28 (30):4562-4567. doi:10.1200/jco.2010.30.7025
12. Vermunt MAC, Robbrecht DGJ, Devriese LA, Janssen JM, Thijssen B, Keessen M, van Eijk M, Kessels R, Eskens F, Beijnen JH, Mehra N, Bergman AM (2021) ModraDoc006, an oral docetaxel formulation in combination with ritonavir (ModraDoc006/r), in metastatic castration-resistant prostate cancer patients: A phase Ib study. *Cancer Rep (Hoboken)* 4 (4):e1367. doi:10.1002/cnr2.1367
13. Yu H, Janssen JM, Sawicki E, van Hasselt JGC, de Weger VA, Nuijen B, Schellens JHM, Beijnen JH, Huitema ADR (2020) A Population Pharmacokinetic Model of Oral Docetaxel Coadministered With Ritonavir to Support Early Clinical Development. *J Clin Pharmacol* 60 (3):340-350. doi:10.1002/jcph.1532
14. Koolen SL, Beijnen JH, Schellens JH (2010) Intravenous-to-oral switch in anticancer chemotherapy: a focus on docetaxel and paclitaxel. *Clin Pharmacol Ther* 87 (1):126-129. doi:10.1038/clpt.2009.233
15. Marchetti S, Stuurman F, Koolen S, Moes J, Hendrikx J, Thijssen B, Huitema A, Nuijen B, Rosing H, Keessen M, Voest E, Mergui-Roelvink M, Beijnen J, Schellens J (2012) Phase I study of weekly oral docetaxel (ModraDoc001) plus ritonavir in patients with advanced solid tumors. *J Clin Oncol* 30:2550-2550. doi:10.1200/jco.2012.30.15\_suppl.2550
16. Sukarnjanaset W, Wattanavijitkul T, Jarurattanasirikul S (2018) Evaluation of FOCEI and SAEM Estimation Methods in Population Pharmacokinetic Analysis Using NONMEM(®) Across Rich, Medium, and Sparse Sampling Data. *Eur J Drug Metab Pharmacokinet* 43 (6):729-736. doi:10.1007/s13318-018-0484-8
17. Freijer JI, Post TM, Ploeger BA, DeJongh J, Danhof M (2007) Application of the convection-dispersion equation to modelling oral drug absorption. *Bull Math Biol* 69 (1):181-195. doi:10.1007/s11538-006-9122-8
18. Acharya MR, Baker SD, Verweij J, Figg WD, Sparreboom A (2004) Determination of fraction unbound docetaxel using microequilibrium dialysis. *Anal Biochem* 331 (1):192-194. doi:10.1016/j.ab.2004.03.045
19. Leen E, Cooke TG, Angerson WJ, McArdle CS (1992) Estimation of total hepatic blood flow by duplex ultrasound. *Gut* 33 (9):1293-1294. doi:10.1136/gut.33.9.1293-c
20. Kan MK, Hopkins GB (1979) Measurement of liver volume by emission computed tomography. *J Nucl Med* 20 (6):514-520
21. Hutson PR, Oettel K, Douglas J, Ritter M, Messing E, Staab MJ, Alberti D, Horvath D, Wilding G (2008) Effect of medical castration on CYP3A4 enzyme activity using the erythromycin breath test. *Cancer Chemother Pharmacol* 62 (3):373-377. doi:10.1007/s00280-007-0613-6
22. Yu F, Zhang T, Guo L, Wu B (2018) Liver Receptor Homolog-1 Regulates Organic Anion Transporter 2 and Docetaxel Pharmacokinetics. *Drug Metab Dispos* 46 (7):980-988. doi:10.1124/dmd.118.080895

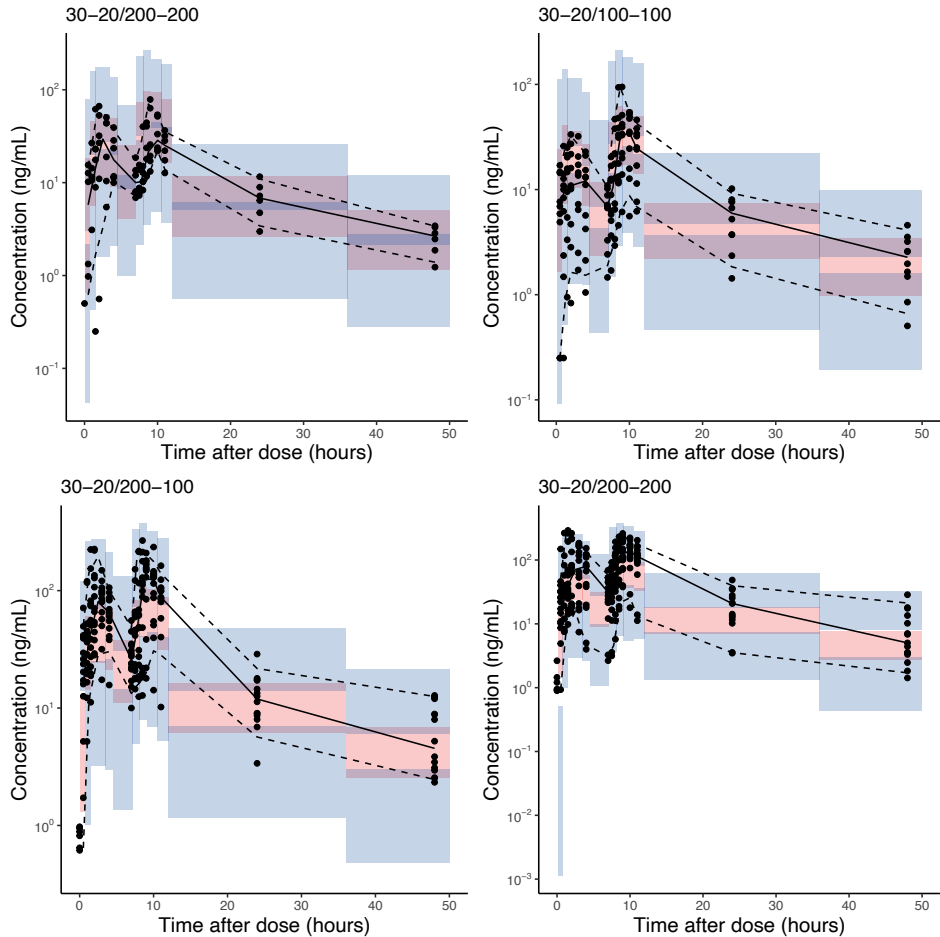
## SUPPLEMENTARY MATERIAL



**Supplementary Figure S1.** Diagnostic plots for the final ritonavir model. A, Population predicted concentrations versus observed concentration; B, Individual predicted concentrations versus observed concentrations. The solid line is the line of unity. The dashed line is the trend line in the data. C, Population predicted concentrations versus conditional weight residuals; D, Time after dose versus conditional weighted residuals.



**Supplementary Figure S2.** Prediction corrected visual predictive check for ritonavir ( $n = 1,000$ ). Solid lines and red areas represent the median observed values and simulated 95% confidence interval. Dashed lines and purple areas represent the 10% and 90% percentiles of the observed values and 95% confidence intervals of the simulated percentiles.



**Supplementary Figure S3.** Visual predictive checks for docetaxel ( $n = 1,000$ ) stratified for the different doses. Solid lines and red areas represent the median observed values and simulated 95% confidence intervals. Dashed lines and purple areas represent the 10% and 90% percentiles of the observed values and 95% confidence intervals of the simulated percentiles.





# Chapter 8

## **Is higher docetaxel clearance in prostate cancer patients explained by higher CYP3A: An in vivo phenotyping study with midazolam**

*Accepted in Journal of Clinical Pharmacology*

Lisa T. van der Heijden  
Claire A. Ribbers  
Marit A.C. Vermunt  
Dick Pluim  
Manon Acda  
Matthijs Tibben  
Hilde Rosing  
Joeri A.J. Douma  
Kishan Naipal  
Andre M. Bergman  
Jos H. Beijnen  
Alwin D.R. Huitema  
Frans L. Opdam

## ABSTRACT

Docetaxel is a well-established anticancer drug in the treatment of solid tumours, including Prostate Cancer (PCa). Patients with PCa have a lower docetaxel exposure for both intravenous (1.8-fold) and oral administration (2.4-fold) than patients with other solid cancers, which could influence efficacy and toxicity. An altered metabolism by Cytochrome P450 3A (CYP3A) due to castration status might explain the observed difference in docetaxel pharmacokinetics. In this *in vivo* phenotyping, pharmacokinetic study, CYP3A activity defined by midazolam clearance (Cl) was compared between patients with PCa and male patients with other solid tumours. All patients with solid tumours who did not use CYP3A modulating drugs were eligible for participation. Patients received 2 mg midazolam orally and 1 mg midazolam intravenously (IV) on two consecutive days. Plasma concentrations were measured with a validated liquid chromatography tandem mass-spectrometry method (LC-MS/MS). Genotyping was performed for CYP3A4 and CYP3A5. Nine patients were included in each group. Oral midazolam Cl was 1.26-fold higher in patients with PCa compared to patients with other solid tumours (geometric mean (CV%): 94.1 (33.5%) L/h vs. 74.4 (39.1%) L/h, respectively;  $p=0.08$ ). IV midazolam Cl did not significantly differ between the two groups ( $p=0.93$ ). Moreover, the metabolic ratio of midazolam to 1'-hydroxy midazolam did not differ between the two groups for both oral administration ( $p=0.67$ ) and IV administration ( $p=0.26$ ). CYP3A4 and CYP3A5 genotypes did not influence midazolam pharmacokinetics. The observed difference in docetaxel pharmacokinetics between both patient groups therefore appears to be neither explained by a difference in midazolam Cl nor by a difference in metabolic conversion rate of midazolam.

## 1 INTRODUCTION

Docetaxel is a well-established anticancer drug for the treatment of patients with multiple solid tumours including metastatic breast cancer, non-small cell lung cancer, prostate cancer, gastric cancer, and squamous cell carcinoma of the head and neck [1]. Docetaxel is commonly administered as a 1-hour intravenous infusion at a dose of 75 mg/m<sup>2</sup> or 100 mg/m<sup>2</sup> every 3 weeks [2,3]. To decrease patient burden and toxicity associated with intravenous (IV) docetaxel, oral formulations have been designed and investigated in clinical trials [4-8].

Recent studies have reported a difference in docetaxel pharmacokinetics between patients with prostate cancer and male patients with other solid tumours. A meta-analysis reported a 1.8-fold lower area-under-the-plasma-concentration-time curve (AUC) for IV docetaxel in patients with metastatic castration resistant prostate cancer (mCRPC) compared to male patients with other solid tumours [9]. Furthermore, these mCRPC patients had a 2.2-fold lower odds of developing grade 3/4 neutropenia [9], indicating the possible clinical significance of a lower docetaxel AUC. Moreover, oral docetaxel administration resulted in an even more pronounced 2.4-fold decrease in docetaxel AUC in mCRPC patients as compared to male patients with other solid tumours [8]. The lower docetaxel exposure appears to be independent of disease-status since patients with metastatic hormone-sensitive prostate cancer (mHSPC) had a similar pharmacokinetic profile for docetaxel as mCRPC patients [10].

Since docetaxel is predominantly metabolized by Cytochrome P450 3A (CYP3A) [11,12], altered CYP3A activity in patients with prostate cancer might explain the observed difference in docetaxel pharmacokinetics. The hypothesis behind the altered CYP3A activity is an induction of the CYP3A enzyme caused by the castration-status of prostate cancer patients [8]. However, *in vivo* phenotyping studies, using the erythromycin breath test, found no significant difference in hepatic CYP3A activity between the above-described patient groups [13,14]. On the other hand, erythromycin is not a specific and not a validated substrate for CYP3A [15-17]. Therefore, there is a need for a more accurate investigation of hepatic and intestinal CYP3A activity in patients with prostate cancer and male patients with other solid tumours.

The aim of the current study was to quantify *in vivo* CYP3A activity in patients with prostate cancer and male patients with other solid tumours using the Cl of the specific CYP3A substrate midazolam as a more accurate metric for enzyme

activity. Midazolam is a short acting benzodiazepine which is, like docetaxel, almost exclusively metabolized by CYP3A into its predominant metabolite 1'-hydroxy midazolam and the lesser metabolite 4'-hydroxy midazolam [18]. Both midazolam AUC and metabolic clearance to 1'-hydroxy midazolam correlate well with hepatic CYP3A content [19,20]. In general, midazolam plasma Cl is an accepted accurate metrics for CYP3A activity due to its specificity and sensitivity to changes in CYP3A activity [21]. Usually, oral midazolam doses of 2-7.5 mg and IV doses of 1-3 mg are used for *in vivo* phenotyping [21]. Secondary objectives were the comparison of midazolam AUC, and the midazolam metabolic ratio to 1'-hydroxy midazolam between the two patient groups with a differentiation between intestinal and hepatic CYP3A activity by administrating oral and IV midazolam.

## 2 METHODS

### 2.1 Study design and patients

A prospective, interventional pharmacokinetic study was designed to compare midazolam pharmacokinetics between patients with prostate cancer and male patients with other solid tumours. The study was conducted in Antoni van Leeuwenhoek Hospital and the study protocol was approved by the local accredited medical ethics committee (The Netherlands Cancer Institute, Amsterdam). The study was performed in accordance with the declaration of Helsinki. Written consent was obtained for all participating patients before the start of study procedures. The study was registered in ClinicalTrials.gov (NCT05518799).

Male patients ( $\geq 18$  years) with histological or cytological proof of a solid tumour were eligible for study participation independent of disease status. Patients with prostate cancer had to have a castration level of testosterone ( $\leq 1.73$  nmol/L) [22]. Adequate hematologic, hepatic, and renal function were required for participation. Patients using concomitant CYP3A modulating drugs, herbs, or food 14 days before the start of the study or within five half-lives of the drug, and patients who smoked during or within 7 days before the start of the study were excluded.

All patients received 2 mg oral midazolam, and 1 mg IV midazolam on two consecutive days. After administration of midazolam, pharmacokinetic exposure was determined. Blood samples (4 mL, K<sub>2</sub>EDTA) were drawn at 7 time points: predose, 0.25, 0.5, 1, 2, 4, and 8 hours after administration. Immediately after collection, samples were centrifuged for 10 minutes at 1500 g at 4 °C. Plasma was collected and stored at -80 °C until analysis.

### 2.2 Bioanalysis

Plasma concentrations of midazolam, 1'-hydroxy midazolam, and 4'-hydroxymidazolam were determined using a liquid-chromatography tandem mass spectrometry method (LC-MS/MS). Sample preparation consisted of liquid-liquid extraction with tert-butylmethylether (TBME) using 200  $\mu$ L plasma aliquots. Stable isotopically labelled midazolam and 1'-hydroxy midazolam were used as internal standards. Plasma aliquots were prepared by adding 1000  $\mu$ L TBME and 20  $\mu$ L internal standard. Samples were mixed with an automatic shaker (1,250 rpm, 10 minutes) and centrifuged (18,626  $\times$  g, 5 minutes). After snap freezing, the organic layer was transferred to a clean tube and evaporated until dryness under a gentle stream of nitrogen (40 °C). The residue was reconstituted with a mixture of 100  $\mu$ L 20 mM ammonium formate in water (pH 3.5) and methanol

(7:3, v/v). Samples were centrifuged ( $18,626 \times g$ , 5 minutes) before transferring the supernatant in vials for analysis. LC-MS/MS apparatus employed were Nexera X2 chromatograph LC (Shimadzu, Kyoto, Japan) and API4000 triple quadrupole MS/MS (Sciex, Framingham, MA, USA), equipped with a turbo ion spray interface, operated in the positive mode. Separation was accomplished using an Acquity BEH C18 analytical column (50 x 2.1 mm ID, 1.7  $\mu\text{m}$  particles) using gradient elution with 20 mM ammonium formate (pH 3.5)-methanol (7:3, v/v) and methanol. Detection and quantification were performed using mass/charge transitions  $m/z$  325.9  $\rightarrow$  291.0 for midazolam,  $m/z$  342.1  $\rightarrow$  203.1 for 1'-hydroxy midazolam, and  $m/z$  342.1  $\rightarrow$  234.0 for 4'-hydroxy midazolam. The method was validated according to international guidelines [23, 24], over a concentration range of 0.1-50 ng/mL for all three analyses. Accuracy was  $\pm 7.9\%$  and precision was  $\leq 5.6\%$ , at all concentration levels during method validation.

### 2.3 Pharmacokinetics and statistical analysis

The primary aim of the current study was the comparison of midazolam Cl between patients with prostate cancer and male patients with other solid tumours. For sample size calculation, a midazolam Cl of 81.7 L/h with a standard deviation of 41.5 L/h was used for male patients with other solid tumours [25]. With 9 patients per group, there will be 80% power to detect a two-fold change in midazolam Cl, assuming a coefficient of variation on the original scale of 50.8% and alpha 0.05 (two-sided). Therefore, 9 evaluable patients in each patient group were required. Midazolam Cl was calculated using non-compartmental analysis. The secondary aim of the study was the determination of AUC to 8 hours ( $\text{AUC}_{0-8}$ ) and AUC extrapolated to infinity ( $\text{AUC}_{\text{inf}}$ ), which were calculated using the linear-log trapezoidal method. The metabolic ratio was calculated by dividing  $\text{AUC}_{\text{inf}}$  of 1'-hydroxy midazolam by  $\text{AUC}_{\text{inf}}$  of midazolam. Other pharmacokinetic metrics were derived from the non-compartmental analysis such as the highest measured concentration over 8 hours ( $C_{\text{max}}$ ), time to  $C_{\text{max}}$  ( $T_{\text{max}}$ ), and volume of distribution ( $V_d$ ) were derived from the  $\text{AUC}_{\text{inf}}$ . Oral bioavailability was defined as the dose-corrected ratio between oral midazolam  $\text{AUC}_{\text{inf}}$  and IV midazolam  $\text{AUC}_{\text{inf}}$ . Samples below the lower limit of quantification (LLOQ) were imputed with half of LLOQ (0.05 ng/mL) if they were necessary for a reliable estimation of the elimination rate constant [26]. Non-compartmental analysis, statistical analysis, and power calculation were performed using R version 4.1.2 (R-project, Vienna, Austria). Wilcoxon signed (rank test was used to determine p-values for the comparison of pharmacokinetics between the two patient groups. A p-value of  $\leq 0.05$  was considered statistically significant. In case of significant difference, post hoc analysis would be performed to differentiate between intestinal and hepatic CYP3A activity.

## 2.4 Genotyping

For genotyping of CYP3A, 4 mL blood was collected in K<sub>2</sub>EDTA vials and stored at -20 °C until analysis. The following single nucleotide polymorphism (SNPs) were determined: *CYP3A4\*2* (664T>C), *CYP3A4\*17* (566T>C), *CYP3A4\*22* (15389C>T) and *CYP3A5\*3* (6987A>G). DNA was extracted with QIAmp DNA Mini Kit (Qiagen, Hilden, Germany). DNA concentrations were measured at 260 nm using a nanodrop nd-1000 UV-VIS spectrometer (Thermo Fischer scientific, Ashville, NC, USA). Genotyping was performed with TaqMan SNP genotyping assays (Applied biosystems, Carlsbad, CA, USA) according to manufacturer's protocol. Reactions were performed with the Applied Biosystems StepOne™. Two negative and 2 positive quality control samples were included on each plate in the TaqMan SNP genotyping assay.

**Table 1.** Demographics of the included patients. Data is presented as median [range] or frequency (percentage%) unless otherwise specified.

	Prostate cancer group	Other solid tumour group
<b>Demographics</b>		
Number of patients	9	9
Ethnicity		
Caucasian	9 (100%)	9 (100%)
Age (years)	69 [58-79]	64 [38-71]
Bodyweight (kg)	81.8 [65-100]	91 [62.5-131]
<b>Disease information</b>		
WHO score		
0	9 (100%)	8 (89%)
1	0 (0%)	1 (11%)
Primary tumour		
Colorectal	0 (0%)	4 (44%)
Melanoma	0 (0%)	4 (44%)
Prostate	9 (100%)	0 (0%)
SCLC	0 (0%)	1 (12%)
Disease stage		
Local	0 (0%)	2 (22%)
Locally advanced	1 (11%)	0 (0%)
Metastatic	8 (89%)	7 (78%)

**Table 1.** Continued.

	Prostate cancer group	Other solid tumour group
<b>Clinical chemistry<sup>#</sup></b>		
<i>ALAT (&lt;45 U/L)</i>	22 [17-36]	22 [9-35]
<i>ASAT (&lt;35 U/L)</i>	32 [22-69]	28 [19 - 42]
<i>eGFR (&gt;60 mL/min)</i>	90 [71-108]	84 [66-96]
<i>Serum creatinine (50-105 µmol/L)</i>	72 [61-90]	84 [66 - 99]
<i>Testosterone (3.0-33.0 nmol/L)</i>	0.03 [0.02-0.5]	9 [6.3-29]
<i>Total bilirubin (≤24 µmol/L)</i>	9 [6-23]	6 [6-18]
<b>Medical history</b>		
Prior therapy		
No	6 (67%)	5 (56%)
Chemotherapy	3 (33%)	1 (11%)
Hormone therapy	3 (33%)	2 (22%)
Immune therapy	0 (0%)	4 (44%)
Chronic concomitant medication		
<i>Abiraterone</i>	6 (67%)	0 (0%)
<i>Anti-acida including PPIs</i>	2 (22%)	4 (44%)
<i>Antibiotics</i>	0 (0%)	1 (11%)
<i>Antihistamines</i>	1 (11%)	0 (0%)
<i>Asthma medication</i>	0 (0%)	1 (11%)
<i>Cardiovascular medication</i>	8 (89%)	4 (44%)
<i>Corticosteroids</i>	3 (33%)	2 (22%)
<i>Encorafenib</i>	0 (0%)	1 (11%)
<i>Hormone therapy</i>	7 (78%)	0 (0%)
<i>Immune therapy</i>	0 (0%)	6 (67%)
<i>Laxatives</i>	1 (11%)	4 (44%)
<i>Osteoporosis prophylaxis</i>	4 (44%)	0 (0%)
<i>Paracetamol</i>	2 (22%)	2 (22%)
<i>Thyreominetics</i>	0 (0%)	1 (11%)

*Abbreviations:* ALAT, alanine aminotransferase; ASAT; aspartate aminotransferase; eGFR, estimated glomerular filtration rate, PPI, proton pump inhibitors; SCLC, small cell lung cancer; WHO, world health organization performance score.

<sup>#</sup> Normal ranges for laboratory provided.



## 3 RESULTS

### 3.1 Patient characteristics

Demographic characteristics of the included patients are summarised in Table 1. All included patients were of Caucasian ethnicity. Median age was similar between the two patient groups. The patients with solid tumours consisted of colorectal carcinoma (n=4), melanoma (n=4), and small cell lung cancer (n=1). Most patients had metastatic disease; 1 patient with prostate cancer had locally advanced disease while 2 patients with other solid tumours had localized disease. Patients with prostate cancer used relatively more chronic concomitant medications, especially cardiovascular drugs, abiraterone, and hormone therapy. Furthermore, 5 patients used corticosteroids which consisted of either prednisolone (max. 10 mg, n=4) or locally applied budesonide (n=1) during the study.

### 3.2 Pharmacokinetic analysis

A summary of the pharmacokinetic metrics is provided in Table 2. The pharmacokinetic profiles of midazolam, 1'-hydroxy midazolam, and 4'-hydroxy midazolam are depicted in Figure 1. Individual pharmacokinetics profiles of midazolam and its metabolites are depicted in Supplementary Figure S1.

#### 3.2.1 Midazolam

Oral midazolam Cl was 1.26-fold higher in patients with prostate cancer compared to male patients with other solid tumours (geometric mean (CV%): 94.1 (33.5%) L/h vs. 74.4 (39.1%) L/h, respectively;  $p=0.08$ ), which was not statistically significant (Figure 2). On the other hand, there was no significant difference in IV midazolam Cl (42.6 (35.1%) L/h vs. 40.6 (40.0%) L/h, respectively;  $p=0.93$ ). Consistently, oral  $AUC_{inf}$  was lower in the prostate cancer group compared to the other solid tumour group (21.3 (33.5%) vs. 26.9 (39.1%) ng/mL\*h, respectively;  $p = 0.08$ ), which was statistically insignificant, while IV  $AUC_{inf}$  was similar between the two groups (23.5 (35.1%) vs. 24.6 (40.0%), respectively,  $p=0.93$ ). Oral bioavailability was lower for patients with prostate cancer compared to patients with other solid tumours, but again not statistically significant (45.3% (24.7%) vs. 54.5% (28.3%),  $p=0.22$ ). In the current study no correlation was observed between testosterone levels and midazolam clearance (Supplementary Figure S2).

**Table 2.** Pharmacokinetic parameters of midazolam and 1'-hydroxy midazolam.

	Oral administration			Intravenous administration		
	Prostate cancer	Other solid tumours	P-value	Prostate cancer	Other solid tumours	P-value
<b>Midazolam</b> Geometric mean (CV%)						
$C_{max}$ (ng/mL)	11.33 (24.9)	8.94 (29.5)	0.10	-	-	-
$T_{max}$ (h)	0.5	0.6	0.35	-	-	-
$AUC_{0-8}$ (ng/mL*h)	19.9 (30.7)	24.0 (32.8)	0.09	21.9 (31.8)	21.4 (36.5)	0.93
$AUC_{inf}$ (ng/mL*h)	21.3 (33.5)	26.9 (39.1)	0.08	23.5 (35.1)	24.6 (40.0)	0.93
$t_{1/2}$ (h <sup>-1</sup> )	1.58 (46.6)	2.18 (37.8)	0.19	1.63 (52.3)	2.47 (37.9)	0.06
Cl/F (L/h)	94.1 (33.5)	74.4 (39.1)	0.08	-	-	-
Cl (L/h)	-	-	-	42.6 (35.1)	40.6 (40.0)	0.93
$V_d/F$ (L)	214 (35.7)	234 (20.2)	0.34	-	-	-
$V_d$ (L)	-	-	-	100 (44.3)	144 (37.1)	0.14
F (%)	45.3 (24.7)	54.5 (28.3)	0.22	-	-	-
<b>1'-hydroxy midazolam</b> Geometric mean (CV%)						
$AUC_{0-8}$ (ng/mL*h)	4.58 (57.0)	4.92 (68.9)	1.00	3.35 (30.7)	2.81 (120)	0.39
$AUC_{inf}$ (ng/mL*h)	4.98 (56.3)	5.33 (67.6)	1.00	3.73 (31.5)	3.41 (111)	0.67
Metabolic ratio	0.23 (40.8)	0.19 (78.5)	0.67	0.16 (18.4)	0.14 (99.2)	0.26

*Abbreviations:*  $AUC_{0-8}$ , area under the concentration time curve from zero to eight hours after administration;  $AUC_{inf}$ , area-under-the-plasma-concentration-time curve extrapolated to infinity,  $C_{max}$ , maximum concentration; Cl, clearance; Cl/F, oral clearance; CV, coefficient of variation; F, oral bioavailability; metabolic ratio,  $AUC_{0-8}$  of 1'-hydroxy midazolam divided by the  $AUC_{0-8}$  of midazolam;  $t_{1/2}$ , half-life,  $T_{max}$ , time to maximum concentration;  $V_d$ , volume of distribution;  $V_d/F$ , oral volume of distribution.

### 3.2.2 1'-hydroxy midazolam

Pharmacokinetics of 1'-hydroxy midazolam demonstrated high inter-patient variability (Figure 1C-D) with higher variability for patients with other solid tumours than prostate cancer. There was no significant difference in 1'-hydroxy midazolam  $AUC_{inf}$  for oral administration (4.98 (56.3%) ng/mL\*h vs. 5.33 (67.6%) ng/mL\*h, respectively,  $p=1.00$ ) and for IV administration (3.73 (31.5%) ng/mL\*h vs. 3.41 (111%) ng/mL\*h, respectively,  $p=0.67$ ). Correspondingly, there was no significant difference in metabolic ratio of 1-hydroxy midazolam to midazolam for both oral administration (0.23 (40.8%) and 0.19 (78.5%),  $p=0.67$ ) and IV administration (0.16 (18.4%) vs. 0.14 (99.2%),  $p=0.26$ ).

### 3.2.3 4'-hydroxy midazolam

The pharmacokinetic profile of 4'-hydroxy midazolam also demonstrated high inter-patient variability (Figure 1E-F). The plasma concentrations of 4'-hydroxy midazolam were lower than anticipated. The frequency of <LLOQ samples did not differ between patients with prostate cancer and patients with other solid tumours (46.3% (50 samples, 10 patients) vs. 47.2% (51 samples, 8 patients), respectively). Moreover, the inter-quartile range of the measured plasma concentrations did not differ between patients with prostate cancer (0.134-0.284 ng/mL) and patients with other solid tumours (0.138-0.273 ng/mL). However, 4'-hydroxy midazolam plasma concentrations for male patients with other solid tumours exhibited a prolonged time above the LLOQ (Supplementary Figure S1), suggesting a trend towards lower 4'-hydroxy midazolam exposure in prostate cancer patients. The outlier at four hours after administration of midazolam depicted in Figure F could not be explained by errors in sampling time or a bioanalytical error.

### 3.3 Genotyping

Pharmacogenetic analysis revealed three single nucleotide polymorphisms (SNPs) in the CYP3A gene. One patient with prostate cancer was heterozygous for CYP3A4\*2 and homozygous for CYP3A5\*3 (nonexpressor phenotype). CYP3A4\*2 is *in vitro* associated with decreased activity (-83% decrease in the predictor of *in vivo* intrinsic midazolam Cl; the ratio of maximum reaction rate ( $V_{\max}$ ) and the Michaelis-Menten rate constant ( $K_m$ ) of CYP3A4 [27]. The influence of CYP3A4\*2 on the *in vivo* pharmacokinetics of midazolam is unclear due to the low prevalence of the SNP [28]. Two patients (one in each patient group) were homozygous for CYP3A4\*1 and heterozygous for CYP3A5\*3 (expressor phenotype). This genotype is associated with the phenotype of an extensive metabolizer [29]. The influence of CYP3A5\*3 on the pharmacokinetics of midazolam seems to be inconsistent. Previous studies reported either no significant difference [30,28] or significant difference [25,31] in midazolam pharmacokinetics. The presence of SNPs did not significantly affect the results from the pharmacokinetic analysis. Both patients who were heterozygous for CYP3A5\*3 (expressor phenotype) had midazolam Cl values within the established range of Cl for both oral and IV administration. The patient who was heterozygous for CYP3A\*2 had the highest oral midazolam Cl. This is inconsistent with the expected decreased CYP3A4 activity. Therefore, it was concluded there was limited effect of the detected SNPs on the pharmacokinetics of midazolam in our study.

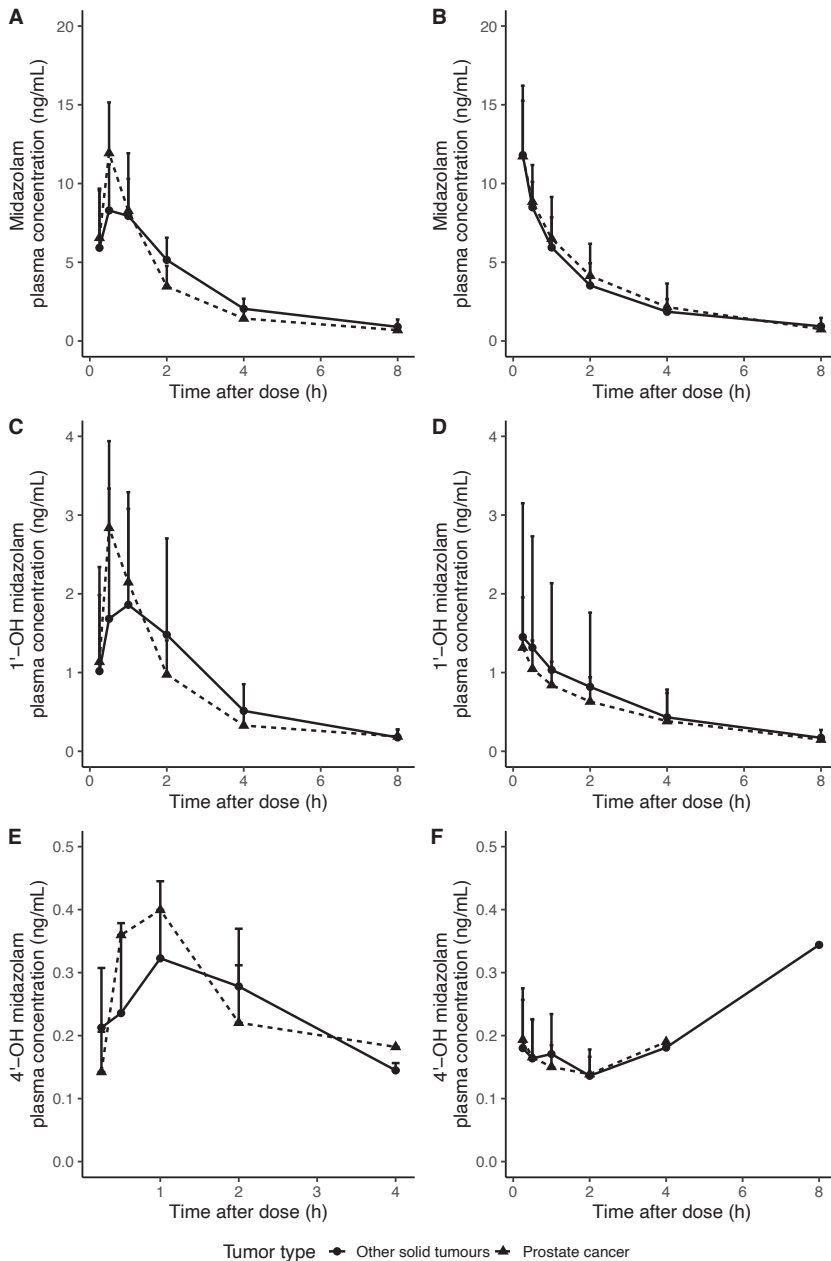


**Figure 1.** Pharmacokinetic profiles of midazolam, 1'-hydroxy midazolam, and 4'-hydroxy midazolam after oral administration (A, C, E) and intravenous administration (B, D, F). The solid dots and solid line represent the pharmacokinetic profile of male patients with other solid tumours and the solid triangles and dashed lines represent the pharmacokinetic profile of patients with prostate cancer. The error bars represent the standard deviation in plasma concentration.

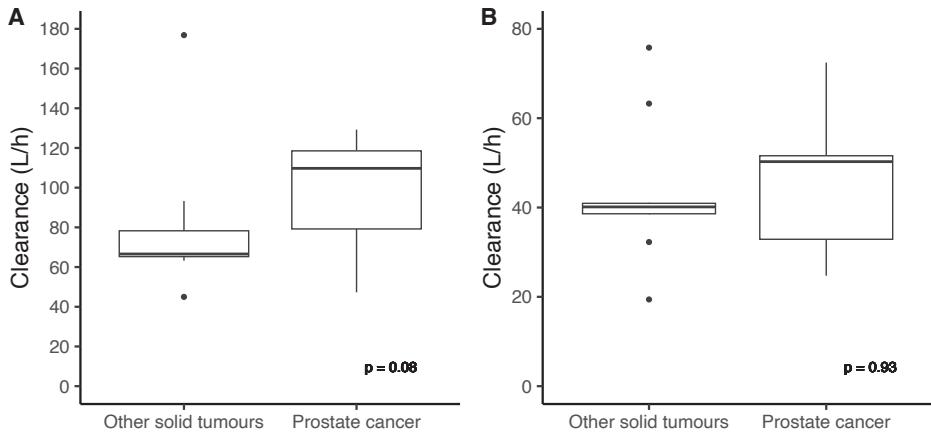


**Figure 2.** Oral midazolam clearance (A) and intravenous midazolam Cl (B) for patients with other solid tumours and patients with prostate cancer.

## 4 DISCUSSION

The primary aim of the current study was to quantify CYP3A activity, defined as midazolam Cl, in patients with prostate cancer compared to patients with other solid tumours. Oral midazolam Cl was 1.26-fold higher in patients with prostate cancer compared to patients with other solid tumours. This non-significant increase in oral clearance only partially explains the observed 2.4-fold difference in oral docetaxel exposure [8]. Moreover, the secondary objectives, midazolam AUC and metabolic ratio, were also not significantly different between patients with prostate cancer and patients with other solid cancers. Because no significant differences between the groups were established, no post hoc analysis was performed to differentiate between intestinal and hepatic CYP3A activity. However, there was a trend towards a higher clearance for oral administration, suggesting a possible higher intestinal CYP3A activity for patients with prostate cancer.

The current study was able to reject the hypothesis of an increased CYP3A activity as the sole physiological mechanism behind the 1.8 - 2.4-fold lower docetaxel exposure observed in patients with prostate cancer [9,8]. Two other studies have also investigated CYP3A activity in patients with prostate cancer. One study in male castrated patients and male non-castrated patients reported no significant difference in hepatic CYP3A activity determined with the erythromycin breath test [13]. Another study observed no significant change in hepatic CYP3A activity, determined with the erythromycin breath test, in eleven men with prostate cancer before the start of luteinizing hormone releasing hormone (LHRH) agonists and two months after the start of therapy [14]. These studies have two important limitations. First, erythromycin is not fully specific for CYP3A activity since it is also a substrate of several drug transporters including P-gp and it is not a validated CYP3A probe [15]. Secondly, the erythromycin breath test quantifies only hepatic CYP3A activity and not intestinal CYP3A activity. The current study used midazolam Cl as a measure for CYP3A activity which is a generally accepted and validated metric for CYP3A activity [21]. Moreover, midazolam was administered both orally and intravenously to enable the quantification of both intestinal and hepatic CYP3A activity. While the current study found a 1.26-fold higher oral midazolam Cl for patients with prostate cancer, it cannot fully explain the observed difference in docetaxel pharmacokinetics [8].

An alternative explanation for the observed difference in docetaxel pharmacokinetics could be increased hepatic uptake due to increased expression of hepatic drug transporters. Preclinical studies in rats reported a significantly

higher docetaxel exposure in the liver of castrated rats compared to non-castrated rats (37.0 vs. 18.0  $\mu\text{g}/\text{mL}\cdot\text{h}$ ,  $p=0.01$ ) [13]. The expression of solute carrier genes encoding for organic cation transporters *rOct1* (*Slc22a1*), organic anion transporter *rOat2* (*Slc22a7*), and organic anion transporter polypeptide *rOatp1a1* (*Slco1a1*) were increased in rat hepatic biopsies [13]. We suspect *rOat2* to mainly contribute to the altered docetaxel pharmacokinetics because docetaxel is both a substrate for *rOat2* and *rOatp1a1*, and erythromycin is only a substrate for *rOatp1a1* [13]. Furthermore, midazolam is neither a substrate for *OATP1a1* and *a2*, while it is still unknown whether it is a substrate for *OAT2* [32, 33]. Cells *ex vivo* overexpressing *rOat2* demonstrated a 3.7-fold increase in docetaxel-mediated cytotoxicity compared to control cells and an approximately 2-fold increase in docetaxel uptake [13]. *rOat2* expression seems to be regulated by liver receptor homolog 1 (*Lrh-1*) [34]. Overexpression of *Lrh-1* resulted in a 2.2-fold increase in *rOat2* mRNA, while *Lrh-1* knockout mice demonstrated a decrease in *rOat2* mRNA [32]. Accordingly, *Lrh-1* knockout mice demonstrated increased docetaxel  $C_{\text{max}}$  and AUC in plasma with lowered hepatic docetaxel concentrations [34]. Lastly, several studies have investigated the relationship between androgens, such as testosterone, and *Lrh-1*, however, the exact relationship remains to be elucidated [35-39]. In the current study no correlation was observed between testosterone levels and midazolam clearance. Moreover, a comparison in oral docetaxel pharmacokinetics between mCRPC patients and newly diagnosed hormone sensitive prostate cancer found no differences between the two groups [10].

The current study has several limitations. Firstly, the majority of the patients had metastatic disease. Disease state could be associated with CYP3A enzyme activity [40]. Prostate cancer tumours are reported to express CYP3A proteins [41]. Furthermore, SNPs in CYP3A are associated with prostate cancer risk and aggressiveness [41]. With such a small sample size, one patient with local disease and two patients with locally advanced disease could influence the current results. However, a comparison of intravenous docetaxel pharmacokinetics between mCRPC patients and newly diagnosed hormone sensitive prostate cancer found no differences between the two groups [10]. Lastly, all included patients were of Caucasian ethnicity. This could limit the extrapolation of the current study to different patient populations. However, the effect of CYP3A genotype, which can differentiate between different ethnicities, appears to be limited to *CYP3A4\*22* [42,43], which was not present in patients enrolled in the current study. Additionally, the effect of *CYP3A5\*3* on midazolam pharmacokinetics is inconsistent [25,28,30,31]. Our study also has several strengths. We used midazolam, which, as a more specific and sensitive probe for CYP3A activity [21],

is recommended by both the European Medicines Agency (EMA) and the US Food and Drug Administration (FDA) [44,45]. Secondly, hepatic and intestinal CYP3A activity could be investigated by administration of midazolam both intravenously and orally, while previous studies measured only hepatic CYP3A enzyme activity [13,14]. Lastly, short time interval pharmacokinetic sampling in the absorption phase ensured the capture of both the absorption phase of midazolam and the early formation of both 1'-hydroxy midazolam and 4'-hydroxy midazolam.

## **5 CONCLUSIONS**

Oral midazolam Cl was 1.26-fold higher in patients with prostate cancer compared to patients with solid tumours, while IV midazolam Cl was similar between the two patient groups. Although not statistically significant, these results suggest a trend towards an increased intestinal CYP3A activity in patients with prostate cancer. However, the observed difference in oral midazolam Cl could not explain the observed 1.8 to 2.4-fold difference in docetaxel exposure between patients with prostate cancer and patients with other solid tumours as observed in other studies. An alternative (but currently hypothetical) explanation for the difference in docetaxel pharmacokinetics could be the upregulation of hepatic OAT2, increasing hepatic uptake and Cl of docetaxel.

## **ACKNOWLEDGEMENTS**

Our gratefulness goes out to all patients who participated in the clinical study.



## REFERENCES

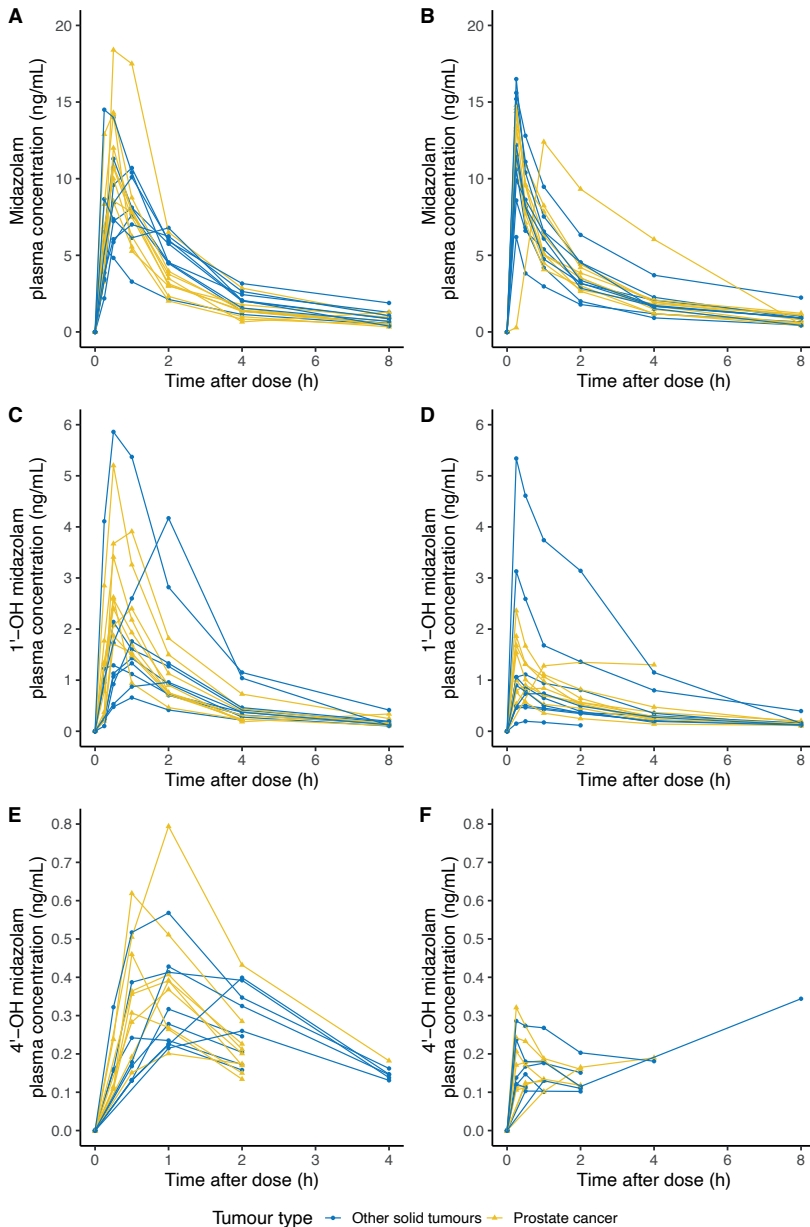
1. Sanofi-Aventis (2005) Taxotere, INN-docetaxel—European Medicines Agency. Summary of product characteristics. <https://www.ema.europa.eu/en/medicines/human/EPAR/taxotere>. Accessed 25 Jan 2023.
2. Di Maio M, Perrone F, Chiodini P, Gallo C, Camps C, Schuette W, Quoix E, Tsai CM, Gridelli C (2007) Individual patient data meta-analysis of docetaxel administered once every 3 weeks compared with once every week second-line treatment of advanced non-small-cell lung cancer. *J Clin Oncol* 25 (11):1377-1382. doi:10.1200/jco.2006.09.8251
3. Camps C, Massuti B, Jiménez A, Maestu I, Gómez RG, Isla D, González JL, Almenar D, Blasco A, Rosell R, Carrato A, Viñolas N, Batista N, Girón CG, Galán A, López M, Blanco R, Provencio M, Diz P, Felip E (2006) Randomized phase III study of 3-weekly versus weekly docetaxel in pretreated advanced non-small-cell lung cancer: a Spanish Lung Cancer Group trial. *Ann Oncol* 17 (3):467-472. doi:10.1093/annonc/mdj115
4. de Weger VA, Stuurman FE, Hendrikx J, Moes JJ, Sawicki E, Huitema ADR, Nuijen B, Thijssen B, Rosing H, Keessen M, Mergui-Roelvink M, Beijnen JH, Schellens JHM, Marchetti S (2017) A dose-escalation study of bi-daily once weekly oral docetaxel either as ModraDoc001 or ModraDoc006 combined with ritonavir. *Eur J Cancer* 86:217-225. doi:10.1016/j.ejca.2017.09.010
5. de Weger VA, Stuurman FE, Koolen SLW, Moes JJ, Hendrikx J, Sawicki E, Thijssen B, Keessen M, Rosing H, Mergui-Roelvink M, Huitema ADR, Nuijen B, Beijnen JH, Schellens JHM, Marchetti S (2019) A Phase I Dose Escalation Study of Once-Weekly Oral Administration of Docetaxel as ModraDoc001 Capsule or ModraDoc006 Tablet in Combination with Ritonavir. *Clin Cancer Res* 25 (18):5466-5474. doi:10.1158/1078-0432.Ccr-17-2299
6. Moes JJ, Koolen SL, Huitema AD, Schellens JH, Beijnen JH, Nuijen B (2011) Pharmaceutical development and preliminary clinical testing of an oral solid dispersion formulation of docetaxel (ModraDoc001). *Int J Pharm* 420 (2):244-250. doi:10.1016/j.ijpharm.2011.08.041
7. Vermunt MAC, Robbrecht DGJ, Devriese LA, Janssen JM, Thijssen B, Keessen M, van Eijk M, Kessels R, Eskens F, Beijnen JH, Mehra N, Bergman AM (2021) ModraDoc006, an oral docetaxel formulation in combination with ritonavir (ModraDoc006/r), in metastatic castration-resistant prostate cancer patients: A phase Ib study. *Cancer Rep (Hoboken)* 4 (4):e1367. doi:10.1002/cnr2.1367
8. Vermunt MAC, van der Heijden LT, Hendrikx J, Schinkel AH, de Weger VA, van der Putten E, van Triest B, Bergman AM, Beijnen JH (2021) Pharmacokinetics of docetaxel and ritonavir after oral administration of ModraDoc006/r in patients with prostate cancer versus patients with other advanced solid tumours. *Cancer Chemother Pharmacol* 87 (6):855-869. doi:10.1007/s00280-021-04259-5
9. de Vries Schultink AHM, Crombag MBS, van Werkhoven E, Otten HM, Bergman AM, Schellens JHM, Huitema ADR, Beijnen JH (2019) Neutropenia and docetaxel exposure in metastatic castration-resistant prostate cancer patients: A meta-analysis and evaluation of a clinical cohort. *Cancer Med* 8 (4):1406-1415. doi:10.1002/cam4.2003

10. Vermunt MAC, van Nuland M, van der Heijden LT, Rosing H, Beijnen JH, Bergman AM (2022) Comparison of docetaxel pharmacokinetics between castration-resistant and hormone-sensitive metastatic prostate cancer patients. *Cancer Chemother Pharmacol* 89 (6):785-793. doi:10.1007/s00280-022-04433-3
11. Royer I, Monsarrat B, Sonnier M, Wright M, Cresteil T (1996) Metabolism of docetaxel by human cytochromes P450: interactions with paclitaxel and other antineoplastic drugs. *Cancer Res* 56 (1):58-65
12. de Weger VA, Beijnen JH, Schellens JH (2014) Cellular and clinical pharmacology of the taxanes docetaxel and paclitaxel-a review. *Anticancer Drugs* 25 (5):488-494. doi:10.1097/cad.000000000000093
13. Franke RM, Carducci MA, Rudek MA, Baker SD, Sparreboom A (2010) Castration-dependent pharmacokinetics of docetaxel in patients with prostate cancer. *J Clin Oncol* 28 (30):4562-4567. doi:10.1200/jco.2010.30.7025
14. Hutson PR, Oettel K, Douglas J, Ritter M, Messing E, Staab MJ, Alberti D, Horvath D, Wilding G (2008) Effect of medical castration on CYP3A4 enzyme activity using the erythromycin breath test. *Cancer Chemother Pharmacol* 62 (3):373-377. doi:10.1007/s00280-007-0613-6
15. Franke RM, Baker SD, Mathijssen RH, Schuetz EG, Sparreboom A (2008) Influence of solute carriers on the pharmacokinetics of CYP3A4 probes. *Clin Pharmacol Ther* 84 (6):704-709. doi:10.1038/clpt.2008.94
16. Frassetto LA, Poon S, Tsourounis C, Valera C, Benet LZ (2007) Effects of uptake and efflux transporter inhibition on erythromycin breath test results. *Clin Pharmacol Ther* 81 (6):828-832. doi:10.1038/sj.clpt.6100148
17. Kurnik D, Wood AJ, Wilkinson GR (2006) The erythromycin breath test reflects P-glycoprotein function independently of cytochrome P450 3A activity. *Clin Pharmacol Ther* 80 (3):228-234. doi:10.1016/j.clpt.2006.06.002
18. Nguyen HQ, Kimoto E, Callegari E, Obach RS (2016) Mechanistic Modeling to Predict Midazolam Metabolite Exposure from In Vitro Data. *Drug Metab Dispos* 44 (5):781-791. doi:10.1124/dmd.115.068601
19. Thummel KE, Shen DD, Podoll TD, Kunze KL, Trager WF, Hartwell PS, Raisys VA, Marsh CL, McVicar JP, Barr DM, et al. (1994) Use of midazolam as a human cytochrome P450 3A probe: I. In vitro-in vivo correlations in liver transplant patients. *J Pharmacol Exp Ther* 271 (1):549-556
20. Thummel KE, Shen DD, Podoll TD, Kunze KL, Trager WF, Bacchi CE, Marsh CL, McVicar JP, Barr DM, Perkins JD, et al. (1994) Use of midazolam as a human cytochrome P450 3A probe: II. Characterization of inter- and intraindividual hepatic CYP3A variability after liver transplantation. *J Pharmacol Exp Ther* 271 (1):557-566
21. Hohmann N, Haefeli WE, Mikus G (2016) CYP3A activity: towards dose adaptation to the individual. *Expert Opin Drug Metab Toxicol* 12 (5):479-497. doi:10.1517/17425255.2016.1163337
22. Lee TY, Pierrillas PB, Lin YW, de Greef R, Zandvliet AS, Schindler E, Migoya E (2023) Population PK and Semimechanistic PK/PD Modeling and Simulation of Relugolix Effects on Testosterone Suppression in Men with Prostate Cancer. *Clin Pharmacol Ther* 113 (1):124-134. doi:10.1002/cpt.2743

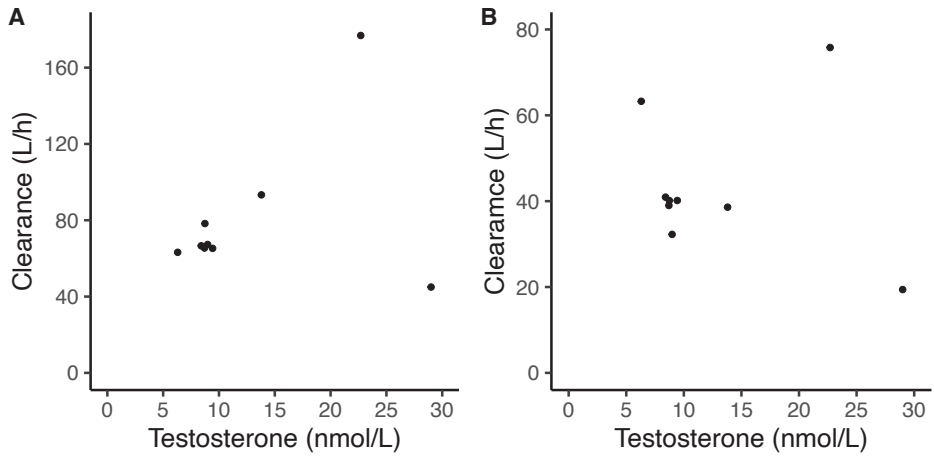
23. European Medicines Agency (EMA) (2011) Guideline on Bioanalytical Method Validation. Committee for Medicinal Products for Human Use and European Medicines Agency. Accessed 8 May 2022
24. US Food and Drug Administration (FDA) (2018) Bioanalytical Method Validation. Silver Springs, Maryland: US Food and Drug Administration. Accessed 9 May 2022
25. Wong M, Balleine RL, Collins M, Liddle C, Clarke CL, Gurney H (2004) CYP3A5 genotype and midazolam clearance in Australian patients receiving chemotherapy. *Clin Pharmacol Ther* 75 (6):529-538. doi:10.1016/j.clpt.2004.02.005
26. Irby DJ, Ibrahim ME, Dauki AM, Badawi MA, Illamola SM, Chen M, Wang Y, Liu X, Phelps MA, Mould DR (2021) Approaches to handling missing or “problematic” pharmacology data: Pharmacokinetics. *CPT Pharmacometrics Syst Pharmacol* 10 (4):291-308. doi:10.1002/psp4.12611
27. Miyazaki M, Nakamura K, Fujita Y, Guengerich FP, Horiuchi R, Yamamoto K (2008) Defective activity of recombinant cytochromes P450 3A4.2 and 3A4.16 in oxidation of midazolam, nifedipine, and testosterone. *Drug Metab Dispos* 36 (11):2287-2291. doi:10.1124/dmd.108.021816
28. Eap CB, Buclin T, Hustert E, Bleiber G, Golay KP, Aubert AC, Baumann P, Telenti A, Kerb R (2004) Pharmacokinetics of midazolam in CYP3A4- and CYP3A5-genotyped subjects. *Eur J Clin Pharmacol* 60 (4):231-236. doi:10.1007/s00228-004-0767-7
29. Sanchez Spitman AB, Moes D, Gelderblom H, Dezentje VO, Swen JJ, Guchelaar HJ (2017) Effect of CYP3A4\*22, CYP3A5\*3, and CYP3A combined genotypes on tamoxifen metabolism. *Eur J Clin Pharmacol* 73 (12):1589-1598. doi:10.1007/s00228-017-2323-2
30. de Jonge H, de Loor H, Verbeke K, Vanrenterghem Y, Kuypers DR (2013) Impact of CYP3A5 genotype on tacrolimus versus midazolam clearance in renal transplant recipients: new insights in CYP3A5-mediated drug metabolism. *Pharmacogenomics* 14 (12):1467-1480. doi:10.2217/pgs.13.133
31. Seng KY, Hee KH, Soon GH, Sapari NS, Soong R, Goh BC, Lee LS (2014) CYP3A5\*3 and bilirubin predict midazolam population pharmacokinetics in Asian cancer patients. *J Clin Pharmacol* 54 (2):215-224. doi:10.1002/jcph.230
32. Ziesenitz VC, Weiss J, Haefeli WE, Mikus G (2013) Cytochrome P450-3A phenotyping using midazolam is not altered by OATP1B1 polymorphisms. *Clin Pharmacol Ther* 93 (5):388. doi:10.1038/clpt.2013.46
33. Imanaga J, Kotegawa T, Imai H, Tsutsumi K, Yoshizato T, Ohyama T, Shirasaka Y, Tamai I, Tateishi T, Ohashi K (2011) The effects of the SLCO2B1 c.1457C > T polymorphism and apple juice on the pharmacokinetics of fexofenadine and midazolam in humans. *Pharmacogenet Genomics* 21 (2):84-93. doi:10.1097/fpc.0b013e32834300cc
34. Yu F, Zhang T, Guo L, Wu B (2018) Liver Receptor Homolog-1 Regulates Organic Anion Transporter 2 and Docetaxel Pharmacokinetics. *Drug Metab Dispos* 46 (7):980-988. doi:10.1124/dmd.118.080895
35. Wu YG, Bennett J, Talla D, Stocco C (2011) Testosterone, not 5 $\alpha$ -dihydrotestosterone, stimulates LRH-1 leading to FSH-independent expression of Cyp19 and P450scc in granulosa cells. *Mol Endocrinol* 25 (4):656-668. doi:10.1210/me.2010-0367
36. Wu Y, Baumgarten SC, Zhou P, Stocco C (2013) Testosterone-dependent interaction between androgen receptor and aryl hydrocarbon receptor induces liver receptor homolog 1 expression in rat granulosa cells. *Mol Cell Biol* 33 (15):2817-2828. doi:10.1128/mcb.00011-13

37. Yang X, Wang Q, Wang Y, Song T, Zheng Y, Wang W, Shi Y (2021) LRH-1 high expression in the ovarian granulosa cells of PCOS patients. *Endocrine* 74 (2):413-420. doi:10.1007/s12020-021-02774-2
38. Xiao L, Wang Y, Xu K, Hu H, Xu Z, Wu D, Wang Z, You W, Ng CF, Yu S, Chan FL (2018) Nuclear Receptor LRH-1 Functions to Promote Castration-Resistant Growth of Prostate Cancer via Its Promotion of Intratumoral Androgen Biosynthesis. *Cancer Res* 78 (9):2205-2218. doi:10.1158/0008-5472.Can-17-2341
39. Zhou J, Wang Y, Wu D, Wang S, Chen Z, Xiang S, Chan FL (2021) Orphan nuclear receptors as regulators of intratumoral androgen biosynthesis in castration-resistant prostate cancer. *Oncogene* 40 (15):2625-2634. doi:10.1038/s41388-021-01737-1
40. Zanger UM, Schwab M (2013) Cytochrome P450 enzymes in drug metabolism: regulation of gene expression, enzyme activities, and impact of genetic variation. *Pharmacol Ther* 138 (1):103-141. doi:10.1016/j.pharmthera.2012.12.007
41. van Eijk M, Boosman RJ, Schinkel AH, Huitema ADR, Beijnen JH (2019) Cytochrome P450 3A4, 3A5, and 2C8 expression in breast, prostate, lung, endometrial, and ovarian tumors: relevance for resistance to taxanes. *Cancer Chemother Pharmacol* 84 (3):487-499. doi:10.1007/s00280-019-03905-3
42. Vanhove T, de Jonge H, de Loor H, Oorts M, de Hoon J, Pohanka A, Annaert P, Kuypers DRJ (2018) Relationship between In Vivo CYP3A4 Activity, CYP3A5 Genotype, and Systemic Tacrolimus Metabolite/Parent Drug Ratio in Renal Transplant Recipients and Healthy Volunteers. *Drug Metab Dispos* 46 (11):1507-1513. doi:10.1124/dmd.118.081935
43. Matthaei J, Bonat WH, Kerb R, Tzvetkov MV, Strube J, Brunke S, Sachse-Seeboth C, Sehrt D, Hofmann U, von Bornemann Hjelmborg J, Schwab M, Brockmöller J (2020) Inherited and Acquired Determinants of Hepatic CYP3A Activity in Humans. *Front Genet* 11:944. doi:10.3389/fgene.2020.00944
44. European Medicines Agency. Guideline on the investigation of drug interactions. (2012) European Medicines Agency (EMA). Accessed 27 Feb 2023
45. Guidance for industry drug interaction studies – study design, data analysis, implications for dosing, and labeling recommendations. (2012) US Food and Drug Administration (FDA). Accessed 27 Feb 2023

## SUPPLEMENTARY MATERIAL



**Supplementary Figure S1.** Individual pharmacokinetic profiles of midazolam, 1'-hydroxy midazolam, and 4'-hydroxy midazolam after oral administration (A, C, E) and intravenous administration (B, D, F). The yellow lines represent the patients with prostate cancer while the blue lines represent the patients with other solid tumours.



**Supplementary Figure S2.** Correlation between oral midazolam clearance and testosterone (A) and intravenous midazolam clearance and testosterone (B) for patients with other solid tumours.









# Part 4

**Optimisation of vincristine  
exposure in paediatric populations**



# Chapter 9

## **A highly sensitive bioanalytical method for the quantification of vinblastine, vincristine, vinorelbine and 4-O-deacetylvinorelbine in human plasma using LC-MS/MS**

*Journal of Pharmaceutical and Biomedical Analysis. 2022;215:114772*

Lisa T. van der Heijden  
Abadi Gebretensae  
Bas Thijssen  
Lotte van Andel  
A. Laura Nijstad  
Yaogeng Wang  
Hilde Rosing  
Alwin D.R. Huitema  
Jos H. Beijnen

## ABSTRACT

A highly sensitive method was developed for the quantification of vinblastine, vincristine, vinorelbine, and its active metabolite 4-O-deacetylvinorelbine in human plasma using liquid chromatography-tandem mass spectrometry (LC-MS/MS). Deuterated isotopes were used as internal standard and liquid-liquid extraction with tertbutyl methyl ether (TBME) was used for sample pre-treatment. The final extract was injected on a C18 column (50 × 2.1 mm ID, 5 µm). Gradient elution was used in combination with Reversed Phase chromatography to elute the analytes and internal standards from the column in 5 min and the API4000 triple quadrupole MS detector was operating in the positive ion mode. The calibration model, accuracy and precision, selectivity and specificity, dilution integrity, carryover, matrix factor and recovery, and stability were evaluated over a concentration range from 0.025 to 10 ng/mL for vinblastine, vinorelbine, and 4-O-deacetylvinorelbine and from 0.1 to 40 ng/mL for vincristine. The intra- and inter-assay bias and precisions were within ±12.4% and ≤10.6%, respectively. This method was successfully applied to study the pharmacokinetics of vincristine in paediatrics and vinorelbine and 4-O-deacetylvinorelbine using *in vivo* mouse models.

## 1 INTRODUCTION

Vinca-alkaloids are a group of cytotoxic drugs targeting  $\beta$ -tubulin assembly. Their interaction with  $\beta$ -tubulin molecules leads to disruption of the mitotic spindle formation, directly causing metaphase arrest and cell death [1–3]. These anticancer agents have played a major role in the treatment of several cancers including Hodgkin's lymphoma, breast cancer and lung cancer, either as a single agent or as combination therapy, since the 1960s [4,5].

There is still much unknown about the pharmacokinetic properties of vinca-alkaloids and the factors influencing their pharmacokinetics, especially in specific patient populations (e.g., paediatrics). To support pharmacokinetic trials in these populations, a highly sensitive bioanalytical method is essential. Liquid chromatography tandem-mass spectrometry (LC-MS/MS) is a useful and frequently applied analytical technique for the quantification of drug concentrations.

LC-MS/MS methods for the quantification of the vinca-alkaloids in human plasma have been reported in literature by our research group [6–8] and others [9–16]. These assays have lower limit of quantification (LLOQ) 0.1 ng/mL [7–9,14], which could be limiting for the full characterisation of the pharmacokinetics of these compounds. An exception is a vincristine assay developed by Dennison et al., which had a LLOQ of 12 pg/mL [10]. This assay was limited to a single vinca-alkaloid.

The objectives of this study were to develop a generic method for the quantification of the most commonly clinically used vinca-alkaloids: vinblastine, vincristine, vinorelbine, and its active metabolite 4-O-deacetylvinorelbine in human plasma and to improve the sensitivity of this assay when compared to previously published assays. To our knowledge, this is the first LC-MS/MS method for vinca-alkaloids quantification using stable isotopically labelled internal standards with LLOQs between 0.025 and 0.1 ng/mL and with runtimes of 5 min only. This sensitive, fast method was successfully applied to paediatric pharmacokinetic studies and in vivo mouse models.

## 2 MATERIALS AND METHODS

### 2.1 Chemicals

Vinblastine sulphate and vincristine sulphate were purchased from Selleckchem (Houston, Texas, USA). Vinorelbine ditartrate and 4-O-deacetylvinorelbine sulphate were obtained from Toronto Research Chemicals (Toronto, ON, Canada).  $^2\text{H}_3$ -vinblastine sulphate,  $^2\text{H}_3$ - vincristine sulphate,  $^2\text{H}_3$ -vinorelbine ditarte, and  $^2\text{H}_3$ -4-O-deacetylvinorelbine sulphate were manufactured by Alsachim (Illkirch Graffen- staden, France). Methanol (HPLC Supra-Gradient), acetonitrile, and water (LC-MS) were obtained from Biosolve (Valkenswaard, The Netherlands). Tert-butyl methyl ether (TBME) and ammonium acetate were purchased from Merck (Darmstadt, Germany). Blank human potassium ethylenediaminetetraacetic acid (K2EDTA) plasma was obtained from Atal Medial (Amsterdam, The Netherlands).

### 2.2 Stock and working solutions

Independent stock solutions for each analyte at a concentration of 1 mg/mL in methanol were used for the preparation of combined working solutions (in methanol). These working solutions contained 0.5–200 ng/ mL for vinblastine, vinorelbine and 4-O-deacetylvinorelbine and from 2 to 800 ng/mL for vincristine and were used for the preparation of the calibration standards. The same procedure was followed for the preparation of the working solutions for the Quality Control (QC) samples. In this way, working solutions in methanol were obtained containing 0.5, 1, 5, 1 and 150 ng/mL for vinblastine, vinorelbine and 4-O-deacetylvinorelbine, and at 2, 6, 40 and 600 ng/mL for vincristine.

Eight non-zero calibration standards were prepared by diluting the working solutions 20-fold with control human K2EDTA plasma. The final concentration range was from 0.025 to 10 ng/mL for vinblastine, vinorelbine and 4-O-deacetylvinorelbine, and from 0.1 to 40 ng/mL for vincristine. A blank (control matrix spiked with internal standard) and a double blank (control matrix) were also prepared.

QC samples were prepared at four concentration levels: LLOQ (QC LLOQ), low (QC L), medium (QC M) and high (QC H), by a 20-fold dilution in control human K2EDTA plasma of the corresponding working solutions. The final concentrations were 0.025, 0.075, 0.5 and 7.5 ng/mL for vinblastine, vinorelbine and 4-O-deacetylvinorelbine, and 0.1, 0.3, 2 and 30 ng/mL for vincristine.

### 2.3 Internal standard

A combined stock solution was prepared in methanol at 1 mg/mL for  $^2\text{H}_3$ -vinblastine,  $^2\text{H}_3$ -vincristine,  $^2\text{H}_3$ -vinorelbine, and  $^2\text{H}_3$ -4-O-deacetylvinorelbine. The stock solution was further diluted with methanol to obtain a working solution with a final concentration of 50 ng/mL for each stable labelled isotope.

### 2.4 Sample preparation

An aliquot of 200  $\mu\text{L}$  plasma was used for sample preparation. Each aliquot was spiked with 10  $\mu\text{L}$  of internal standard working solution (50 ng/mL) except the double blank calibration standards. Liquid-liquid extraction was performed by adding 1 mL of TBME to each sample prior to mixing and centrifuging (14,000 rpm for 5 min). The samples were snap frozen and the supernatant was collected. The supernatant was dried under a gentle stream of nitrogen (40 °C) prior to reconstitution with 75  $\mu\text{L}$  of methanol-acetonitrile-water (1:1:2, v/v/v). Subsequently, the samples were vortex mixed and centrifuged (14,000 rpm for 5 min) before 65  $\mu\text{L}$  of the final extract was transferred into vials prior analysis. Liquid-liquid extraction with TBME had preference over the previously reported protein precipitation [6,7] because it resulted in satisfactory LLOQ values for all analytes.

### 2.5 Liquid chromatography equipment and conditions

The chromatographic system consisted of a Nexera X2 chromatograph (Shimadzu, Kyoto, Japan) equipped with a binary pump (Nexera LC30-AD), a degasser (Nexera DGU-20A3R), an autosampler (Nexera SIL-30ACMP) and a column oven (Nexera CTO-20AC). The analytes were separated using a reversed phase C18 column (Waters Xbridge 50  $\times$  2.1 mm ID, 5  $\mu\text{m}$  particles) coupled to a guard column (Waters, 0.2  $\mu\text{m}$ ). The mobile phase consisted of ammonium acetate in water (pH 10.5; 1 mM)-acetonitrile (7:3, v/v, eluent A) and methanol (eluent B) and the flow was 0.4 mL/min. The applied gradient program was 30% B (0.0–0.5 min), 30–100% B (0.5–3.0 min), 100%B (3.0–3.5 min), 100–30% B (3.5–3.51 min), and 30% (3.51–5.0 min). A volume of 10  $\mu\text{L}$  was injected.

### 2.6 Mass spectrometry equipment and conditions

An API4000 triple quadrupole mass spectrometer (MS) equipped with a turbo ion spray interface, operating in positive ion mode was used (Sciex, Framingham, MA, USA). Multiple reaction monitoring (MRM) was used for quantification. The chromatograms were processed using Analyst™ software (Sciex, version 1.6.2). The MS operating parameters are summarised in Table 1 and the proposed fragmentations are depicted in Figure. 1. For the internal standard a product ion  $[\text{M H}]^+$  was chosen to prevent cross-analyte interference.

## 2.7 Validation procedures

The method was validated based on the current FDA and EMA guidelines for bioanalytical method validation [17,18].

**Table 1.** Above: General mass spectrometric parameters. Below: Analyte specific mass spectrometric parameters for vinblastine, vincristine, vinorelbine, 4-O-deacetylvinorelbine and the internal standards.

Mass-spectrometer					
Run duration	5 min				
Ionspray voltage	3500 V				
Nebulizer gas	60 au				
Polarity	positive				
Turbo gas / heater gas	50 au				
Curtain gas	13 au				
Collision gas	9 au				
Temperature	750 °C				
	MRM (m/z)	Collision energy (V)	Collision exit potential (V)	Declustering potential (V)	Dwell time (ms)
Vinblastine	811.4 →224.2	59	14	93	150
Vinblastine-IS	815.5 →224.2				
Vincristine	825.4 →144.2	99	10	151	150
Vincristine-IS	829.4 →144.2				
Vinorelbine	779.3 →122.1	79	8	106	75
Vinorelbine-IS	783.3 →122.1				
4-O-deacetylvinorelbine	737.4 →122.1	79	10	106	75
4-O-deacetylvinorelbine-IS	741.4 →122.1				

Abbreviations: IS = internal standard, MRM = multiple reaction monitoring.



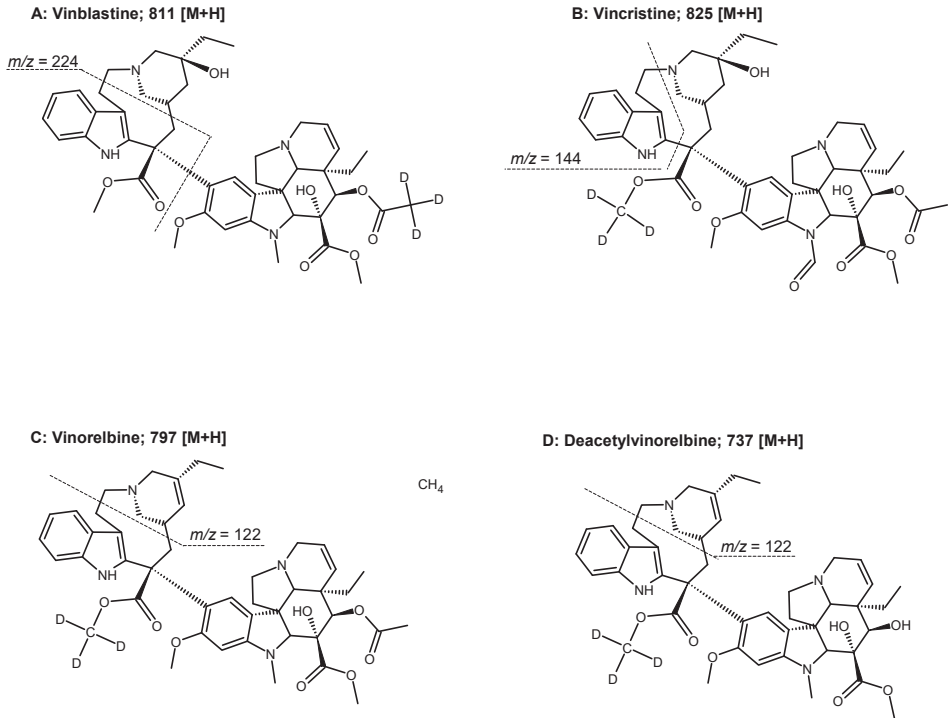


**Figure 1.** Chemical structures of (A) vinblastine, (B) vincristine, (C) vinorelbine, and (D) 4-O-deacetyl vinorelbine including the proposed fragmentation. The position of deuterium labelling is indicated with the letter D.

## 3 RESULTS

### 3.1 Validation

#### 3.1.1 Calibration model

The calibration model was determined using eight calibration standards for each of the four analytes. The concentration (x)-response correlation was described using linear regression with  $1/x^2$  weighting for vinblastine and vincristine and quadratic regression with  $1/x^2$  weighting was used for vinorelbine and 4-O-deacetylvinorelbine. The validated concentration range was from 0.025 to 10 ng/mL for vinblastine, vinorelbine and 4-O-deacetylvinorelbine, and from 0.1 to 40 ng/mL for vincristine. All the calibration standards were within  $\pm 6.5\%$  of their nominal concentrations and therefore met the acceptance criteria of  $\pm 15\%$  ( $\pm 20\%$  for LLOQ).

#### 3.1.2 Accuracy and precision

To determine accuracy and precision, five replicates of QC samples were analysed in three separate runs. Accuracy was defined as the bias (%) and precision as the relative standard error (%). Intra-assay variability was determined from the mean measured concentration per run. Inter-assay variability was calculated from the overall mean measured concentration. One-way analysis of variance was used to calculate intra- and inter-assay variation. Data on accuracy and precision are presented in Table 2. The intra-assay accuracy and precision and inter-assay accuracy and precision were within the required  $\pm 15\%$  of their nominal concentration ( $\pm 20\%$  for QC LLOQ).

#### 3.1.3 Endogenous interference

To determine the impact of endogenous interferences, six different batches of blank control human K2EDTA plasma were spiked at the LLOQ for each analyte. The back-calculated concentrations of these spiked samples were within the required 20% of the nominal concentrations. Continuing, blank samples did not contain interferences coeluting at the retention time of vincristine, vinorelbine, and 4-O-deacetylvinorelbine for the analytes and their internal standards (Figure 2). For vinblastine, one out of the six blank samples demonstrated endogenous interferences of 24.7%. However, the acceptance criteria of four out of six blank samples with endogenous interferences 20% (5% for internal standards) were met. Therefore, endogenous interference was deemed acceptable.

#### 3.1.4 Cross-analyte/IS interference

Cross-analyte/IS interference experiments were executed to investigate the extent of any interferences caused by metabolites of the analytes or from degradation products formed during sample preparation. For the evaluation of

cross-analyte/internal standard interferences, the analytes and their internal standards were separately spiked to blank control human K2EDTA plasma at their ULOQ. The interference at the retention times of the analytes and internal standards were calculated as percentage of area of their respective LLOQ. The cross-analyte/internal standard interferences did not meet the acceptance criteria of 20% (5% for internal standards) for the following compounds: vinblastine (28.3% from vincristine), vincristine (3157% from vinblastine), vinorelbine (22.4% from vincristine), and  $^2\text{H}_3$ -vincristine (22.7% from  $^2\text{H}_3$ -vinblastine). The cross analyte/internal standard interferences were found to be irrelevant for clinical application for several reasons: 1) Vinca- alkaloids are not part of combination therapy with each other, 2) the concentrations of the analytes of the calibration standards and the QC samples are within the same range, and 3) there was no cross-analyte interference observed for vinorelbine and its metabolite, 4-O- deacetylvinorelbine.

**Table 2.** Assay performance data for vinblastine, vincristine, vinorelbine and its metabolite 4-O-deacetylvinorelbine.

Analyte	Nominal conc. (ng/mL)	Intra-assay (n = 15)		Inter-assay (n = 15)	
		Bias (%)	Precision (%)	Bias (%)	Precision (%)
Vinblastine	0.025	±13.2	≤15.9	-8.9	-*
	0.075	±3.7	≤8.2	-0.4	-*
	0.500	±12.4	≤3.3	-11.7	-*
	7.50	±5.7	≤4.4	0.5	5.4
Vincristine	0.100	±6.9	≤15.5	2.3	-*
	0.300	±9.9	≤5.8	2.9	5.7
	2.00	±4.4	≤7.1	2.9	-*
	30.0	±3.5	≤6.5	0.1	2.7
Vinorelbine	0.025	±10.8	≤9.8	-4.2	4.9
	0.075	±10.9	≤8.0	-5.6	4.4
	0.500	±3.4	≤4.4	-2.9	-*
	7.50	±10.3	≤5.3	-3.9	8.8
4-O-deacetylvinorelbine	0.025	±8.1	≤16.3	5.0	-*
	0.075	±5.2	≤10.6	-3.1	-*
	0.500	±3.2	≤5.0	-1.8	-*
	7.50	±3.9	≤2.3	-1.5	3.4

\* No significant additional variation due to the performance of the assay in different runs was found. Nominal conc. = Nominal concentration.

### 3.1.5 Dilution integrity

Five replicate control human K<sub>2</sub>EDTA plasma samples with a concentration around 10 times of the ULOQ were diluted 20-fold with control human K<sub>2</sub>EDTA plasma to determine the dilution integrity. The accuracy of the 20-fold diluted samples was  $\pm 8.0\%$ ,  $\pm 4.7\%$ ,  $\pm 3.8\%$  and  $\pm 1.7\%$  for vinblastine, vincristine, vinorelbine and 4-O-deacetylvinorelbine, respectively. An accuracy of within  $\pm 15\%$  of the nominal concentration was required.

### 3.1.6 Carry-over

Carry-over was determined by injecting two double blank control human K<sub>2</sub>EDTA plasma samples after a calibration standard at ULOQ concentration level. Carry-over was not detected except for vinorelbine and 4-O-deacetylvinorelbine, which was 9.6% and 15.8% of the area of the LLOQ of these analytes, respectively. However, carry-over was found to be acceptable since less than 20% of the area of the analytes at LLOQ level was detected.

### 3.1.7 Extraction recovery and matrix effect

Recovery was investigated in control human K<sub>2</sub>EDTA plasma at QC L and QC H concentrations in triplicate. The sample pre-treatment recovery was calculated by dividing the peak area in the processed sample by the peak area in presence of the matrix for the analyses and the internal standards. Overall recovery was defined as the peak area in the processed sample divided by the peak area in the absence of matrix. Sample pre-treatment recovery ranged from 70.7% to 79.4% for vinblastine, from 75.6% to 76.5% for vincristine, 104–111% for vinorelbine, and 101–118% for 4-O-deacetylvinorelbine. Overall recovery varied between 111% and 131%, 68.3% and 72.1%, 127% and 138%, and 128% and 146% for vinblastine, vincristine, vinorelbine, and 4-O-deacetylvinorelbine, respectively. The internal standardised matrix factor (measure of ion suppression and/or enhancement) ranged from 0.829 and 0.982 for vinblastine, 0.926 and 0.999 for vincristine, 0.938 and 1.01 for vinorelbine, and 0.889 and 1.04 for 4-O-deacetylvinorelbine. Although there is both ion enhancement as suppression for the different analytes, the results were reproducible with coefficient of variations of 3.4%, 8.8%, 3.6%, and 8.3% for vinblastine, vincristine, vinorelbine and 4-O-deacetylvinorelbine, respectively. These values met the acceptance criteria of  $\leq 15\%$ .

### 3.1.8 Stability

Stability in control human K<sub>2</sub>EDTA plasma was determined for short-term storage at ambient temperature, long-term storage at 70 °C, and after three freeze/thaw cycles. One freeze/thaw cycle consisted of unassisted thawing at room temperature and

subsequently freezing at 70 °C for at least 12 h. Stability of the stock solutions were determined for short-term storage at room temperature and long-term storage at - 70 °C. Furthermore, the stability of the dry extract and the final extract was determined. If 85–115% (15%) of the initial concentration of the analytes in bioanalytical samples was recovered, the analytes were considered to be stable. For stock solutions, a range of 95–105% ( $\pm 5\%$ ) was applied. Stability data depicted in Table 3. All analytes were stable at ambient temperature for 6 h and for 3 freeze/ thaw cycles. Furthermore, vinblastine and vinorelbine were stable in plasma at 70 °C for at least 16.8 months (505 days), while vincristine and 4-O-deacetylvinorelbine were unstable. For the latter, stability was confirmed over a shorter time period of 9.1 months (273 days). Moreover, dry extract stability was established for vinorelbine and 4-O-deacetylvinorelbine for six days at 2–8 °C while vinblastine and vincristine did not meet the stability criteria. For vinblastine, a shorter stability period for the dry extract was established of 3 days, while the dry extract of vincristine remained unstable. Therefore, the dry extract of vincristine has to be processed to the final extract before storage. The final extracts of vinblastine and vinorelbine were stable for four days at 2–8 °C, while the final extracts of vincristine and 4-O-deacetylvinorelbine were stable for 7 days at 2–8 °C. Finally, all stock solutions were stable at ambient temperature for 6 h and for at least 16.7 months (500 days) at 70 °C. Long-term stability at 20 °C was not investigated due to the previously reported limited long-term stability of vincristine, vinorelbine, and 4-O-deacetylvinorelbine at 20 °C by our institute [6,7], and the limited long-term stability of vincristine and 4-O-deacetylvinorelbine at - 70 °C in the current study.

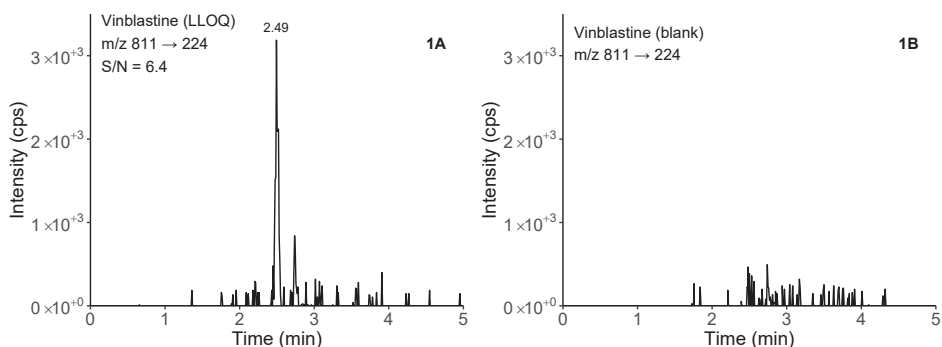


**Figure 2.** Representative LC-MS/MS chromatograms of the lower limit of quantification (A-series) and a blank sample (B-series) of vinblastine (1), vincristine (2), vinorelbine (3) and 4-O-deacetylvinorelbine (4). The concentration at LLOQ level was 0.025 ng/mL for vinblastine, vinorelbine, and 4-O-deacetylvinorelbine, and 0.1 ng/mL for vincristine. S/N are the signal-to-noise ratios for each analyte.

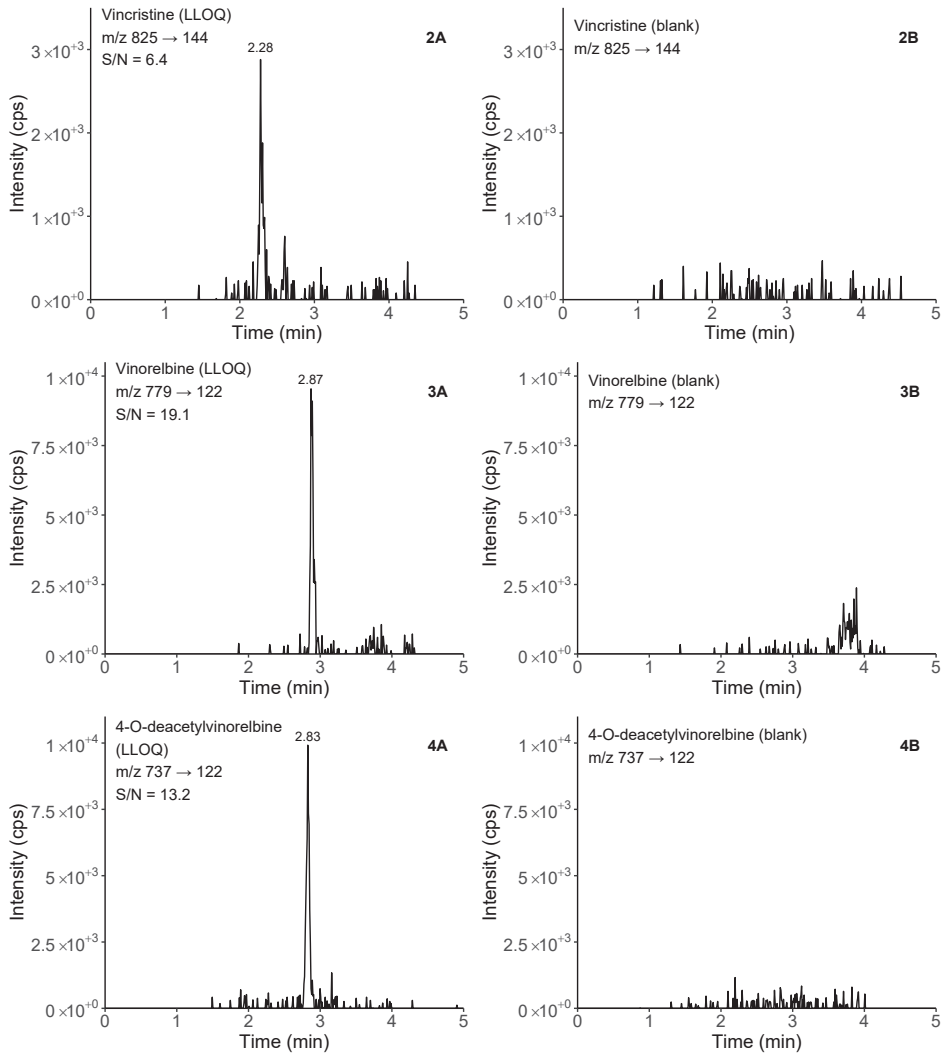


**Figure 2.** Continued.

### 3.2 Clinical application

The bioanalytical method was used to support pharmacokinetic studies in paediatric patients and in mice. Pharmacokinetics of two subjects from both studies are depicted in Figure. 3. The validated concentrations ranges were lower than the expected concentrations in (pre-) clinical samples to prevent carry-over. Samples with concentrations above the validated concentration ranges were diluted with control human plasma. The LLOQ was sufficient to measure plasma.

## 4 CONCLUSION

A sensitive, fast LC-MS/MS method was developed and validated for the quantification of vinblastine, vincristine, vinorelbine, and 4-O-deacetylvinorelbine in human plasma. Linearity over a concentration range of 0.025–10 ng/mL for vinblastine, vinorelbine, and 4-O-deacetyl- vinorelbine and 0.1–40 ng/mL for vincristine were established. This method was successfully applied to pharmacokinetic studies of vincristine in children and pharmacokinetic studies of vinorelbine and 4-O-deacetylvinorelbine in mice.

**Table 3.** Stability parameters for vinblastine, vincristine, vinorelbine and 4-O-deacetyl- vinorelbine.

Analyte	Matrix	Conditions	Nom. Conc. (ng/mL)	Bias (%)	C.V. (%)	n
Vinblastine	Plasma	3 F/T cycles (-70 °C/ambient)	0.0750	2.5	7.0	3
			7.50	4.9	5.0	3
	Plasma	6 h, ambient temperature	0.0750	5.9	3.8	3
			7.50	-2.8	4.0	3
	Plasma	505 days, -70 °C	0.0750	13.9	6.7	3
			7.50	4.6	7.7	3
	Dry extract	3 days, 2-8°C	0.0750	-0.1	7.6	3
			7.50	11.3	2.0	3
	Dry extract	6 days, 2-8°C	0.0750	-11.6	12.1	3
			7.50	-18.8	12.7	3
	Final extract	4 days, 2-8°C	0.0750	-4.9	10.6	3
			7.50	-11.0	5.0	3
MeOH (stock)	6 h, ambient temperature	1.00*10 <sup>6</sup>	2.4	1.0	3	
MeOH (stock)	503 days, -70 °C	1.00*10 <sup>6</sup>	0.7	1.2	3	
Vincristine	Plasma	3 F/T cycles (-70 °C/ambient)	0.300	4.9	3.7	3
			30.0	-2.1	3.1	3
	Plasma	6 h, ambient temperature	0.300	1.1	14.0	3
			30.0	-3.2	2.0	3
	Plasma	273 days, -70 °C	0.300	-12.3	5.9	3
			30.0	-2.4	1.9	3
	Plasma	505 days, -70 °C	0.300	-28.4	3.0	3
			30.0	-27.3	4.9	3
	Dry extract	3 days, 2-8 °C	0.300	-27.2	7.8	3
			30.0	-38.2	9.1	3
	Final extract	7 days, 2-8 °C	0.300	2.4	11.3	3
			30.0	5.4	7.4	3
MeOH (stock)	6 h, ambient temperature	1.00*10 <sup>6</sup>	-1.5	3.2	3	
MeOH (stock)	503 days, -70 °C	1.00*10 <sup>6</sup>	4.7	1.3	3	

**Table 3.** Continued

Analyte	Matrix	Conditions	Nom. Conc. (ng/mL)	Bias (%)	C.V. (%)	n
Vinorelbine	Plasma	3 F/T cycles (-70 °C/ambient)	0.0750	4.1	1.3	3
			7.50	4.2	5.7	3
	Plasma	6 h, ambient temperature	0.0750	-7.9	6.2	3
			7.50	6.2	3.3	3
	Plasma	505 days, -70 °C	0.0750	-7.0	3.9	3
			7.50	-8.4	4.3	3
	Dry extract	6 days, 2-8 °C	0.0750	-7.6	8.9	3
			7.50	-0.8	3.8	3
	Final extract	4 days, 2-8 °C	0.0750	-7.4	7.8	3
			7.50	4.3	2.4	3
MeOH (stock)	6 h, ambient temperature	1.00*10 <sup>6</sup>	2.7	2.4	3	
MeOH (stock)	501 days, -70 °C	1.00*10 <sup>6</sup>	3.2	2.5	3	
4-O-deacetyl-vinorelbine	Plasma	3 F/T cycles (-70 °C/ambient)	0.0750	-7.2	9.2	3
			7.50	5.3	2.6	3
	Plasma	6 h, ambient temperature	0.0750	-10.6	7.2	3
			7.50	-2.1	1.4	3
	Plasma	273 days, -70 °C	0.0750	-14.4	4.7	3
			7.50	-9.9	1.4	3
	Plasma	505 days, -70 °C	0.0750	-17.4	1.8	3
			7.50	-12.3	2.1	3
	Dry extract	6 days, 2-8 °C	0.0750	0.8	4.5	3
			7.50	3.7	1.2	3
	Final extract	7 days, 2-8 °C	0.0750	-4.0	7.3	3
			7.50	8.4	1.3	3
	MeOH (stock)	6 h, ambient temperature	1.00*10 <sup>6</sup>	1.4	2.7	3
	MeOH (stock)	500 days, -70 °C	1.00*10 <sup>6</sup>	0.9	4.9	3

Abbreviations: C.V. = coefficient of variation; F/T = freeze/thaw; Nom. Conc., nominal concentration; MeOH = methanol.



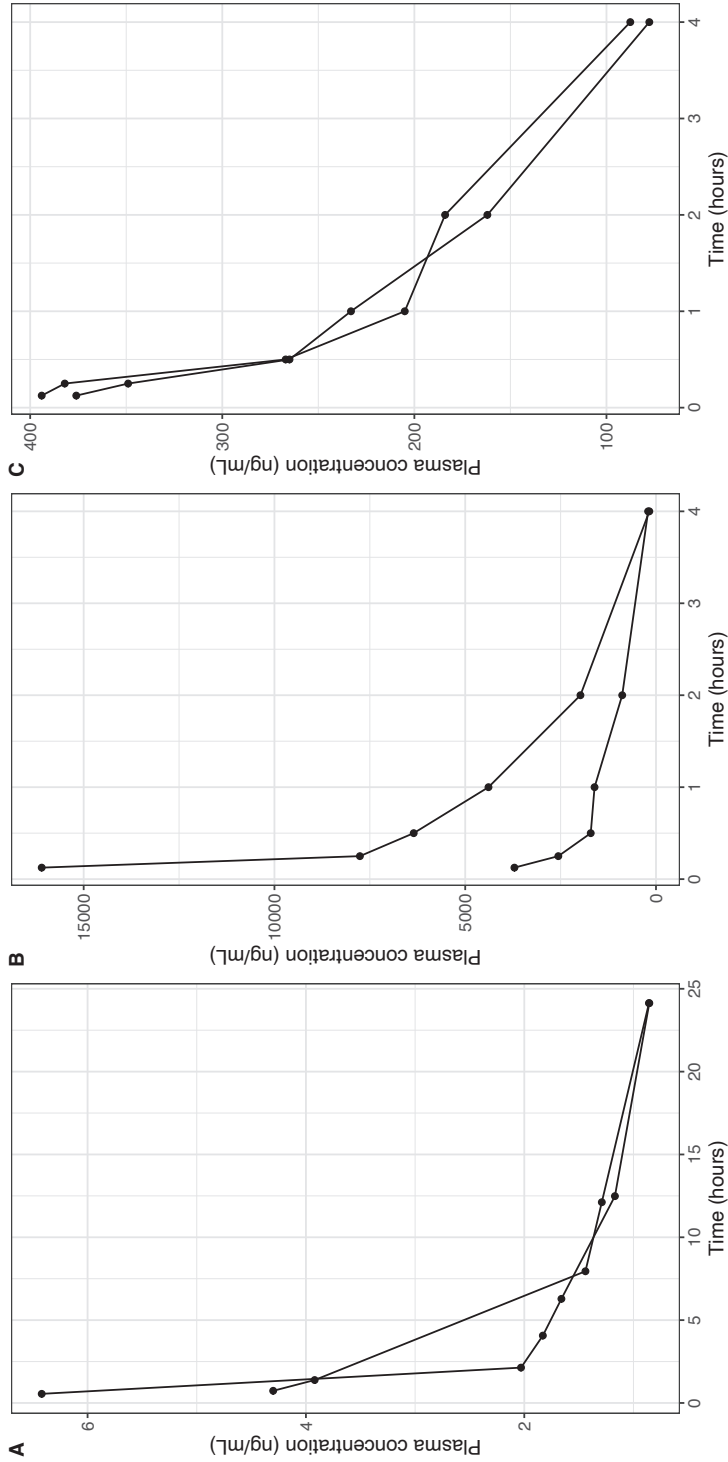


**Figure 3.** Pharmacokinetics of vincristine (A), vinorelbine (B), and 4-O-deacetylvinorelbine (C). Vincristine plasma samples were obtained from two paediatric subjects receiving 1.5–2 mg/m<sup>2</sup> vincristine intravenously according to standard of care. These two pharmacokinetic curves demonstrated the method's clinical application to quantify vincristine pharmacokinetics in paediatric patients. Vinorelbine and 4-O-deacetylvinorelbine plasma samples were obtained from two mice from an *in vivo* mouse study. Vinorelbine was administered to the mice after a 3 h fast either intravenously or orally with a dose of 10 mg/kg. These pharmacokinetics curved demonstrated the method's application to quantify vinorelbine and 4-O-deacetylvinorelbine pharmacokinetics in mice.

## REFERENCES

1. Gan PP, Kavallaris M (2008) Tubulin-targeted drug action: functional significance of class II and class IV $\beta$  tubulin in vinca alkaloid sensitivity. *Cancer Res* 68 (23):9817-9824. doi:10.1158/0008-5472.CAN-08-1501
2. Pasquier E, Kavallaris M (2008) Microtubules: a dynamic target in cancer therapy. *IUBMB Life* 60 (3):165-170. doi:10.1002/iub.25
3. Kavallaris M, Annereau JP, Barret JM (2008) Potential mechanisms of resistance to microtubule inhibitors. *Semin Oncol* 35 (3 Suppl 3):S22-27. doi:10.1053/j.seminoncol.2008.01.006
4. Martino E, Casamassima G, Castiglione S, Cellupica E, Pantalone S, Papagni F, Rui M, Siciliano AM, Collina S (2018) Vinca alkaloids and analogues as anti-cancer agents: Looking back, peering ahead. *Bioorg Med Chem Lett* 28 (17):2816-2826. doi:10.1016/j.bmcl.2018.06.044
5. Lucas DM, Still PC, Perez LB, Grever MR, Kinghorn AD (2010) Potential of plant-derived natural products in the treatment of leukemia and lymphoma. *Curr Drug Targets* 11 (7):812-822. doi:10.2174/138945010791320809
6. Damen CW, Israels T, Caron HN, Schellens JH, Rosing H, Beijnen JH (2009) Validated assay for the simultaneous quantification of total vincristine and actinomycin-D concentrations in human EDTA plasma and of vincristine concentrations in human plasma ultrafiltrate by high-performance liquid chromatography coupled with tandem mass spectrometry. *Rapid Commun Mass Spectrom* 23 (6):763-774. doi:10.1002/rcm.3938
7. Damen CW, Lagas JS, Rosing H, Schellens JH, Beijnen JH (2009) The bioanalysis of vinorelbine and 4-O-deacetylvinorelbine in human and mouse plasma using high-performance liquid chromatography coupled with heated electrospray ionization tandem mass-spectrometry. *Biomed Chromatogr* 23 (12):1316-1325. doi:10.1002/bmc.1255
8. Damen CW, Rosing H, Tibben MM, van Maanen MJ, Lagas JS, Schinkel AH, Schellens JH, Beijnen JH (2008) A sensitive assay for the quantitative analysis of vinorelbine in mouse and human EDTA plasma by high-performance liquid chromatography coupled with electrospray tandem mass spectrometry. *J Chromatogr B Analyt Technol Biomed Life Sci* 868 (1-2):102-109. doi:10.1016/j.jchromb.2008.04.046
9. Corona G, Casetta B, Sandron S, Vaccher E, Toffoli G (2008) Rapid and sensitive analysis of vincristine in human plasma using on-line extraction combined with liquid chromatography/tandem mass spectrometry. *Rapid Commun Mass Spectrom* 22 (4):519-525. doi:10.1002/rcm.3390
10. Dennison JB, Renbarger JL, Walterhouse DO, Jones DR, Hall SD (2008) Quantification of vincristine and its major metabolite in human plasma by high-performance liquid chromatography/tandem mass spectrometry. *Ther Drug Monit* 30 (3):357-364. doi:10.1097/FTD.0b013e31816b92c9
11. Gao S, Zhou J, Zhang F, Miao H, Yun Y, Feng J, Tao X, Chen W (2014) Rapid and sensitive liquid chromatography coupled with electrospray ionization tandem mass spectrometry method for the analysis of paclitaxel, docetaxel, vinblastine, and vinorelbine in human plasma. *Ther Drug Monit* 36 (3):394-400. doi:10.1097/FTD.000000000000010

12. Gong X, Yang L, Zhang F, Liang Y, Gao S, Liu K, Chen W (2017) Validated UHPLC-MS/MS assay for quantitative determination of etoposide, gemcitabine, vinorelbine and their metabolites in patients with lung cancer. *Biomed Chromatogr* 31 (11). doi:10.1002/bmc.3989
13. Guilhaumou R, Solas C, Rome A, Giocanti M, Andre N, Lacarelle B (2010) Validation of an electrospray ionization LC/MS/MS method for quantitative analysis of vincristine in human plasma samples. *J Chromatogr B Analyt Technol Biomed Life Sci* 878 (3-4):423-427. doi:10.1016/j.jchromb.2009.12.015
14. Qian J, Wang Y, Chang J, Zhang J, Wang J, Hu X (2011) Rapid and sensitive determination of vinorelbine in human plasma by liquid chromatography-tandem mass spectrometry and its pharmacokinetic application. *J Chromatogr B Analyt Technol Biomed Life Sci* 879 (9-10):662-668. doi:10.1016/j.jchromb.2011.01.039
15. Skolnik JM, Barrett JS, Shi H, Adamson PC (2006) A liquid chromatography-tandem mass spectrometry method for the simultaneous quantification of actinomycin-D and vincristine in children with cancer. *Cancer Chemother Pharmacol* 57 (4):458-464. doi:10.1007/s00280-005-0065-9
16. Van Heugen JC, De Graeve J, Zorza G, Puozzo C (2001) New sensitive liquid chromatography method coupled with tandem mass spectrometric detection for the clinical analysis of vinorelbine and its metabolites in blood, plasma, urine and faeces. *J Chromatogr A* 926 (1):11-20. doi:10.1016/s0021-9673(01)00993-1
17. US Food and Drug Administration (FDA) (2019) Guidance for industry: Bioanalytical method validation. <https://www.fda.gov/files/drugs/published/Bioanalytical-Method-Validation-Guidance-for-Industry.pdf> Accessed 5 January 2021
18. European Medicines Agency (EMA) (2011) Guideline on bioanalytical method validation [https://www.ema.europa.eu/en/documents/scientific-guideline/guideline-bioanalytical-method-validation\\_en.pdf](https://www.ema.europa.eu/en/documents/scientific-guideline/guideline-bioanalytical-method-validation_en.pdf) Accessed 5 January 2021



# Chapter 10

## **A sensitive liquid chromatographic-mass spectrometry method for the quantification of vincristine in whole blood collected with volumetric absorptive microsampling**

*Journal of Pharmaceutical and Biomedical Analysis. 2023;225:115232*

Lisa T. van der Heijden

Aniek Uittenboogaard

A. Laura Nijstad

Abadi Gebretensae

Gertjan J.L. Kaspers

Jos H. Beijnen

Alwin D.R. Huitema

Hilde Rosing

## ABSTRACT

Vincristine is a well-established cytotoxic drug. In paediatric populations blood collection via venipuncture is not always feasible. Volumetric absorptive microsampling (VAMS) is a less invasive method for blood collection. Furthermore, VAMS lacks the haematocrit effect on the recovery known with dried blood spots. Therefore, a liquid chromatography tandem-mass spectrometry method was developed and validated for the quantification of vincristine in whole blood collected with VAMS devices. Samples were prepared using solid-liquid extraction with 0.2% formic acid in water and acetonitrile. The final extract was injected on a C18 column (2.0 x 50 mm, 5  $\mu$ m). Gradient elution was used, and quantification was performed with a triple quadruple mass spectrometer operating in the positive mode. The validated concentration range was from 1 to 50 ng/mL with an intra- and inter-accuracy and precision of  $\pm$ 10.9% and  $\leq$ 7.3%, respectively. This method was successfully applied to quantify vincristine concentrations in whole blood collected with VAMS from paediatric oncology patients. Vincristine concentrations in whole blood were non-linearly associated with plasma concentrations, which could be described with a saturable binding equilibrium model.

## 1 INTRODUCTION

Vincristine is a cytotoxic drug from the vinca-alkaloid group. It plays a major role in the treatment of both solid and non-solid tumours in adult and paediatric populations [1]. The cytotoxic effect of vincristine is achieved by binding to the  $\beta$ -subunit of tubulin. This drug-tubulin binding leads to inhibition of microtubule formation, resulting in cell arrest in the metaphase [2,3]. Vincristine is administered intravenously as a bolus or short infusion [1]. The pharmacokinetics of vincristine is characterised by a fast initial distribution with a half-life of 5 minutes, followed by a long terminal elimination phase with a half-life of 19-155 hours [4]. Vincristine is metabolized by Cytochrome P450 (CYP) enzymes, predominately by isoforms CYP3A4 and CYP3A5, and is biliary excreted through efflux transporter P-glycoprotein (P-gp) [5]. Furthermore, the pharmacokinetics of vincristine show large inter-individual variability with recent pharmacokinetics studies reporting inter-individual variability of 17-66% in adults and 48-67% in children [6,7].

Despite the long clinical use of vincristine, there is no complete understanding of factors that explain the observed high inter-individual variability in vincristine pharmacokinetics [8,9]. The effect of different covariates such as demographic, clinical, and biomedical data have been studied but no conclusive relationships have been found so far [6,8,10,11-13,14-18]. However, recent clinical studies support the possible effect of ethnicity on vincristine pharmacokinetics [10,19-21-23]. Therefore, pharmacokinetic studies are needed to further investigate the possible effects of ethnicity and other factors on vincristine pharmacokinetics.

Sensitive bioanalytical methods for the quantification of vincristine are essential to support future pharmacokinetic studies; several have been described in literature [24-29]. The collection of plasma samples might be undesirable in more vulnerable patient populations such as (young) children and in resource limited settings due to the invasiveness of a venepuncture and the relatively large volume of matrix collected. In these settings, whole blood sampling from a finger prick, such as dried blood spots, might be preferred over plasma sampling. The quantification of vincristine from dried blood spots has been described in literature [30,31]. A limiting factor of dried blood spots is the haematocrit effect on the recovery of the analyte which influences the spread of the blood droplet on the dried blood spot card [32].

An alternative for dried blood spots is volumetric absorptive microsampling (VAMS), which allows for accurate sampling of a specific volume of whole blood [33,34]. By sampling an exact volume of whole blood before the sample is dried, the effect of haematocrit on sample preparation is minimised. The aim of the current study was to develop a sensitive liquid chromatography tandem mass spectrometry (LC-MS/MS) method to quantify vincristine in whole blood using VAMS sampling devices that will be able to support a future pharmacokinetic trial in Kenyan paediatric oncology patients. During this study three VAMS samples will be collected within one to four hours after vincristine administration. To quantify the collected VAMS samples, a lower limit of quantification (LLOQ) of 1 ng/mL was deemed essential and an upper lower limit of quantification (ULOQ) of 50 ng/mL was deemed appropriate based on the expected concentration at 4 hours after administration [35]. The developed method was validated based on the EMA and FDA guidelines [36,37]. To our knowledge, this is the first bioanalytical assay using VAMS sampling devices for the quantification of vincristine in human whole blood. A bioanalytical assay using VAMS sampling devices for the quantification of vincristine in mice whole blood has been published previously [38].



## 2 MATERIALS AND METHODS

### 2.1 Chemicals

Vincristine sulphate was purchased from Selleckchem (Houston, Texas, USA).  $^2\text{H}_3$ -vincristine sulphate (internal standard) was obtained from Toronto Research Chemicals (Toronto, ON, Canada). Acetonitrile, formic acid, methanol, and water (all ULC-MS grade) were supplied by Biosolve (Valkenswaard, the Netherlands). Ammonia and ammonium acetate were both obtained from Merck (Darmstadt, Germany). VAMS sampling devices (Mitra®) were purchased from Neoteryx (Torrance, CA, USA). Control human whole blood was collected from healthy volunteers.

### 2.2 Stock solutions and working solutions

Stock solutions were prepared in methanol at a concentration of 1 mg/mL. Separate stock solutions were used for the preparation of the calibration standards and the quality control (QC) samples. The stock solutions were diluted in methanol to obtain working solutions for the calibration standards with a concentration range of 20-1,000 ng/mL. Working solutions of the QC samples were prepared by diluting the stock solution in methanol to a concentration range of 20-800 ng/mL. A stock solution of internal standard was prepared in methanol at a concentration of 1 mg/mL. The working solution of the internal standard was made by diluting of the internal standard stock solution with methanol to a final concentration of 50 ng/mL. All stock and working solutions were stored at -70 °C.

### 2.3 Calibration standards, quality control samples

Calibration standards and QC samples were prepared in batches prior to the validation of the method since it was difficult to obtain fresh control human whole blood for each validation run. Fresh whole blood was collected in  $\text{K}_2\text{EDTA}$  tubes. The stability in the biomatrix (dried whole blood on Mitra® sampling devices) was determined afterwards. The haematocrit of the whole blood was measured and adjusted to a haematocrit of 0.35, as it was the expected mean in the study population, by adding either plasma or red blood cells. The haematocrit was confirmed after adjustment. The calibration standards were prepared by diluting the working solutions 20-fold to concentrations of 1, 2, 5, 10, 20, 30, 40, and 50 ng/mL. QC samples were prepared in the same manner as the calibration standards. Working solutions were diluted 20-fold with whole blood at concentrations of 1, 3, 20, and 40 ng/mL for QC LLOQ, QC-LOW, QC-MID, and QC-HIGH. A single blank (control matrix with internal standard), and a double blank (control matrix) were also prepared. The spiked whole blood calibration standards and QC

samples were gently homogenized for 10 minutes to prevent haemolysis before sampling 10  $\mu\text{L}$  whole blood with the VAMS sampling devices. After sampling, the VAMS sampling devices were dried overnight at ambient temperature in its original packaging for both calibration standards and QC samples. All calibration standards and QC samples were stored in Ziploc bags with desiccant in the dark at ambient temperature.

#### 2.4 Sample preparation

The sponge of the VAMS sampling devices was transferred to 2.0 mL reaction tubes (Eppendorf, Hamburg, Germany). Two grinding beads (stainless steel, 3.96 mm) were added to all reaction tubes prior adding 400  $\mu\text{L}$  0.2% formic acid in water to all samples. The double blank samples were spiked with 20  $\mu\text{L}$  methanol while all other samples were spiked with 20  $\mu\text{L}$  internal standard (50 ng/mL). All reaction tubes were placed in a genogrinder (Genogrinder Spex Sample prep 2010, Instrument solutions, Nieuwegein, the Netherlands) for 10 minutes at 1250 rpm. Protein precipitation was performed by adding 1000  $\mu\text{L}$  acetonitrile to all reaction tubes. The samples were vortex mixed and centrifuged at 15,000 rpm for 5 minutes. Supernatant was transferred into clean 2.0 mL reaction tubes and was evaporated with nitrogen (40 °C). The samples were reconstituted with 100  $\mu\text{L}$  methanol-acetonitrile-water (1:1:2, v/v/v) before centrifuging for 5 minutes at 15,000 rpm. The clear supernatant was transferred into the 200  $\mu\text{L}$  insert of the autosampler vials for analysis.

#### 2.5 LC equipment and conditions

The chromatographic system used was a UPLC I-class pump with an inline degasser connected to an UPLC-LC I-class autosampler, set at 4 °C and I-class column oven (series, Waters corporation, Milford, MA, USA). Chromatographic separation was achieved using a Gemini C18 analytical column (Phenomenex, Torrance, CA, USA; 50 x 2.0 mm ID, 5  $\mu\text{m}$  particles). The column temperature was kept at 40 °C. The purge and strong wash solvent consisted of 0.1% formic acid in water-methanol (50:50, v/v). The mobile phase consisted of ammonium acetate in water (1 mM, pH 10.5)-acetonitrile (7:3, v/v, eluent A) and methanol (eluent B) with a flow rate of 0.4 mL/min. The pH of the ammonium acetate buffer in eluent A was adjusted to pH 10.5 with ammonia. The applied gradient program was 30% B (0-1.00 min), 30-45% B (1.00-2.50 min), 45% B (2.50-3.50 min), 45-30% (3.50-3.51 min), and 30% B (3.51-5.00 min).

## 2.6 MS equipment and conditions

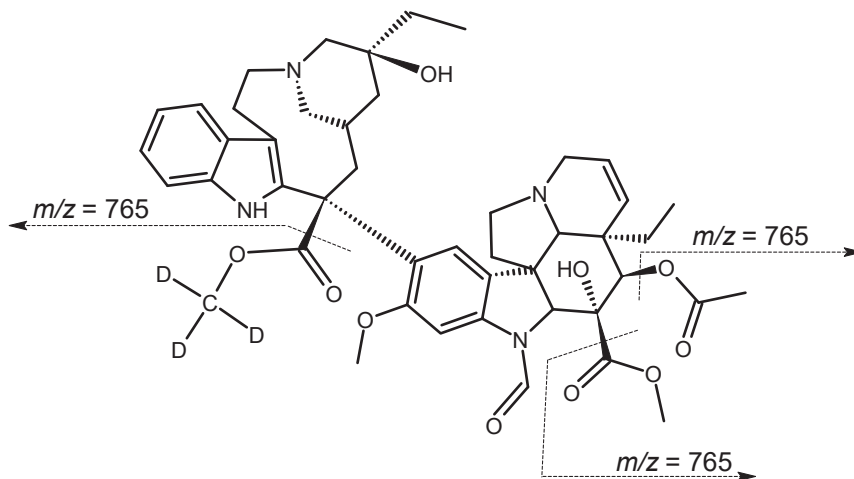
Detection was performed using a QTRAP5500 (Sciex, Framingham, MA, USA) with a turbo ionspray interface operating in positive ion method. Multiple reaction monitoring (MRM) was used to quantify vincristine  $[M+H]^+$  using the transitions of  $m/z$  825.2  $\rightarrow$  765.4 and deuterated vincristine (internal standard) with  $m/z$  828.2  $\rightarrow$  768.4. The proposed fragmentation pattern is depicted in Figure 1. MS operating parameters are summarised in Table 1. Data acquisition and processing were performed with Analyst<sup>TM</sup> software (Sciex, version 1.7.2.).

**Table 1.** Above: general mass spectrometric parameters. Below: Analyte specific mass spectrometric parameters for vincristine and  $^2[H]_3$ -vincristine.

Mass-spectrometer		
Run duration	5 min	
Ionspray voltage	5000 V	
Nebuliser gas	45 au	
Polarity	Positive	
Turbo gas/heater gas	60 au	
Curtain gas	30 au	
Collision gas	10 au	
Temperature	700 °C	
	Vincristine	$^2[H]_3$ -vincristine
MRM ( $m/z$ )	825.2 $\rightarrow$ 765.4	828.2 $\rightarrow$ 768.4
Collision energy (V)	51	53
Collision exit potential (V)	6	12
Declustering potential (V)	286	290
Entrance potential (V)	10	12
Dwell time (msec)	75	75

## 2.7 Validation procedures

The validation of the current method was based on the current FDA and EMA guidelines for bioanalytical method-validation [36,37]. Calibration model (linearity), LLOQ, accuracy and precision, carry-over, dilution integrity, matrix factor, haematocrit effect, endogenous interference, cross-analyte/internal standard interference, and stability were investigated.

**Vincristine: 825 [M+H]**

**Figure 1.** Chemical structure of vincristine including the proposed fragmentation. The position of the deuterium labelling is indicated with the letter D.

### 2.7.1. Calibration model and lower limited of quantification

Eight non-zero calibration standards ranging from 1 to 50 ng/mL were prepared in duplicate for each validation run. Linear regression was performed on the ratio of the analyte peak and the internal standard peak versus the nominal analyte concentration ( $x$ ) with a weighting factor of  $1/x^2$ . Deviations from the mean for each non-zero calibration standards should be within  $\pm 15\%$  ( $\pm 20\%$  for the LLOQ) for at least 75% of the non-zero standards. The LLOQ should have a signal-to-noise ratio of  $\geq 5:1$  compared to the single blank sample.

### 2.7.2 Accuracy and precision

Intra- and inter-assay accuracy and precision were determined by analysing five replicates of QC samples in three separate validation runs. The concentration levels were LLOQ (1 ng/mL), LOW (3 ng/mL), MID (20 ng/mL), and HIGH (40 ng/mL). The concentration of the QC samples was determined using the calibration standards prepared and analysed in the same analytical batch. Accuracy was defined as the bias from the nominal concentration and precision was defined as the coefficient of variation (CV %). Intra-assay bias was the bias of the mean measured concentration per analytical run compared to the nominal concentration. Inter-assay bias was the mean measured concentration in three analytical runs compared to the nominal concentration. The inter-run precision was calculated with a one-way ANOVA. The accuracy values should be within  $\pm 15\%$  ( $\pm 20\%$  at the LLOQ) and the precision values should be within  $\leq 15\%$  ( $\leq 20\%$  for the LLOQ).

### 2.7.3 Carry-over

Carry-over was investigated by injecting two double blank samples after the upper limit of quantification (ULOQ, 50 ng/mL) sample of the calibration standard. The peak areas at the retention times of the analyte and the internal standard in the double blank samples were compared to the mean area of the analyte and internal standard in five replicates of LLOQ samples. The peaks of the analyte and the internal standard found in the first double blank should be  $\leq 20\%$  and  $\leq 5\%$ , respectively.

### 2.7.4 Specificity and selectivity

Specificity and selectivity were evaluated in control human whole blood batches (haematocrit of 0.35) obtained from six different healthy volunteers. Co-eluting peaks at the retention time of the analyte and the internal standard from endogenous interferences were assessed in the double blank samples and compared to the QC MID samples. The peak areas present in the double blank samples should be  $\leq 15\%$  for the analyte and  $\leq 5\%$  for the internal samples. Bias of the QC MID samples should be  $\pm 15\%$  of the nominal concentration in at least 4 of 6 tested human whole blood batches.

Cross-analyte/internal standard interference was investigated by spiking the analyte at ULOQ level (50 ng/mL) and separately the internal standard at internal standard level. Interference of the analyte with the internal standard should be  $\leq 5\%$  of the peak area of the LLOQ samples. Interference of the internal standard with the analyte should be  $\leq 20\%$  of the LLOQ sample.

### 2.7.5 Matrix factor and sample preparation recovery

Matrix effect and recovery of the assay were determined using control human whole blood batches (haematocrit of 0.35) from three individuals at QC MID level (20 ng/mL). To successfully apply the current method to clinical practice, it is important to collect, spike and sample (with VAMS sampling devices) control human whole blood within one workday. Therefore, it was chosen to use three batches and one concentration level in these experiments. The absolute matrix factor was calculated as analyte or internal standard peak area between matrix present and matrix absent samples. The internal standard-normalised matrix factor was calculated as the ratio between the absolute matrix effect and the internal standard. The CV% of the internal standard-normalised matrix factor should be  $\leq 15\%$ . The sample preparation recovery was computed as the ratio between peak areas of the processed QC sample and spiked blank matrix sample.

### 2.7.6 Dilution integrity

Dilution integrity was determined by preparing >ULOQ samples (250 ng/mL, haematocrit 0.35) in 5-fold. After sample preparation, the final extract was diluted 20-fold with the final extract of single blank samples containing internal standard but no analyte. The accuracy and precision of the diluted samples should be  $\pm 15\%$  and  $\leq 15\%$ , respectively.

### 2.7.7 Haematocrit effect

The effect of haematocrit was investigated in a single batch of control human whole blood. Haematocrit was adjusted by adding red blood cells (to obtain a higher haematocrit value) or plasma (to obtain a lower haematocrit value) to a fixed volume of whole blood. Haematocrit was confirmed after adjustment. Whole blood was centrifuged for 10 minutes at 3,000 rpm to obtain red blood cells and plasma. The final haematocrit values were 0.25, 0.30, 0.35, 0.40, 0.50, and 0.60. The concentration of the samples was determined using the calibration standard prepared and measured in the same batch at a haematocrit of 0.35. Accuracy and precision of these samples should be  $\pm 15\%$  and  $\leq 15\%$ , respectively.

### 2.7.8 Stability

Long-term stability of vincristine in VAMS sampling devices was investigated. VAMS sampling devices were stored in Ziploc bags with desiccant in the dark at ambient temperature (21-22 °C) and in two climate cabinets at 25 °C and 40 °C with a relative humidity (RH) of 60% and 75%, respectively. Stability experiments were performed at QC MID level. Short and long-term stability of the stock solution has been described previously [27] and is at least 6 h at ambient temperature and 273 days at -70 °C. The acceptance criteria for the accuracy and precision of the long-term storage of QC samples were  $\pm 15\%$  bias and  $\leq 15\%$  CV.

## 2.8 Clinical application

Whole blood was obtained from paediatric patients treated with vincristine using VAMS 10  $\mu\text{L}$  sampling devices. The paediatric patients (0-17 years old) were included in a clinical trial performed at the Princess Máxima Center (Utrecht, The Netherlands). The study was conducted in accordance with the Declaration of Helsinki and the study protocol was approved by the medical ethics committee of Erasmus Medical Center (Rotterdam, The Netherlands). The study was registered in the Dutch trial register (NL63037.078.18). Vincristine was administered according to standard of care with a dose of 1.5-2  $\text{mg}/\text{m}^2$  (max 2 mg). Whole blood samples were collected from a central venous line. For 7 patients, 10  $\mu\text{L}$  whole blood was collected with VAMS sampling devices prior to centrifuging. After centrifuging the

samples, plasma was collected and stored at  $-80\text{ }^{\circ}\text{C}$  until analysis. A previously validated LC-MS/MS method was used for the quantification of vincristine in plasma samples [27]. In short, liquid-liquid extraction was performed with tert-butyl methyl ether (TBME). Subsequently, samples were snap frozen and the supernatant collected. The samples were dried under a gentle stream of nitrogen ( $40\text{ }^{\circ}\text{C}$ ) and reconstituted with methanol-acetonitrile-water (1:1:2, v/v/v). Separation was obtained with a gradient using ammonium acetate in water (1 mM, pH 10.5)-acetonitrile (7:3, v/v, eluent A) and methanol (eluent B), a flow rate of 0.4 mL/min., and a reversed phase C18 column (Waters Xbridge 50 x 2.1 mm ID, 5  $\mu\text{m}$  particles). Detection was performed using a API4000 (Sciex, Framingham, MA, USA) with a turbo ion spray interface operating in positive ion mode and MRM was used to quantify vincristine concentrations. Deuterated vincristine was used as internal standards. The LLOQ of the bioanalytical method was 0.1 ng/mL with the intra- and inter-assay bias and precisions were within  $\pm 12.4\%$  and  $\leq 10.6\%$ , respectively. The relationship between vincristine plasma concentrations and vincristine whole blood concentrations was investigated.

## 3 RESULTS AND DISCUSSION

### 3.1 Development

#### 3.1.1 Sample preparation

The challenge of the current method was to achieve the desired LLOQ of 1 ng/mL with a limited sample volume (10  $\mu$ L whole blood). Maximal recovery of vincristine from the VAMS sampling devices was of utmost importance to achieve the desired sensitivity. Therefore, the focus of the sample preparation was the optimisation of the recovery. The initial sample preparation was a previously published method for the bioanalysis of vincristine in dried blood spots [31]. This method extracts vincristine from the dried blood spot with acetonitrile-methanol-water (1:1:1, v/v/v) before sonication of the samples for 15 minutes. The samples were centrifuged, and the clear extract was transferred to a glass autosampler [31]. While this method was able to quantify vincristine from dried blood spots with a LLOQ of 1 ng/mL, this sensitivity could not be achieved with VAMS sampling devices. Therefore, different extraction solvents were investigated: Ethanol, Tert-Butyl Methyl Ether (TBME), methanol-acetonitrile-water (1:1:2, v/v/v), 0.5 M phosphoric acid and TBME, methanol, and 0.2% formic acid in water. The latter resulted in the highest signal-to-noise ratio and thus recovery of the analyte and internal standard.

Additionally, we compared extraction using sonication to using a genogrinder. The hypothesis was that the genogrinder would result in a higher signal due to the pressing force of the grinding beads on the VAMS sponge. Samples processed with the genogrinder resulted in a modest increase in signal, however, demonstrated less variability when compared to sonication. Therefore, the genogrinder was preferred over sonication. Increasing the extraction time of the samples in the genogrinder did not improve the signal-to-noise ratio and 10 min at 1250 rpm was found to be optimal.

To increase sensitivity of the method, a concentrating step was introduced in the sample preparation. Evaporation with nitrogen (40 °C) and reconstitution with methanol-acetonitrile-water (1:1:2, v/v/v) was chosen because it was an effective method for increasing the sensitivity of the bioanalysis method for vincristine in human plasma [27]. Due to the above-described evaporation step, a LLOQ of 1 ng/mL was achieved. A protein precipitation step was included after the extraction step to reduce the noise and therefore enhance the signal-to-noise ratio. Acetonitrile was chosen as the precipitation solvent and a LLOQ



level of 1 ng/mL was achieved with acceptable accuracy and precision. While the final sample preparation was relatively more complex than the previously published plasma methods [24-29], all the steps in the sample preparation were necessary to obtain the desired LLOQ.

### 3.1.2 Chromatography and mass spectrometry

Optimisation of the chromatography and mass spectrometry was crucial to achieve the desired LLOQ of 1 ng/mL with the small sample volume of 10  $\mu$ L. Furthermore, linearity was desired up to a concentration of 50 ng/mL to support a future pharmacokinetic study where VAMS samples will be collected at 1, 1.5, and 4 hours after vincristine administration. A previously published method for the quantification of vincristine in VAMS in mice whole blood reported an ULOQ of 1200 ng/mL [38]. However, regarding human pharmacokinetics of vincristine, an ULOQ of 50 ng/mL was deemed suitable to quantify VAMS samples collected at the above-described time points [35]. In literature, acidic and alkaline environments have been described for the chromatography of vincristine [24,39]. Both environments were investigated to determine the optimal chromatography system with the highest signal-to-noise ratio.

The mobile phase of the acidic environment consisted of 0.2% formic acid in water (Eluent A) and methanol (Eluent B) [39]. In this environment, the signal of the double charged parent ion ( $m/z$  413) was optimal compared to the mono charged molecular ion ( $m/z$  825). However, monitoring of the bivalent molecule ion resulted in a high offset which reduced the signal-to-noise ratio significantly. Different combinations of 0.2% formic acid with methanol for Eluent A were investigated. However, the high offset remained which caused a reduction in the sensitivity and reproducibility of the bioanalytical method.

For the alkaline conditions, ammonium acetate (1 mM, pH 10.5)-acetonitrile (7:3, v/v) was used as Eluent A and methanol as Eluent B. The ammonium acetate buffer was adjusted to a pH 10.5 with ammonia. With this chromatographic system, the molecule ion with a  $m/z$  of 825 was detected with the highest relative abundance and the transition of  $m/z$  825  $\rightarrow$  765 resulted in the lowest offset and the highest signal-to-noise ratio and was therefore further optimized. A qualifier ion was not included in the method. The current presented method will be used to support a future pharmacokinetic trial. VAMS collected during the study will contain vincristine and co-administration of other drugs will be closely monitored and registered. Due to the high mass and unique molecular structure

of vincristine (Figure 1), inclusion of a qualifier ion was deemed unnecessary. The alkaline environment had the preference over the acidic environment due to a superior signal-to-noise ratio and a decrease in signal variability.

## 3.2 Validation procedures

### 3.2.1 Calibration model

The method was linear over a concentration range of 1 to 50 ng/mL. The linear regression of ratio of the peak area of the analyte and internal standard versus the concentration was weighted with  $1/x^2$  (the reciprocal of the squared concentration) to obtain the minimum total bias and the most constant bias across the range. A linear fit ( $R^2 \geq 0.998$ ) was obtained in all validation runs. The back-calculated concentrations had a bias of  $\pm 2.9\%$  and a precision of  $\leq 8.1\%$  for all calibration levels. The LLOQ was established at 1 ng/mL with a minimum signal-to-noise ratios of 5.7:1, 5.5:1, and 5.0:1 for the three different validation runs, respectively, which met the acceptance criteria. Representative chromatograms of double blank, single blank, LLOQ and ULOQ are depicted in Figure 2.

### 3.2.2 Accuracy and precision

The accuracy and precision data are given in Table 2. The intra- and inter-assay bias was  $\pm 10.9\%$  and  $\pm 9.6\%$  over all concentration levels, respectively. Intra- and inter-assay precision was  $\leq 7.3\%$  and  $\leq 2.7\%$  over all concentration levels, respectively. Therefore, the accuracy and precision data met the acceptance criteria.

**Table 2.** Assay performance data for vincristine.

Nominal vincristine concentration (ng/mL)	Intra-assay (n=15)		Inter-assay (n=15)	
	Bias (%)	Precision (%)	Bias (%)	Precision (%)
1	2.2-9.4	$\leq 7.3$	6.3	2.7
3	7.6-9.9	$\leq 3.6$	8.6	*
20	0.3-4.9	$\leq 4.3$	2.7	1.7
40	-0.3-2.9	$\leq 5.2$	0.9	*

\* No additional variation was found by performing the assay between days (mean square between groups is less than mean square within groups).

### 3.2.3 Carry-over

Carry-over was investigated by comparing the peak area present in the first double blank sample following an ULOQ sample to the mean peak area of LLOQ samples in five-fold. The carry-over in three validation runs was  $\leq 3.7\%$  for vincristine and  $\leq 0.1\%$  for the internal standard, which is within the acceptance criteria of  $\leq 20\%$ .

### 3.2.4 Specificity and selectivity

Selectivity was determined in six individual human whole blood batches at the blank and LLOQ levels. There was no interference at the retention times of vincristine and the internal standard. The accuracy of vincristine at the QC MID level was also established for all six whole blood batches of which five had a deviation of  $\leq 13.5\%$  and one sample a deviation of  $\leq 16.5\%$  compared to the nominal concentration. Vincristine at ULOQ level did not show any interference with the internal standard and the internal standard did not show any interference with vincristine. Therefore, the acceptance criteria of specificity and selectivity were met.

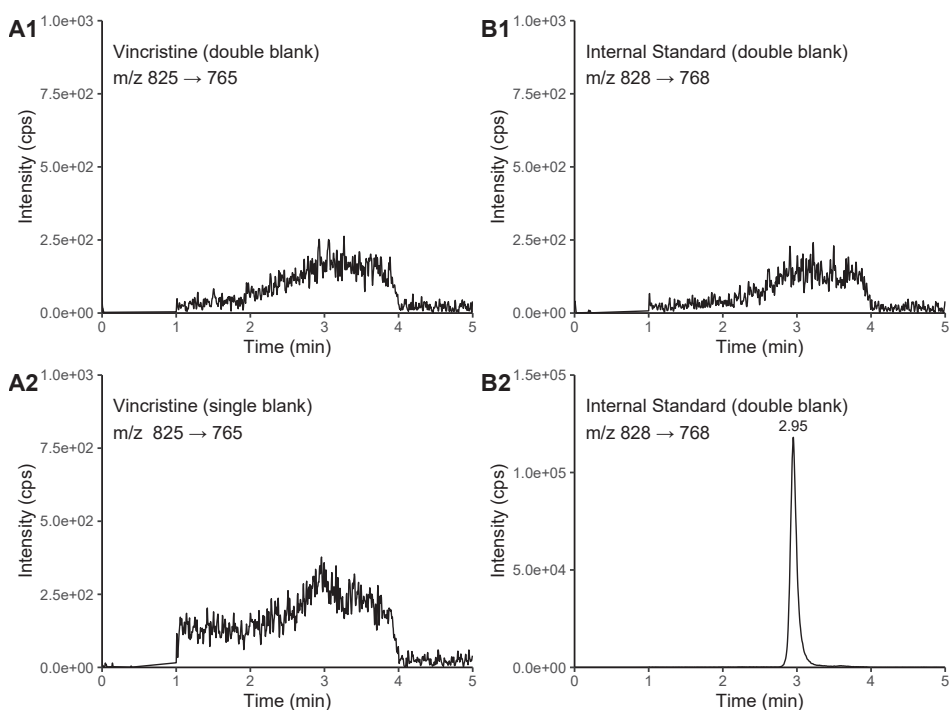


**Figure 2.** Representative LC-MS/MS chromatograms of vincristine (A-series) and the internal standard (B-series). The vincristine concentration at LLOQ and ULOQ level is 1 ng/mL and 50 ng/mL, respectively.

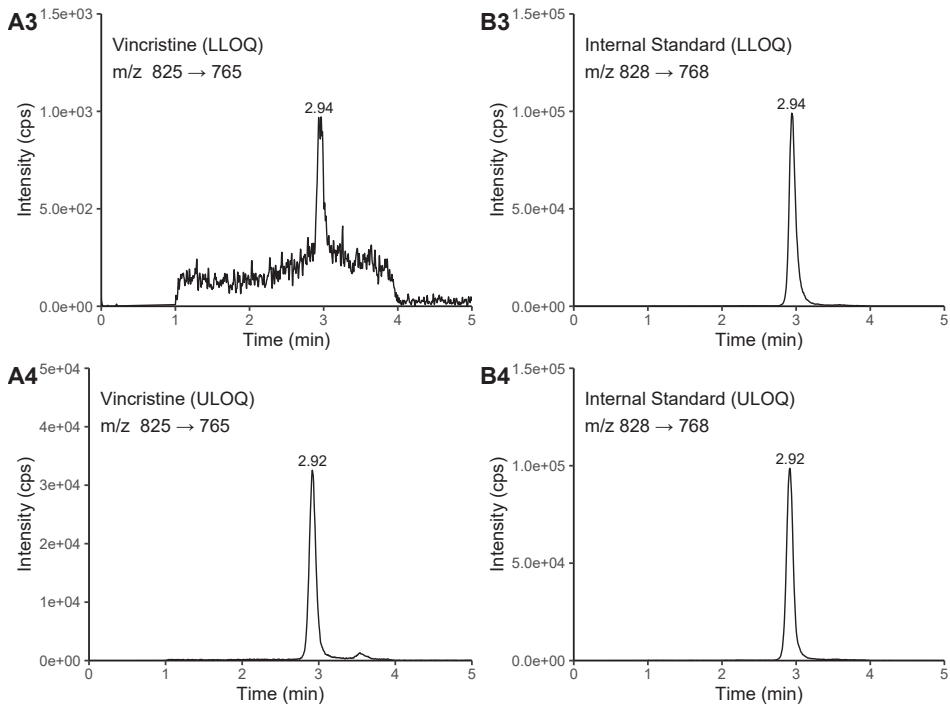


**Figure 2.** Continued

### 3.2.5 Matrix effect and recovery

The matrix factor of vincristine and the internal standard were 0.38 and 0.33, respectively. This resulted in the internal standard-normalised matrix factor of 1.15 with a CV% of 0.87. This met the acceptance criteria of  $\leq 15\%$ . The sample preparation recovery at QC MID was 71.8%. The recovery could not be improved by increasing the retention time but resulted in the loss of sensitivity due to a decrease in in signal-to-noise ratio.

### 3.2.6 Dilution integrity

Final extractions of samples  $>ULOQ$  were diluted 20-fold with the final extractions of single blank samples. The intra-assay bias and precision for the diluted samples were  $\pm 5.8\%$  and  $\leq 13.4\%$ , respectively. Therefore, it can be concluded at samples with a concentration  $>ULOQ$  can be diluted 20-fold.

### 3.2.7 Haematocrit effect

Haematocrit effect was determined in triplicate in a range of haematocrit values (0.25-0.60). The data is presented in Table 3. The back-calculated concentrations had an accuracy of  $\pm 8.7\%$  and a precision of  $\leq 7.9\%$  and therefore met the acceptance criteria. Vincristine in whole blood collected with VAMS sampling devices can thus be quantified over a wide range of haematocrit values from 0.25 to 0.60.

**Table 3.** Haematocrit effect on assay performance (n=3).

Haematocrit (%)	Nominal vincristine concentration (ng/mL)	Mean measured vincristine concentration (ng/mL)	Bias (%)	Precision (%)
0.25	26.0	25.3	6.4	-2.7
0.30	26.0	23.9	-7.9	1.1
0.35	26.0	27.2	4.6	7.9
0.40	26.0	25.4	-2.4	1.5
0.50	26.0	27.1	4.1	3.2
0.60	26.0	28.3	8.7	2.8

### 3.2.8 Stability

The stability of vincristine in whole blood collected with VAMS sampling devices was investigated under various conditions (see Table 4). Vincristine in whole blood collected with VAMS was stable for 3 months at ambient temperatures and 1 month at 25 °C (RH 60%) and unstable at 1 week at 40 °C (RH 75%). The effect of temperature on the long-term stability of the samples could be caused by thermo-dependent degradation of vincristine or reduced recovery of vincristine from the VAMS sampling devices stored at higher temperatures. Differences in relative humidity could potentially explain the difference in stability between storage conditions at ambient temperatures and at 25 °C (RH 60%). The stability data demonstrated the importance of consistent storage conditions of VAMS samples. Stability remained a problem for long term storage. Therefore, it is recommended to store VAMS samples in Ziploc bags with desiccant in the dark at ambient temperature and analyse them within 3 months after collection. The stability was not a problem for the clinical application of this method, since the samples of the future pharmacokinetic study will be quantified and reported within one week after collection.

**Table 4:** Stability parameters for vincristine (n=3).

Matrix	Nominal concentration (ng/mL)	Conditions	Bias (%)	C.V. (%)	N
VAMS	20	3 months, ambient temperature	-14.2	5.2	3
		6 months, ambient temperature	-33.5	1.4	3
		1 month, 25°C (HR 60%)	-6.5	5.6	3
		3 months, 25 °C (HR 60%)	-24.6	3.7	3
		1 week, 40 °C (HR 75%)	-32.2	8.1	3
		1 month, 40 °C (HR 75%)	-45.0	4.0	3
		3 months, 40 °C (HR 75%)	-60.9	1.9	3

Abbreviation: HR = relative humidity, VAMS = volumetric absorptive microsampling.

### 3.3 Clinical application

The currently described method was able to quantify vincristine in whole blood from the VAMS sampling devices. The measured vincristine concentrations had a range of 1.27 to 242 ng/mL for whole blood and 0.129 to 247 ng/mL for plasma. A total of 9 samples were <LLOQ of which 5 were VAMS samples and 4 were plasma samples. These samples were either collected a long time after administration (>50 hours) or just before administration. The plasma sample with a concentration of 0.129 ng/mL was excluded from the data analysis, because the corresponding VAMS sample was <LLOQ. In total 21 complete sample pairs with a range of 1-6 sample pairs per patient were included in the study. A representative chromatogram of a patient sample is depicted in Figure 3.

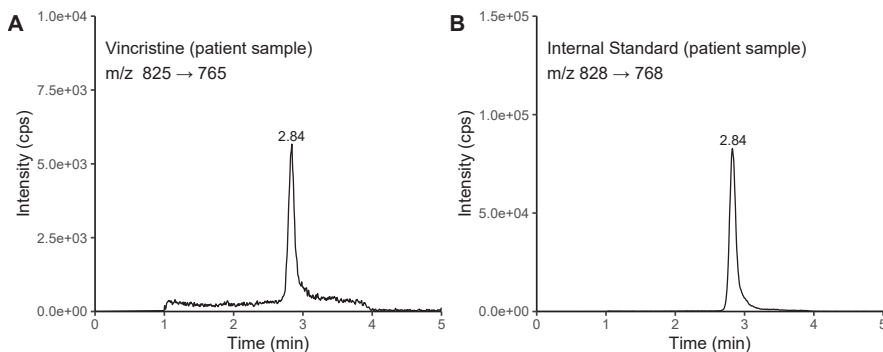


**Figure 3.** Representative LC-MS/MS chromatogram of a clinical sample of one patient. A, vincristine at a quantified concentration of 7.56 ng/mL. B, the internal standard. The patient received 1.5-2 mg/m<sup>2</sup> vincristine intravenously and the sample was collected 2 hours and 50 minutes after administration.

The relationship between vincristine concentrations in whole blood and plasma demonstrated non-linearity (See Figure 4A-B). The current observed non-linearity between whole blood and plasma vincristine concentrations differentiated from the previously reported linear correlation between vincristine whole blood and plasma concentrations [38]. This discrepancy was attributed to two differences in study design. Firstly, Rosser., *et al* (2022) quantified vincristine in murine whole blood while the current study quantified vincristine in human whole blood [38]. Secondly, Rosser., *et al* (2022) performed an *ex vivo* experiment in which the whole blood and plasma samples were spiked with vincristine [38]. In the current study, whole blood and plasma samples collected from paediatric oncology patients were quantified. The currently observed non-linearity was observed in the difference between whole blood and plasma concentrations which deviated over the measured concentration range (Figure 4G) demonstrating relatively high whole blood concentrations at low plasma concentrations. To describe the relationship between vincristine whole blood and plasma concentrations a saturable binding equilibrium model was fitted to the data (Equation 1 and 2).

$$C_b = \frac{B_{max} \times C_p}{C_p + K_d} \quad (\text{Equation 1})$$

$$C_{wb} = C_b \times HTC + C_p \times (1 - HTC) \quad (\text{Equation 2})$$

In these equations,  $C_b$  is the bound vincristine concentration to blood cells,  $B_{max}$  is the maximal binding capacity to blood cells,  $C_p$  the vincristine plasma concentration,  $K_d$  is the equilibrium dissociation constant,  $C_{wb}$  vincristine concentration in whole blood, and  $HTC$  the haematocrit. The estimation of the  $B_{max}$  and  $K_d$  were 243 ng/mL and 21.4 ng/mL, respectively. This indicates that bound vincristine was half-maximal at a plasma concentration of 21.4 ng/mL. The saturable binding equilibrium model was able to describe the general trend in the data (Figure 4C-F). However, large variability in the data as well as the bias in the weighted residuals remained unexplained. Therefore, whole blood concentrations cannot be extrapolated to plasma concentrations. The saturable binding of vincristine in whole blood could be explained by vincristine's binding to blood cells (e.g., thrombocytes or erythrocytes). *In vitro* and *in vivo* studies have reported extensive binding of vinca-alkaloids including vincristine to thrombocytes [40-44]. Furthermore, a clinical pharmacokinetic trial in adults reported decreased vincristine plasma exposure in patients with higher thrombocyte levels [45]. A future pilot pharmacokinetic trial in Kenyan paediatric patients will study the implementation of finger prick sampling and while the blood distribution of vincristine will be studied in a future *in vitro* blood distribution study.

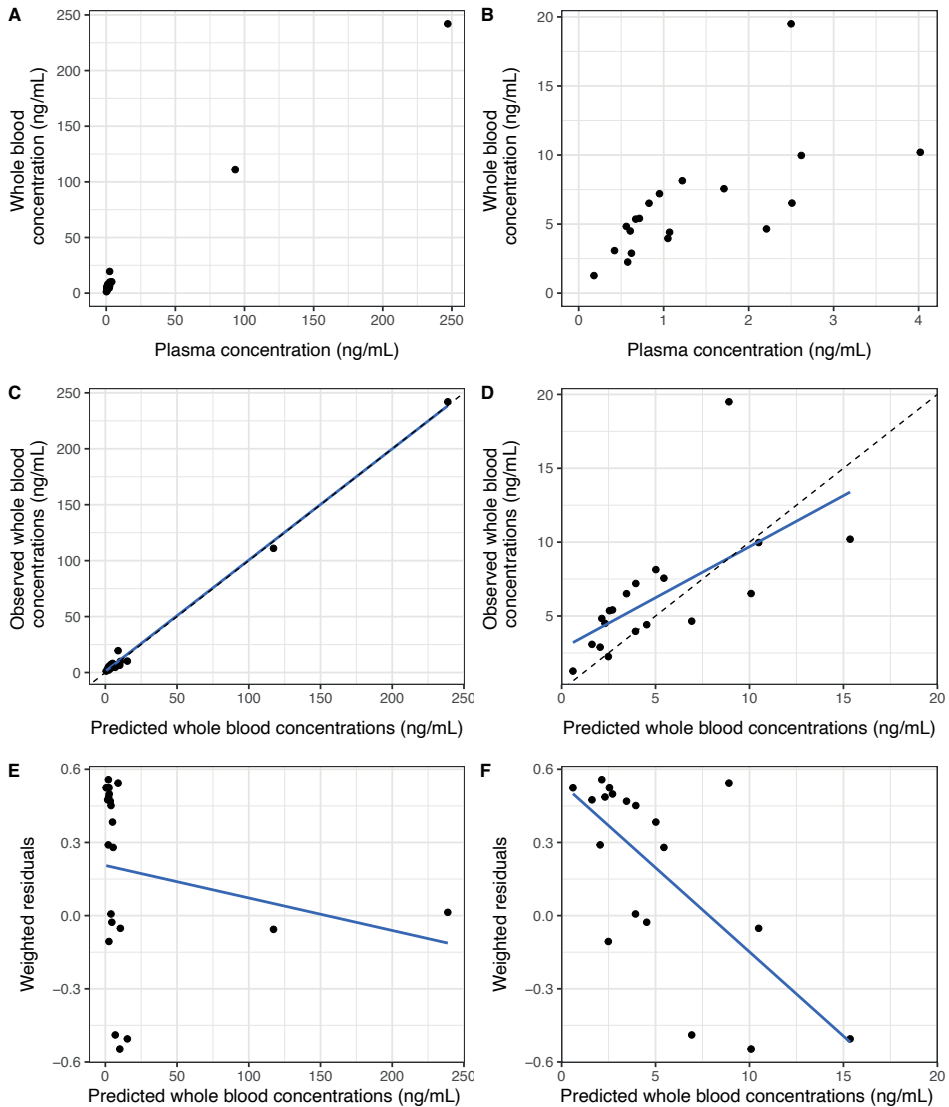


**Figure 4.** Vincristine concentrations in human whole blood and human plasma. A, Plasma concentrations versus whole blood concentrations. B, Plasma concentrations versus whole blood concentrations zoomed in. C, Predicted versus observed whole blood concentrations with saturable distribution kinetics. D, Predicted versus observed whole blood concentrations zoomed in. E, Predicted whole blood concentrations versus the weighted residuals. F, Predicted whole blood concentrations versus the weight residuals zoomed in. The blue dashed line represents the trend in the data, and the black dashed line represent the line of unity where prediction equals observation. The black dots are the individual measurements.



## 4 CONCLUSION

A sensitive bioanalytical method for the quantification of vincristine in whole blood collected with VAMS sampling devices was developed and validated. The validated range was from 1 to 50 ng/mL using a stable isotope with an accuracy  $\pm 10.9\%$  and precision of  $\leq 7.3\%$ . To our knowledge this is the first bioanalytical method for the quantification of vincristine in whole blood collected with VAMS sampling devices. The method has been successfully used to quantify patient samples. The relationship between vincristine whole blood concentrations and plasma concentrations was found to be non-linear. Future research should further investigate the implementation of finger prick sampling and the blood distribution of vincristine.

## REFERENCES

1. Rowinsky EK, Donehower RC (1991) The clinical pharmacology and use of antimicrotubule agents in cancer chemotherapeutics. *Pharmacol Ther* 52 (1):35-84. doi:10.1016/0163-7258(91)90086-2
2. Coccia PF, Altman J, Bhatia S, Borinstein SC, Flynn J, George S, Goldsby R, Hayashi R, Huang MS, Johnson RH, Beaupin LK, Link MP, Oeffinger KC, Orr KM, Pappo AS, Reed D, Spraker HL, Thomas DA, von Mehren M, Wechsler DS, Whelan KF, Zebrack BJ, Sundar H, Shead DA (2012) Adolescent and young adult oncology. Clinical practice guidelines in oncology. *J Natl Compr Canc Netw* 10 (9):1112-1150. doi:10.6004/jnccn.2012.0117
3. Stryckmans PA, Lurie PM, Manaster J, Vamecq G (1973) Mode of action of chemotherapy in vivo on human acute leukemia--II. Vincristine. *Eur J Cancer* 9 (9):613-620. doi:10.1016/0014-2964(73)90002-9
4. Teva Summary of product characteristics: Vincristine sulphate (NL). (2020).at <[https://www.geneesmiddeleninformatiebank.nl/smpc/h100081\\_smpc.pdf](https://www.geneesmiddeleninformatiebank.nl/smpc/h100081_smpc.pdf)>.
5. Zhou XJ, Rahmani R (1992) Preclinical and clinical pharmacology of vinca alkaloids. *Drugs* 44 Suppl 4:1-16; discussion 66-19. doi:10.2165/00003495-199200444-00002
6. van de Velde ME, Panetta JC, Wilhelm AJ, van den Berg MH, van der Sluis IM, van den Bos C, Abbink FCH, van den Heuvel-Eibrink MM, Segers H, Chantrain C, van der Werff Ten Bosch J, Willems L, Evans WE, Kaspers GL (2020) Population Pharmacokinetics of Vincristine Related to Infusion Duration and Peripheral Neuropathy in Pediatric Oncology Patients. *Cancers (Basel)* 12 (7). doi:10.3390/cancers12071789
7. Igarashi T, Kishi S, Hosono N, Higashi T, Iwao T, Yano R, Tsukamoto H, Goto N, Yamauchi T, Ueda T (2021) Population pharmacokinetic model development and exposure-response analysis of vincristine in patients with malignant lymphoma. *Cancer Chemother Pharmacol* 87 (4):501-511. doi:10.1007/s00280-020-04220-y
8. Gidding CE, Meeuwssen-de Boer GJ, Koopmans P, Uges DR, Kamps WA, de Graaf SS (1999) Vincristine pharmacokinetics after repetitive dosing in children. *Cancer Chemother Pharmacol* 44 (3):203-209. doi:10.1007/s002800050968
9. Anghelescu DL, Faughnan LG, Jeha S, Relling MV, Hinds PS, Sandlund JT, Cheng C, Pei D, Hankins G, Pauley JL, Pui CH (2011) Neuropathic pain during treatment for childhood acute lymphoblastic leukemia. *Pediatr Blood Cancer* 57 (7):1147-1153. doi:10.1002/pbc.23039
10. Frost BM, Lönnerholm G, Koopmans P, Abrahamsson J, Behrendtz M, Castor A, Forestier E, Uges DR, de Graaf SS (2003) Vincristine in childhood leukaemia: no pharmacokinetic rationale for dose reduction in adolescents. *Acta Paediatr* 92 (5):551-557
11. Guilhaumou R, Simon N, Quaranta S, Verschuur A, Lacarelle B, Andre N, Solas C (2011) Population pharmacokinetics and pharmacogenetics of vincristine in paediatric patients treated for solid tumour diseases. *Cancer Chemother Pharmacol* 68 (5):1191-1198. doi:10.1007/s00280-010-1541-4
12. Moore AS, Norris R, Price G, Nguyen T, Ni M, George R, van Breda K, Duley J, Charles B, Pinkerton R (2011) Vincristine pharmacodynamics and pharmacogenetics in children with cancer: a limited-sampling, population modelling approach. *J Paediatr Child Health* 47 (12):875-882. doi:10.1111/j.1440-1754.2011.02103.x

13. Barnett S, Kong J, Makin G, Veal GJ (2021) Over a decade of experience with carboplatin therapeutic drug monitoring in a childhood cancer setting in the United Kingdom. *Br J Clin Pharmacol* 87 (2):256-262. doi:10.1111/bcp.14419
14. Crom WR, de Graaf SS, Synold T, Uges DR, Bloemhof H, Rivera G, Christensen ML, Mahmoud H, Evans WE (1994) Pharmacokinetics of vincristine in children and adolescents with acute lymphocytic leukemia. *J Pediatr* 125 (4):642-649. doi:10.1016/s0022-3476(94)70027-3
15. de Graaf SS, Bloemhof H, Vendrig DE, Uges DR (1995) Vincristine disposition in children with acute lymphoblastic leukemia. *Med Pediatr Oncol* 24 (4):235-240. doi:10.1002/mpo.2950240405
16. Groninger E, Meeuwssen-de Boer T, Koopmans P, Uges D, Sluiter W, Veerman A, Kamps W, de Graaf S (2002) Pharmacokinetics of vincristine monotherapy in childhood acute lymphoblastic leukemia. *Pediatr Res* 52 (1):113-118. doi:10.1203/00006450-200207000-00021
17. Plasschaert SL, Groninger E, Boezen M, Kema I, de Vries EG, Uges D, Veerman AJ, Kamps WA, Vellenga E, de Graaf SS, de Bont ES (2004) Influence of functional polymorphisms of the MDR1 gene on vincristine pharmacokinetics in childhood acute lymphoblastic leukemia. *Clin Pharmacol Ther* 76 (3):220-229. doi:10.1016/j.clpt.2004.05.007
18. Groninger E, Meeuwssen-de Boer T, Koopmans P, Uges D, Sluiter W, Veerman A, Kamps W, de Graaf S (2005) Vincristine pharmacokinetics and response to vincristine monotherapy in an up-front window study of the Dutch Childhood Leukaemia Study Group (DCLSG). *Eur J Cancer* 41 (1):98-103. doi:10.1016/j.ejca.2004.10.006
19. van de Velde ME, Kaspers GL, Abbink FCH, Wilhelm AJ, Ket JCF, van den Berg MH (2017) Vincristine-induced peripheral neuropathy in children with cancer: A systematic review. *Crit Rev Oncol Hematol* 114:114-130. doi:10.1016/j.critrevonc.2017.04.004
20. Diouf B, Crews KR, Lew G, Pei D, Cheng C, Bao J, Zheng JJ, Yang W, Fan Y, Wheeler HE, Wing C, Delaney SM, Komatsu M, Paugh SW, McCorkle JR, Lu X, Winick NJ, Carroll WL, Loh ML, Hunger SP, Devidas M, Pui CH, Dolan ME, Relling MV, Evans WE (2015) Association of an inherited genetic variant with vincristine-related peripheral neuropathy in children with acute lymphoblastic leukemia. *Jama* 313 (8):815-823. doi:10.1001/jama.2015.0894
21. Skiles JL, Chiang C, Li CH, Martin S, Smith EL, Olbara G, Jones DR, Vik TA, Mostert S, Abbink F, Kaspers GJ, Li L, Njuguna F, Sajdyk TJ, Renbarger JL (2018) CYP3A5 genotype and its impact on vincristine pharmacokinetics and development of neuropathy in Kenyan children with cancer. *Pediatr Blood Cancer* 65 (3). doi:10.1002/pbc.26854
22. Jemal A, Thomas A, Murray T, Thun M (2002) Cancer statistics, 2002. *CA Cancer J Clin* 52 (1):23-47. doi:10.3322/canjclin.52.1.23
23. Pollock BH, DeBaun MR, Camitta BM, Shuster JJ, Ravindranath Y, Pullen DJ, Land VJ, Mahoney DH, Jr., Lauer SJ, Murphy SB (2000) Racial differences in the survival of childhood B-precursor acute lymphoblastic leukemia: a Pediatric Oncology Group Study. *J Clin Oncol* 18 (4):813-823. doi:10.1200/jco.2000.18.4.813

24. Damen CW, Israëls T, Caron HN, Schellens JH, Rosing H, Beijnen JH (2009) Validated assay for the simultaneous quantification of total vincristine and actinomycin-D concentrations in human EDTA plasma and of vincristine concentrations in human plasma ultrafiltrate by high-performance liquid chromatography coupled with tandem mass spectrometry. *Rapid Commun Mass Spectrom* 23 (6):763-774. doi:10.1002/rcm.3938
25. Corona G, Casetta B, Sandron S, Vaccher E, Toffoli G (2008) Rapid and sensitive analysis of vincristine in human plasma using on-line extraction combined with liquid chromatography/tandem mass spectrometry. *Rapid Commun Mass Spectrom* 22 (4):519-525. doi:10.1002/rcm.3390
26. Dennison JB, Renbarger JL, Walterhouse DO, Jones DR, Hall SD (2008) Quantification of vincristine and its major metabolite in human plasma by high-performance liquid chromatography/tandem mass spectrometry. *Ther Drug Monit* 30 (3):357-364. doi:10.1097/FTD.0b013e31816b92c9
27. van der Heijden LT, Gebretensae A, Thijssen B, van An del L, Nijstad AL, Wang Y, Rosing H, Huitema ADR, Beijnen JH (2022) A highly sensitive bioanalytical method for the quantification of vinblastine, vincristine, vinorelbine and 4-O-deacetylvinorelbine in human plasma using LC-MS/MS. *J Pharm Biomed Anal* 215:114772. doi:10.1016/j.jpba.2022.114772
28. Guilhaumou R, Solas C, Rome A, Giocanti M, Andre N, Lacarelle B (2010) Validation of an electrospray ionization LC/MS/MS method for quantitative analysis of vincristine in human plasma samples. *J Chromatogr B Analyt Technol Biomed Life Sci* 878 (3-4):423-427. doi:10.1016/j.jchromb.2009.12.015
29. Skolnik JM, Barrett JS, Shi H, Adamson PC (2006) A liquid chromatography-tandem mass spectrometry method for the simultaneous quantification of actinomycin-D and vincristine in children with cancer. *Cancer Chemother Pharmacol* 57 (4):458-464. doi:10.1007/s00280-005-0065-9
30. Agu L, Skiles JL, Masters AR, Renbarger JL, Chow DS (2021) Simultaneous quantification of vincristine and its major M1 metabolite from dried blood spot samples of Kenyan pediatric cancer patients by UPLC-MS/MS. *J Pharm Biomed Anal* 203:114143. doi:10.1016/j.jpba.2021.114143
31. Damen CW, Rosing H, Schellens JH, Beijnen JH (2009) Application of dried blood spots combined with high-performance liquid chromatography coupled with electrospray ionisation tandem mass spectrometry for simultaneous quantification of vincristine and actinomycin-D. *Analytical and bioanalytical chemistry* 394 (4):1171-1182. doi:10.1007/s00216-009-2775-z
32. Zhang J, Majumdar TK, Flarakos J, Tse FLS (2013) Best Practices in LC-MS Method Development and Validation for Dried Blood Spots. In: *Handbook of LC-MS Bioanalysis*. pp 379-389. doi:https://doi.org/10.1002/9781118671276.ch30
33. Ye Z, Gao H (2017) Evaluation of sample extraction methods for minimizing hematocrit effect on whole blood analysis with volumetric absorptive microsampling. *Bioanalysis* 9 (4):349-357. doi:10.4155/bio-2015-0028
34. Kip AE, Kiers KC, Rosing H, Schellens JHM, Beijnen JH, Dorlo TPC (2017) Volumetric absorptive microsampling (VAMS) as an alternative to conventional dried blood spots in the quantification of miltefosine in dried blood samples. *J Pharm Biomed Anal* 135:160-166. doi:10.1016/j.jpba.2016.12.012

35. Nijstad AL, Chu WY, de Vos-Kerkhof E, Enters-Weijnen CF, van de Velde ME, Kaspers GJL, Barnett S, Veal GJ, Lalmohamed A, Zwaan CM, Huitema ADR (2022) A Population Pharmacokinetic Modelling Approach to Unravel the Complex Pharmacokinetics of Vincristine in Children. *Pharm Res* 39 (10):2487-2495. doi:10.1007/s11095-022-03364-1
36. Agency EEM (2011) Guideline on Bioanalytical Method Validation. Committee for Medicinal Products for Human Use and European Medicines Agency. Accessed 8 May 2022
37. Administration FFaD (2018) Bioanalytical Method Validation. Silver Springs, Maryland: US Food and Drug Administration. Accessed 9 May 2022
38. Rosser SPA, Atkinson C, Nath CE, Fletcher JI (2022) Quantification of vincristine and tariquidar by liquid chromatography-tandem mass spectrometry in mouse whole blood using volumetric absorptive microsampling for pharmacokinetic applications. *J Sep Sci* 45 (14):2508-2519. doi:10.1002/jssc.202101013
39. Yang F, Wang H, Liu M, Hu P, Jiang J (2013) Determination of free and total vincristine in human plasma after intravenous administration of vincristine sulfate liposome injection using ultra-high performance liquid chromatography tandem mass spectrometry. *J Chromatogr A* 1275:61-69. doi:10.1016/j.chroma.2012.12.026
40. Secret CJ, Hadfield JR, Beer CT (1972) Studies on the binding of (<sup>3</sup>H)vinblastine by rat blood platelets in vitro. Effects of colchicine and vincristine. *Biochem Pharmacol* 21 (11):1609-1624. doi:10.1016/0006-2952(72)90311-5
41. Leandro-García LJ, Leskelä S, Inglada-Pérez L, Landa I, de Cubas AA, Maliszewska A, Comino-Méndez I, Letón R, Gómez-Graña Á, Torres R, Ramírez JC, Álvarez S, Rivera J, Martínez C, Lozano ML, Cascón A, Robledo M, Rodríguez-Antona C (2012) Hematologic  $\beta$ -tubulin VI isoform exhibits genetic variability that influences paclitaxel toxicity. *Cancer Res* 72 (18):4744-4752. doi:10.1158/0008-5472.Can-11-2861
42. Gout PW, Wijcik LL, Beer CT (1978) Differences between vinblastine and vincristine in distribution in the blood of rats and binding by platelets and malignant cells. *Eur J Cancer* 14 (11):1167-1178. doi:10.1016/0014-2964(78)90222-0
43. Urien S, Brée F, Breillout F, Bastian G, Krikorian A, Tillement JP (1993) Vinorelbine high-affinity binding to human platelets and lymphocytes: distribution in human blood. *Cancer Chemother Pharmacol* 32 (3):231-234. doi:10.1007/bf00685841
44. Hebden HF, Hadfield JR, Beer CT (1970) The binding of vinblastine by platelets in the rat. *Cancer Res* 30 (5):1417-1424
45. Sethi VS, Jackson DV, Jr., White DR, Richards F, 2nd, Stuart JJ, Muss HB, Cooper MR, Spurr CL (1981) Pharmacokinetics of vincristine sulfate in adult cancer patients. *Cancer Res* 41 (9 Pt 1):3551-3555



# Chapter 11

## **Age-dependent vincristine binding to $\beta$ -tubulin explains non-linear pharmacokinetics of vincristine: a physiologically based pharmacokinetic approach**

*Manuscript in preparation*

A. Laura Nijstad\*

Wan-Yu Chu\*

Lisa T. van der Heijden

Shelby Barnett

Gareth J. Veal

Arief Lalmohamed

C. Michel Zwaan

Thomas P.C. Dorlo

Alwin D.R. Huitema

*\* Both authors contributed equally to the manuscript*

## ABSTRACT

Vincristine is widely used in pediatric oncology and acts by binding to the  $\beta$ -subunits of tubulin in tumor cells. The expression of  $\beta$ -tubulin in healthy tissue is thought to be highly relevant for the distribution of vincristine throughout the body and is most likely age-dependent. The current physiologically-based pharmacokinetic (PBPK) study has been conducted to optimize a previously published PBPK model by including vincristine binding to  $\beta$ -tubulin in blood cells and to assess age-related differences. Data from 16 adults, 10 adolescents (13-16 years), 23 children (2-10 years) and 17 infants (0-1 years) were included in the model. Using PK-Sim, an adult PBPK model including metabolism and elimination by CYP3A4, CYP3A5 and P-gp and binding to  $\beta$ -tubulin in tissue and blood cells was developed. This model was successfully scaled to adolescents, children and infants. The pediatric model was optimized by simulating a 2.5-fold higher binding capacity of blood- and tissue- $\beta$ -tubulin for infants (0-1 years), a 2-fold higher binding capacity for children (2-10 years) and a 1.5-fold higher binding capacity for adolescents (13-16 years) as compared to adults. A higher binding capacity of vincristine to  $\beta$ -tubulin could lead to a more rapid reduction in the vincristine plasma concentration, reduced amounts of free vincristine, explaining the fact that children are able to tolerate higher relative doses of vincristine. This study forms the basis for further optimization of pediatric dosing guidelines of vincristine.



## 1 INTRODUCTION

Vinca alkaloids are frequently used in the chemotherapeutic treatment of various malignancies. These substances bind to the  $\beta$ -subunits of tubulin, thereby inhibiting microtubule formation and causing arrest of the cell at metaphase. The vinca alkaloid vincristine is widely used in both adult and childhood cancer patients, and is usually dosed at 1.4-2.0 mg/m<sup>2</sup>, with a maximum of 2 mg per dose [1]. The dose is maximized because of the risk of developing vincristine induced peripheral neuropathy (VIPN), which was found to be dose dependent. However, these dosing capping recommendations have been questioned since they are mainly based on empirical experiences [2,3]. For infants, the dose is reduced to 50-80% of the usual BSA based dose or a mg/kg dose (0.025-0.05 mg/kg) is given, even though a pharmacological rationale for these regimens is lacking [4,5].

Optimizing vincristine dosage for individuals remains a challenge, mainly because of lack of knowledge on factors that might influence its pharmacokinetics (PK). This has most recently been highlighted in terms of the challenges of dosing vincristine in neonates and infants as compared to older children [6]. Vincristine is mainly metabolized through hepatic cytochrome P450 (CYP450) enzymes, particularly by the CYP3A4 and CYP3A5 isoforms, with biliary excretion through the hepatic efflux transporter P-glycoprotein (P-gp) [7]. The plasma concentration-time profile of vincristine indicates a rapid distribution phase followed by a relatively long elimination phase, with initial and terminal half-life values of 5 minutes and 19-155 hours, respectively [1]. The PK of vincristine is most commonly described by a two- or three-compartmental model and is characterized by large interindividual variability. For example, in recent population PK studies of vincristine, interindividual variability in PK parameters ranged from 17% to 66% in adults, and 48% to 67% in children [8,9]. The effects of demographic, clinical, and biomedical variables, such as age, body surface area (BSA), dose, and pharmacogenetics, on the PK of vincristine have been studied but no structural covariates on vincristine clearance (CL) or volume of distribution (Vd) have been identified [3,4,6,8,10-17].

Binding of vincristine to  $\beta$ -tubulin in healthy tissue might be key in understanding its unexplained PK variability [5,18]. Saturable binding to  $\beta$ -tubulin was incorporated into a previously published population PK model [5]. Vincristine binding to  $\beta$ -tubulin was found to be dependent on body weight and age.  $\beta$ -tubulin binding capacity decreased with increasing age, which is in line with the PBPK results from Lee et al [18]. They concluded that binding to  $\beta$ -tubulin in healthy

tissue plays a key role in determining differences in vincristine distribution, and a 5-fold higher  $\beta$ -tubulin binding capacity was observed in children as compared to adults [18]. However, a 5-fold higher  $\beta$ -tubulin binding capacity can be seen as physiologically implausible and the PBPK model of Lee et al. only included  $\beta$ -tubulin in tissue as a binding partner of vincristine and did not take  $\beta$ -tubulin in blood (e.g., erythrocytes, leukocytes and thrombocytes) into account. Previously, it has been shown that several isoforms of  $\beta$ -tubulin are expressed in erythrocytes, leukocytes and thrombocytes, so it is necessary to take this into account in the PBPK model as well [19-22].

The current PBPK study was conducted with the aim to improve understanding of the complex non-linear PK profile of vincristine, particularly to comprehend evidence-based dosing regimens for children. The previously published PBPK model of Lee, *et al* [18] was optimized by including vincristine binding to  $\beta$ -tubulin in blood cells and age-related differences were investigated.

## 2 METHODS

### 2.1 Patient data

#### 2.1.1 Data for PBPK model development

Historical data comprising adults from two different PK studies (Villikka., *et al.* and a Newcastle study described by Nijstad., *et al.*) were used for the adult PBPK model development [5,23]. Data from Villikka., *et al.* [23] were digitized using GetData Graph Digitizer (version 2.26.0.20). Plasma concentrations from Villikka., *et al.* [23] were used for the adult training dataset, and plasma concentrations from the Newcastle study [5] for the adult evaluation dataset.

Data from pediatric patients originated from a prospective, observational study performed in the Princess Máxima Center for Pediatric Oncology in the Netherlands, previously described by Nijstad., *et al.* [5] Data from patients aged 0-1 years, 2-10 years and 13-16 years, with at least 1 sample between 0 and 24 hours after dose, were included in this PBPK analysis. Regarding the infants, only patients treated with a dose of 0.05 mg/kg were included.

All patients were treated with vincristine as standard of care, with doses according to local protocols. Doses, varying from 1 to 2 mg/m<sup>2</sup> with a maximum of 2 mg or 0.05 mg/kg for infants, were administrated as bolus infusion. Vincristine plasma concentrations were quantified using a liquid chromatography (tandem) mass spectrometry (LC-MS/MS) assay [5, 23-26].

#### 2.1.2 Vincristine whole blood concentrations

For a selection of patients included in the prospective, observational study performed in the Princess Máxima Center for Pediatric Oncology in the Netherlands, previously described by Nijstad., *et al.* [5], vincristine whole blood concentrations were determined using a validated LC-MS/MS method [27].

Whole blood was collected using a Mitra® (10  $\mu$ L, Neoteryx, Torrance, USA) device. The sponge of the Mitra® was transferred into a 2.0 mL reaction tube. Two grinding beads were added to all reaction tubes. A two-step extraction was performed. First, 400  $\mu$ L 0.2% formic acid in water was added to all samples. The double blanks (CALO/0) were spiked with 20  $\mu$ L methanol. All other samples were spiked with 20  $\mu$ L internal standard in methanol (vincristine-d<sub>3</sub>, 50 ng/mL). The first extraction step was performed by placing all samples in a genogrinder for 10 minutes (1250 rpm). The second extraction step consisted of liquid-liquid extraction with acetonitrile prior to centrifuging (15,000 rpm for 5 minutes). The

supernatant was collected and dried under a gentle stream of nitrogen (40 °C) prior to reconstitution with 100 µL methanol:acetonitrile:water (1:1:2, v/v/v). Continuing, the samples were vortex mixed and centrifuged (15,000 rpm for 5 minutes) before the supernatant was transferred to vials prior to analysis. The final extracts were analyzed with a validated LC-MS/MS method. The method was validated according to the EMA and FDA guidelines on bioanalytical method validation over a linear range of 1-50 ng/mL. The lower limited of quantification (LLOQ) was 1 ng/mL. The intra- and inter-assay bias and precisions were within ±9.9% and ≤7.3%.

Plasma concentrations for the corresponding time point were available as well. Concentrations in blood cells were calculated by subtracting the plasma concentration from the whole blood concentration, taking the hematocrit level into account:

$$C_{Blood\ cell} = \frac{C_{Whole\ blood} - C_{Plasma} \times (1 - Hematocrit)}{Hematocrit}$$

## 2.2 PBPK model development

A schematic workflow for the PBPK model development is presented in Figure 1.

### 2.2.1 Adult base model

Firstly, an adult base model was built and evaluated. Physiochemical properties, binding partners, metabolism and elimination processes of vincristine were included based on Lee., *et al* [18]. Expression levels of CYP3A4, CYP3A5, P-gp (ABCB1) and tissue-β-tubulin were incorporated using the genome expression arrays from ArrayExpress [28]. For tissue-β-tubulin, TUBB (Gene ID: 203068) was selected to represent overall tissue-β-tubulin binding, since it is expressed in most human tissues. The initial model was simulated based on virtual adults following a single bolus dose of 2 mg vincristine and fitted to the data of the adult training dataset.

### 2.2.2 Adult model including blood-β-tubulin as binding partner

After development of the base adult model, binding of vincristine to β-tubulin in blood cells was implemented. A dummy protein binding partner, only expressed in the blood cell compartment defined by PK-Sim, was added to the base model. Binding parameters (i.e., dissociation constant ( $K_D$ ) and dissociation rate ( $k_{off}$ )) of tissue-β-tubulin binding as presented by Lee et al. were used as initial estimates [18].

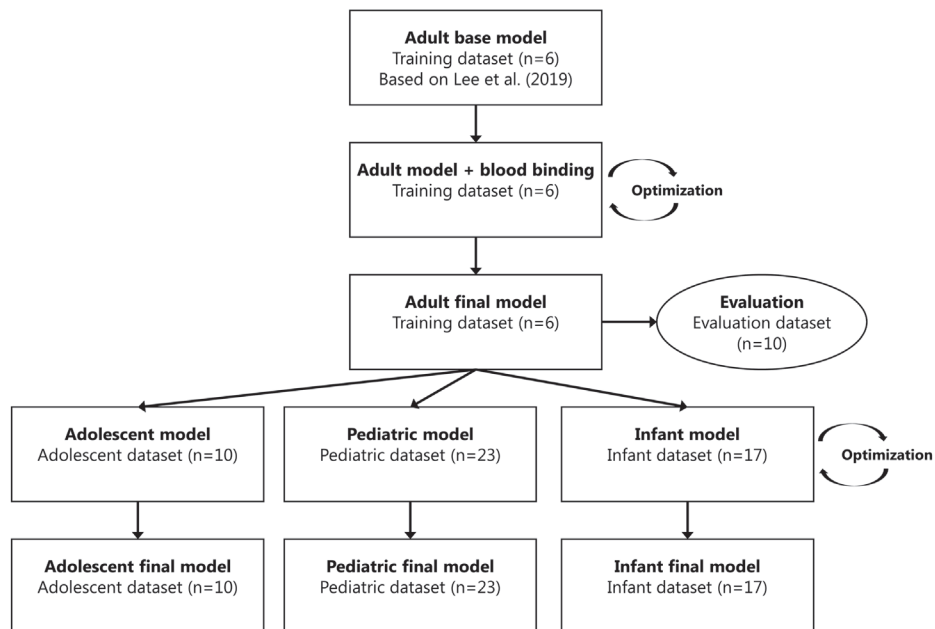


**Figure 1.** Schematic workflow for the PBPK model development

### 2.2.3 Model fitting and evaluation

Model parameter optimization was conducted by fitting the model to the adult training dataset. The reference concentrations of blood- $\beta$ -tubulin as well as tissue- $\beta$ -tubulin and binding parameters of blood- $\beta$ -tubulin were optimized. Within each step, the rationality of parameterization was evaluated by reported values in literature and served as the key determinant to include subsequent binding partners.

For model evaluation, a virtual adult population of 100 individuals was generated based on patient demographics of the adult evaluation dataset. Models were evaluated visually and were accepted if simulated concentration-time profiles fit the overall shape of observed profiles and most observed concentration data fell within the 95% prediction interval (PI) for simulated data.

Sensitivity analyses were performed in order to evaluate the impact of blood- and tissue- $\beta$ -tubulin-binding on vincristine distribution. Input parameters related to blood- and tissue- $\beta$ -tubulin-binding ( $K_D$ ,  $k_{off}$  and reference concentration) were selected for sensitivity analyses performances and were evaluated with a 100% variation to determine their relative impact on the area under the concentration-time curve from 0-24h post-infusion ( $AUC_{0-24}$ ),  $AUC_{\infty}$ ,  $V_d$ ,  $V_{ss}$ , CL and terminal half-life ( $t_{1/2}$ ).

#### 2.2.4 Pediatric model

The final adult population model was scaled to an infant, pediatric and adolescent population of 100 individuals based on patient demographics of the infant, pediatric and adolescent dataset. Age-dependent variations and maturations in anatomy, physiology, and biochemistry were implemented [29-31]. Age-dependent organ volumes, tissue compositions, blood flow rates, etc. were scaled by the implemented algorithm in PK-Sim within the limits of the International Commission on Radiological Protection (ICRP) [32]. Ontogeny of CYP3A4 was included based on the built-in PK-Sim ontogeny function.

Virtual infant patients were dosed with a single vincristine bolus of 0.05 mg/kg and pediatric patients until the age of 12 years were dosed with a single vincristine bolus of 1.5 mg/m<sup>2</sup>. For model evaluation, simulated concentration-time profiles were compared with plasma observations from the pediatric datasets.

#### 2.3 Software

PBPK modeling was performed using PK-Sim (version 7.10, Open Systems Pharmacology Suite) [33]. Simulations were carried out using the Schmitt partition coefficient calculation method. Model input parameter optimization was accomplished using the Levenberg-Marquardt algorithm implemented in PK-Sim. Sensitivity analyses were performed using the PK-Sim built-in tool for model evaluation. R (version 3.4.3) was used for data handling and visualization [34].

### 3 RESULTS

#### 3.1 Patient data

Data from 66 patients (16 adults, 10 adolescents (13-16 years), 23 children (2-10 years) and 17 infants (0-1 years)) were included. Plasma concentrations of 6 adult patients were used for the training dataset and the remaining 10 adult patients for the evaluation dataset. Patient characteristics are displayed in Table 1.

**Table 1.** Patient characteristics

	Adults		Adolescents	Children	Infants
	Training dataset <sup>23</sup>	Evaluation dataset <sup>5</sup>	13-16 years <sup>5</sup>	2-10 years <sup>5</sup>	0-1 years <sup>5</sup>
	N=6	N=10	N=10 (12 OCC)	N=23 (27 OCC)	N=17
Female sex [n (%)]	3 (50%)	3 (30%)	2 (20%)	10 (43%)	7 (41%)
Age, years [median (range)]	46.5 (40-54)	20.3 (18.3-33.9)	14.0 (13.2-15.3)	5.3 (2.9-10.0)	0.5 (0.04-0.98)
Body weight, kg [median (range)]	NA	90.1 (42.5-126)	43.8 (35.0-59.9)	20.2 (11.8-33.1)	5.8 (2.9-11.0)
BMI, kg/m <sup>2</sup> [median (range)]	24.5 (17-32)	NA	NA	NA	NA
Absolute dose, mg [median (range)]	2	2	2	1.2 (0.8-1.7)	0.4 (0.2-0.69)

BMI, Body mass index; NA, not applicable; OCC, Occasions

#### 3.2 PBPK model development

##### 3.2.1 Adult base model

An adult base model was built and evaluated. Metabolism and elimination processes were included identically to Lee., *et al* [18]: CYP3A4, CYP3A5, P-gp (ABCB1). Tissue- $\beta$ -tubulin was incorporated as binding partner of vincristine.

The fit of this model to the training dataset was assessed visually and optimized manually. An optimized tissue- $\beta$ -tubulin reference concentration of over 10  $\mu$ M was necessary to adequately describe vincristine distribution in the first few hours post-dose. The model with only tissue- $\beta$ -tubulin as a specific binding partner of vincristine was, therefore, considered not physiological plausible to describe vincristine distribution. This was considered to indicate of additional binding of vincristine by blood cells.

### 3.2.2 Adult model including blood- $\beta$ -tubulin as binding partner

The adult base model was optimized by including blood- $\beta$ -tubulin as a binding partner of vincristine. This model improved the description of the vincristine observations within the first 2 hours after administration (Figure 2A).

As a starting point,  $k_{\text{off}}$  was set to  $1.93 \times 10^{-3}$  /s and  $K_D$  to  $0.05 \mu\text{M}$  based on literature of tissue- $\beta$ -tubulin [18].  $K_D$  was optimized to  $0.20 \mu\text{M}$ . Optimized reference concentrations of tissue- and blood- $\beta$ -tubulin were  $1.0 \mu\text{M}$  and  $1.2 \mu\text{M}$ , respectively.

The model was evaluated with the adult evaluation dataset. Population-based simulations were performed for virtual adults with similar patient characteristics as the evaluation dataset (Table 1). As shown in Figure 2B, the majority of observed concentration data points were within the 95% PI of simulated vincristine plasma concentrations, indicating that the established model with blood- $\beta$ -tubulin-binding was adequate.

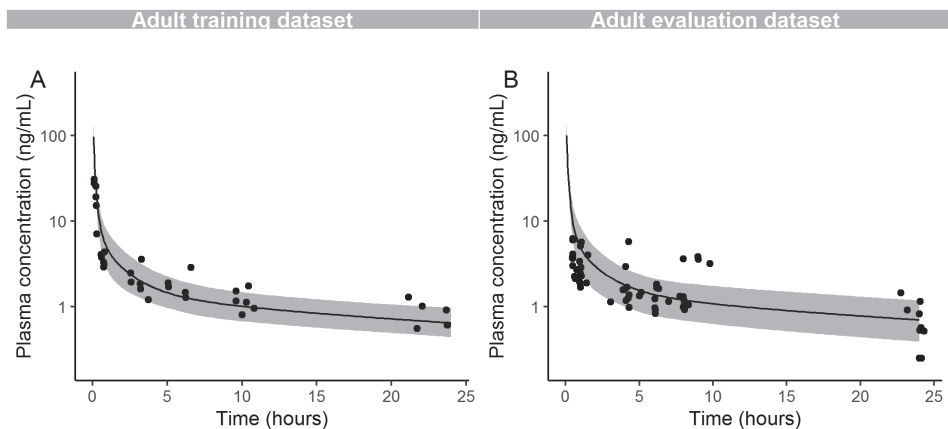


**Figure 2.** Simulated plasma concentration time curves for the adult training dataset (A) and the adult evaluation dataset (B). The solid line represents the simulated mean and the grey area the 95% prediction interval.

The sensitivity analysis (Table 2) showed that most PK parameters were more sensitive to variations in blood- $\beta$ -tubulin expression level than in tissue- $\beta$ -tubulin expression level. For example, 100% increases in blood- or tissue- $\beta$ -tubulin reference concentrations led to decreases in  $\text{AUC}_{0-24}$  of 34% and 5%, and increases in  $V_{\text{ss}}$  of 88% and 11%, respectively. Changes in the  $K_D$  of vincristine-blood- $\beta$ -tubulin binding also led to a greater impact on PK parameters than that of tissue-



$\beta$ -tubulin binding. Moreover, the effect of blood- $\beta$ -tubulin-binding impacted on PK parameters related to both the period shortly after infusion and the later time points, as suggested by the changes in  $V_{ss}$  and  $V_d$ . The CL of vincristine was marginally influenced by variations in either blood- or tissue- $\beta$ -tubulin reference concentration, suggesting that the binding processes mostly affected vincristine distribution.

**Table 2.** Sensitivity analyses

Binding partner	Input parameter	Relative change in PK parameter with a 100% variation in selected input parameters (%)					
		AUC <sub>0-24</sub>	AUC <sub>∞</sub>	V <sub>ss</sub>	V <sub>d</sub>	CL	t <sub>1/2</sub>
Blood- $\beta$ -tubulin	Ref Conc	-34%	-0.1%	88%	87%	0.1%	87%
	K <sub>D</sub>	24%	7%	-54%	-56%	-7%	-50%
	k <sub>off</sub>	-0.04%	-0.03%	-0.06%	-0.24%	0.03%	-0.26%
Tissue- $\beta$ -tubulin	Ref Conc	-5%	-2%	11%	11%	2%	9%
	K <sub>D</sub>	5%	2%	-11%	-11%	-2%	-9%
	k <sub>off</sub>	-0.01%	-0.42%	-0.67%	-0.66%	0.42%	-1.00%

Abbreviations: AUC, area under the curve; CL, total body clearance; K<sub>D</sub>, dissociation constant; k<sub>off</sub>, dissociation rate, PK, pharmacokinetics; t<sub>1/2</sub>, half-life; V<sub>d</sub>, volume of distribution during terminal phase; V<sub>ss</sub>, volume of distribution at steady state

This adult PBPK model considering possible binding between vincristine and blood- $\beta$ -tubulin demonstrated physiologically appropriate tissue- $\beta$ -tubulin and blood- $\beta$ -tubulin reference concentrations. Therefore, this model strengthened the relevant binding of vincristine to blood- $\beta$ -tubulin in addition to tissue- $\beta$ -tubulin.

### 3.2.3 Pediatric model

The final adult population model was scaled to an adolescent (13-16 years), a pediatric (2-10 years) and an infant (0-1 years) population of 100 individuals with characteristics similar to patient demographics of the corresponding datasets (Table 1).

For both the adolescent, the pediatric and the infant population, the simulated concentration-time curve overpredicted plasma concentrations in the first hours after administration (Figure 3A-C), suggesting that vincristine distribution was still not well described in the model, despite incorporating vincristine binding to blood- $\beta$ -tubulin.

Lee et al. have shown the same misspecification when scaling the adult PBPK model to children aged 2 to 9 years, solving it by assuming a 5-fold higher tissue- $\beta$ -tubulin expression in children [18]. However, as the developed adult PBPK model demonstrated the importance of blood- $\beta$ -tubulin-binding in vincristine distribution, a higher vincristine binding capacity, which might be due to increasing tissue- or blood- $\beta$ -tubulin affinity, could also attribute to the more extensive distribution in children. Therefore, a 2 to 5-fold increase with steps of 0.5 in both blood- and tissue- $\beta$ -tubulin expression was evaluated. For adolescents, increasing the vincristine binding capacity of blood- and tissue- $\beta$ -tubulin 1.5-fold led to improved overall predictions, whereas in children 2-10 years, increasing the blood- and tissue- $\beta$ -tubulin reference concentrations 2-fold was considered optimal. For infants until 1 years of age, the initial distribution phase was even more pronounced. As a consequence, a 2.5-fold higher reference concentration was considered optimal to fit the infant data. The final PBPK model evaluation in adolescents, children and infants are shown in Figure 3D-F and final model parameters in Table 3.

### 3.3 Vincristine whole blood concentrations

In total, 21 whole blood concentrations of 6 pediatric patients (1.0-17.6 years) were available. A nonlinear relationship between whole blood and plasma concentrations was observed. The simulated blood cell-, whole blood- and plasma concentration-time curves based on the final PBPK model are displayed in Figure 4. The observed concentrations closely followed the simulated curves. Vincristine disposition in blood cells seems saturable.

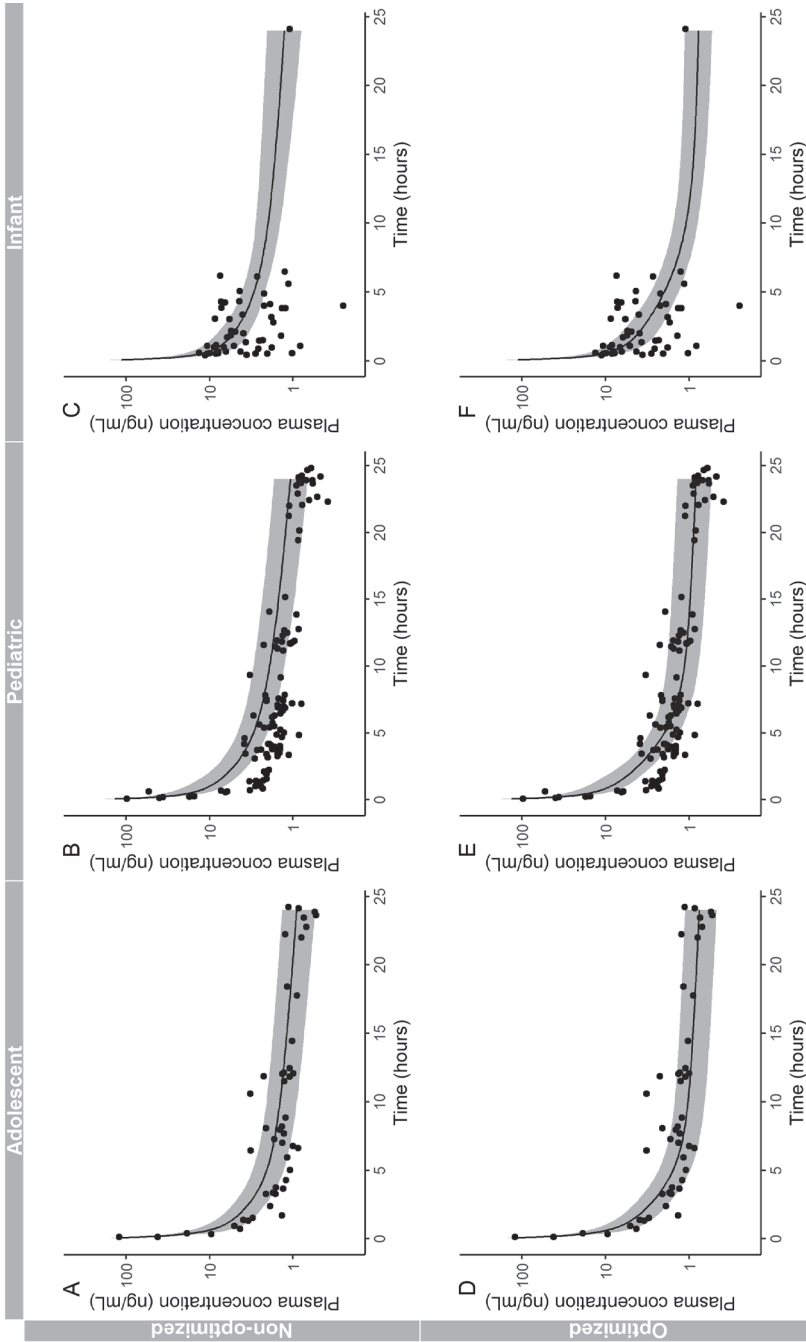


**Figure 3.** Non-optimized (upper panels A, B and C) versus optimized (lower panels D, E and F) simulated plasma concentration time curves for the adolescent population (A and D respectively), pediatric (B and E respectively) and infant population (C and F, respectively). The solid line represents the simulated mean and the grey area the 95% prediction interval.

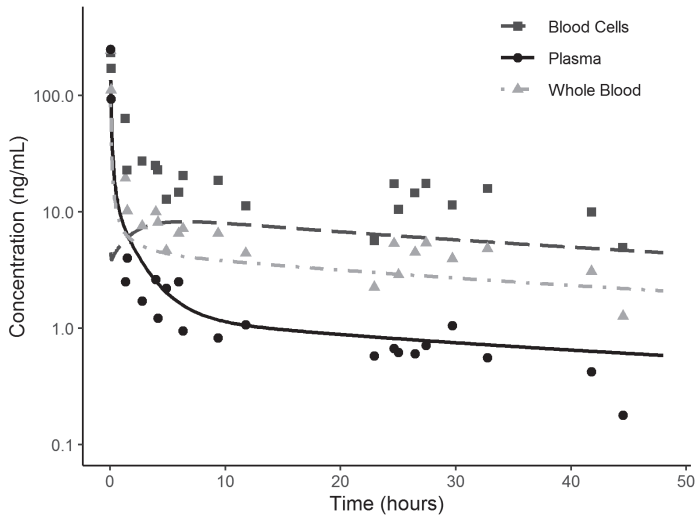


**Figure 4.** Simulated blood cell- (darkgray, dashed line), whole blood- (lightgray, dotdashed line) and plasma (black, solid line) concentration time-curves for the pediatric population.

**Table 3.** Final parameters used for the adult and pediatric vincristine PBPK model.

Parameter	Value *
Molecular weight, g/mol	824.958
Solubility, mg/L	2.27
LogP	2.82
pK <sub>a</sub>	5.00 and 7.4
f <sub>u</sub>	0.51 ( $\alpha$ -1-acid glycoprotein)
<i>CYP3A4 metabolism</i>	
V <sub>max</sub> (pmol/min/pmol enzyme)	0.9
K <sub>m</sub> ( $\mu$ M)	19.8
<i>CYP3A5 metabolism</i>	
V <sub>max</sub> (pmol/min/pmol enzyme)	8.1
K <sub>m</sub> ( $\mu$ M)	14.3
<i>P-gp transport</i>	
J <sub>max</sub> (pmol/mL/min)	416.1
K <sub>m</sub> ( $\mu$ M)	17.1
Binding to $\beta$ -tubulin in tissue	
k <sub>off</sub> (1/s)	1.93 * 10 <sup>-3</sup>
K <sub>D</sub> ( $\mu$ M)	0.05
Reference concentration ( $\mu$ M)	1.00
Relative expression	1.0 (adult) 1.5 (adolescent) 2.0 (pediatric) 2.5 (infant)
Binding to $\beta$ -tubulin in blood	
k <sub>off</sub> (1/s)	1.93 * 10 <sup>-3</sup>
K <sub>D</sub> ( $\mu$ M)	0.20
Reference concentration ( $\mu$ M)	1.20
Relative expression	1.0 (adult) 1.5 (adolescent) 2.0 (pediatric) 2.5 (infant)

Abbreviations: f<sub>u</sub>, unbound fraction; J<sub>max</sub>, maximal rate of transport; K<sub>D</sub>, dissociation constant; K<sub>m</sub>, Michaelis-Menten constant; k<sub>off</sub>, dissociation rate; LogP, partition coefficient; P-gp, P-glycoprotein; V<sub>max</sub>, maximum rate of metabolism.

\*All parameters, except for binding to  $\beta$ -tubulin in blood, were based on the model of Lee., et al [18].

## 4 DISCUSSION

In this current study, the complex interplay between binding of vincristine to  $\beta$ -tubulin including binding to blood components was successfully modelled using a PBPK approach. The age dependent effects of  $\beta$ -tubulin binding on the PK of vincristine were incorporated, providing a mechanistic explanation for the observed age dependency of plasma vincristine PK. We have shown that incorporation of blood- $\beta$ -tubulin-binding improves the adult PBPK model as published by Lee et al. and explains the observed differences between children and adults [18]. Our final adult model incorporated metabolism by CYP3A4 and CYP3A5, elimination by P-gp and binding to  $\beta$ -tubulin in peripheral tissue and blood cells.

We have shown that vincristine binding to  $\beta$ -tubulin in blood mainly affects the distribution phase in the first hours after administration. This is explained by the fact that blood cells are the first components that are exposed to the drug after intravenous administration. Moreover, the findings on the non-linear and saturable binding in blood components (Figure 4) show that vincristine binding to blood- $\beta$ -tubulin explains the non-linear PK of vincristine and the rapid distribution in the first period after infusion. Binding of vinca alkaloids to blood cells has been previously shown in several *in vivo* and *in vitro* studies [19, 35-37]. In addition, a high affinity to thrombocytes was previously described [36].

In the first step of model development, the adult optimized PBPK model was scaled to children. Evaluation of this model on pediatric data indicated that children (2-10 years) had a 2-fold higher binding capacity of blood- and tissue- $\beta$ -tubulin, while this was 1.5-fold higher for adolescents (13-16 years) and 2.5-fold higher for infants (0-1 years) as compared to adults. Previously, Lee, *et al.*, found a 5-fold higher binding capacity of tissue- $\beta$ -tubulin for children (0-12 years) as compared to adults, albeit without taking binding to blood- $\beta$ -tubulin into account [18]. The expression of  $\beta$ -tubulin in the in-built expression database of PK-Sim is limited to peripheral tissue. The current study demonstrated that including blood- $\beta$ -tubulin-binding on top of tissue- $\beta$ -tubulin-binding not only provided an adequate description of the vincristine distribution phase for both plasma and whole blood concentrations but also resulted in biologically more plausible parameter estimations.

The observed age dependent PK of vincristine is explained in our model by a higher expression of  $\beta$ -tubulin in tissue as well as blood cells in children as compared to adults. Tubulin in microtubules plays a significant role in cell division. Since cell division is more dominant in younger patients, a higher  $\beta$ -tubulin expression in children as

compared to adults is highly likely. Even though evidence for age related differences in the exposition of  $\beta$ -tubulin is not available, previous immunohistochemical research showed that expression of  $\beta$ 2-tubulin was higher in neonatal tissue compared to tissue of older children and adults. Also, expression decreased with increasing age [38]. The same could be expected for other isotypes of  $\beta$ -tubulin. Our findings are in line with our previous observations from a vincristine population PK model in children [5]. Here, a decrease in maximal vincristine binding capacity to  $\beta$ -tubulin associated with an increase in age was identified.

A lower expression of  $\beta$ -tubulin for adults as compared to children would lead to a lower binding capacity of vincristine in blood and peripheral tissue, which would lead to higher amounts of free vincristine in the central compartment. This higher amount of free vincristine in the central compartment could have several implications. Firstly, higher amounts of free vincristine are available to distribute to peripheral tissue, where it could lead to VIPN. Secondly, higher amounts of vincristine are available to bind to tumor cells, and could, theoretically, be more effective in terms of treatment. This last implication would suggest that vincristine could be less effective in children. However, in current practice, children already receive a higher  $\text{mg}/\text{m}^2$  dose than adults, due to the fact that children are able to tolerate higher doses of vincristine. Children are dosed based on BSA, while adults receive a standard capped dose of 2 mg, corresponding to lower  $\text{mg}/\text{m}^2$  doses than administered to children with a BSA below  $1 \text{ m}^2$ . The difference in  $\beta$ -tubulin binding capacity between children and adults provides a physiologically plausible reason for higher relative doses of vincristine in children and capping the vincristine dose to 2 mg in adolescents and adults. This also explains why considerably higher doses of vincristine can be administered via a long continuous infusion. In that case, vincristine concentrations remain below the concentrations necessary to saturate the  $\beta$ -tubulin binding capacity [39,40].

The higher expression of  $\beta$ -tubulin for infants as compared to children and adults strengthens the hypothesis that extra dose reductions for very young patients as compared to older children might not be justified [5]. However, we did observe a higher variability in vincristine plasma concentrations in the first 6 hours after infusion for infants than for children and adolescents, which might indicate that some variability in the distribution phase in this population is still unexplained.

Despite the fact that children are able to tolerate higher doses of vincristine, VIPN remains a serious side effect, which also occurs in children. To date, no convincing predictors for VIPN in children have been found [41]. However, a substantial

interindividual variability (up to 7-fold) in  $\beta$ -tubulin VI expression in blood cells has been observed [22]. The high variability in  $\beta$ -tubulin VI expression could explain the variability in observed VIPN, which is still poorly understood [41].

In addition, DNA missense variations in  $\beta$ -tubulin VI expression, altering myelosuppressive action, have been characterized in a previous study. One of these variations significantly decreased sensitivity to paclitaxel induced tubulin polymerization [22]. Moreover, these polymorphisms were thought to contribute to decreased myelosuppression, associated with the use of microtubule-binding drugs, like paclitaxel and vinca alkaloids. Genetic variations in other  $\beta$ -tubulin isoforms in tumor cells have also been described and are associated with resistance to microtubule-binding drugs [42,43]. These results lead to the question whether genetic variations in  $\beta$ -tubulin isoforms in neurons could explain variability in sensitivity to VIPN. However, evidence to support this hypothesis are lacking.

Previous studies have shown that children of African-American origin are at a lower risk of developing VIPN than children of Caucasian origin [41]. This difference is thought to be associated to differences in CYP polymorphisms between the populations. However, the current study indicates that it could possibly be related to differences in  $\beta$ -tubulin expression or polymorphisms in the encoding genes, but this hypothesis should be confirmed by studying the  $\beta$ -tubulin expression and/or genotype in various populations.

A limitation of the current study concerns explaining the variability in vincristine binding capacity. In the current study, we have shown that vincristine binding to blood cells impacts vincristine distribution throughout the body. It could be expected that variability in blood cell counts explains variability in vincristine PK. However, previous research [5] did not find an effect of thrombocyte levels on the maximal binding capacity of vincristine. Future studies could include data on blood cell counts (e.g., erythrocytes, leukocytes and thrombocytes) to study this effect.

In conclusion, the presented vincristine PBPK model describes the plasma and whole blood pharmacokinetics of vincristine in children and adults and demonstrates a substantial effect of blood- $\beta$ -tubulin-binding on vincristine distribution. A 2-fold higher  $\beta$ -tubulin expression in children compared to adults was found for tissue as well as for blood cells, potentially explaining the fact that children are able to tolerate higher doses of vincristine. The previously reported, high variability in  $\beta$ -tubulin expression and DNA polymorphisms, altering sensitivity to vincristine, could explain the poor understood variability in VIPN between patients.



## REFERENCES

1. Teva (209) Vincristine sulphate - Summary of product characteristics: Vincristine sulphate (NL) [https://www.geneesmiddeleninformatiebank.nl/smpc/h100081\\_smpc.pdf](https://www.geneesmiddeleninformatiebank.nl/smpc/h100081_smpc.pdf). Accessed 21 July 2023.
2. McCune, J. S. & Lindley, C (1997). Appropriateness of maximum-dose guidelines for vincristine. *American Journal of Health-System Pharmacy* 54, 1755–1758.
3. Frost, B. M. et al (2003) Vincristine in childhood leukaemia: no pharmacokinetic rationale for dose reduction in adolescents. *Acta paediatrica* 92, 551–7
4. Nijstad, A. L. et al (2022) Clinical pharmacology of cytotoxic drugs in neonates and infants: Providing evidence-based dosing guidance. *Eur J Cancer* 164, 137–154.
5. Nijstad, A. L. et al (2022) A Population Pharmacokinetic Modelling Approach to Unravel the Complex Pharmacokinetics of Vincristine in Children. *Pharm Res* 39, 2487–2495
6. Barnett, S. et al. (2021) Vincristine dosing, drug exposure and therapeutic drug monitoring in neonate and infant cancer patients. *European Journal of Cancer*. doi:10.1016/j.ejca.2021.09.014
7. Zhou, X.-J. & Rahmani, R (1992) Preclinical and Clinical Pharmacology of Vinca Alkaloids. *Drugs* 44, 1–16
8. Velde, M. E. van de et al (2020) Population pharmacokinetics of vincristine related to infusion duration and peripheral neuropathy in pediatric oncology patients. *Cancers* 12, 1–15
9. Igarashi, T. et al (2021). Population pharmacokinetic model development and exposure–response analysis of vincristine in patients with malignant lymphoma. *Cancer Chemotherapy and Pharmacology* 87, 501–511
10. Guilhaumou, R. et al (2011) Population pharmacokinetics and pharmacogenetics of vincristine in paediatric patients treated for solid tumour diseases. *Cancer Chemotherapy and Pharmacology* 68, 1191–1198
11. Moore, A. S. et al (2011) Vincristine pharmacodynamics and pharmacogenetics in children with cancer: A limited-sampling, population modelling approach. *Journal of Paediatrics and Child Health* 47, 875–882
12. Gidding, C. E. M. et al (1999). Vincristine pharmacokinetics after repetitive dosing in children. *Cancer chemotherapy and pharmacology* 44, 203–9
13. Crom, W. R. et al (1994). Pharmacokinetics of vincristine in children and adolescents with acute lymphocytic leukemia. *The Journal of pediatrics* 125, 642–9
14. Graaf, S. S. N. De, Bloemhof, H., Vendrig, D. E. M. M. & Uges, D. R. A (1995). Vincristine disposition in children with acute lymphoblastic leukemia. *Medical and Pediatric Oncology* 24, 235–240
15. Groninger, E. et al (2002) Pharmacokinetics of Vincristine Monotherapy in Childhood Acute Lymphoblastic Leukemia. *Pediatric Research* 52, 113–118
16. Plasschaert, S. L. A. et al (2004) Influence of functional polymorphisms of the MDR1 gene on vincristine pharmacokinetics in childhood acute lymphoblastic leukemia. *Clinical Pharmacology and Therapeutics* 76, 220–229
17. Groninger, E. et al (2005). Vincristine pharmacokinetics and response to vincristine monotherapy in an up-front window study of the Dutch Childhood Leukaemia Study Group (DCLSG). *European Journal of Cancer* 41, 98–103

18. Lee, C. M., Zane, N. R., Veal, G. & Thakker, D. R (2019) Physiologically Based Pharmacokinetic Models for Adults and Children Reveal a Role of Intracellular Tubulin Binding in Vincristine Disposition. *CPT Pharmacometrics Syst Pharmacol* 8, 759–768
19. Secret, C. J., Hadfield, J. R. & Beer, C. T (1972). Studies on the binding of [<sup>3</sup>H]vinblastine by rat blood platelets in vitro. Effects of colchicine and vincristine. *Biochemical Pharmacology* 21, 1609–1624
- Sethi, V. S. et al. Pharmacokinetics of Vincristine Sulfate in Adult Cancer Patients. *Cancer Research* 41, 3551 LP – 3555 (1981).
20. Leandro-García, L. J. et al (2010) Tumoral and tissue-specific expression of the major human  $\beta$ -tubulin isoforms. *Cytoskeleton* 67, 214–223
21. Leandro-García, L. J. et al (2012) Hematologic  $\beta$ -Tubulin VI Isoform Exhibits Genetic Variability That Influences Paclitaxel Toxicity. *Cancer Research* 72, 4744–4752
22. Villikka, K., Kivistö, K. T., Mäenpää, H., Joensuu, H. & Neuvonen, P. J (1999). Cytochrome P450-inducing antiepileptics increase the clearance of vincristine in patients with brain tumors. *Clin Pharmacol Ther* 66, 589–593
23. Israels, T. et al (2010). Malnourished Malawian patients presenting with large Wilms tumours have a decreased vincristine clearance rate. *Eur J Cancer* 46, 1841–1847
24. Damen, C. W. N. et al (2009). Validated assay for the simultaneous quantification of total vincristine and actinomycin-D concentrations in human EDTA plasma and of vincristine concentrations in human plasma ultrafiltrate by high-performance liquid chromatography coupled with tandem mass spectrometry. *Rapid Communications in Mass Spectrometry* 23, 763–774
25. Heijden, L. T. van der et al (2022). A highly sensitive bioanalytical method for the quantification of vinblastine, vincristine, vinorelbine and 4-O-deacetylvinorelbine in human plasma using LC-MS/MS. *J Pharm Biomed Anal* 114772 doi:10.1016/j.jpba.2022.114772
26. Heijden, L. T. van der et al (2023). A sensitive liquid chromatographic-mass spectrometry method for the quantification of vincristine in whole blood collected with volumetric absorptive microsampling. *J Pharm Biomed Anal* 115232 doi:10.1016/j.jpba.2023.115232
27. Meyer, M., Schneckener, S., Ludewig, B., Kuepfer, L. & Lippert, J (2012). Using expression data for quantification of active processes in physiologically based pharmacokinetic modeling. *Drug Metabolism and Disposition* 40, 892–901
28. Barrett, J. S., Casa Alberighi, O. Della, Läer, S. & Meibohm, B (2012) Physiologically Based Pharmacokinetic (PBPK) Modeling in Children. *Clinical Pharmacology & Therapeutics* 92, 40–49
29. Maharaj, A. R., Barrett, J. S. & Edginton, A. N. A (2013) workflow example of PBPK modeling to support pediatric research and development: Case study with lorazepam. *AAPS Journal* 15, 455–464
30. Maharaj, A. R. & Edginton, A. N (2014) Physiologically based pharmacokinetic modeling and simulation in pediatric drug development. *CPT: Pharmacometrics and Systems Pharmacology* 3,
31. ICRP Basic Anatomical and Physiological Data for Use in Radiological Protection Reference Values. ICRP Publication 89. *Ann. ICRP* 32, (3-4) (2002).
32. Open Systems Pharmacology Suite PK-Sim Version 7.10. (2021).
33. RC Team R: a language and environment for statistical computing. R Foundation for Statistical Computing, Vienna (2009).

34. Gout, P. W., Wijcik, L. L. & Beer, C. T (1978). Differences between vinblastine and vincristine in distribution in the blood of rats and binding by platelets and malignant cells. *European Journal of Cancer* (1965) 14, 1167–1178
35. Urien, S. et al (1993). Vinorelbine high-affinity binding to human platelets and lymphocytes: distribution in human blood. *Cancer Chemotherapy and Pharmacology* 32, 231–234
36. Hebden, H. F., Hadfield, J. R. & Beer, C. T (1970). The binding of vinblastine by platelets in the rat. *Cancer Research* 30, 1417–1424
37. Oda, E., Nakamura, Y., Yamamoto, M. & Kojiro, M (2005). Immunohistochemical Distribution of Tubulin beta II in Human Normal and Neoplastic Tissues. *The Kurume Medical Journal* 52, 117–125
38. Pinkerton, C. R. et al (1988). Continuous vincristine infusion as part of a high dose chemoradiotherapy regimen: drug kinetics and toxicity. *Cancer Chemotherapy and Pharmacology* 22, 271–274
39. Kellie, S. J. et al (2004). Increasing the dosage of vincristine: A clinical and pharmacokinetic study of continuous-infusion vincristine in children with central nervous system tumors. *Cancer* 100, 2637–2643
40. Velde, M. E. van de et al (2017). Vincristine-induced peripheral neuropathy in children with cancer: A systematic review. *Critical Reviews in Oncology/Hematology* 114, 114–130
41. Giannakakou, P. et al (1997). Paclitaxel-resistant Human Ovarian Cancer Cells Have Mutant  $\beta$ -Tubulins That Exhibit Impaired Paclitaxel-driven Polymerization. *Journal of Biological Chemistry* 272, 17118–17125
42. Kavallaris, M. et al (2001). Multiple microtubule alterations are associated with Vinca alkaloid resistance in human leukemia cells. *Cancer research* 61, 5803–9



# Chapter 12

## **Development of a Therapeutic Drug Monitoring strategy for the optimization of vincristine treatment in paediatric oncology populations in Africa**

*Therapeutic Drug Monitoring. 2023;45(3):354-363*

Lisa T. van der Heijden  
A. Laura Nijstad  
Aniek Uittenboogaard  
Jos H. Beijnen  
Thomas P.C. Dorlo  
Gertjan Kaspers  
Alwin D.R. Huitema

## ABSTRACT

**Background:** Recent studies have reported ethnic differences in vincristine exposure and outcomes such as toxicity. This resulted in the hypothesis of subtherapeutic dosing in African children. To optimize individual treatment, a strategy to identify subtherapeutic exposure using therapeutic drug monitoring (TDM) is essential. The aim of the current study was to develop a strategy for TDM of vincristine in African children to meet the following criteria: (1) identify patients with low vincristine exposure with sufficient sensitivity ( $> 70\%$ ), (2) determine vincristine exposure with a limited sampling strategy design of three samples, and (3) allow all samples to be collected within 4 h after administration.

**Methods:** An *in silico* simulation study was performed using a previously described population pharmacokinetic model and real-life demographic dataset of Kenyan and Malawian pediatric oncology patients. Two different TDM strategies were evaluated: (1) Bayesian approach and (2) pharmacometric nomogram. The sampling design was optimized using the constraints described above. Sensitivity analysis was performed to investigate the influence of missing samples, erroneous sampling times, and different boundaries on the nomogram weight bands.

**Results:** With the Bayesian approach, 43.3% of the estimated individual exposure values had a prediction error of  $\geq 20\%$  owing to extremely high shrinkage. The Bayesian approach did not improve with alternative sampling designs within sampling constraints. However, the pharmacometric nomogram could identify patients with low vincristine exposure with a sensitivity, specificity, and accuracy of 75.1%, 76.4%, and 75.9%, respectively. The pharmacometric nomogram performed similarly for different weight bands.

**Conclusions:** The Pharmacometric nomogram was able to identify patients with low vincristine exposure with high sensitivity with three blood samples collected at 1, 1.5, and 4 hours after administration. Missing samples should be avoided, and the three scheduled samples should be collected within 15, 5, and 15 min of 1, 1.5, and 4 h after administration, respectively.

## 1 INTRODUCTION

Vincristine is a chemotherapeutic drug belonging to the vinca alkaloid group [1]. Its use in clinical practice has been well established since the 1960s [2] in the treatment of both solid and nonsolid tumors in various populations [3]. Vincristine is administered intravenously via either a bolus injection or short infusion [3]. After administration, vincristine pharmacokinetics are characterized by a fast distribution phase within the first few hours, followed by a slow elimination phase [4,5]. The distribution phase contains a saturable component because of its binding to  $\beta$ -tubulin [6,7]. Elimination occurs predominantly through metabolism, particularly by cytochrome P450 (CYP) enzymes CYP3A4 and CYP3A5 [8]. Vincristine pharmacokinetics demonstrate large inter-individual variability [9]. Recent pharmacokinetic studies have reported inter-individual variability in pharmacokinetic parameters in children, ranging from 48-67% [10,11].

The mechanism of action of vincristine relies on its interference with the microtubules in the mitotic spindle, which causes a cytostatic effect [12,13]. Its major side effect is neurotoxicity (vincristine-induced peripheral neuropathy (VIPN)), which mainly affects longer neurons and is dose limiting. VIPN is characterized by sensory loss, neuropathic pain, and muscle weakness [2]. VIPN is probably associated with vincristine dose, given that increased vincristine doses (2 mg/m<sup>2</sup>, max 2.5 mg) resulted in an unacceptably high incidence of VIPN compared to lower vincristine doses (1.5 mg/m<sup>2</sup>, max. 2 mg) in children with B-acute lymphoblastic leukemia (B-ALL) (78.8% Caucasian) [13].

Despite the longstanding use of vincristine in clinical practice, the covariates that explain inter-individual variability in pharmacokinetics and toxicity remain largely unknown [15,16]. Ethnicity may explain some of the observed variability. Caucasian children are more affected by VIPN than are non-Caucasian children [2,17,18]. Moreover, in a cohort of Kenyan children, the prevalence of high CYP3A5 expression was 91%, while it was only 14% in a predominantly Caucasian U.S. cohort [19]. The high-expression genotype was associated with lower plasma exposure (and thus, increased clearance). It was not associated with VIPN, which is likely due to the low incidence (9%) of non-high CYP3A5 expressers [19]. It is possible that the high incidence of the high-expresser CYP3A5 genotype, and thus higher clearance of vincristine, may contribute to the overall poorer treatment outcome seen in non-Caucasian

children with cancer, since their vincristine exposure might be lower [20, 21]. In addition to ethnicity, nutritional status might also play a role in the clinical pharmacology of vincristine, since Malawian children suffering from malnutrition experienced more toxicity and had lower vincristine clearance compared to Caucasian children with a better nutritional status [22,23].

These observations led to the hypothesis that the current vincristine dose regimen (2 mg/m<sup>2</sup>, max. 2.5 mg) is subtherapeutic for African pediatric patients who are relatively underdosed compared with their Caucasian peers [19]. Dose adjustments based on therapeutic drug monitoring (TDM) could be a potential strategy to safely optimize vincristine treatment in African pediatric oncology patients, ultimately aiming to improve treatment outcomes. The aim of the current study was to develop a pragmatic strategy for TDM of vincristine to identify African pediatric oncology patients with low vincristine exposure relative to their Caucasian peers. The TDM strategy had to meet the following criteria for implementation in the clinic: (1) identify patients with low vincristine exposure with sufficient sensitivity (>70%), (2) determine vincristine exposure with a limited sampling strategy design of three samples, and (3) allow all samples to be collected within 4 h after administration. Two TDM strategies were investigated: (1) Bayesian estimation, and (2) a nomogram based on body weight and plasma concentration ratios. An *in silico* simulation study was performed using a previously described pediatric population pharmacokinetic model [7] and a real-life demographic dataset of Kenyan and Malawian pediatric oncology patients. Sensitivity analysis was performed to identify the critical aspects of the TDM strategy and define the time intervals for sample collection.



## 2 MATERIALS AND METHODS

### 2.1 Clinical Setting and Practical Constraints

The TDM strategy was developed to support future pharmacokinetic studies in Kenyan pediatric oncology patients. The aim of this clinical study is to optimize vincristine treatment in this population using a TDM approach. To reduce the burden on patients and the number of hospital visits, the number of blood samples was limited to a maximum of three within 4 h after administration. Children will receive vincristine as part of standard care as a 5-minute IV push injection at a dose of 2 mg/m<sup>2</sup> (max. 2.5 mg).

### 2.2 *In silico* Pharmacokinetic Simulations

#### 2.2.1 Population pharmacokinetic model

Vincristine pharmacokinetics were simulated using a previously published population pharmacokinetic model [7], which was developed on a dataset containing 1297 samples of 206 paediatric and adult patients with a median age of 8.3 years (range 0.04–33.9 years). Vincristine pharmacokinetics were described using a three-compartment model consisting of a central compartment, a peripheral compartment, and a saturable tubulin-binding compartment with linear elimination from the central compartment. The saturable binding of vincristine to  $\beta$ -tubulin was described using Equations 1 (differential equation) and 2:

$$\frac{dA(\text{bound})}{dt} = K_{on} \times A(Vc) \times \left(1 - \frac{A(\text{bound})}{B_{max}}\right) - K_{off} \times A(\text{bound}) \quad (\text{Equation 1})$$

$$B_{max} = B_{max,70\text{ kg}} \times \frac{WT}{70} \times \left(\frac{AGE}{18}\right)^{\theta_{B_{max} \sim AGE}} \quad (\text{Equation 2})$$

where  $K_{on}$  is the association rate constant,  $A(Vc)$  is the amount of vincristine in the central compartment  $Vc$ ,  $A(\text{bound})$  is the amount of vincristine bound to  $\beta$ -tubulin,  $B_{max}$  is the maximum amount of vincristine able to bind to  $\beta$ -tubulin for an individual,  $K_{off}$  is the dissociation rate constant,  $B_{max,70\text{ kg}}$  is the maximum amount of vincristine able to bind to  $\beta$ -tubulin for a typical individual with a body weight of 70 kg,  $WT$  is body weight in kg,  $AGE$  is age in years, and  $\theta_{B_{max} \sim AGE}$  is the power coefficient for the correlation between  $B_{max}$  and  $AGE$ .

Body weight was included as a covariate for clearance and volume of distribution for both the central and peripheral compartments with allometric scaling. Furthermore, inter-occasion variability was included in  $B_{max}$  to account for the

effect of chemotherapeutics on the number of dividing cells in the body. Residual variability was described using a proportional error model. The final parameter estimates are reported in Table S1 in Supplemental Digital Content 1 [7].

### 2.2.2 Virtual Patient Population

A demographic dataset of 1003 Kenyan and Malawian children was used to create a virtual pediatric patient population to ensure clinical applicability [24-27]. An overview of the demographic data is presented in Table S2 in Supplemental Digital Content 1. The final dataset consisted of 1001 children aged between 0.2 and 17 years, with a body weight between 5 and 59 kg, and a weight-for-height z-score (W-H-Z-score) between -8 and 8.3. Of these children, 12% were considered severely malnourished (Z-score < -3.0) and 14% were moderately malnourished (Z-score -2.0).

### 2.2.3 Simulations

Vincristine pharmacokinetics were simulated for 1000 patients as a 5-minute push injection at a dose of 2 mg/m<sup>2</sup> (max. 2.5 mg), according to the standard of care in Kenya. Vincristine plasma concentrations were simulated every 15 min for 4 h after the end of the push injection.

### 2.2.4 Bayesian Estimation for Therapeutic Drug Monitoring

One of the TDM strategies investigated was Bayesian estimation of vincristine clearance. Bayesian estimation of pharmacokinetic parameters has been well established for pharmacokinetic-guided dosing. Therefore, the Bayesian estimation of clearance was investigated for individual dose adaptations of vincristine. A sampling design with samples collected at 1, 1.5, and 4 h after the completion of vincristine administration was deemed clinically feasible. Vincristine clearance obtained from population pharmacokinetic simulations (see section Simulations) was defined as the true clearance ( $CL_{true}$ ), and Bayesian estimation was defined as the predicted clearance ( $CL_{pred}$ ). Bias and precision were calculated as the mean relative prediction error (MRPE) and root mean squared relative prediction error (RMSE), respectively, using Equations 3 and 4:

$$MRPE = \frac{\sum_{i=1}^n \frac{(Cl_{pred,i} - Cl_{true,i})}{Cl_{true,i}}}{n} \quad \text{(Equation 3)}$$

$$RMSE = \sqrt{\frac{\sum_{i=1}^n \left(\frac{(Cl_{pred,i} - Cl_{true,i})}{Cl_{true,i}}\right)^2}{n}}, \quad \text{(Equation 4)}$$

where  $n$  is the total number of subjects,  $CL_{pred,i}$  is the Bayesian estimate of vincristine clearance for individual  $i$  and  $CL_{true,i}$  is the vincristine clearance used in the simulation step for individual  $i$ . Furthermore, the fraction of mean prediction errors  $< 10\%$  and  $< 20\%$  was determined.

### 2.2.5 Pharmacometric Nomogram for Therapeutic Drug Monitoring

An alternative TDM strategy for Bayesian estimation was designed. This strategy was based on the assumption that vincristine exposure might be classified as low or adequate based on the ratio between the individual observed vincristine concentration and the median vincristine concentration of the population ( $R_t$ ) at different time points. However, using the median vincristine concentration of the complete pediatric population might lead to misclassification because vincristine pharmacokinetics are influenced by body weight and age (see section Population Pharmacokinetic Model). It was assumed that body weight had a more relevant effect on vincristine exposure than age because of the effect of the covariate on the respective pharmacokinetic parameters. Therefore, it was proposed to stratify patients based on their body weight (weight bands) and calculate  $R_t$ 's with the median vincristine concentration of the Caucasian pediatric population within the respective weight band. Vincristine exposure was classified as low when two or more  $R_t$  were  $\leq 0.80$ .

A pharmacometric nomogram was developed in several steps. First, the time points for sample collection were optimized for a typical (Caucasian) patient (18 years, 70 kg). Second, the performance of the pharmacometric nomogram with the optimized sampling strategy was investigated for each predefined weight band. Lastly, vincristine plasma concentrations were simulated using the optimal sampling strategy for 1001 virtual African pediatric oncology patients (see section Virtual Patient Population). The vincristine exposure of each patient was classified using a pharmacometric nomogram.

### 2.2.6 Weight Bands and Reference Patients

Weight bands were developed to stratify the patients into groups with similar vincristine pharmacokinetics to ensure sufficient accuracy of the pharmacometric nomogram. Weight bands were defined based on the effect of body weight on vincristine exposure in relation to the variability in the population [7]. This resulted in weight bands of 5 kg up to a body weight of 40 kg due to the high variability in body weight, age, and vincristine dose in smaller children, while weight bands of 10 kg were defined above a body weight of 40 kg due to relatively low variability in body weight, age, and reaching the capped maximum dose of 2.5 mg in larger children.

For each weight band, a typical (Caucasian) patient was developed as a reference for patients with body weight within the respective weight band. The patient had a specific body weight, age, and body surface area (BSA). Body weight was defined as the median body weight within the weight band. Age was defined as the median age of the children in the demographic dataset with body weight within the respective weight band. The corresponding BSA was calculated using a previously described method [28]. Patient characteristics are presented in Table 2. These reference patients were used for the simulation of reference concentrations (median concentration at each time point;  $C_{T,REF}$ ).

### 2.2.7 Optimization of the sampling strategy

The sampling strategy was optimized according to Figure 1 using the simulated pharmacokinetics of a typical (Caucasian) patient (18 years old, 70 kg). The true exposure classification was obtained by dividing the individual area under the concentration-time curve (AUC) with the median AUC ( $AUC_{REF}$ ) using the same threshold of  $\leq 0.80$  as for plasma concentration ratios. Different sampling strategies were tested by alternating sampling times in three predefined sampling windows: 0-1 h, 1.5-2.5 h, and 3-4 h after a 5-minute push injection. The sensitivity, specificity, and accuracy were determined to evaluate the performance of the nomogram. Sensitivity was weighted more than specificity and accuracy in the evaluation of different sampling designs because the aim of the TDM strategy was to identify patients with low exposure. The risk of overexposure due to false positives was considered low because the toxicity profile (e.g., presence of VIPN) and nutritional status of the patients also played a role in dose adjustments. A clinically feasible sampling design, with samples collected at 1, 1.5, and 4 h after vincristine administration, was used as the starting point.

### 2.2.8 Performance of the pharmacometric nomogram.

To investigate the performance of the nomogram, vincristine plasma concentrations were simulated using the model described in section Population pharmacokinetic model, and the virtual patient population described in section Virtual patient populations. The exposure of these virtual patients was classified using the reference concentrations as described in section Weight bands and reference patients.

## 2.3 Sensitivity Analysis

A sensitivity analysis was performed to check the robustness and limitations of the pharmacometric nomogram. The influence of missing samples, sampling errors, and alternative body weight bands on the performance of the pharmacometric nomogram was investigated.

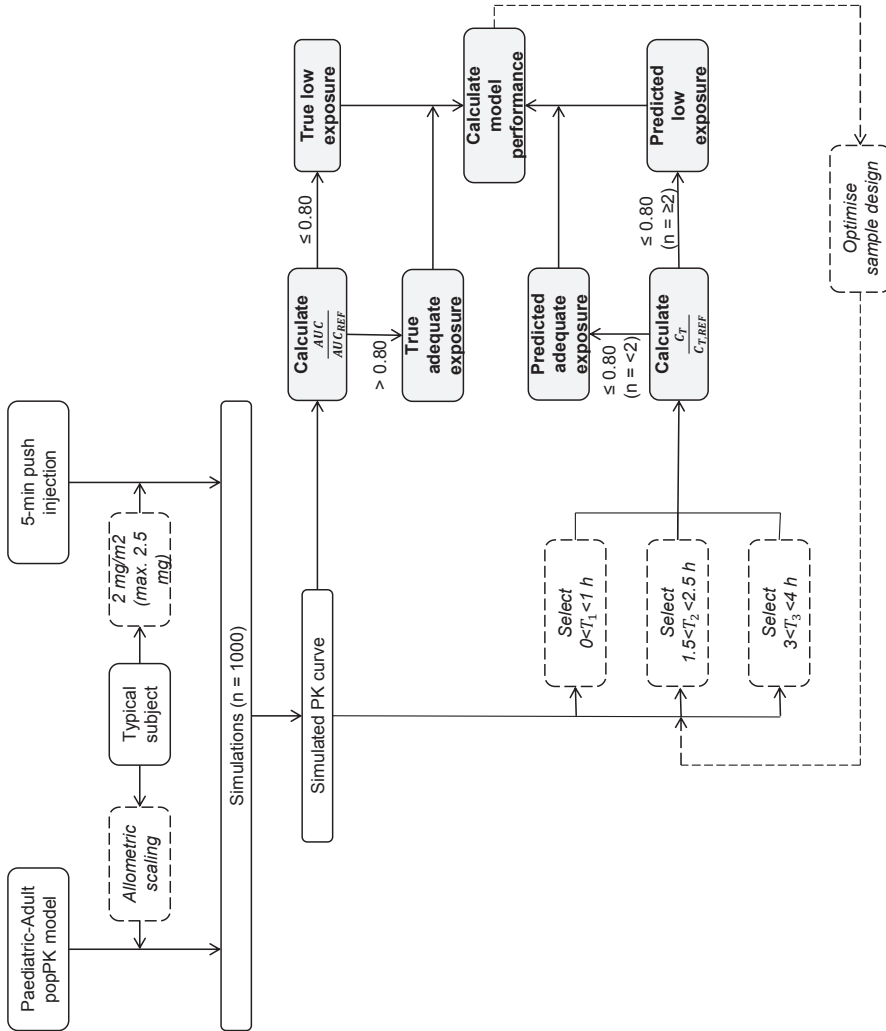


Figure 1. Flowchart of the simulation method.

## 3 RESULTS

### 3.1 Bayesian estimation for Pharmacokinetic-guided Dosing

The Bayesian estimation of vincristine clearance based on three plasma concentrations collected within the first four hours after administration was characterized by extreme shrinkage (see Figure 2). Generally, there was an underprediction of higher vincristine clearances, whereas the lower vincristine clearances were overpredicted, with prediction errors of up to 300%. The prediction errors could not be improved by changing the sampling strategy. In particular, extreme overpredictions would make dose individualization based on Bayesian estimation not only difficult but also potentially highly dangerous. The poor performance of Bayesian estimation was not observable in the MRPE, which ranged between 2.2% and 10.1%, while it was more pronounced in the RMSE, which ranged between 31.5% and 46.3% (see Table S3, Supplemental Digital Content 1). Therefore, it was concluded that Bayesian estimation was not an appropriate method for the exposure estimation of vincristine in the context of the practical constraints associated with the study design.

### 3.2 Pharmacometric Nomogram Development

#### 3.2.1 Study design optimization

The results of study design optimization are presented in Table 1. A clinically feasible study design, with sampling at 1, 1.5, and 4 h after a 5-minute push injection, was chosen as the starting point. The use of a sampling time point between 0-1 h post administration did not substantially improve the performance of the nomogram. The sensitivity, specificity, and accuracy ranged from 70.8% to 71.7%, 75.9% to 80.2%, and 74.2% to 77.3%, respectively. A sampling time of 1 h was chosen because it is the most pragmatic sampling time for the clinic. The sensitivity of the nomogram decreased from 70.8% to a minimum of 57.5% when the concentration-time point in sampling window 2 (1.5-2.5 h) was taken later than 1.5 hour after the push injection (Table 1). However, the specificity increased to approximately 85% and the accuracy was similar. The sensitivity of the nomogram decreased similarly when the concentration-time point in sampling window 3 (3-4 h) was considered earlier. A study design with concentration-time points of 1, 1.5, and 4 h after a 5 minute push-injection was chosen as the optimal study design because of its high sensitivity, specificity, accuracy, and clinical feasibility. The final nomogram is depicted in Supplemental Figure S1.

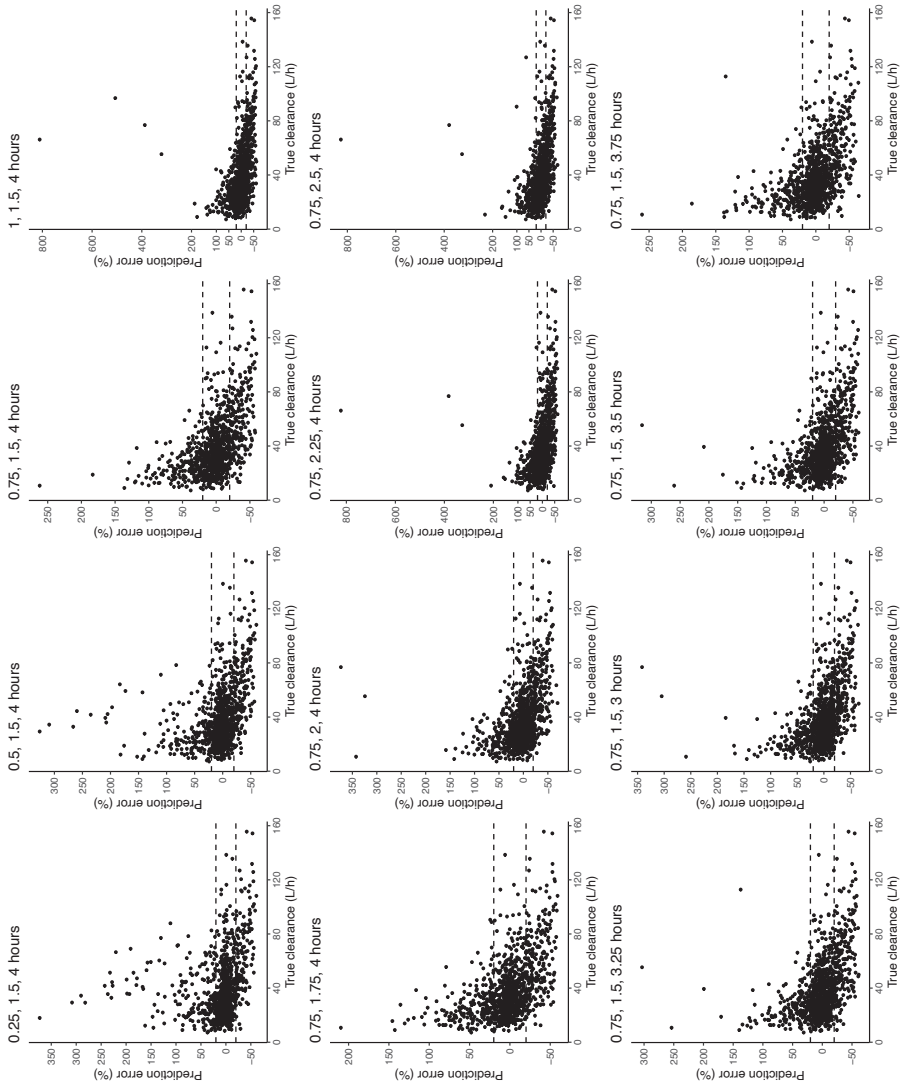


**Figure 2.** Prediction errors plotted against true clearance for different study designs. Dashed lines represent -20% and 20% boundaries.

**Table 1.** Study design optimization of the pharmacometric nomogram.

	Study design (hours)	Sensitivity (%)	Specificity (%)	Accuracy (%)
Final	1, 1.5, 4	70.8	75.9	74.2
Window 1	0.25, 1.5, 4	71.7	80.2	77.3
	0.5, 1.5, 4	70.5	78.2	75.6
	0.75, 1.5, 4	70.8	76.7	74.7
	1, 1.5, 4	70.8	75.9	74.2
Window 2	1, 1.75, 4	69.9	77.0	74.6
	1, 2, 4	57.5	85.8	76.2
	1, 2.25, 4	57.5	85.8	76.2
	1, 2.5, 4	57.8	85.8	76.3
Window 3	1, 1.5, 3.75	57.8	85.8	76.3
	1, 1.5, 3.5	57.8	85.3	76.0
	1, 1.5, 3.25	57.2	85.3	75.8
	1, 1.5, 3	56.9	84.9	75.4

### 3.2.2 Nomogram performance

Using the pharmacokinetic nomogram, it was possible to adequately classify the simulated vincristine exposure of 1001 pediatric oncology patients into low- and adequate-exposure groups. The overall model sensitivity was 75.1%, with a specificity of 76.4% and accuracy of 75.9%. The sensitivity was  $\geq 70\%$  for most weight categories (Table 2), indicating that patients with low exposure were identifiable for seven of the nine weight bands. Weight band 9 (50–60 kg) had the lowest sensitivity of 33.3%, probably because of the low number of virtual patients inside that weight band ( $n = 5$ ). Weight band 1 (5–10 kg) had a sensitivity of just below the desired 70%. This may be due to the relatively high variability in age, body weight, and dose in relation to the number of patients in that weight band.

### 3.3 Sensitivity Analysis


The sensitivity analysis demonstrated the strengths and limitations of the pharmacometric nomogram. The results of the sensitivity analysis are shown in Figure 3.



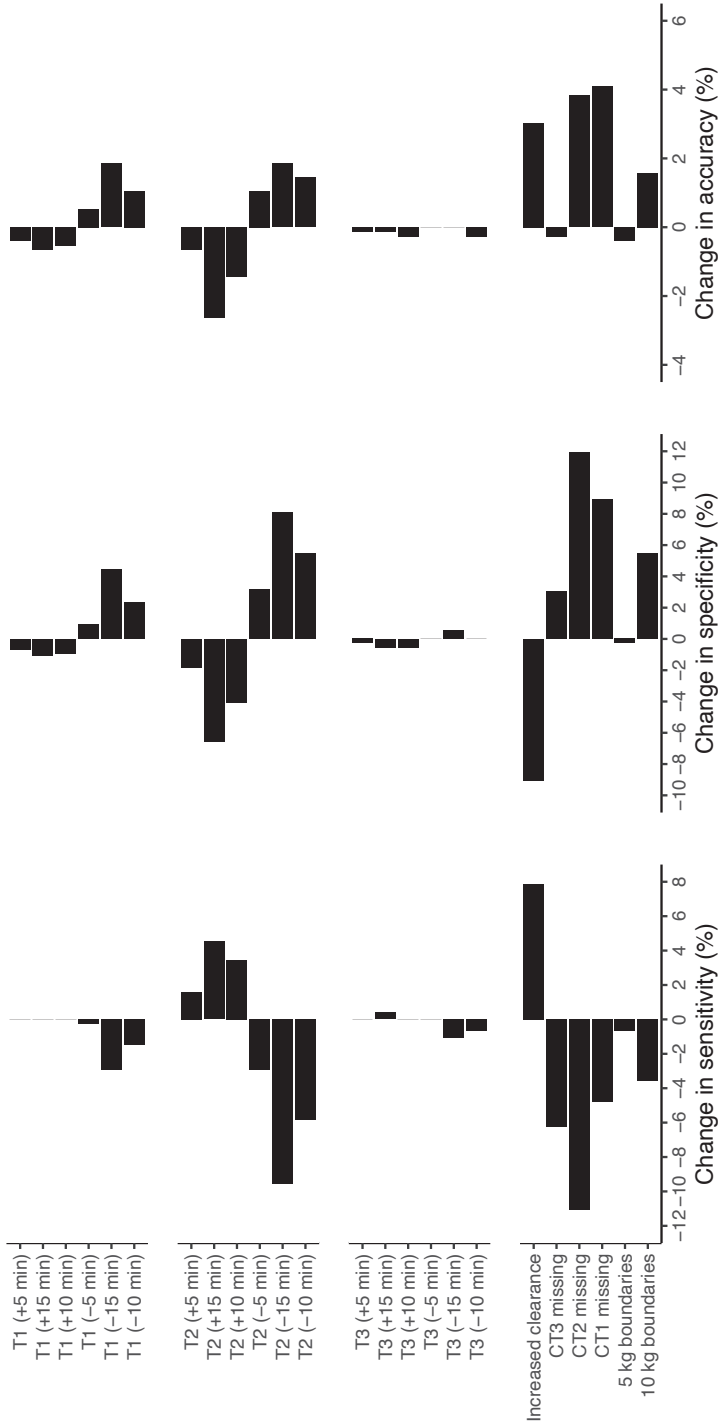


**Figure 3.** Results of the sensitivity analysis depicted as the change in sensitivity, specificity, and accuracy compared to the optimal study design. Abbreviations: CTi, concentration-time points of the respective sampling windows. Ti, time of sample collection within the respective sampling windows.

**Table 2.** Performance of the pharmacometric nomogram on simulated vincristine pharmacokinetics of African pediatric oncology patients. Demographic data are depicted as median (range).

Data	Demographic data				Reference patients		
	n	Age (yrs)	Weight (kg)	Dose (mg)	Age (yrs)	Weight (kg)	BSA (m <sup>2</sup> )
All data	1001	6 (0.2-17.0)	17.5 (5.0-59)	1.5 (0.4-2.5)			
Weight band 1	88	1.46 (0.25-4.30)	8.75 (5.0-9.9)	0.9 (0.6-1)	1.5	7.5	0.40
Weight band 2	299	3.1 (0.2-10.1)	12.4 (10-14.9)	1.1 (0.4-1.5)	3.1	12.5	0.575
Weight band 3	193	5.7 (0.6-12.0)	17 (15-19.9)	1.4 (1.2-1.7)	5.7	17.5	0.725
Weight band 4	171	8.2 (2.0-14.0)	22 (20-24.9)	1.8 (1.5-2)	8.2	22.5	0.86
Weight band 5	126	11 (1.3-15.1)	27 (25-29.8)	2 (1.8-2.2)	11.0	27.5	0.985
Weight band 6	69	12 (6.8-17.0)	31.7 (30-34.9)	2.2 (2-2.4)	12.0	32.5	1.10
Weight band 7	24	13 (2.75-15.0)	36 (35-39.9)	2.5 (2.1-2.5)	13.0	37.5	1.2
Weight band 8	26	13 (5.17-15.0)	42 (40-49.5)	2.5 (2.4-2.5)	13.0	45.0	1.4
Weight band 9	5	14 (12.8-14.2)	56.1 (51-59)	2.5	14.0	55.0	1.6

Abbreviations: BSA, body surface area; Ref. conc, reference concentration; Yrs, years.

Nomogram		Nomogram performance					
Weight bands (kg)	Ref. conc. (ng/mL) <sup>#</sup>	Predicted exposure	True low (n =)	True adequate (n =)	Sensitivity (%)	Specificity (%)	Accuracy (%)
		Low	269	152	75.1	76.4	75.9
5-10	6.89	Low	23	10	67.6	81.5	76.1
	4.33	Adequate	89	491			
10-15	6.40	Low	81	37	70.4	79.9	76.3
	3.88	Adequate	11	44			
15-20	6.40	Low	81	37	70.4	79.9	76.3
	1.50	Adequate	34	147			
15-20	5.90	Low	43	33	71.7	75.2	74.1
	3.49	Adequate	17	100			
20-25	5.75	Low	51	28	83.6	74.5	77.8
	3.32	Adequate	10	82			
25-30	5.58	Low	39	22	81.2	71.8	75.4
	3.22	Adequate	9	56			
30-35	5.72	Low	17	14	81.0	70.8	73.9
	3.25	Adequate	4	34			
35-40	5.77	Low	6	4	75.0	75.0	75.0
	3.28	Adequate	2	12			
40-50	5.85	Low	8	4	100	77.8	84.6
	3.32	Adequate	0	14			
50-60	5.68	Low	1	0	33.3	100	60
	3.23	Adequate	2	2			
50-60	5.68	Low	1	0	33.3	100	60
	1.11	Adequate	2	2			

<sup>#</sup> The reference concentrations are depicted in the order of sample collection, 1, 1.5, and 4 h after the end of a 5-minute push injection, respectively

The performance of the pharmacometric nomogram was sensitive to missing samples and early or delayed sample collection. In particular, when the second sample was missing or it deviated from the nominal sampling time, relatively large changes in the sensitivity, specificity, and accuracy were observed. However, the decrease in sensitivity was relatively limited, allowing 66.8% of the patients with low vincristine exposure to be correctly identified. Missing plasma concentrations at the first or third sample collection time resulted in a decrease in sensitivity by 5% and 6%, respectively, while the specificity and accuracy increased. The increase in sensitivity and accuracy due to missing samples was due to patients with vincristine concentrations that were close to the reference concentration. These patients were misclassified when all three samples were considered, but correctly classified when the second or third samples were missing. Furthermore, the second sample should be collected within  $\pm 5$  min of the intended sample collection time (1.5 h after a 5-minute push injection). For the first and third samples, a time interval of  $\pm 15$  min around the planned sample collection time resulted in an acceptable performance of the pharmacometric nomogram.

Changing the body weight boundaries to 5 or 10 kg did not influence the performance of the pharmacometric nomogram. Using 5 kg body weight boundaries instead of a combination of 5 and 10 kg body weight boundaries resulted in a decrease in sensitivity of -0.7%, while 10 kg body weight boundaries resulted in a decrease in sensitivity of -3.6%. The impact of 5 kg body weight boundaries on specificity and accuracy was negligible, while 10 kg body weight boundaries had a small increase of 5.5% and 1.6%, respectively.

Overall, the performance of the pharmacometric nomogram was relatively sensitive to missing samples and the exact timing of sample collection of the second sample. Nonetheless, the pharmacometric nomogram performed robustly with a sensitivity of 66.8–78.5%.

## 4 DISCUSSION

The current study aimed to develop a pharmacometric nomogram for the identification of pediatric patients with low vincristine exposure. A study design consisting of three samples collected at 1, 1.5, and 4 h after a 5-minute push injection resulted in the optimal performance of the pharmacometric nomogram. The pharmacometric nomogram could identify African pediatric oncology patients with simulated low vincristine exposure with high sensitivity, specificity, and accuracy (75.1%, 76.4%, and 75.9%, respectively) in a clinical setting with practical constraints. A decision tree of the pharmacometric nomogram is shown in Figure S1 in Supplemental Digital Content 1. The sensitivity analysis demonstrated the relative robustness of the pharmacometric nomogram. Furthermore, sensitivity analysis demonstrated that collection intervals of  $\pm 15$  min of the intended collection times are acceptable for the first and third samples, whereas the second sample should be collected within 5 min of the intended collection time. Finally, care should be taken to avoid missing samples, especially the second sample, as indicated by the sensitivity analysis.

The pharmacometric nomogram presented here was developed to identify African pediatric oncology patients with low vincristine exposure relative to their Caucasian peers. The Caucasian population seemed to be an appropriate reference because the pharmacokinetics, safety, and efficacy of vincristine have mainly been evaluated in the Caucasian population. Identification of African pediatric patients with low vincristine exposure is relevant because low exposure is currently clinically ignored, whereas high exposure may result in toxicity leading to dose reductions. Furthermore, there are several indications that African pediatric patients are currently underdosed with vincristine. First, non-Caucasian patients are less affected by VIPN than Caucasian patients, possibly due to racial differences in CYP3A5 expression [2, 17, 18, 29]. The incidence of CYP3A5 high-expressers in Kenyan children was found to be 91% versus 14% in a U.S. cohort, corresponding to a reduction in exposure of 58% [19], indicating that Kenyan children metabolize vincristine faster than Caucasian children. One study in adult lymphoma patients [11] and one study in pediatric acute lymphoblastic leukemia patients [30] reported an association between vincristine exposure and clinical outcomes, indicating that vincristine exposure may influence clinical outcomes. This has been confirmed by the observation that non-Caucasian oncology patients have poorer outcomes for several pediatric oncology diseases than Caucasian patients [20,21]. In addition, variability in vincristine exposure in African pediatric populations should be considered. Significantly lower vincristine

clearance ( $p = 0.001$ ) and higher vincristine exposure ( $p = 0.003$ ) were observed in Malawian pediatric patients ( $n = 11$ ) than in British pediatric patients ( $n = 8$ ) [22]. Nutritional status explained the difference in vincristine exposure ( $p = 0.043$ ) [22]. The relatively higher vincristine exposure in Malawian children may contribute to the considerable toxicity observed in Malawian children suffering from malnutrition receiving preoperative chemotherapy [23]. Therefore, dose optimization might be beneficial in improving vincristine treatment in African pediatric oncology patients. TDM could be a strategy to increase the dose of vincristine in low-exposure patients and finding an optimal dose in this patient population and prevent dose reductions due to toxicity in patients with high exposure. The pharmacometric nomogram enabled TDM by identifying patients with low vincristine exposure.

Since its introduction, the Bayesian estimation of pharmacokinetic parameters and its use in pharmacokinetic-guided dosing have been well established. It has been described for numerous drugs including vancomycin [31,32], mycophenolic acid [33], theophylline [34,35], aminoglycoside antibiotics [36-38], antiepileptic drugs [38-40], digoxin [41], and chemotherapeutics such as paclitaxel [42] and carboplatin [43]. However, for vincristine exposure, Bayesian estimation is not suitable under current clinical constraints. The complex pharmacokinetics of vincristine makes it difficult to accurately estimate vincristine exposure with only three concentrations collected within 4 h after administration. Vincristine demonstrates distribution pharmacokinetics with a fast initial distribution phase and long elimination phase [4,5]. Owing to the distribution pharmacokinetics of vincristine, it was difficult to capture AUC with the current limited sampling design, resulting in underprediction and extreme overprediction of vincristine clearance (Figure 2). The Bayesian estimation of individual concentrations would likely improve the performance of the Bayesian estimation. These Bayesian estimations of individual concentrations can be used as inputs for the pharmacometric nomogram. However, this would complicate the implementation of the pharmacometric nomogram in clinical practice, especially since the pharmacometric nomogram with simulated observed concentrations performs adequately.

This pharmacokinetic nomogram cannot be clinically evaluated until a future clinical study is conducted, in which the exposure of Kenyan pediatric patients will be classified according to the pharmacometric nomogram (see Supplemental Figure S1). The primary objective of this clinical trial is to optimize vincristine dosing in this patient population. Children with low vincristine exposure are eligible

for a dose increase of 20%. The sensitivity, specificity, and accuracy are thought to be representative of the performance of the pharmacometric nomogram in the study population because it was developed based on demographic data of real African pediatric oncology patients treated in the same treatment center where the algorithm is going to be implemented and evaluated. The high sensitivity of the pharmacometric nomogram ensures that enough patients with low vincristine exposure are identified to attain the primary objective of the study. Moreover, the risk of overdosing is low owing to the high specificity of the pharmacometric nomogram. However, approximately 23.6% of patients with adequate vincristine exposure will be incorrectly identified as having low exposure and could theoretically receive an unjustified dose increase. Theoretically, this could result in toxicity. However, dose increases should not be solely based on the outcome of the pharmacometric nomogram. Other factors such as nutritional status [22,23] and toxicity profile (e.g., development of VIPN) should also be taken into account, and the final decision should be made by the treating physician. Therefore, only patients with classified low vincristine exposure who are clinically expected to tolerate an increased dose will be considered for dose increase, minimizing the risk of overdosing and toxicity. Approximately 25% of patients with actual low vincristine exposure will be wrongly classified and therefore be at risk of continued underdosing, especially for patients with a body weight between 5-10 kg (see Table 2). Owing to practical limitations, the sensitivity could not be improved by, for example, extending the study design with an additional plasma concentration at a later time point. Finally, when samples of a patient are collected outside the recommended sampling windows or are missing, the impact on the classification of the patient should be estimated based on the sensitivity analysis (Figure 3). The risk of potential misclassification due to erroneous sampling or missing samples should be considered in the benefit-risk evaluation of a potential dose increase.

Pharmacometric nomograms offer several advantages. First, the pharmacometric nomogram does not rely on assumptions regarding the parameter distributions in African pediatric patients. This is important because the distribution of pharmacokinetic parameters is not necessarily similar between two pediatric populations. However, the reference concentrations used in the pharmacometric nomogram are based on the assumptions of parameter distributions in (predominantly) Caucasian patients. Second, the pharmacometric nomogram is a relatively simple method and, therefore, easy to use for clinicians unfamiliar with pharmacokinetic models. Furthermore, the pharmacometric nomogram uses a limited sampling strategy, with all samples collected within 4 h after administration. Patients will be able to go home relatively soon compared to

a Bayesian estimation strategy that might require a 24 h sample. Lastly, the pharmacometric nomogram can be extrapolated to different settings, such as other chemotherapeutics that have similar distribution pharmacokinetics as vincristine (e.g., doxorubicin, gemcitabine, and docetaxel). Owing to the pronounced and rapid distribution pharmacokinetics followed by slow terminal elimination, the application of classical TDM approaches such as Bayesian estimation is limited; therefore, our proposed approach could be a practical alternative. Furthermore, the pharmacometric nomogram can also be used to identify patients with high levels of exposure. A limitation of the pharmacometric nomogram is the loss of information. While the output of the pharmacometric nomogram is a binary exposure variable (low or non-low), each of these groups will contain a range of exposure values. Patient concentrations much lower than the reference concentrations will be considered for the same dose increase as patients with concentrations just below the reference concentrations.

## 5 CONCLUSION

A pharmacometric nomogram was developed to identify pediatric oncology patients with low vincristine exposure to support therapeutic drug monitoring of vincristine in Kenyan pediatric patients. The nomogram uses body weight and three plasma concentrations collected at 1, 1.5, and 4 h after a 5-minute push injection. The pharmacometric nomogram had a sensitivity of 75.1%, specificity of 76.4%, and accuracy of 75.9%. Missing samples should be avoided, and the three plasma concentrations should be collected within 15, 5, and 15 min of 1, 1.5, and 4 h after administration of a 5-minute push injection, respectively.



## REFERENCES

1. Stearn WT (1975) A Synopsis of the Genus *Catharanthus* (apocynaceae). The *Catharanthus* Alkaloids. pp. 9-45
2. van de Velde ME, Kaspers GL, Abbink FCH, Wilhelm AJ, Ket JCF, van den Berg MH (2017) Vincristine-induced peripheral neuropathy in children with cancer: A systematic review. *Crit Rev Oncol Hematol* 114:114-130. doi:10.1016/j.critrevonc.2017.04.004
3. Rowinsky EK, Donehower RC (1991) The clinical pharmacology and use of antimicrotubule agents in cancer chemotherapeutics. *Pharmacol Ther* 52 (1):35-84. doi:10.1016/0163-7258(91)90086-2
4. Minev B (2011) Cancer Management in Man: Chemotherapy, Biological Therapy, Hyperthermia and Supporting Measures. doi:10.1007/978-90-481-9704-0
5. Van den Berg HW, Desai ZR, Wilson R, Kennedy G, Bridges JM, Shanks RG (1982) The pharmacokinetics of vincristine in man: reduced drug clearance associated with raised serum alkaline phosphatase and dose-limited elimination. *Cancer Chemother Pharmacol* 8 (2):215-219. doi:10.1007/bf00255487
6. Guilhaumou R, Simon N, Quaranta S, Verschuur A, Lacarelle B, Andre N, Solas C (2011) Population pharmacokinetics and pharmacogenetics of vincristine in paediatric patients treated for solid tumour diseases. *Cancer Chemother Pharmacol* 68 (5):1191-1198. doi:10.1007/s00280-010-1541-4
7. Nijstad AL, Chu WY, de Vos-Kerkhof E, Enters-Weijnen CF, van de Velde ME, Kaspers GJL, Barnett S, Veal GJ, Lalmohamed A, Zwaan CM, Huitema ADR (2022) A Population Pharmacokinetic Modelling Approach to Unravel the Complex Pharmacokinetics of Vincristine in Children. *Pharm Res*. doi:10.1007/s11095-022-03364-1
8. Zhou XJ, Rahmani R (1992) Preclinical and clinical pharmacology of vinca alkaloids. *Drugs* 44 Suppl 4:1-16; discussion 66-19. doi:10.2165/00003495-199200444-00002
9. Gidding CE, Kellie SJ, Kamps WA, de Graaf SS (1999) Vincristine revisited. *Crit Rev Oncol Hematol* 29 (3):267-287. doi:10.1016/s1040-8428(98)00023-7
10. van de Velde ME, Panetta JC, Wilhelm AJ, van den Berg MH, van der Sluis IM, van den Bos C, Abbink FCH, van den Heuvel-Eibrink MM, Segers H, Chantrain C, van der Werff Ten Bosch J, Willems L, Evans WE, Kaspers GL (2020) Population Pharmacokinetics of Vincristine Related to Infusion Duration and Peripheral Neuropathy in Pediatric Oncology Patients. *Cancers (Basel)* 12 (7). doi:10.3390/cancers12071789
11. Igarashi T, Kishi S, Hosono N, Higashi T, Iwao T, Yano R, Tsukamoto H, Goto N, Yamauchi T, Ueda T (2021) Population pharmacokinetic model development and exposure-response analysis of vincristine in patients with malignant lymphoma. *Cancer Chemother Pharmacol* 87 (4):501-511. doi:10.1007/s00280-020-04220-y
12. Coccia PF, Altman J, Bhatia S, Borinstein SC, Flynn J, George S, Goldsby R, Hayashi R, Huang MS, Johnson RH, Beaupin LK, Link MP, Oeffinger KC, Orr KM, Pappo AS, Reed D, Spraker HL, Thomas DA, von Mehren M, Wechsler DS, Whelan KF, Zebrack BJ, Sundar H, Shead DA (2012) Adolescent and young adult oncology. Clinical practice guidelines in oncology. *J Natl Compr Canc Netw* 10 (9):1112-1150. doi:10.6004/jncn.2012.0117
13. Stryckmans PA, Lurie PM, Manaster J, Vamecq G (1973) Mode of action of chemotherapy in vivo on human acute leukemia--II. Vincristine. *Eur J Cancer* 9 (9):613-620. doi:10.1016/0014-2964(73)90002-9

14. Lew G, Chen Y, Lu X, Rheingold SR, Whitlock JA, Devidas M, Hastings CA, Winick NJ, Carroll WL, Wood BL, Borowitz MJ, Pulsipher MA, Hunger SP (2021) Outcomes after late bone marrow and very early central nervous system relapse of childhood B-acute lymphoblastic leukemia: a report from the Children's Oncology Group phase III study AALL0433. *Haematologica* 106 (1):46-55. doi:10.3324/haematol.2019.237230
15. Frost BM, Lönnerholm G, Koopmans P, Abrahamsson J, Behrendtz M, Castor A, Forestier E, Uges DR, de Graaf SS (2003) Vincristine in childhood leukaemia: no pharmacokinetic rationale for dose reduction in adolescents. *Acta Paediatr* 92 (5):551-557
16. Gidding CE, Meeuwssen-de Boer GJ, Koopmans P, Uges DR, Kamps WA, de Graaf SS (1999) Vincristine pharmacokinetics after repetitive dosing in children. *Cancer Chemother Pharmacol* 44 (3):203-209. doi:10.1007/s002800050968
17. Anghelescu DL, Faughnan LG, Jeha S, Relling MV, Hinds PS, Sandlund JT, Cheng C, Pei D, Hankins G, Pauley JL, Pui CH (2011) Neuropathic pain during treatment for childhood acute lymphoblastic leukemia. *Pediatr Blood Cancer* 57 (7):1147-1153. doi:10.1002/pbc.23039
18. Diouf B, Crews KR, Lew G, Pei D, Cheng C, Bao J, Zheng JJ, Yang W, Fan Y, Wheeler HE, Wing C, Delaney SM, Komatsu M, Paugh SW, McCorkle JR, Lu X, Winick NJ, Carroll WL, Loh ML, Hunger SP, Devidas M, Pui CH, Dolan ME, Relling MV, Evans WE (2015) Association of an inherited genetic variant with vincristine-related peripheral neuropathy in children with acute lymphoblastic leukemia. *Jama* 313 (8):815-823. doi:10.1001/jama.2015.0894
19. Skiles JL, Chiang C, Li CH, Martin S, Smith EL, Olbara G, Jones DR, Vik TA, Mostert S, Abbink F, Kaspers GJ, Li L, Njuguna F, Sajdyk TJ, Renbarger JL (2018) CYP3A5 genotype and its impact on vincristine pharmacokinetics and development of neuropathy in Kenyan children with cancer. *Pediatr Blood Cancer* 65 (3). doi:10.1002/pbc.26854
20. Jemal A, Thomas A, Murray T, Thun M (2002) Cancer statistics, 2002. *CA Cancer J Clin* 52 (1):23-47. doi:10.3322/canjclin.52.1.23
21. Pollock BH, DeBaun MR, Camitta BM, Shuster JJ, Ravindranath Y, Pullen DJ, Land VJ, Mahoney DH, Jr., Lauer SJ, Murphy SB (2000) Racial differences in the survival of childhood B-precursor acute lymphoblastic leukemia: a Pediatric Oncology Group Study. *J Clin Oncol* 18 (4):813-823. doi:10.1200/jco.2000.18.4.813
22. Israels T, Damen CW, Cole M, van Geloven N, Boddy AV, Caron HN, Beijnen JH, Molyneux EM, Veal GJ (2010) Malnourished Malawian patients presenting with large Wilms tumours have a decreased vincristine clearance rate. *Eur J Cancer* 46 (10):1841-1847. doi:10.1016/j.ejca.2010.03.002
23. Israels T, Chagaluka G, Pidini D, Caron H, de Kraker J, Kamiza S, Borgstein E, Molyneux L (2012) The efficacy and toxicity of SIOP preoperative chemotherapy in Malawian children with a Wilms tumour. *Pediatr Blood Cancer* 59 (4):636-641. doi:10.1002/pbc.24088
24. van Weelderen RE, Njuguna F, Klein K, Mostert S, Langat S, Vik TA, Olbara G, Kipng'etich M, Kaspers GJL (2021) Outcomes of pediatric acute myeloid leukemia treatment in Western Kenya. *Cancer Rep (Hoboken)*:e1576. doi:10.1002/cnr2.1576
25. Olbara G, van der Wijk T, Njuguna F, Langat S, Mwangi H, Skiles J, Vik TA, Kaspers GJL, Mostert S (2021) Childhood acute lymphoblastic leukemia treatment in an academic hospital in Kenya: Treatment outcomes and health-care providers' perspectives. *Pediatr Blood Cancer* 68 (12):e29366. doi:10.1002/pbc.29366

26. Uittenboogaard A, Njuguna F, Mostert S, Langat S, van de Velde ME, Olbara G, Vik TA, Kaspers GJL (2022) Outcomes of Wilms tumor treatment in western Kenya. *Pediatr Blood Cancer* 69 (4):e29503. doi:10.1002/pbc.29503
27. Huibers MHW, Manda G, Silverstein A, Wanda W, Mtete I, Makuti S, Westmoreland KD, Mehta P, Ozuah NW (2022) The Burden of Malnutrition in Childhood Cancer in Malawi - Risk Regardless of Age. *Nutr Cancer* 74 (9):3322-3328. doi:10.1080/01635581.2022.2076888
28. Sharkey I, Boddy AV, Wallace H, Mycroft J, Hollis R, Picton S (2001) Body surface area estimation in children using weight alone: application in paediatric oncology. *Br J Cancer* 85 (1):23-28. doi:10.1054/bjoc.2001.1859
29. Renbarger JL, McCammack KC, Rouse CE, Hall SD (2008) Effect of race on vincristine-associated neurotoxicity in pediatric acute lymphoblastic leukemia patients. *Pediatr Blood Cancer* 50 (4):769-771. doi:10.1002/pbc.21435
30. Lönnerholm G, Frost BM, Abrahamsson J, Behrendtz M, Castor A, Forestier E, Heyman M, Uges DR, de Graaf SS (2008) Vincristine pharmacokinetics is related to clinical outcome in children with standard risk acute lymphoblastic leukemia. *Br J Haematol* 142 (4):616-621. doi:10.1111/j.1365-2141.2008.07235.x
31. Neely MN, Kato L, Youn G, Kraler L, Bayard D, van Guilder M, Schumitzky A, Yamada W, Jones B, Minejima E (2018) Prospective Trial on the Use of Trough Concentration versus Area under the Curve To Determine Therapeutic Vancomycin Dosing. *Antimicrob Agents Chemother* 62 (2). doi:10.1128/aac.02042-17
32. Pai MP, Neely M, Rodvold KA, Lodise TP (2014) Innovative approaches to optimizing the delivery of vancomycin in individual patients. *Adv Drug Deliv Rev* 77:50-57. doi:10.1016/j.addr.2014.05.016
33. Barraclough KA, Isbel NM, Staatz CE (2010) Evaluation of the mycophenolic acid exposure estimation methods used in the APOMYGERE, FDCC, and Optcept trials. *Transplantation* 90 (1):44-51. doi:10.1097/TP.0b013e3181e06584
34. Chrystyn H, Ellis JW, Mulley BA, Peake MD (1988) The accuracy and stability of Bayesian theophylline predictions. *Ther Drug Monit* 10 (3):299-305. doi:10.1097/00007691-198803000-00011
35. Hurley SF, McNeil JJ (1988) A comparison of the accuracy of a least squares regression, a Bayesian, Chiou's and the steady-state clearance method of individualising theophylline dosage. *Clin Pharmacokinet* 14 (5):311-320. doi:10.2165/00003088-198814050-00003
36. Burton ME, Chow MS, Platt DR, Day RB, Brater DC, Vasko MR (1986) Accuracy of Bayesian and Sawchuk-Zaske dosing methods for gentamicin. *Clin Pharm* 5 (2):143-149
37. Kraus DM, Dusik CM, Rodvold KA, Campbell MM, Kecskes SA (1993) Bayesian forecasting of gentamicin pharmacokinetics in pediatric intensive care unit patients. *Pediatr Infect Dis J* 12 (9):713-718. doi:10.1097/00006454-199309000-00002
38. Rodvold KA, Pryka RD, Kuehl PG, Blum RA, Donahue P (1990) Bayesian forecasting of serum gentamicin concentrations in intensive care patients. *Clin Pharmacokinet* 18 (5):409-418. doi:10.2165/00003088-199018050-00005
39. Kuranari M, Chiba S, Ashikari Y, Kodama Y, Sakata T, Takeyama M (1996) Clearance of phenytoin and valproic acid is affected by a small body weight reduction in an epileptic obese patient: a case study. *Journal of clinical pharmacy and therapeutics* 21 (2):83-87. doi:10.1111/j.1365-2710.1996.tb00005.x

40. Boucher BA, Rodman JH, Fabian TC, Cupit GC, Ludden TM, West ME, Ray MW (1987) Disposition of phenytoin in critically ill trauma patients. *Clin Pharm* 6 (11):881-887
41. el Desoky E, Meinshausen J, Bühl K, Engel G, Harings-Kaim A, Drewelow B, Klotz U (1993) Generation of pharmacokinetic data during routine therapeutic drug monitoring: Bayesian approach vs. pharmacokinetic studies. *Ther Drug Monit* 15 (4):281-288. doi:10.1097/00007691-199308000-00004
42. de Jonge ME, van den Bongard HJ, Huitema AD, Mathôt RA, Rosing H, Baas P, van Zandwijk N, Beijnen JH, Schellens JH (2004) Bayesian pharmacokinetically guided dosing of paclitaxel in patients with non-small cell lung cancer. *Clin Cancer Res* 10 (7):2237-2244. doi:10.1158/1078-0432.ccr-03-0060
43. Huitema AD, Mathôt RA, Tibben MM, Schellens JH, Rodenhuis S, Beijnen JH (2000) Validation of techniques for the prediction of carboplatin exposure: application of Bayesian methods. *Clin Pharmacol Ther* 67 (6):621-630. doi:10.1067/mcp.2000.106827

## SUPPLEMENTARY MATERIAL.

**Supplementary Table S1.** Vincristine pharmacokinetic parameter estimates of the final model.

Parameter	Estimate	95% CI
$CL_{70\text{kg}}$ (L/h)	30.6	27.6 – 33.0
$Q_{70\text{kg}}$ (L/h)	63.2	57.2 – 70.1
$Vc_{70\text{kg}}$ (L)	5.39	4.23 – 6.46
$Vp_{70\text{kg}}$ (L)	400	357 – 463
$Bmax_{18\text{yrs},70\text{kg}}$ ( $\mu\text{g}$ )	0.525	0.479 – 0.602
$k_{\text{on}}$ (/h)	1300 fixed	
$k_{\text{off}}$ (/h)	11.5	9.2 – 14.5
Age on $Bmax$	-0.199	-0.304 – -0.090
IIV CL (%)	47.7	41.0 – 54.3
IIV Q (%)	38.1	26.2 – 49.0
IIV $Vc$ (%)	122.5	98.7 – 158.3
IIV $Vp$ (%)	57.1	48.8 – 69.7
IIV $k_{\text{on}}$ (%)	126.5	108.7 – 147.8
IIV $k_{\text{off}}$ (%)	24.1	11.1 – 33.8
IOV $Bmax$ (%)	59.1	50.7 – 66.1
Proportional residual error (%)	30.1	28.9 – 31.4

Abbreviations:  $Bmax$ , maximal binding capacity; CI, Confidence interval obtained by sampling importance resampling; CL, Clearance; IIV, Interindividual variability; IOV, interval variability;  $k_{\text{off}}$ , dissociation rate constant;  $k_{\text{on}}$ , association rate constant; PK, pharmacokinetics (s); Q, Intercompartmental clearance;  $Vc$ , central compartment;  $Vp$ , peripheral compartment.

$Bmax$  corresponds to a subject aged 18 years weighing 70 kg, while other population estimates correspond to a subject weighing 70 kg and are adjusted to an individual value using allometric scaling.

The final parameter estimates are obtained from Nijstad *et al.*, (2022) [7].

**Supplementary Table S2.** Demographic data of 1001 Kenyan and Malawian paediatric oncology patients.

	Kenya	Malawi
Number of in children	689	312
Boys (%)	43.8	59.9
Age (years)	5.8 (0.2-16.3)	6 (0.3-17)
Bodyweight (kg)	17.5 (5-59)	17 (6-51)
BSA (m <sup>2</sup> )	0.7 (0.3-1.6)	0.7 (0.2-1.5)
Z-score	-1 (-8-8.3)	-1 (-6.3-5.9)

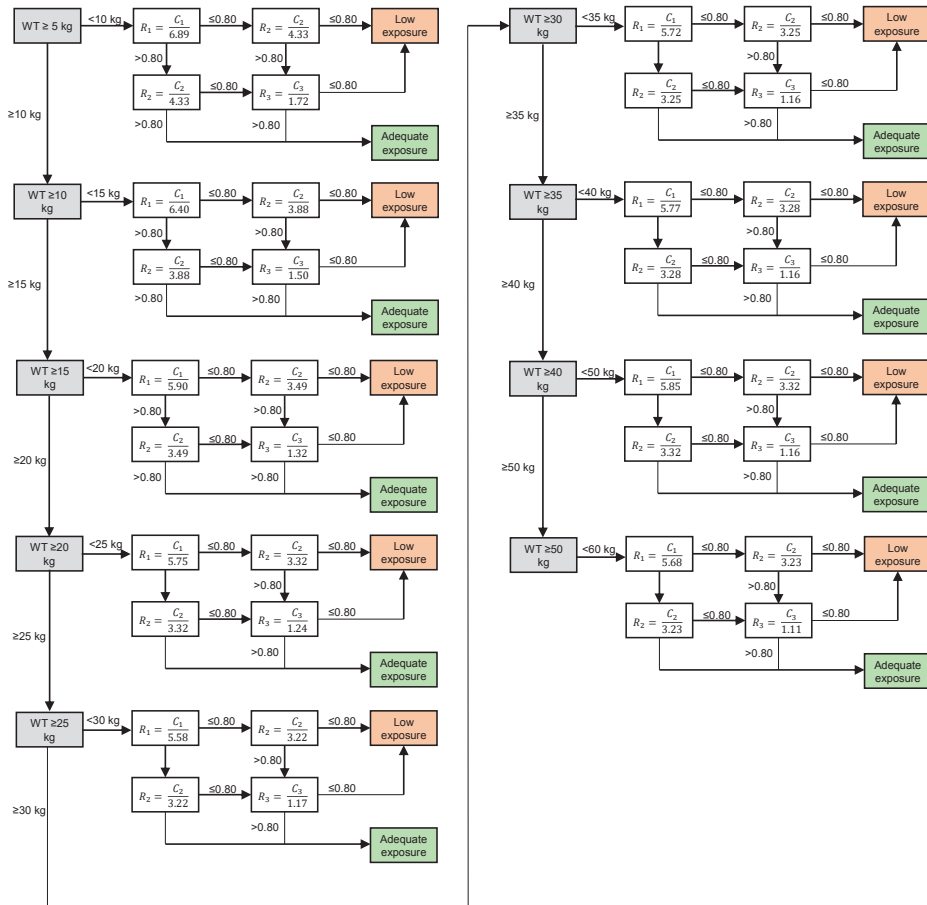
All values are presented as medians (range), unless otherwise specified.

Abbreviations: BSA, body surface area.

**Supplementary Table S3.** Numerical results of Bayesian estimation of vincristine clearance performance.

Study design (hours)	MRPE (%)	RMSE (%)	Fraction $\pm$ 10% (%)	Fraction $\pm$ 20% (%)
0.25, 1.5, 4	10.1	45.4	50.8	67.7
0.5, 1.5, 4	5.6	39.9	44.8	64.9
0.75, 1.5, 4	2.4	31.7	38.8	60.2
1, 1.5, 4	3.0	46.3	35.6	56.7
0.75, 1.75, 4	2.6	31.5	38.4	57.4
0.75, 2.25, 4	3.3	36.5	34.8	56.2
0.75, 2.25, 4	3.3	43.9	34.5	56.6
0.75, 2.25, 4	4.1	44.5	34.1	54.4
0.75, 1.5, 3.25	2.6	33.8	38.2	60.5
0.75, 1.5, 3	2.7	35.6	37.5	60.8
0.75, 1.5, 3.5	2.8	33.7	38.9	61.0
0.75, 1.5, 3.75	2.2	32.3	37.6	59.3

Abbreviations: MRPE, mean relative prediction error. RMSE, root mean squared relative prediction error.



**Supplementary Figure S1.** Decision tree of the pharmacometric nomogram. Abbreviations:  $C_1$ , vincristine plasma concentration collected 1 h after complete administration.  $C_2$ , vincristine plasma concentration collected 1.5 hours after complete administration.  $C_3$ , vincristine plasma concentration, collected 4 h after complete administration.  $R_1$ , ratio of the measured plasma concentration to the reference concentration 1 h after complete administration.  $R_2$ , ratio of the measured plasma concentration to the reference concentration at 1.5 hours after complete administration.  $R_3$ , the ratio of the measured plasma concentration to the reference concentration at 4 h after complete administration.





# Chapter 13

## **Conclusions and Perspectives**



## CONCLUSIONS AND PERSPECTIVES

Despite the need for an improved dose selection in early development of anticancer agents, many dose-escalating Phase I clinical trials still define the recommended Phase 2 dose (RP2D) on toxicity data [1,2]. However, for improved dose selection, characterisation of exposure-response relationships is essential. This thesis focusses on three important methods for the support of dose finding in oncology drug development: sensitive bioanalytical methods, microdosing and pharmacometric modelling. The main findings and implications of the work described in this thesis on these three topics are summarized in Figure 1.

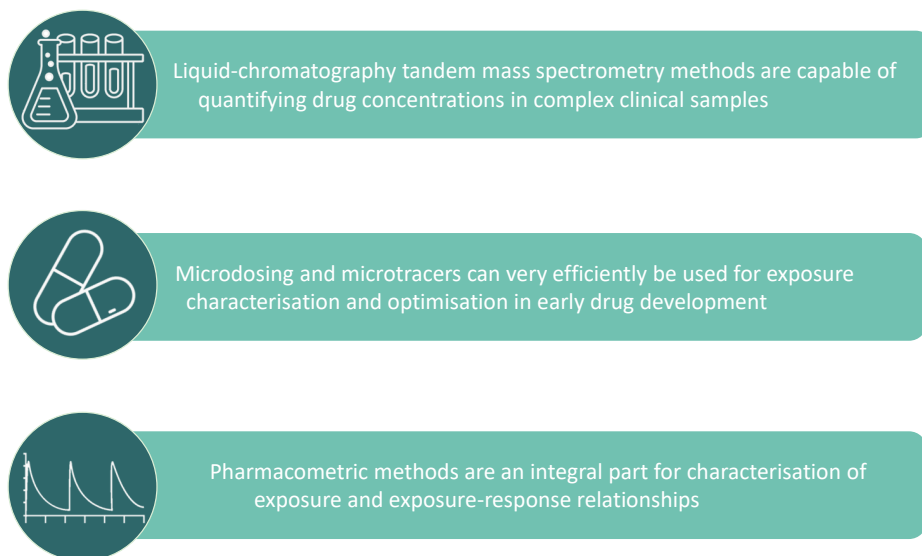


**Figure 1.** Key points extracted from this thesis.

### **Ultra-sensitive liquid-chromatography tandem mass spectrometry methods are capable of quantifying drug concentrations in complex clinical samples**

The ability to quantify drug concentrations in biological matrices over a clinically relevant concentration range is essential for the characterisation of pharmacokinetics and thus for dose finding. Previously, accelerated mass spectrometry (AMS) was necessary to quantify concentrations in the picogram per millilitre (pg/mL) range (or lower) [3]. Application of AMS is complicated by its limited availability and the use of radioactive labelled compounds [3]. Recent advances within the field of bioanalysis made it possible to quantify

increasingly lower drug concentrations with liquid chromatography tandem mass spectrometry (LC-MS/MS). In comparison to AMS, LC-MS/MS is more readily available in laboratories and is independent on the radioactive labelling of compounds, making it a suitable equipment to support clinical trials [3]. In this thesis, the development and validation of several fit-for-purpose LC-MS/MS methods have been described that contribute to exposure characterisation and exposure optimisation of several anticancer agents.

Two LC-MS/MS methods were used for the quantification of vincristine in human plasma (**Chapter 9**) and whole blood collected with volumetric absorptive microsampling (VAMS; **Chapter 10**). The bioanalysis of vincristine in plasma is a relatively straightforward LC-MS/MS method but still with a lower limit of quantitation in the low ng/mL range. Despite the long-established clinical use of vincristine, covariates explaining the inter-individual variability observed in vincristine pharmacokinetics remain largely unknown [4,5]. Due to these two sensitive LC-MS/MS methods vincristine pharmacokinetics in plasma and whole blood could be investigated resulting in the conclusion that children have a lower  $\beta$ -tubulin binding capacity compared to adults as described in **Chapter 11** and by Nijstad, *et al* [6], which might explain the fact that children are able to tolerate higher doses of vincristine.

These studies paved the way for further dose optimisation of vincristine in children. However, for this population, an assay requiring minimal volumes of blood is necessary, which demands ultrasensitive detection. Therefore, an assay for vincristine in VAMS was developed (**Chapter 10**). This LC-MS/MS contributed to the feasibility of a pharmacokinetic study for the optimisation of vincristine dosing in Kenyan children (NCT05844670). VAMS is an alternative sampling method, which requires small volumes ( $\leq 20$   $\mu$ L) of whole blood and uses a less invasive method for sample collection (e.g., finger prick instead for venepuncture) [7,8]. Therefore, VAMS might be a more desirable sampling method for vulnerable and frail patient populations, such as paediatrics. Additional advantages of VAMS sampling are stability due to the dried matrix form (dried whole blood) making shipment at ambient temperatures possible and the possibility of home sampling. Since LC-MS/MS methods are capable of quantifying drug concentrations in human whole blood collected with VAMS, VAMS can be considered as a sampling method in future clinical studies not only for special populations such as paediatrics [9] but also adult populations [10].

Further dose optimisation of anticancer agents could be achieved with target-site bioanalysis with LC-MS/MS. Tissue drug concentrations could improve our understanding of exposure-response relationship. Target-site bioanalysis early in drug development is possible since biopsy collection at start and during treatment has become more common practice in Phase I clinical trials [11]. While intratumour sunitinib concentrations were higher compared to plasma for glioblastoma [12], it is unknown if this will be the case for every drug. Therefore, sensitive LC-MS/MS methods are essential for the quantification of tissue drug concentrations.

Lastly, LC-MS/MS methods can also support novel clinical trial designs such as microdose and microtracer studies. These compounds are usually administered at extreme low doses ( $\leq 100 \mu\text{g}$ ) and therefore ultrasensitive bioanalytical assays are essential for the feasibility of these studies. Moreover, these bioanalytical methods, especially for the support of microtracer studies, are challenged by isotope interference due to the large difference in concentration range between microtracer (stable isotopically labelled drug) and the unlabelled drug ( $\geq 1,000$ -fold). **Chapter 2** demonstrated that concentrations as low as  $1 \text{ pg/mL}$  of  $^2\text{H}_6$ -alectinib (microtracer) could be quantified with an accuracy and precision of  $\pm 15.9\%$  and  $\leq 12.5\%$ , respectively, in presence of  $\geq 400 \text{ ng/mL}$  alectinib. The methods of correction for spectral isotope interference described in this chapter can be applied to other LC-MS/MS bioanalytical methods with microdose and microtracer studies.

Taken together, relatively simple LC-MS/MS methods are capable of quantifying drug concentrations in complex clinical samples. Ultrasensitive LC-MS/MS methods enable pharmacokinetic studies which were not possible before, and which can make important contributions to dose optimization for instance in special populations like paediatrics.

### **Microdosing and microtracers can very efficiently be used for exposure characterisation and optimisation in early drug development**

Microdoses are sub-therapeutic doses at  $1/100^{\text{th}}$  of the (anticipated) therapeutic dose with a maximum dose of  $100 \mu\text{g}$  [5]. These microdoses are administered to study participants with the aim of an early assessment of *in vivo* pharmacokinetics prior to Phase I clinical trials [5]. The predictive value of a microdose is usually determined by performing non-compartmental analysis for both the microdose and the therapeutic dose, where the dose-normalised pharmacokinetic metrics should fall within 2-fold of each other [13,14]. Based on this methodology, the predictive value of a microdose was found to be between 62-68% for oral drugs and 94-100% for intravenous drugs [15,16].

The predominant disadvantage of this methodology is its inability to extrapolate to different therapeutic doses. Extrapolation to therapeutic doses can be performed using naïve pooled data (NPD) pharmacokinetic models (**Chapter 1**). These extrapolations can be used to inform dose selection in dose-escalating Phase I trials. Dose selection for dose-escalating Phase I trials could be further improved by using physiologically-based pharmacokinetic (PBPK) modelling to combine microdose pharmacokinetics with preclinical data. Drug characteristics, disease biology, and preclinical data such as *in vitro* enzyme/transporter kinetic data, could be used for the development of a PBPK model for a new anticancer agent, while *in vivo* microdose pharmacokinetics could be used for model optimisation.

Microdosing has also been applied to other study design, such as drug-drug interaction studies, pharmacokinetic studies in vulnerable populations, metabolic profiling, and site of action studies [15,17,18]. Extrapolation of these studies to therapeutic dose level can also be achieved with the NPD pharmacokinetic models. Moreover, microdosing has increasingly been used for *in vivo* phenotyping of Cytochrome P450 (CYP) enzymes (**Chapter 4**). *In vivo* phenotyping at microdose level would allow characterisation of drug elimination in early drug development without pharmacological adverse events. Moreover, *in vivo* phenotyping at microdose level could be used for individualised dose-adaptations such as for simvastatin [19].

Microtracers, like microdoses, are administered at a maximum dose of 100 µg. Unlike microdoses, they are stable isotopically labelled drugs that are co-administered with an unlabelled therapeutic dose [20]. Due to the difference in molecular weight, both labelled and unlabelled drug can be quantified within the same sample, and therefore pharmacokinetics of both labelled and unlabelled drug can be determined simultaneously. Due to this characteristic, microtracers were originally used for the determination of absolute bioavailability [20]. Despite absolute bioavailability, other pharmacokinetic processes such as drug absorption can be investigated using microtracers. For example, a microtracer food-effect study would allow the determination of the food-effect on the pharmacokinetics of the microtracer, while the treatment with the unlabelled drug is unaffected (**Chapter 3**). Using this trial design, the patient burden of food-effect studies in patients for drugs with long half-lives can be decreased. This is clinically relevant since food-effect on drug exposure can differ between single dose pharmacokinetics in healthy volunteers compared to steady-state pharmacokinetics in patients as for lapatinib [21,22] and abiraterone [23].

In summary, microdoses and microtracers can very efficiently be used for the characterisation of pharmacokinetic processes in early drug development. Data obtained during microdose/microtracer studies can inform dose selection for subsequent clinical trials. Therefore, these study designs should become an integral part of drug development for new anticancer agents.

### **Pharmacometric methods are an integral part of the characterisation of exposure and exposure-response relationships**

Quantitative mathematical models are fundamental for the characterisation of drug exposure and exposure-response relationships. The importance of pharmacometrics in drug development has been recognized by the US Food and Drug Administration (FDA) [24]. While pharmacometrics has been embraced by the pharmaceutical industry, it has yet to be implemented consistently in decision-making regarding dose selection in early drug development [25-27]. This is a missed opportunity since pharmacometrics can contribute to an improved dose selection in early drug development.

First, pharmacokinetic models can identify patient subpopulations with different pharmacokinetic profiles who might need dose adaptations. By investigating factors (covariates) affecting inter-individual variability in pharmacokinetics an improved understanding of population pharmacokinetics can be obtained (**Chapter 7**). Moreover, PBPK models can investigate the influence of physiological processes on pharmacokinetics since they quantitatively describe human physiology to accurately predict concentration-time profiles of drugs in different tissues. Thereby, hypotheses can be mechanistically investigated as demonstrated for the influence of vincristine binding to  $\beta$ -tubulin in blood cells on vincristine pharmacokinetics (**Chapter 11**). Identification of subpopulations with deviant pharmacokinetic profiles is important to rationalise dose selection in these subpopulations such as children (**Chapter 11**), African children (**Chapter 12**), and patients with a specific tumour type such as metastatic castration resistant prostate cancer (**Chapter 7**).

In addition to identification of patient subpopulations, these pharmacokinetic models can extrapolate pharmacokinetics across subpopulations to inform doses for future clinical studies. Both PBPK and population pharmacokinetic models can be used for extrapolation. PBPK models extrapolate based on physiological mechanistic differences between populations, such as difference in drug-target binding (**Chapter 11**), and thereby able to predict drug exposure in multiple tissues. Population pharmacokinetic models can extrapolate drug exposure to

patient subpopulations based on clinically relevant covariates, such as tumour type (**Chapter 12**). Using these models, dosing regimens can be compared to each other or the achievement of a desired target, and thereby rationalising dose selection for future clinical studies in these populations. These models can be improved by incorporating emerging (clinical) data. For example, the PBPK model for vincristine in **Chapter 11** might be improved by the incorporation of the CEP72 mutation [28].

A next step to improve dose selection would be the development of pharmacokinetic-pharmacodynamic (PK-PD) models, in which pharmacokinetics is linked to clinical outcomes such as efficacy or toxicity (**Chapter 6**). These PK-PD models can be used to extrapolate different dose regimens and investigate which dose regimen result in exposure with an optimal efficacy/toxicity profile. In this manner, these models can help select doses for future trials by selecting a dose with an optimal exposure-response profile or prioritising future dose levels based on their response (**Chapter 6**). PK-PD models could be improved by incorporating mechanistic models describing drug action resulting in efficacy or toxicity. Inclusion of drug action mechanisms in PK-PD could increase the confidence in predictions under different conditions. An improved understanding of drug efficacy and toxicity could be obtained with patient derived organoids (**Chapter 5**).

Lastly, pharmacometrics can improve study design by assessing study design characteristics and their influence on study endpoints. Power analyses can be performed with pharmacokinetic models to rationalise sample sizes (**Chapter 3**). Moreover, different sampling strategies can be investigated for the identification of informative sampling times (**Chapter 12**) or minimising number of samples without influencing the endpoint of the study (**Chapter 3**). Lastly, sensitivity analyses can be performed to identify critical aspects in study design such as missing data or erroneous sampling times (**Chapter 12**). Using pharmacokinetic models for optimising study design can rationalise minimalistic study designs which can influence patient burden positively.

Summarising, pharmacometric modelling is a powerful tool for the characterisation and extrapolation of drug exposure and exposure-response relationships. Thereby these models can inform dose selection for future clinical studies. Lastly, pharmacometrics can optimise clinical study design and thereby reduce patient burden of these studies.



**Final remarks**

Currently dose selection in oncology drug development is predominantly based on toxicity. Dose selection can be improved by taking both exposure–efficacy and exposure–toxicity relationships into account. A thorough characterisation of exposure–response relationship is therefore fundamental to improve dose selection in early drug development of anticancer. Ultrasensitive LC-MS/MS methods enable innovative pharmacokinetic studies essential for the characterisation of exposure–response relationships, especially in patient subpopulations. Microdoses and microtracers can be efficiently applied for the characterisation of drug exposure in early drug development. Therefore, such study designs should be implemented in drug development programs. Lastly, future drug development programs should apply pharmacometrics early in development and continuously update pharmacokinetic models with emerging clinical data to improve exposure–response characterisation and thereby dose selection. By implementing these considerations, dose selection of anticancer agents in early drug development could potentially be improved.

## REFERENCES

1. Araujo D, Greystoke A, Bates S, Bayle A, Calvo E, Castelo-Branco L, de Bono J, Drilon A, Garralda E, Ivy P, Kholmanskikh O, Melero I, Pentheroudakis G, Petrie J, Plummer R, Ponce S, Postel-Vinay S, Siu L, Spreafico A, Stathis A, Steeghs N, Yap C, Yap TA, Ratain M, Seymour L (2023) Oncology phase I trial design and conduct: time for a change - MDICT Guidelines 2022. *Ann Oncol* 34 (1):48-60. doi:10.1016/j.annonc.2022.09.158
2. Fourie Zirkelbach J, Shah M, Vallejo J, Cheng J, Ayyoub A, Liu J, Hudson R, Sridhara R, Ison G, Amiri-Kordestani L, Tang S, Gwise T, Rahman A, Pazdur R, Theoret MR (2022) Improving Dose-Optimization Processes Used in Oncology Drug Development to Minimize Toxicity and Maximize Benefit to Patients. *J Clin Oncol* 40 (30):3489-3500. doi:10.1200/jco.22.00371
3. Yamane N, Tozuka Z, Kusama M, Maeda K, Ikeda T, Sugiyama Y (2011) Clinical relevance of liquid chromatography tandem mass spectrometry as an analytical method in microdose clinical studies. *Pharm Res* 28 (8):1963-1972. doi:10.1007/s11095-011-0423-8
4. Frost BM, Lönnerholm G, Koopmans P, Abrahamsson J, Behrendtz M, Castor A, Forestier E, Uges DR, de Graaf SS (2003) Vincristine in childhood leukaemia: no pharmacokinetic rationale for dose reduction in adolescents. *Acta Paediatr* 92 (5):551-557
5. Gidding CE, Meeuwse-de Boer GJ, Koopmans P, Uges DR, Kamps WA, de Graaf SS (1999) Vincristine pharmacokinetics after repetitive dosing in children. *Cancer Chemother Pharmacol* 44 (3):203-209. doi:10.1007/s002800050968
6. Nijstad AL, Chu WY, de Vos-Kerkhof E, Enters-Weijnen CF, van de Velde ME, Kaspers GJL, Barnett S, Veal GJ, Lalmohamed A, Zwaan CM, Huitema ADR (2022) A Population Pharmacokinetic Modelling Approach to Unravel the Complex Pharmacokinetics of Vincristine in Children. *Pharm Res*. doi:10.1007/s11095-022-03364-1
7. Ye Z, Gao H (2017) Evaluation of sample extraction methods for minimizing hematocrit effect on whole blood analysis with volumetric absorptive microsampling. *Bioanalysis* 9 (4):349-357. doi:10.4155/bio-2015-0028
8. Kip AE, Kiers KC, Rosing H, Schellens JHM, Beijnen JH, Dorlo TPC (2017) Volumetric absorptive microsampling (VAMS) as an alternative to conventional dried blood spots in the quantification of miltefosine in dried blood samples. *J Pharm Biomed Anal* 135:160-166. doi:10.1016/j.jpba.2016.12.012
9. Moorthy GS, Vedar C, Downes KJ, Fitzgerald JC, Scheetz MH, Zuppa AF (2021) Microsampling Assays for Pharmacokinetic Analysis and Therapeutic Drug Monitoring of Antimicrobial Drugs in Children: A Critical Review. *Ther Drug Monit* 43 (3):335-345. doi:10.1097/ftd.0000000000000845
10. Grassin-Delyle S, Lamy E, Semeraro M, Runge I, Treluyer JM, Mansukhani R, Arribas M, Roberts I, Shakur-Still H (2021) Clinical Validation of a Volumetric Absorptive Micro-Sampling Device for Pharmacokinetic Studies With Tranexamic Acid. *Front Pharmacol* 12:764379. doi:10.3389/fphar.2021.764379
11. El-Osta H, Hong D, Wheler J, Fu S, Naing A, Falchook G, Hicks M, Wen S, Tsimberidou AM, Kurzrock R (2011) Outcomes of research biopsies in phase I clinical trials: the MD anderson cancer center experience. *Oncologist* 16 (9):1292-1298. doi:10.1634/theoncologist.2011-0043

12. van Linde ME, Labots M, Brahm CG, Hovinga KE, De Witt Hamer PC, Honeywell RJ, de Goeij-de Haas R, Henneman AA, Knol JC, Peters GJ, Dekker H, Piersma SR, Pham TV, Vandertop WP, Jiménez CR, Verheul HMW (2022) Tumor Drug Concentration and Phosphoproteomic Profiles After Two Weeks of Treatment With Sunitinib in Patients with Newly Diagnosed Glioblastoma. *Clin Cancer Res* 28 (8):1595-1602. doi:10.1158/1078-0432.Ccr-21-1933
13. Rowland M (2007) Commentary on ACCP position statement on the use of microdosing in the drug development process. *J Clin Pharmacol* 47 (12):1595-1596; author reply 1597-1598. doi:10.1177/0091270007310548
14. Lappin G, Garner RC (2008) The utility of microdosing over the past 5 years. *Expert Opin Drug Metab Toxicol* 4 (12):1499-1506. doi:10.1517/17425250802531767
15. Lappin G, Noveck R, Burt T (2013) Microdosing and drug development: past, present and future. *Expert Opin Drug Metab Toxicol* 9 (7):817-834. doi:10.1517/17425255.2013.786042
16. van Nuland M, Rosing H, Huitema ADR, Beijnen JH (2019) Predictive Value of Microdose Pharmacokinetics. *Clin Pharmacokinet* 58 (10):1221-1236. doi:10.1007/s40262-019-00769-x
17. Mikus G (2019) Probes and Cocktails for Drug-Drug Interaction Evaluation: The Future Is Microdosing? *Clin Pharmacol Ther* 105 (6):1335-1337. doi:10.1002/cpt.1350
18. Foerster KI, Burhenne J (2020) Microdosing drugs: a versatile technique to detect and assess drug-drug interactions. *Expert Opin Drug Metab Toxicol* 16 (6):447-448. doi:10.1080/17425255.2020.1758666
19. Stoll F, Burhenne J, Lausecker B, Weiss J, Thomsen T, Haefeli WE, Mikus G (2013) Reduced exposure variability of the CYP3A substrate simvastatin by dose individualization to CYP3A activity. *J Clin Pharmacol* 53 (11):1199-1204. doi:10.1002/jcph.161
20. Roosendaal J, Rosing H, Beijnen JH (2020) Stable Isotopically Labeled Intravenous Microdose Pharmacokinetic Trials as a Tool to Assess Absolute Bioavailability: Feasibility and Paradigm to Apply for Protein Kinase Inhibitors in Oncology. *Clin Pharmacol Drug Dev* 9 (5):552-559. doi:10.1002/cpdd.840
21. Devriese LA, Koch KM, Mergui-Roelvink M, Matthys GM, Ma WW, Robidoux A, Stephenson JJ, Chu QS, Orford KW, Cartee L, Botbyl J, Arya N, Schellens JH (2014) Effects of low-fat and high-fat meals on steady-state pharmacokinetics of lapatinib in patients with advanced solid tumours. *Invest New Drugs* 32 (3):481-488. doi:10.1007/s10637-013-0055-4
22. Koch KM, Reddy NJ, Cohen RB, Lewis NL, Whitehead B, Mackay K, Stead A, Beelen AP, Lewis LD (2009) Effects of food on the relative bioavailability of lapatinib in cancer patients. *J Clin Oncol* 27 (8):1191-1196. doi:10.1200/jco.2008.18.3285
23. Chi KN, Spratlin J, Kollmannsberger C, North S, Pankras C, Gonzalez M, Bernard A, Stieltjes H, Peng L, Jiao J, Acharya M, Kheoh T, Griffin TW, Yu MK, Chien C, Tran NP (2015) Food effects on abiraterone pharmacokinetics in healthy subjects and patients with metastatic castration-resistant prostate cancer. *J Clin Pharmacol* 55 (12):1406-1414. doi:10.1002/jcph.564
24. Woodcock J, Woosley R (2008) The FDA critical path initiative and its influence on new drug development. *Annu Rev Med* 59:1-12. doi:10.1146/annurev.med.59.090506.155819

25. Lalonde RL, Kowalski KG, Hutmacher MM, Ewy W, Nichols DJ, Milligan PA, Corrigan BW, Lockwood PA, Marshall SA, Benincosa LJ, Tensfeldt TG, Parivar K, Amantea M, Glue P, Koide H, Miller R (2007) Model-based drug development. *Clin Pharmacol Ther* 82 (1):21-32. doi:10.1038/sj.clpt.6100235
26. Milligan PA, Brown MJ, Marchant B, Martin SW, van der Graaf PH, Benson N, Nucci G, Nichols DJ, Boyd RA, Mandema JW, Krishnaswami S, Zwillich S, Gruben D, Anziano RJ, Stock TC, Lalonde RL (2013) Model-based drug development: a rational approach to efficiently accelerate drug development. *Clin Pharmacol Ther* 93 (6):502-514. doi:10.1038/clpt.2013.54
27. Visser SA, Aurell M, Jones RD, Schuck VJ, Egnell AC, Peters SA, Brynne L, Yates JW, Jansson-Löfmark R, Tan B, Cooke M, Barry ST, Hughes A, Bredberg U (2013) Model-based drug discovery: implementation and impact. *Drug Discov Today* 18 (15-16):764-775. doi:10.1016/j.drudis.2013.05.012
28. Uittenboogaard A, Neutel CLG, Ket JCF, Njuguna F, Huitema ADR, Kaspers GJL, van de Velde ME (2022) Pharmacogenomics of Vincristine-Induced Peripheral Neuropathy in Children with Cancer: A Systematic Review and Meta-Analysis. *Cancers (Basel)* 14 (3). doi:10.3390/cancers1403061







# Appendices

**Summary**

**Nederlandse samenvatting**

**Author affiliations**

**Author contribution**

**List of Publications**

**Dankwoord**

**Curriculum vitae**





## SUMMARY

In recent years the focus of drug development in oncology has switched from conventional cytotoxic drugs to targeted therapies. Despite this change in focus, dose selection of anticancer agents in early drug development is still often based on toxicity. Dose selection can be improved by using both exposure-efficacy and exposure-toxicity relationships for decision making regarding dose selection. Therefore, a thorough understanding of these exposure-response relationships in early drug development is essential. Methodologies for exposure optimisation and characterization of exposure-response relationship are, therefore, needed. Moreover, exposure-response relationships might differ between patient subpopulations. Methods for exposure extrapolation across patient subpopulations need to be investigated. In this thesis, several methodologies for the optimisation of drug exposure and exposure-response relationships are described, contributing to improving dose selection of anticancer agents in early drug development.

In **Part 1** the application of microdoses and microtracers for exposure optimisation of anticancer agents was discussed. **Chapter 1** described a new methodology for the extrapolation of microdose pharmacokinetics to therapeutic pharmacokinetics. Naïve pooled data (NPD) pharmacokinetic models for gemcitabine, its metabolite 2',2'-difluorodeoxyuridine (dFdU) and anastrozole were developed based on microdose data. Subsequently, these pharmacokinetic models were used for extrapolation to therapeutic dose. Comparison between the predicted and observed therapeutic pharmacokinetic curve showed discrepancies of gemcitabine and dFdU but showed great similarity for anastrozole. These results demonstrated the application of NPD pharmacokinetic models for microdose extrapolation to therapeutic doses, which can contribute to dose selection for future dose-escalating Phase I trials.

**Chapter 2** and **3** described an innovative design for food-effect trials: microtracer food-effect study exemplified by alectinib. In this study, 100 µg  $^2\text{H}_6$ -alectinib (microtracer) will be co-administered with 600 mg alectinib with and without food. In **Chapter 2** the bioanalytical method for the quantification of  $^2\text{H}_6$ -alectinib in alectinib-containing human plasma for the support of this microtracer food-effect study was described. Samples collected during this study will contain a  $\geq 5,000$ -fold difference in concentration between the two analytes. The method was validated according to the FDA and EMA guidelines over a concentration range of 1-10 pg/mL with a bias and precision of  $\pm 3.5\%$  and  $\leq 5.7\%$  ( $\pm 15.9\%$

and  $\leq 12.5\%$  for the lower limit of quantification (LLOQ)), respectively. Several methods for correction of isotope interference were investigated and validated. Stability experiments demonstrated the stability of  $^2\text{H}_6$ -alectinib in the biomatrix for 2 days at ambient temperature and for 44 days at  $-20\text{ }^\circ\text{C}$ .

**Chapter 3** focussed on the feasibility of the study design of alectinib microtracer food-effect study. An *in silico* simulation study was performed using a previously published population pharmacokinetic model. Pharmacokinetics of a  $100\text{ }\mu\text{g}$  dose of  $^2\text{H}_6$ -alectinib were simulated. The proposed study design of 10 patients on steady state treatment, 10 blood samples collected within 24 hours after administration of the microtracer and an assumed food-effect of 40% had a power of 99.9%. The mean estimated food-effect was 39.8% (80% confidence interval (CI): 31.0-48.6%). These findings support the feasibility of a microtracer food-effect study for alectinib.

Moreover, in **Chapter 4** the application of microdosing to *in vivo* phenotyping of Cytochrome P450 (CYP) enzymes was discussed. There is sufficient evidence to support *in vivo* phenotyping of CYP2C19 and CYP3A with microdoses of omeprazole and midazolam, respectively. For CYP1A2, CYP2C9, CYP2D6, and CYP2E1 evidence for sensitivity to changes in enzyme activity at microdose level were lacking. Before microdose phenotyping test can be used for individualised dose adaptations, validation studies to establish sensitivity of probes to changes in enzyme activity at microdose level need to be conducted.

**Part 2** described the challenging dose optimisation of combination therapy consisting of mitogen-activated protein kinase kinase (MEK) inhibitors and human epidermal growth factor receptor (pan-HER) inhibitors. **Chapter 5** described the safety and pharmacokinetics of the first four dose levels of a dose-escalation study with lapatinib (pan-HER inhibitor), binimetinib (MEK inhibitor), and vinorelbine (microtubule targeting agent) in patients with RAS mutated metastatic colorectal cancer. At data cut-off, 14 patients were included. Most frequent toxicities were diarrhoea ( $n=10$ ), rash ( $n=11$ ), and anaemia ( $n=4$ ). An intermittent dose regimen of 1000 mg lapatinib QD, 30 mg binimetinib BID with once weekly administration of  $17.5\text{ mg/m}^2$  vinorelbine was found to be tolerable. Pharmacokinetic data showed a dose-exposure relationship for binimetinib but not for lapatinib, which was consistent with their relative increasing in exposure.

In **Chapter 6** a pharmacokinetic-toxicity model was developed linking the pharmacokinetics of pan-HER inhibitors (lapatinib, dacomitinib, and afatinib) and MEK inhibitors (binimetinib, trametinib, mirdametinib, and selumetinib) to toxicity

using a latent variable representing cumulative toxic effects. Development of a dose-limiting toxicity (DLT) was modelled using a logistic regression model. The relative contribution of MEK inhibitors compared to pan-HER inhibitors to overall toxicity was estimated as 7.6-fold (95% CI: 7.5-7.8). The maximum predicted probability of DLT increased from 6% within the first week of treatment to 17% in week four, which corresponded to the observed incidence of DLT of 22%. These results suggest in terms of toxicity, dose-escalation of MEK inhibitors should be prioritised to dose-escalation of pan-HER inhibitors. Lastly, this model can be used to predict the probability of DLTs for new dose levels of these or similar drug combinations.

**Part 3** focused on dose finding of oral docetaxel co-administered with the booster ritonavir for patients with metastatic castration-resistant prostate cancer (mCRPC). Previous studies have reported significant lower exposure of both intravenous and oral docetaxel for mCRPC patients compared to patients with other solid tumours. This observed difference in docetaxel pharmacokinetics is thought to be caused by an increased CYP3A activity or increased hepatic uptake resulting in higher clearance.

In **Chapter 7** the difference in oral docetaxel and ritonavir pharmacokinetics between these two patient populations was quantified using a population pharmacokinetic model. mCRPC patients had an estimated 2.3-fold (relative standard error (RSE%): 7.1) higher ritonavir clearance and a 1.5-fold (RSE%: 14.6) docetaxel intrinsic clearance. Oral docetaxel exposure for mCRPC patients was predicted for 16 different dosing regimens of docetaxel and ritonavir, with several dosing regimens resulting in similar docetaxel exposure. The pharmacokinetic profiles of these dosing regimens differentiated which could potentially result in differences in efficacy and toxicity.

**Chapter 8** investigated the difference in CYP3A activity between patients with prostate cancer and male patients with other solid tumours. Midazolam clearance was determined as a measurement of CYP3A activity. Oral midazolam clearance was 1.26-fold higher in patients with prostate cancer compared to patients with other solid tumours (geometric mean (CV%): 94.1 (33.5%) L/h vs. 74.4 (39.1%) L/h, respectively;  $p=0.08$ ). Intravenous midazolam clearance did not significantly differ between the two groups ( $p=0.93$ ). Furthermore, the metabolic ratio of midazolam to 1'-hydroxy midazolam did not differ between the two patient groups. Based on these results it can be concluded that the observed difference in docetaxel pharmacokinetics between the two patient groups cannot be fully explained by a difference in CYP3A activity.

**Part 4** addressed the exposure optimisation of vincristine in paediatric populations. A LC-MS/MS method for the quantification of the vinca-alkaloids vincristine, vinblastine, vinorelbine and its metabolite 4-O-deacetyl vinorelbine in human plasma was described in **Chapter 9**. The method was validated according to the FDA and EMA guidelines over a concentration range of 0.025 to 10 ng/mL for vinblastine, vinorelbine, and 4-O-deacetyl vinorelbine and 0.1 to 40 ng/mL for vincristine. The bias and precision were within  $\pm 12.4\%$  and  $\leq 10.6\%$  ( $\pm 13.2\%$  and  $\leq 16.3\%$  at LLOQ), respectively. The method was successfully used for the quantification of vincristine for a paediatric pharmacokinetic study and the quantification of vinorelbine and its metabolite for a preclinical mouse study.

**Chapter 10** described a LC-MS/MS method for the quantification of vincristine in human whole blood collected in volumetric absorptive microsampling (VAMS). The method was validated according to the EMA and FDA guidelines over a concentration of 1 to 50 ng/mL with the use of only 10 microliters of whole blood. The accuracy and precision were  $\pm 9.9\%$  and  $\leq 7.3\%$  ( $\pm 9.4\%$  and  $\leq 7.3\%$  at LLOQ), respectively. Samples exceeding the upper limit of quantification could be diluted 20 times. Quantification of vincristine in VAMS was independent on the haematocrit of whole blood. Stability showed that vincristine was stable in the biomatrix for 3 months at ambient temperature and 1 month at 25 °C and a relative humidity of 60%. Comparison of vincristine plasma concentrations to vincristine whole blood concentrations demonstrated a non-linear relationship.

A PBPK model was used to improve understanding of the complex non-linear pharmacokinetics of vincristine in **Chapter 11**. The hypothesis of vincristine binding to  $\beta$ -tubulin in blood cells was investigated. The PBPK model including blood cell binding adequately described vincristine pharmacokinetics. A higher binding capacity to  $\beta$ -tubulin for tissue and blood for infants (2.5-fold), children (2.0-fold), and adolescents (1.5-fold) compared to adults was necessary for the adequate description of pharmacokinetics in these populations. A higher  $\beta$ -tubulin binding capacity resulted in a more pronounced initial distribution phase of vincristine. Decreased free vincristine concentrations in the central compartment could potentially result in a lower risk of peripheral neuropathy, since less free vincristine is able to distribute to peripheral tissue where it can cause peripheral neuropathy. The higher binding capacity might explain the fact that children are able to tolerate higher relative doses of vincristine and the need for dose capping in adults.

Clinical outcomes of vincristine treatment (e.g., efficacy and toxicity) differ between Caucasian children and African children, which resulted in the hypothesis that African children are currently underdosed compared to their Caucasian peers. In **Chapter 12** a pharmacometric nomogram based on reference vincristine concentrations and bodyweight was used to identify patients with low vincristine exposure with a sensitivity, specificity, and accuracy of 75.1%, 76.4%, and 75.9%, respectively. The pharmacometric nomogram performed consistently for the different weight categories. The pharmacometric nomogram could contribute to optimisation of vincristine dosing in African children, by identifying patients who might need a dose increase and will be implemented in a planned prospective clinical trial.

In conclusion, this thesis aimed to improve dose finding in early drug development of anticancer agents by investigating novel methods for exposure optimization and exposure extrapolation. It was demonstrated that ultrasensitive and innovative LC-MS/MS methods enable novel pharmacokinetic studies essential for the characterisation of exposure-response relationships. Moreover, the application of microdoses and microtracers as efficient strategies for early characterisation of drug exposure was established. Lastly, several pharmacometrics methods were used for exposure optimisation of anticancer agents, confirming its essential role in drug development. Implementation of these methods might improve dose selection of anticancer agents in in early drug development.



## NEDERLANDSE SAMENVATTING

In de afgelopen jaren is de focus gedurende de ontwikkeling van oncologische geneesmiddelen veranderd van conventionele chemotherapie naar doelgerichte therapie. Ondanks deze verandering in focus, is toxiciteit vroeg in het ontwikkelingstraject nog vaak bepalend bij de doseringsselectie van oncologische middelen. Doseringselectie kan verbeterd worden door blootstelling-effectiviteit en blootstelling-toxiciteit relaties van geneesmiddelen te betrekken bij de besluitvorming. Een diepgaand inzicht in deze blootstelling-effect relaties vroeg in het ontwikkelingstraject van geneesmiddelen is essentieel. Hiervoor is methodologie voor het optimaliseren van de blootstelling en voor het beschrijven van de blootstelling-effect relatie nodig. Daarnaast kan een blootstelling-effect relatie verschillen tussen patiënten subpopulaties (bijvoorbeeld tussen volwassenen en kinderen). Methoden voor de extrapolatie van de blootstelling over patiënt-subpopulaties moeten daarom onderzocht worden. Dit proefschrift beschrijft verschillende methoden om de blootstelling te optimaliseren en blootstelling-effect relaties te beschrijven. Hierbij wordt bijgedragen aan de verbetering van doseringselectie van oncologische geneesmiddelen vroeg in het ontwikkelingstraject.

In **Deel 1** van dit proefschrift wordt beschreven hoe microdoses en microtracers gebruikt kunnen worden om de blootstelling van oncologische middelen te optimaliseren. **Hoofdstuk 1** beschreef een nieuwe methodologie om de farmacokinetiek van microdoses te extrapoleren naar therapeutische doseringen. Naïve pooled data (NPD) farmacokinetiek modellen zijn ontwikkeld voor gemcitabine, de metaboliet 2',2'-difluorodeoxyuridine (dFdU) en anastrozole. Deze farmacokinetiek modellen zijn vervolgens gebruikt voor de extrapolatie naar therapeutische doseringen. De voorspelde therapeutische concentraties weken af van de gemeten therapeutische concentraties voor gemcitabine en dFdU, maar waren gelijkwaardig voor anastrozole. Dit resultaat demonstreerde de toepassing van NPD farmacokinetiek modellen voor de extrapolatie van microdoses naar therapeutische doseringen. Deze modellen kunnen gebruikt worden voor besluitvorming rondom doseringen voor toekomstige dosisesescalatie Fase I studies.

**Hoofdstuk 2** en **3** beschreven een innovatieve studie opzet voor voedsel-effect studies: een microtracer voedsel-effect studie waarbij alectinib als voorbeeld is genomen. In deze microtracer voedsel-effect studie wordt  $100 \mu\text{g } ^2\text{H}_6$ -alectinib (microtracer) samen ingenomen met 600 mg alectinib met een maaltijd en of op een nuchtere maag. In **Hoofdstuk 2** wordt de bioanalyse methode voor de

kwantificatie van  $^2\text{H}_6$ -alectinib in humaan plasma met alectinib beschreven. Deze bioanalyse methode zal ter ondersteuning gebruikt worden voor de toekomstige microtracer voedsel-effect studie. De plasmaconcentraties van  $^2\text{H}_6$ -alectinib en alectinib in de monsters die gedurende de toekomstige studie verzameld zullen worden, zullen een  $\geq 5,000$ -voud van elkaar verschillen. De methode werd gevalideerd volgens de FDA en EMA-richtlijnen met een gevalideerde concentratie range van 1-10 pg/mL met een nauwkeurigheid van  $\pm 3.5\%$  en een precisie van  $\leq 5.7\%$  ( $\pm 15.9\%$  en  $\leq 12.5\%$  voor de laagste kwantificatielimiet (LLOQ)), respectievelijk. Verschillen methoden om de monsters te corrigeren voor isotoop interferentie zijn onderzocht en gevalideerd.  $^2\text{H}_6$ -alectinib was stabiel in humaan plasma voor 2 dagen op kamertemperatuur en 44 dagen op  $^{\circ}\text{C}$ .

De focus van **Hoofdstuk 3** lag op de haalbaarheid van de toekomstige alectinib microtracer voedsel-effect studie. Om de haalbaarheid van de studie opzet te bestuderen was er een *in silico* simulatie studie uitgevoerd. Hierbij was een eerder gepubliceerd populatie farmacokinetiek model gebruikt. Farmacokinetiek van een  $100\ \mu\text{g}$   $^2\text{H}_6$ -alectinib dosering werd gesimuleerd voor de voorgestelde studie opzet voor 10 patiënten op steady-state alectinib behandeling waarbij 10 monster worden afgenomen binnen 24 uur na inname van de microtracer met een aangenomen voedsel-effect van 40%. Deze studie opzet had een power van 99.9% met een gemiddeld geschatte voedsel-effect van 39.8% (80% betrouwbaarheidsinterval (CI): 31.0-48.6%). Deze resultaten ondersteunen de haalbaarheid van een microtracer voedsel-effect studie voor alectinib.

**Hoofdstuk 4** beschreef de toepassing van microdoses voor *in vivo* fenotypering van Cytochroom P450 (CYP) enzymen. Er was voldoende bewijs voor de toepassing van microdosing voor de *in vivo* fenotypering van CYP2C19 en CYP3A met omeprazol en midazolam microdoses, respectievelijk. Voor CYP1A2, CYP2C9, CYP2D6 en CYP2E1 was er te weinig bewijs dat de fenotyperingsmiddelen (probes) gevoelig waren voor veranderingen in enzymactiviteit op microdose niveau. Daarom moeten er validatie studies uitgevoerd worden om deze gevoeligheid vast te stellen voordat microdose fenotypering gebruikt kan worden voor individuele doseeraanpassingen.

**Deel 2** beschreef de uitdagende optimalisatie van de combinatie behandeling van mitogen-activated protein kinase kinase (MEK) remmers en remmers van meerdere human epidermal growth factor receptoren (pan-HER). In **Hoofdstuk 5** werden de veiligheid en farmacokinetiek van de eerste vier doseerlevels van een dosisescalatie studie met lapatinib (pan-HER remmer), binimetinib (MEK



remmer) en vinorelbine (microtubule targeting agent) in patiënten met RAS gemuteerde gemetastaseerde colorectaal kanker beschreven. Op het moment van data-analyse waren er 14 patiënten geïncludeerd. De meest voorkomende bijwerkingen waren diarree (n=10), huiduitslag (n=11) en bloedarmoede (n=4). Een intermitterend doseerschema van 1000 mg lapatinib eenmaal daags, 30 mg binimetinib tweemaal daags, en een wekelijkse toediening van 17.5 mg/m<sup>2</sup> vinorelbine werd beschouwd als veilig. Farmacokinetische data lieten een dosis-blootstellingsrelatie zien voor binimetinib, maar niet voor lapatinib. Dit was consistent met hun relatieve toename in blootstelling.

In **Hoofdstuk 6** werd een farmacokinetiek-toxiciteit model ontwikkeld. In dit model werd de farmacokinetiek van pan-HER remmers (lapatinib, dacomitinib, afatinib) en MEK remmers (binimetinib, trametinib, mirdametinib, en selumetinib) gelinkt aan toxiciteit met een latente variabele die de cumulatieve toxische effecten van de behandeling weergeeft. De ontwikkeling van een dosis limiterende toxiciteit (DLT) werd voorspeld met behulp van logistische regressie. De relatieve bijdragen van MEK-remmers ten opzichte van pan-HER remmers aan de algehele toxiciteit werd geschat als 7.6-voud (95% CI: 7.5-7.8). De maximale voorspelde kans op een DLT nam toe van 6% gedurende de eerste week van de behandeling tot 17% in week 4. Dit correspondeerde met de geobserveerde incidentie van 22%. Deze resultaten suggereren dat de dosisescalatie van MEK remmers de prioriteit moet hebben over de dosisescalatie van pan-HER remmers betreffende de toxiciteit van de behandeling. Tenslotte kan dit model gebruikt worden om de kans op DLTs te voorspellen voor toekomstige doseerlevels voor zowel deze combinaties als gelijkwaardige combinaties.

De focus van **Deel 3** lag op het vinden van een geschikte dosis voor orale docetaxel gecombineerd met de booster ritonavir voor patiënten met gemetastaseerde castratie-resistente prostaatkanker (mCRPC). Eerder studies rapporteerden voor mCRPC patiënten een significante lagere blootstelling voor zowel intraveneus als oraal docetaxel vergeleken met patiënten met andere solide tumoren. De hypothese achter dit verschil in blootstelling is een verhoogd CYP3A activiteit of een verhoogde hepatische opname in mCRPC patiënten resulterend in een hogere klaring en een lagere blootstelling.

**Hoofdstuk 7** beschreef de kwantificatie van het geobserveerde verschil in de farmacokinetiek van docetaxel en ritonavir tussen mCRPC patiënten en patiënten met andere solide tumoren. De geschatte klaring voor mCRPC patiënten was 2.5-voud hoger voor de ritonavir klaring (relatieve standaardfout (RSE%): 7.1)

en 1.5-voud hoger voor docetaxel intrinsieke klaring (RSE%: 14.6) ten opzichte van patiënten met andere solide tumoren. De blootstelling van orale docetaxel voor mCRPC patiënten werd voorspeld voor 16 verschillende doseerschemas voor docetaxel en ritonavir. Meerdere doseringen resulteerde in een gelijkwaardige blootstelling, maar hadden verschillende farmacokinetische profielen wat mogelijk de effectiviteit en veiligheid zou kunnen beïnvloeden.

**Hoofdstuk 8** onderzocht het potentiële verschil in CYP3A activiteit tussen patiënten met prostaatkanker en mannelijke patiënten met andere solide tumoren. CYP3A activiteit werd gedefinieerd als midazolam klaring, omdat dit een algemeen geaccepteerde maat is voor CYP3A activiteit. Orale midazolam klaring was 1.26-voud hoger in patiënten met prostaatkanker ten opzichte van mannelijke patiënten met andere solide tumoren (geometrisch gemiddelde (CV%): 94.1 (33.5%) L/h vs. 74.4 (39.1%), respectievelijk,  $p = 0.08$ ). Intraveneuze midazolam klaring verschilde niet tussen de twee patiëntengroepen ( $p=0.93$ ) evenals de metabole ratio van midazolam naar 1'-hydroxy midazolam. Op basis van deze resultaten kon geconcludeerd worden dat de geobserveerde verschillen in docetaxel farmacokinetiek tussen deze patiëntengroepen niet volledig verklaard kan worden door een verschil in CYP3A activiteit.

**Deel 4** beschreef de optimalisatie van de vincristine blootstelling in kinderen. Een bioanalyse methode voor de kwantificatie van vincristine, vinblastine, vinorelbine en zijn metaboliet 4-O-deacetylvinorelbine in humaan plasma werd beschreven in **Hoofdstuk 9**. De methode werd gevalideerd volgens de richtlijnen van de FDA en EMA over een concentratie range van 0.025 tot 10 ng/mL voor vinblastine, vinorelbine, en 4-O-deacetylvinorelbine en 0.1 tot 40 ng/mL voor vincristine. De nauwkeurigheid en precisie was respectievelijk  $\pm 12.4\%$  en  $\leq 10.6\%$  ( $\pm 13.2\%$  en  $\leq 16.3\%$  voor de LLOQ). Deze methode was succesvol in het kwantificeren van vincristine plasmaconcentraties voor een farmacokinetische studie in kinderen en in het kwantificeren van vinorelbine en zijn metaboliet voor een preklinische studie met muizen.

**Hoofdstuk 10** beschreef een bioanalyse methode voor de kwantificatie van vincristine in humaan volbloed dat werd verzameld met volumetric absorptive microsampling (VAMS). De methode werd gevalideerd volgens de richtlijnen van de EMA en FDA over een concentratie range van 1 tot 50 ng/mL met een sample volume van 10  $\mu$ L volbloed. De nauwkeurigheid en precisie waren respectievelijk  $\pm 9.9\%$  en  $\leq 7.3\%$  ( $\pm 9.4\%$  en  $\leq 7.3\%$  voor de LLOQ). Monsters met een concentratie boven de bovenste grens van kwantificatie konden 20 keer verdund

worden. De kwantificatie van vincristine in volbloed verzameld met VAMS was onafhankelijk van de hematocriet waarde van de volbloed. Vincristine was stabiel in de droge volbloed voor 3 maanden op kamertemperatuur en 1 maand op 25 °C bij een relatieve luchtvochtigheid van 60%. De vergelijking tussen vincristine concentratie in plasma en volbloed lied een non-lineaire relatie zien.

Een fysiologisch gebaseerd farmacokinetiek (PBPK) model was gebruikt om de complexe farmacokinetiek van vincristine te bestuderen in **Hoofdstuk 11**. De hypothese van de binding van vincristine aan  $\beta$ -tubuline in bloedcellen werd onderzocht. Het PBPK-model waarbij de binding van vincristine aan bloedcellen werd meegenomen, beschreef de vincristine farmacokinetiek goed. Een hogere bindingscapaciteit aan  $\beta$ -tubuline in weefsel en bloed was nodig om de farmacokinetiek adequaat te beschrijven in baby's (2.5-voud), kinderen (2.0-voud) en adolescenten (1.5-voud) vergeleken met volwassenen. Een hogere bindingscapaciteit voor  $\beta$ -tubuline resulteerde in een duidelijker initiële distributie fase voor vincristine. Afgenomen vrije vincristine concentraties in het centrale compartiment kunnen potentieel zorgen voor een lager risico op perifere neuropathie, omdat er mindere vincristine beschikbaar is voor het perifere weefsel waar de perifere neuropathie kan veroorzaken. Een hogere bindingscapaciteit voor vincristine aan  $\beta$ -tubuline zou daarom kunnen verklaren dat kinderen een hogere vincristine dosis kunnen verdragen en waarom er een maximale tolereerbare vincristine dosering is bij volwassenen.

Klinische uitkomsten van de behandeling met vincristine (bijvoorbeeld effectiviteit of toxiciteit) verschillen tussen Kaukasische kinderen en Afrikaanse kinderen. Deze observatie leidde tot de hypothese dat Afrikaanse kinderen mogelijk een te lage dosering krijgen in vergelijking tot Kaukasische kinderen. In **Hoofdstuk 12** wordt er een farmacometrische nomogram beschreven gebaseerd op referentie van vincristine concentraties en lichaamsgewicht. Dit nomogram kon patiënten identificeren met een lage vincristine blootstelling met een sensitiviteit, specificiteit en nauwkeurigheid van 75.1%, 76.4%, en 75.9%, respectievelijk. Het farmacometrische nomogram functioneerde consistent over de verschillende categorieën voor lichaamsgewicht. Dit nomogram kan bijdragen aan het optimaliseren van de vincristine doseringen in Afrikaanse kinderen door de identificatie van patiënten die mogelijk een dosis verhoging nodig hebben. Het farmacometrische nomogram zal gebruikt worden in een toekomstige prospectieve klinische studie.

Concluderend had dit proefschrift als doel een bijdrage te leveren aan het verbeteren van de dosis selectie van oncologische middelen vroeg in de geneesmiddelontwikkeling door nieuwe methoden te onderzoeken voor het optimaliseren van de blootstelling en extrapolatie van blootstelling. Er is aangetoond dat ultra-sensitieve en innovatieve bioanalyse methoden nodig zijn ter ondersteuning van nieuwe farmacokinetische studies. Deze studies zijn essentieel voor de beschrijving van blootstelling-effect relaties van nieuwe geneesmiddelen. Verder zijn microdoses en microtracers efficiënte strategieën om de blootstelling van een nieuw oncologisch middel vroeg in de ontwikkeling in kaart te brengen. Tenslotte zijn er verschillende farmacometrische methoden gebruikt voor de optimalisatie van de blootstelling van verschillende oncologische middelen. Hierbij wordt bevestigd dat farmacometrie essentieel is gedurende geneesmiddelontwikkeling. De implementatie van deze methoden zou kunnen bijdragen aan de verbetering van dosisselectie van oncologische geneesmiddelen vroeg in de geneesmiddelontwikkeling.





## AUTHOR AFFILIATIONS

A. Laura Nijstad	Department of Clinical Pharmacy, University Medical Center Utrecht, CX Utrecht, The Netherlands Department of Pharmacology, Princess Máxima Center for Pediatric Oncology, Utrecht, The Netherlands
Abadi Gebretensae	Department of Pharmacy & Pharmacology, Antoni van Leeuwenhoek/The Netherlands Cancer Institute, Amsterdam, The Netherlands
Alwin D.R. Huitema	Department of Clinical Pharmacy, University Medical Center Utrecht, Utrecht, the Netherlands Department of Pharmacology, Princess Máxima Center for Pediatric Oncology, Utrecht, The Netherlands Department of Pharmacy & Pharmacology, Netherlands Cancer Institute, Amsterdam, The Netherlands
Andre M. Bergman	Department of Medical Oncology, The Netherlands Cancer Institute, Amsterdam, The Netherlands Department of Oncogenomics, The Netherlands Cancer Institute, Amsterdam, The Netherlands
Aniek Uittenboogaard	Princess Máxima Center for Pediatric Oncology, Utrecht, The Netherlands Emma Children's Hospital, Amsterdam UMC, Vrije Universiteit Amsterdam, Pediatric Oncology/Global Child Health Group, Amsterdam, The Netherlands
Arco J. Teske	Department of Cardiology, University Medical Center Utrecht, Utrecht, The Netherlands
Arief Lalmohamed	Department of Clinical Pharmacy, University Medical Center Utrecht, Utrecht, The Netherlands Utrecht Institute for Pharmaceutical Sciences, Utrecht University, Utrecht, The Netherlands
Bas Thijssen	Department of Pharmacy & Pharmacology, Antoni van Leeuwenhoek/The Netherlands Cancer Institute, Amsterdam, The Netherlands

C. Michel Zwaan	Princess Máxima Center for Pediatric Oncology, Utrecht, The Netherlands Department of Pediatric Oncology, Erasmus MC-Sophia Children's Hospital, Rotterdam, The Netherlands
Claire A. Ribbers	Department of Pharmacy & Pharmacology, Antoni van Leeuwenhoek/The Netherlands Cancer Institute, Amsterdam, The Netherlands Pharmaceutical Sciences, Utrecht University, Utrecht, The Netherlands
Dick Pluim	Department of Clinical Pharmacology, The Netherlands Cancer Institute - Antoni van Leeuwenhoek Hospital, Amsterdam, The Netherlands
Eelke H. Gort	Department of Medical Oncology, UMC Utrecht Cancer Center, Utrecht, The Netherlands
Emilie van Brummelen	Centre for Human Drug Research, Leiden, The Netherlands
Filip Y.F.L. de Vos	Department of Medical Oncology, University Medical Center Utrecht, Utrecht, The Netherlands
Frans L. Opdam	Department of Medical Oncology, The Netherlands Cancer Institute - Antoni van Leeuwenhoek Hospital, Amsterdam, The Netherlands
Gareth J. Veal	Newcastle University Centre for Cancer, Newcastle University, Newcastle Upon Tyne, UK
Geert W.J. Frederix	Julius Center for Health Sciences and Primary Care, University Medical Center Utrecht and Utrecht University, Utrecht, The Netherlands Department of Genetics, Utrecht University Medical Center, Utrecht, The Netherlands
Gertjan J.L. Kaspers	Emma Children's Hospital, Amsterdam UMC, University of Amsterdam, Paediatric Oncology, Amsterdam, The Netherlands Dutch Childhood Oncology Group, Utrecht, The Netherlands Princess Maxima Center for Pediatric Oncology, Utrecht, The Netherlands



---

Heleen A. Crommelin	Interstitial Lung Diseases Center of Excellence, Department of Pulmonology, St Antonius Hospital, Nieuwegein, The Netherlands Division Laboratory and Pharmacy, Department of Clinical Pharmacy, University Medical Center Utrecht, The Netherlands
Helena M. Klein Wolterink	Department of Medical Oncology, UMC Utrecht Cancer Center, Utrecht, The Netherlands
Henk M.W. Verheul	Department of Medical Oncology, Erasmus Medical Center, Rotterdam, The Netherlands
Hilde H. Nienhuis	Department of Medical Oncology, University of Groningen, University Medical Center Groningen, Groningen, The Netherlands
Hilde Rosing	Department of Pharmacy & Pharmacology, Antoni van Leeuwenhoek/The Netherlands Cancer Institute, Amsterdam, The Netherlands
Hugo J.G. Snippert	Oncode Institute, Center for Molecular Medicine, University Medical Center Utrecht, Utrecht, The Netherlands
Jeanine M.L. Roodhart	Oncode Institute, Center for Molecular Medicine, University Medical Center Utrecht, Utrecht, The Netherlands Department of Medical Oncology, University Medical Center Utrecht, Utrecht, The Netherlands
Joeri A.J. Douma	Department of Clinical Pharmacology, Division of Medical Oncology, Antoni van Leeuwenhoek/The Netherlands Cancer Institute, The Netherlands Department of Internal Medicine, Medisch Centrum Leeuwarden, Leeuwarden, The Netherlands
Johannes L. Bos	Oncode Institute, Center for Molecular Medicine, University Medical Center Utrecht, Utrecht, The Netherlands

Jos H. Beijnen	Department of Pharmacy & Pharmacology, Antoni van Leeuwenhoek/The Netherlands Cancer Institute, Amsterdam, The Netherlands Department of Pharmaceutical Sciences, Utrecht University, Utrecht, The Netherlands Modra Pharmaceuticals B.V., Amsterdam, The Netherlands
Kishan Naipal	Department of Clinical Pharmacology, Division of Medical Oncology, Antoni van Leeuwenhoek/The Netherlands Cancer Institute, The Netherlands
Leon Aardenburg	Department of Pharmacy & Pharmacology, Antoni van Leeuwenhoek/The Netherlands Cancer Institute, Amsterdam, The Netherlands
Lot A. Devriese	Department of Medical Oncology, UMC Utrecht Cancer Center, University Medical Center Utrecht, Utrecht, The Netherlands
Lotte van Andel	Department of Pharmacy & Pharmacology, Antoni van Leeuwenhoek/The Netherlands Cancer Institute, Amsterdam, The Netherlands
Maarten A. Huisman	Oncode Institute, Center for Molecular Medicine, University Medical Center Utrecht, Utrecht, The Netherlands
Maida I. Mohmaed Ali	Department of Pharmacy & Pharmacology, Antoni van Leeuwenhoek/The Netherlands Cancer Institute, Amsterdam, The Netherlands
Manon Acda	Department of Pharmacy & Pharmacology, Antoni van Leeuwenhoek/The Netherlands Cancer Institute, Amsterdam, The Netherlands
Manon N.G.J.A. Braat	Department of Radiology, University Medical Centre Utrecht, Utrecht, The Netherlands
Marijke Linschoten	Department of Cardiology, Division Heart and Lungs, University Medical Centre Utrecht, Utrecht, The Netherlands
Marit A.C. Vermunt	Department of Pharmacy & Pharmacology, Antoni van Leeuwenhoek/The Netherlands Cancer Institute, Amsterdam, the Netherlands

---

Matthijs Tibben	Department of Pharmacy & Pharmacology, Antoni van Leeuwenhoek/The Netherlands Cancer Institute, Amsterdam, The Netherlands
Merel van Nuland	Department of Pharmacy & Pharmacology, Antoni van Leeuwenhoek/The Netherlands Cancer Institute, Amsterdam, The Netherlands
Miangela M. Lacle	Department of Pathology, University Medical Center Utrecht, Utrecht University, Utrecht, The Netherlands
Miriam Koopman	Department of Medical Oncology, University Medical Center Utrecht, Utrecht University, Utrecht, The Netherlands
Neeltje Steeghs	Department of Medical Oncology, The Netherlands Cancer Institute, Amsterdam, The Netherlands
Sander Mertens	Oncode Institute, Center for Molecular Medicine, University Medical Center Utrecht, Utrecht, The Netherlands
Shelby Barnett	Newcastle University Centre for Cancer, Newcastle University, Newcastle Upon Tyne, UK
Sjoerd G. Elias	Department of Epidemiology, Julius Center for Health Sciences and Primary Care, Utrecht, The Netherlands
Thomas P.C. Dorlo	Department of Pharmacy and Pharmacology, Antoni van Leeuwenhoek/The Netherlands Cancer Institute, Amsterdam, The Netherlands Department of Pharmacy, Uppsala University, Sweden
Wan-Yu Chu	Department of Pharmacy & Pharmacology, Antoni van Leeuwenhoek/The Netherlands Cancer Institute, Amsterdam, The Netherlands



## AUTHOR CONTRIBUTION

### Chapter 1

I contributed to the conception and design of the study. I developed the pharmacokinetic models and discussed the modelling methodology and interpretation with my supervisory team. I wrote the manuscript and implemented contributions of all co-authors and external reviewers up to final publication.

### Chapter 2

I contributed to the conception and design of the study. I contributed to the development of the bioanalytical method and discussed results of the experiments with my supervisory team. I wrote the manuscript and implemented contributions of all co-authors.

### Chapter 3

I contributed to the conception and design of the study. I performed the data analysis using population pharmacokinetic modelling and discussed the modelling methodology and interpretation of the results with my supervisory team. I wrote the manuscript and implemented contributions of all co-authors and external reviewers.

### Chapter 4

I contributed to the conception and design of the study. I performed the literature search and the subsequent data analysis. I discussed interpretation of results and the future perspectives of microdosing for phenotyping of Cytochrome P450 enzymes. I wrote the manuscript and implemented contributions of all co-authors.

### Chapter 5

I contributed to the design of the study. I performed the quantification of vinorelbine plasma concentration. I performed the pharmacokinetic analysis and discussed the results and interpretation with my supervisory team and the study team. I co-wrote the manuscript, provided feedback, and implemented contributions of all co-authors.

### **Chapter 6**

I contributed to the design of the study. I collected previously analysed pharmacokinetic data. I performed the data analysis using population pharmacokinetic modelling and discussed the modelling methodology and interpretation of results with my supervisory team. I wrote the manuscript and implemented contributions of all co-authors.

### **Chapter 7**

I contributed to the conception and design of the study. I performed the data analysis using population pharmacokinetic modelling and discussed the modelling methodology and interpretation of results with my supervisory team. I wrote the manuscript and implemented contributions of all co-authors.

### **Chapter 8**

I contributed to the conception and design of the study. I collected the data. I developed and validated the bioanalysis method to support the clinical trial. I performed the quantification of drug plasma concentrations. I performed the pharmacokinetic analysis and statistical analysis and discussed the interpretation of the results with my supervisory team. I wrote the manuscript and implemented contributions of all co-authors.

### **Chapter 9**

I performed additional experiments to support the development of the bioanalytical method. I wrote the manuscript and implemented contributions of all co-authors up to final publication.

### **Chapter 10**

I contributed to the conception and design of the study. I performed the development of the bioanalytical method and contributed to the validation. I discussed results of experiments and their interpretation with my supervisory team. I performed the data analysis and discussed the interpretation with my supervisory team. I wrote the manuscript and implemented contributions of all co-authors up to final publication.

### **Chapter 11**

I contributed to the conception and design of the study. I contributed to the supervision on the development of the PBPK model and provided feedback on the interpretation of the results. I provided feedback on the manuscript.

**Chapter 12**

I contributed to the conception and design of the study. I performed the data analysis using population pharmacokinetic modelling and discussed the modelling methodology and interpretation of the results with my supervisory team. I wrote the manuscript and implemented contributions of all co-authors and external reviewers up to final publication.





## LIST OF PUBLICATIONS

**van der Heijden LT**, van den Hondel KE, Olyslager EJH, de Jong LAA, Reijnders UJL, Franssen EJF. Internet-Purchased Sodium Azide Used in a Fatal Suicide Attempt: A Case Report and Review of the Literature. *Toxics*. 2023; 11(7):608.

**van der Heijden LT**, Nijstad AL, Uittenboogaard A, Beijnen JH, Dorlo TPC, Kaspers GJL, Huitema ADR. Development of a Therapeutic Drug Monitoring Strategy for the Optimization of Vincristine Treatment in Pediatric Oncology Populations in Africa. *Ther Drug Monit*. 2023 Jun 1;45(3):354-363.

**van der Heijden L**, van Nuland M, Beijnen J, Huitema A, Dorlo T. A naïve pooled data approach for extrapolation of Phase 0 microdose trials to therapeutic dosing regimens. *Clin Transl Sci*. 2023 Feb;16(2):258-268.

**van der Heijden LT**, Uittenboogaard A, Nijstad AL, Gebretensae A, Kaspers GJL, Beijnen JH, Huitema ADR, Rosing H. A sensitive liquid chromatographic-mass spectrometry method for the quantification of vincristine in whole blood collected with volumetric absorptive microsampling. *J Pharm Biomed Anal*. 2023 Feb 20;225:115232. doi: 10.1016/j.jpba.2023.115232. Epub 2023 Jan 2. PMID: 36608428.

**van der Heijden LT**, Gebretensae A, Thijssen B, van Andel L, Nijstad AL, Wang Y, Rosing H, Huitema ADR, Beijnen JH. A highly sensitive bioanalytical method for the quantification of vinblastine, vincristine, vinorelbine and 4-O-deacetylvinorelbine in human plasma using LC-MS/MS. *J Pharm Biomed Anal*. 2022 Jun 5;215:114772.

Vermunt MAC, van Nuland M, **van der Heijden LT**, Rosing H, Beijnen JH, Bergman AM. Comparison of docetaxel pharmacokinetics between castration-resistant and hormone-sensitive metastatic prostate cancer patients. *Cancer Chemother Pharmacol*. 2022 Jun;89(6):785-793. doi: 10.1007/s00280-022-04433-3. Epub 2022 Apr 25. PMID: 35467095; PMCID: PMC9135852.

Vermunt MAC, **van der Heijden LT**, Hendrikx JJMA, Schinkel AH, de Weger VA, van der Putten E, van Triest B, Bergman AM, Beijnen JH. Pharmacokinetics of docetaxel and ritonavir after oral administration of ModraDoc006/r in patients with prostate cancer versus patients with other advanced solid tumours. *Cancer Chemother Pharmacol*. 2021 Jun;87(6):855-869.

**van der Heijden LT**, Mian P, Hias J, de Winter BCM, Tournoy J, Van der Linden L, Tibboel D, Walgraeve K, Flamaing J, Koch BCP, Allegaert K, Spriet I. Highly Variable Paracetamol Pharmacokinetics After Multiple Oral Dosing in Frail Older People: A Population Pharmacokinetic Analysis. *Drugs Aging*. 2022 Jan;39(1):83-95.





## DANKWOORD

De afgelopen vier jaar heb ik met veel liefde en enthousiasme gewerkt aan mijn onderzoeksprojecten. Nu mijn proefschrift is afgerond voel ik niet alleen de verwachte opluchting, maar ook teleurstelling dat het allemaal ten einde is gekomen. De afgelopen jaren heb ik veel geleerd, gezien en veel gelachen, waardoor het Antoni van Leeuwenhoek aan is gaan voelen als een tweede thuis. Een proefschrift schrijven is geen sinecure, maar het product van de steun en inzet van vele mensen. Daarom wil ik een aantal mensen in het bijzonder bedanken.

Ten eerste wil ik alle **patiënten** bedanken die hebben deelgenomen aan de klinische studies die zijn beschreven in dit proefschrift. Het is bijzonder om te ervaren hoeveel mensen mee willen doen met klinisch onderzoek, wetende dat zij daar zelf weinig baat van zullen hebben. Regelmatig werden de goede zorgen die zij hebben ervaren in het ziekenhuis genoemd als motivatie om mee te doen, zodat toekomstige patiënten nog betere zorg kunnen krijgen. Wegens die reden wil ik ook al het **zorgpersoneel** in het ziekenhuis bedanken.

**Alwin**, je had gelijk: uiteindelijk is het allemaal goed gekomen. Jouw onuitputtelijke enthousiasme en positiviteit hebben mij, vooral in de laatste maanden, feilloos door het promotietraject heen geloosd. Hoe vast ik ook zat in mijn eigen hoofd, jij wist altijd het probleem op een gestructureerde manier te benaderen, waardoor het opeens allemaal heel logisch werd. Ik ben je ontzettend dankbaar voor al kansen die je mij hebt gegeven en het vertrouwen dat je in mij had. Ik had het niet zonder jou kunnen doen.

**Jos**, ook jij gaf mij het vertrouwen dat het allemaal goed zou komen. Jouw kritische blik zorgde ervoor dat elk manuscript naar een hoger niveau getild werden. Onze gesprekken leidden altijd tot nieuwe inzichten waar ik weer mee aan de slag kon. Zo heb ik veel van je kunnen leren. Bedankt voor al de steun en adviezen die jij mij de afgelopen jaren hebt gegeven.

**Thomas**, ik heb ontzettend veel bewondering voor hoe jij, met jouw onderzoeksgroep in Uppsala, de wereld een beetje beter probeert te maken. Ik heb zoveel van je geleerd; niet alleen model-technisch, maar ook hoe je complexe modellen op een simpele en concrete manier uitlegt. Ik wil je bedanken voor alle steun en het vertrouwen dat je mij hebt gegeven.

**Hilde**, het bioanalyse lab was compleet uit mijn comfort zone, maar jij gaf mij het vertrouwen om toch op het lab te gaan staan. Jouw bioanalytische expertise was essentieel tijdens de ontwikkeling van onze bioanalyse methoden. Ondanks dat je het regelmatig druk had, wist je altijd tijd voor mij vrij te maken. Bedankt voor alle inzichten en hulp die jij mij gegeven hebt.

**Frans**, jij was niet alleen de PI van onze farmacokinetiek studie (N2OCYM), maar ook mijn mentor voor de opleiding tot klinisch farmacoloog. Door jouw enthousiaste en betrokken begeleiding heb ik de opleiding met veel plezier afgerond. Ik heb zoveel van jou kunnen leren. Bedankt voor al jouw vertrouwen en alle leuke casuïstiek die je mijn kant opstuurde.

**Bas** en **Matthijs**, dank jullie wel voor jullie enthousiasme, interesse en de tijd om mijn vragen te beantwoorden. **Abadi**, als mijn lab coach was je regelmatig mijn cheerleader op het lab. We hebben veel gelachen samen en dat ik een LC-MS/MS kan bedienen heb ik te danken aan jouw geduldige en duidelijke uitleg. **Leon**, **Manon**, **Danielle**, **Ciska**, **Lianda**, **Luc** en alle andere analisten op het lab. Dank voor jullie hulp en de gezelligheid tijdens de koffiepauzes. **Niels**, ik kan me niet voorstellen hoe mijn promotietraject zonder jou was geweest (een stuk saaier in elk geval). Bedankt dat ik jou altijd mocht lastigvallen met werk- en niet-werk gerelateerde onderwerpen en dat ik bij jou altijd mijzelf kon zijn.

Ik wil ook graag alle **coauteurs** bedanken voor hun waardevolle inbreng op mijn stukken. Daarnaast ben ik ook dankbaar voor alle mensen die hebben bijgedragen aan de klinische studies. **Carla** en **Else** voor het beantwoorden van al mijn vragen. Het **trialbureau** voor de administratieve ondersteuning. De **planning farmacologie** en de **centrale bereidingen** van de apotheek voor het altijd meedenken over de optimale studieplanning voor de patiënt. De **verpleegkundig specialisten**, in het speciaal **Marjolein** en **Coby**, en de **researchverpleegkundigen**, in het speciaal **Lotte**, **Maira** en **Tessa**, voor de prettige samenwerking.

**Aniek** en **Gertjan**, bedankt dat jullie mij betrokken hebben bij de CHAPATI studie. Ik heb erg genoten van onze discussies over de farmacokinetiek van vincristine. **Maarten**, **Jeanine** en **Nikki**, bedankt voor de prettige samenwerking betreffende de RASTRIC studie. **André**, **Kishan** en **Joeri**, dankzij jullie enthousiasme en inzet verliep de inclusie van de N2OCYM erg soepel. Ik ben jullie hier enorm dankbaar voor. **Marit**, dankjewel voor je hulp bij het opzetten van de N2OCYM. **Dick** bedankt voor het genotyperen van CYP3A voor dit project. **Claire**, het was een plezier om jou te mogen begeleiden tijdens je masterstage, welke uiteindelijk geleid heeft

tot een mooi manuscript. **Neeltje**, bedankt voor je hulp met het opzetten van de N20FEA en al jouw nuttige adviezen; ze hebben zeker geholpen. **Raween, Robbert** en **Maïda** bedankt voor jullie inzet om van de N20FEA een succes te maken.

**Paola**, jij verdient een aparte plek in mijn dankwoord. Zonder jouw passie voor onderzoek was ik nooit gaan promoveren. Circa vijf jaar na mijn onderzoeksstage ben jij nog steeds een voorbeeld voor mij. De afgelopen vier jaar kon ik altijd bij jou terecht met mijn verhaal of voor advies. Dankjewel daarvoor.

**Lishi**, dankjewel dat jij mijn paranimf wilt zijn. De afgelopen drie jaar zijn wij goede vrienden geworden. Fijn dat jij altijd naar mijn ideeën wilde luisteren en wilde meedenken. Ons bijna wekelijkse bijkletsuurtje in de trein was een van mijn favoriete momenten van de week. Dankjewel voor al je hulp en gezelligheid.

**Kim**, het is vanzelfsprekend dat jij mijn tweede paranimf bent. Als zus sta je al heel mijn leven naast mij en door je studie kon jij altijd met mij meepraten en het artsenperspectief gegeven op mijn onderzoek. Dankjewel dat je naar mij luisterde elke keer als ik probeerde uit te leggen hoe leuk farmacokinetiek is.

**René**, je was mijn rots in de branding tijdens de moeilijkste periode van mijn PhD, waar ik ontzettend dankbaar voor ben. Je was altijd beschikbaar om te sparren en mee te denken, waar ik veel van geleerd heb. Ik heb je de laatste 1.5 jaar moet missen als PhD-maatje, maar gelukkig zie ik je regelmatig.

Mijn lieve (oud)-kamergenootjes, **Semra, Ignace, Wendy, Maud** en **Merel** die altijd paraat stonden voor advies of om even mee te denken. Jullie zorgden ervoor dat mijn werkdagen gevuld waren met gezelligheid, maar daagden mij ook uit om vanuit een ander perspectief naar mijn onderzoek te kijken.

Alle **OIOs van H3**, bedankt voor alle borrels, etentjes, en OIO-weekenden. Jullie maakten van mijn promotietraject een bijzondere tijd. **Wietse**, dankjewel dat je altijd mee te wilde denken als ik vastzat met lab projecten. **Alaa**, dankjewel dat je altijd voor mij klaar stond. **Hinke**, ik ben dankbaar dat ik met jou kon sparren over mijn modellen.

Lieve  **vrienden** en **familie**, dank voor al jullie steun en interesse in mijn onderzoek en de welkome afleidingen. Lieve **oma** en **Dyonne**, dat ik mijn proefschrift heb moeten afronden zonder jullie was iets wat ik niet had verwacht. Ik mis jullie, maar ik weet dat jullie trots zouden zijn geweest op wat ik heb bereikt.

Lieve **pap** en **mam**, bedankt voor alle onvoorwaardelijke steun. Ondanks dat jullie meestal geen idee hadden waar ik had overhad, deden jullie altijd jullie best om het te begrijpen. Ik ben dankbaar dat ik op mocht groeien binnen zo'n liefdevol gezin. **Ruben**, mijn kleine grote broer, dankjewel voor al je steun de afgelopen jaren. Ik had mij geen lievere broer kunnen wensen.







## CURRICULUM VITAE

Lisa van der Heijden was born on July 12<sup>th</sup>, 1994 in Capelle aan den IJssel, the Netherlands. After her high school graduation from the Emmauscollege in Rotterdam, she started the study Pharmacy at the University of Utrecht in 2013. During her studies she participated in the Descartes College honours program and the Innovation in Pharmacy honours program. As part of her master's program, she performed a scientific internship at the department of paediatric surgery of Erasmus Medical Center Sophia Children's Hospital in Rotterdam, The Netherlands, focusing on pharmacokinetics of oral paracetamol in frail older patients. After her graduation in 2019, she started her PhD research at the department of Pharmacy & Pharmacology of the Netherlands Cancer Institute – Antoni van Leeuwenhoek Hospital, under the supervision of prof. dr. Alwin Huitema prof. dr. Jos Beijnen, dr. Hilde Rosing and dr. Thomas Dorlo. Her PhD mainly focused on methodologies for the optimisation of drug exposure in early drug development. During her PhD, she also did the training to become a clinical pharmacologist. Despite being raised in the Rotterdam area, Amsterdam has grown on her. The city will be her home for the next few years as she will start as a resident in the Onze Lieve Vrouwe Gasthuis (OLVG hospital) in Amsterdam on the 1st of January 2024, to become a hospital pharmacist.





